Persistent luminescence: kinetics and compounds

Koen Van den Eeckhout

Promotoren: Prof. Dr. Dirk Poelman en Prof. Dr. Philippe Smet

Proefschrift ingediend tot het behalen van de academische graad van
Doctor in de wetenschappen: Fysica

Vakgroep Vastestofwetenschappen
Voorzitter: Prof. Dr. Paul Matthys
Faculteit Wetenschappen
Academiejaar 2012-2013

UNIVERSITEIT GENT

Voor Mona

Contents

II Mechanism of persistent luminescence

III Development of persistent phosphors

Dankwoord

Dit doctoraatsproefschrift was er nooit gekomen zonder de hulp en de steun van ongelooflijk veel mensen. Dit is dan ook het ideale moment om hen oprecht te bedanken.

Dirk en Philippe, mijn dierbare promotoren, dankjewel om in mij het vuur van de wetenschap steeds weer aan te wakkeren. Ik herinner mij nog onze eerste ontmoeting, waarbij jullie mij vol enthousiasme de afterglow van een dun laagje $SrAl_2O_4$:Eu,Dy lieten zien. Nu, vijf jaar later, ben ik nog steeds dankbaar dat ik toen voor een thesis bij LumiLab heb gekozen. De combinatie van jullie grenzeloze wetenschappelijke passie, eindeloze fysische kennis en ontembaar enthousiasme zijn voor mij altijd een groot voorbeeld geweest. Dankjewel om mij op de nodige momenten een hart onder de riem (of een schop onder de kont) te geven. Dankjewel voor alle kansen die ik tijdens mijn thesis en doctoraat heb gekregen: presentaties, bijscholingen, ervaringen in het buitenland,... Het heeft de voorbije jaren tot een enorm gevarieerde en leerrijke ervaring gemaakt, en ik kijk er dan ook naar uit om er ook in de toekomst een vruchtbare samenwerking van te maken!

Er was de voorbije jaren geen dag dat ik met tegenzin de S1 ben binnengestapt, en dat is grotendeels de verdienste van mijn collega's bij LumiLab en in de rest van de S1.

Katleen, mijn favoriete 'spobilo', we begonnen samen onze thesis bij LumiLab, we hebben er (ongeveer) samen ons doctoraat verdedigd, en blijven er ook samen nog enkele jaren hangen. Dankjewel voor de ontelbare momenten van ontspannende babbels, muziek en donuts, voor de onvergetelijke trips naar Grenoble, voor de immer begripvolle raad en steun. Ik kijk ernaar uit om nog enkele jaren samen op de S1 door te brengen!

Anthony, Katrien en Heleen, mijn gezellige bureaugenoten, dankjewel om mij elke ochtend weer in een vrolijke stemming te brengen. Dankjewel om de ideale uitlaatklep te zijn voor mijn frustraties, mijn hyperactieve momenten, of wanneer ik gewoon eens zin heb om voor te lezen uit eigen werk. Ik wens jullie alle succes bij jullie eigen onderzoek!

Jonas, Jonas, Nursen, Iolanda, Hajieh, you are also the most amazing colleagues I could have hoped for. Thank you for all the great discussions, the music, the company on our trips to Grenoble, or to conferences. And of course, thank you for all the cakes and sweets! May your future be as bright as the afterglow of $SrAl_2O_4$:Eu,Dy!

Olivier, Nico, Elly en Kristof, dankjewel om steeds klaar te staan bij allerlei praktische en minder praktische problemen en verzoeken! Jullie zijn de onmisbare katalysator van alles wat aan de S1 gebeurt.

I would also like to thank the members of the examination and reading committee, dr. Adrie Bos, dr. Aurélie Bessière, dr. Klaartje De Buysser, dr. Henk Vrielinck, and dr.

Jan Ryckebusch, for their critical review of my text and their valuable comments.

Dankjewel aan mijn goede vrienden voor hun eeuwige steun en hun interesse in mijn werk: Bart, Lieven, Frederik, Pieter, Maarten, Glenn, en vele anderen, teveel om hier op te noemen. Hendrik, bedankt dat je bent blijven aandringen, en daardoor mijn leven een stukje zinvoller hebt gemaakt.

Lieve ouders, het meeste dank ben ik aan jullie verschuldigd. Niet alleen voor de nooit aflatende steun tijdens het werken aan mijn doctoraat en het schrijven van mijn proefschrift, maar voor alle mooie jaren van mijn jeugd. Dankjewel voor de ontelbare kansen die ik van jullie heb gekregen, en de ongelooflijke ervaringen die ik dankzij jullie heb mogen beleven. Dankjewel om mij steeds een liefdevolle thuis te geven. Ik wens jullie nog enorm veel mooie, rustige jaren samen vol uitstapjes, reizen en familiemomenten!

Lieve Hannes, jij hebt de voorbije maanden het meest geleden onder de afwerking van dit doctoraat. Dankjewel om er steeds opnieuw voor mij te zijn en op mij te wachten, ook en vooral op de momenten dat het minder gaat. Jouw vrolijkheid en lach geven mij elke dag opnieuw de energie en het geluk om tot het uiterste van het leven te genieten. Daarvoor kan ik je nooit genoeg bedanken!

Samenvatting

In tegenstelling tot de meeste luminescente materialen blijven persistente luminescente stoffen licht uitzenden gedurende enkele minuten of uren na het einde van de excitatie. Deze opmerkelijke eigenschap heeft voor de hand liggende toepassingen in decoratie en ontwerp, veiligheidssignalisatie, wijzerplaten en displays, maar recent werden ook nieuwe toepassingen ontwikkeld. In het bijzonder zouden persistente luminescente nanodeeltjes gebruikt kunnen worden als alternatief voor radioactieve tracers in *in vivo* medische beeldvorming.

Vandaag de dag is de meerderheid van deze toepassingen gebaseerd op de groene emissie van europium-gedopeerde strontiumaluminaten, omdat dit de enige stoffen zijn met een nalichting lang genoeg voor gebruik in de praktijk. Rood-emitterende persistente fosfors zijn opmerkelijk schaars, hoewel ze bijzonder gewenst zijn voor gebruik in veiligheidssignalisatie en medische beeldvorming.

Ondanks een goed begrip van het basisprincipe achter persistente luminescentie blijven verschillende details tot op de dag van vandaag het onderwerp van discussie. Hierdoor blijft de zoektocht naar helderdere, efficiëntere persistente fosfors een trial-and-error proces. In deze dissertatie proberen we enkele van deze overblijvende mysteries te ontrafelen, in het bijzonder de kenmerken van het trapsysteem en het trapping proces. Bovendien ontwikkelden we een oranje-emitterend persistent luminescent materiaal dat kan gebruikt worden voor medische beeldvorming, en geven we een overzicht van de huidige toestand van het onderzoek naar persistente luminescentie.

Mechanisme van persistente luminescentie

Het fenomeen van persistente luminescentie wordt bepaald door een complex samenspel van gastrooster, luminescente centra, ladingsdragers, trapniveaus, defecten en codopanten. Om meer te weten te komen over de achterliggende processen kan een grote verscheidenheid aan gekende en minder gekende experimentele technieken en simulaties worden ingezet.

Door het construeren van een eenvoudig model met één of twee traps kunnen we de emissie-intensiteit simuleren van de persistente fosforen $Sr_2MgSi_2O_7$:Eu,Dy en $CaAl_2O_4$:Eu,Nd tijdens de excitatie. Deze emissie springt niet ogenblikkelijk naar een constante waarde, maar neemt geleidelijk toe door het samenspel van trapping en recombinatie. Dergelijke simulaties kunnen ons ook leren aan welk tempo en in welke mate de verschillende traps gevuld worden.

Met x-stralen absorptiespectroscopie kan de valentietoestand van de luminescente centra en de codopanten gemeten en gevolgd worden. We kunnen hiermee aantonen

dat de verhouding Eu^{3+} versus Eu^{2+} in $SrAl_2O_4$:Eu,Dy toeneemt tijdens de excitatie, aan hetzelfde tempo als het vullen van de traps (bepaald uit metingen van de radioluminescentie). Dit bewijst dat de activators geoxideerd worden, en dat de hierbij vrijgekomen elektronen in traps terecht komen. Een gelijkaardige verandering van de valentietoestand in de codopanten kon nog niet worden waargenomen.

Thermoluminescentie (TL) metingen bij verschillende excitatiegolflengtes en excitatietemperaturen tonen aan dat het trappingproces thermisch geactiveerd kan zijn, vooral wanneer lange golflengtes gebruikt worden voor de excitatie. Deze thermische barrière wordt bepaald door de afstand tussen het geëxciteerde energieniveau (5d in het geval van Eu^{2+}) en de conductieband, en dus door de thermische quenching. Daarom is het nodig te focussen op stoffen met een lage thermische quenchingtemperatuur in de zoektocht naar Eu^{2+}-gebaseerde persistente fosfors. Hierin kunnen de traps immers makkelijker gevuld worden door excitatie met zichtbaar licht.

Door de totale lichtoutput en duur van de nalichting in $SrAl_2O_4$:Eu,Dy te meten in functie van de excitatie-intensiteit kan het aantal traps in dit materiaal geschat worden. Vanaf een zekere excitatie-intensiteit — bereikt door gebruik van een blauwe laser — nadert de geïntegreerde lichtoutput een maximumwaarde. Dit toont aan dat het maximale aantal traps in het materiaal gevuld is. Uitgaande van deze redenering kunnen we schatten dat het aantal traps in $SrAl_2O_4$:Eu,Dy ongeveer 16% van het aantal luminescente centra bedraagt.

Tot slot beschrijven we een procedure om de structuur van de traps in een persistente fosfor bloot te leggen, uitgaande van een reeks TL experimenten met verschillende excitatieduur en -temperatuur, en de initial rise analysemethode. Op deze manier kan de trapdiepte op een veel betrouwbaardere manier worden bepaald dan wanneer wordt uitgegaan van slechts één enkele TL meting, vooral in het geval van een continue verdeling van trapdieptes. We passen deze procedure toe op de bekende persistente fosfor $CaAl_2O_4$:Eu,Nd, en vinden een continue trapverdeling met een Gausissche vorm die is gecentreerd rond 0.9 eV maar zich uitstrekt van 0.7 tot 1.2 eV.

Ontwikkeling van persistente fosfors

Om het tekort aan persistente fosfors met een lange emissiegolflengte op te vangen, richtten we onze aandacht op de europium-gedopeerde nitrido-silicaten ($M_2Si_5N_8$:Eu, M = Ca, Sr en Ba), een groep oranje-emitterende fosfors die courant in LED toepassingen wordt gebruikt. Al deze materialen vertonen tot op zekere hoogte nalichting, hoewel deze in $Sr_2Si_5N_8$:Eu zeer beperkt blijft. $Ba_2Si_5N_8$:Eu heeft een relatief lange nalichting die pas na ongeveer 400 seconden onder de drempelwaarde 0.32 mcd/m^2 zakt.

Bij codopering met zeldzame aarden wordt de persistente luminescentie sterk beïnvloed. Terwijl de toevoeging van Sm de nalichting in alle onderzochte materialen doet afnemen, leidt de toevoeging van Tm aan $Ca_2Si_5N_8$:Eu tot een verzesvoudiging van de persistente intensiteit. Een maximale nalichtingstijd van 2500 seconden werd gemeten, maar de emissie blijft meerdere uren zichtbaar met het blote (aan het donker aangepaste) oog. De persistente luminescentie kan zowel met UV- als met zichtbaar licht opgewekt worden, wat de stof zeer geschikt maakt voor toepassingen binnenshuis.

SEM metingen en EDX mapping tonen het bestaan aan van niet-luminescente Tm-rijke gebiedjes in $Ca_2Si_5N_8$:Eu,Tm. Dit kan gedeeltelijk vermeden worden door het verlengen van de bereidingsduur, het toevoegen van (co)dopanten in hun fluoride- in plaats van hun oxidevorm, en door geschikte fluxmaterialen te gebruiken (zoals KF of NH_4Cl). Tevens zorgt een tekort van 5% aan Ca in het startmengsel voor een sterke toename in de intensiteit van de nalichting, wellicht omdat de gecreëerde Ca-vacatures het inbouwen van dopanten en codopanten in het gastrooster vergemakkelijken.

De korrelgrootte van het geoptimaliseerde $Ca_2Si_5N_8$:Eu,Tm poeder werd verkleind tot ongeveer 100 nm door malen in oplossing en centrifugeren. Dit maakt de stof beter geschikt voor toepassing als tracers in *in vivo* medische beeldvorming. Als een *proof of concept* werden deze deeltjes gefunctionaliseerd en geïnjecteerd in muizen, door collega's van de onderzoeksgroep LCMCP (Chimie Paristech). Met een gevoelige camera kan de biodistributie duidelijk in beeld gebracht worden, zo'n 15 minuten na injectie in de staartader. Tot slot tonen cytotoxiciteit-experimenten een lage acute toxiciteit ($\lesssim$ 10-20%) van de $Ca_2Si_5N_8$:Eu,Tm nanodeeltjes aan, gebaseerd op LDH en MTT metingen.

De zoektocht naar nieuwe, betere persistente luminescente materialen duurt voort, voornamelijk gemotiveerd door de mogelijke toepassingen. In het bijzonder rode en nabij-infrarode fosfors zijn erg gewenst voor medische beeldvorming en veiligheidssignalisatie. Het blijft een moeilijke opgave om *a priori* de emissie- en nalichtingseigenschappen van een willekeurige combinatie gastrooster-activator te voorspellen. Een intelligente combinatie van simulaties, nieuwe en traditionele experimentele technieken kan ons nochtans een rijkdom aan informatie opleveren over de onderliggende kinetiek en het trapsysteem. Op deze manier blijft onze kennis over persistente luminescentie groeien, en worden voortdurend nieuwe, uitdagende en veelbelovende toepassingen mogelijk gemaakt.

Summary

Contrary to most luminescent materials, persistent luminescent compounds have the ability to continue emitting light for minutes or hours after the excitation has ended. This remarkable phenomenon has obvious uses in decoration and design, safety signage, dials and displays, but recently promising novel applications have been suggested. In particular, persistent luminescent nanoparticles could be an alternative for radioactive tracer particles used for *in vivo* medical imaging.

Today, the majority of these applications relies on the greenish emission of the europium-doped strontium aluminates, since these are the only compounds with an afterglow that is bright and long-lasting enough for practical use. Red-emitting persistent phosphors, although strongly desired for safety signs and medical imaging, are particularly scarce.

Even though the basic principle behind persistent luminescence is by now well understood, many details remain the subject of discussion. This makes the search for brighter, more efficient persistent phosphors a trial-and-error process. In this dissertation, we attempt to unravel some of the remaining mysteries on persistent luminescence, in particular the features of the trap system and the trapping process. Furthermore, we developed an orange-emitting persistent luminescent material which can be used for medical imaging experiments, and we give a state of the art of the persistent luminescence research.

Mechanism of persistent luminescence

The phenomenon of persistent luminescence is governed by a complex interplay between the host compound, luminescent centers, charge carriers, trap levels, defects and codopants. To understand more about the underlying processes, a variety of common and novel experimental techniques and simulations can be used.

By constructing a simple one- or two-trap model we can accurately simulate the emission intensity of the persistent phosphors $Sr_2MgSi_2O_7$:Eu,Dy and $CaAl_2O_4$:Eu,Nd during the excitation. This emission does not immediately jump to a constant value, but slowly increases as the processes of trapping and recombination are competing against each other. These simulations also show us at which rate and to what extent the different traps are filled.

Using x-ray absorption spectroscopy the valence state of the luminescent centers and the codopants can be measured and monitored. We show that the ratio of Eu^{3+} to Eu^{2+} in $SrAl_2O_4$:Eu,Dy increases during the excitation, in the same way as the trap filling rate, which was determined from the radioluminescence. This proves that the

activators are oxidized and that the hereby released electrons are trapped. A similar valence state change in the codopants has yet to be detected.

Thermoluminescence (TL) measurements at various excitation wavelengths and at various temperatures show that the trapping process can be thermally activated, especially when exciting using long wavelengths. This thermal barrier is related to the energy difference between the excited state (5d in the case of Eu^{2+}) and the conduction band, and hence to the thermal quenching. Therefore, when searching for Eu^{2+}-based long-wavelength persistent phosphors, we should focus on those compounds having a relatively low thermal quenching temperature, as this facilitates trap filling of the phosphors with visible light.

By measuring the total light output and duration of the afterglow in $SrAl_2O_4$:Eu,Dy as a function of the excitation intensity we are able to estimate the number of traps in this material. At a certain excitation intensity level, achieved using blue laser excitation, the total light output reaches a saturation value. This indicates that the maximum number of traps in the material has been filled. Based on this reasoning, we can estimate the number of traps in $SrAl_2O_4$:Eu,Dy to be around 16% of the number of luminescent ions.

Finally, we describe a procedure to probe the trap system in a persistent phosphor, by combining series of TL experiments at various excitation durations and temperatures with the initial rise analysis method. In this way, the trap depths can be determined in a much more reliable way than using only a single TL measurement, especially in the presence of a continuous distribution of trap depths. We apply this procedure to the well-known persistent phosphor $CaAl_2O_4$:Eu,Nd, and prove the presence of a continuous trap depth distribution with a Gaussian shape, centered around 0.9 eV with tails extending from roughly 0.7 up to 1.2 eV.

Development of persistent phosphors

In order to alleviate the need for persistent phosphors emitting in the long-wavelength range of the visible spectrum, we focussed our attention on the family of europium-doped nitrido-silicates ($M_2Si_5N_8$:Eu, M = Ca, Sr and Ba), a group of orange-emitting phosphors commonly employed in LED development. All of these show afterglow properties to a certain extent, however, these are very limited in $Sr_2Si_5N_8$:Eu. A relatively long afterglow is detected in $Ba_2Si_5N_8$:Eu, lasting about 400 seconds before dropping below the 0.32 mcd/m^2 threshold.

Upon codoping with rare earths, the persistent luminescent properties are strongly influenced. While the addition of Sm decreases the afterglow intensity in all of the investigated compounds, adding Tm to $Ca_2Si_5N_8$:Eu increases this intensity almost sixfold. A maximum afterglow duration of 2500 seconds was measured, but the emission remains visible for several hours with the dark-adapted eye. The persistent luminescence can be induced by both UV and visible light, which makes the compound perfectly suited for indoor applications.

SEM measurements and EDX mapping revealed the presence of non-luminescent Tm-rich islands in $Ca_2Si_5N_8$:Eu,Tm. This can partially be countered by increasing the preparation duration, adding the (co)dopants in their fluoride rather than their

oxide form, and by using appropriate flux materials such as KF or NH_4Cl. Also, a 5% deficiency of Ca in the starting mixture strongly enhances the afterglow intensity, probably because the increase of Ca vacancies facilitates the incorporation of dopants and codopants in the host lattice.

The grain size of the optimized $Ca_2Si_5N_8$:Eu,Tm powder was reduced to about 100 nm by wet grinding and centrifuging techniques. This makes them more suitable for application as tracer particles in *in vivo* medical imaging. As a proof of concept, these particles were functionalized and injected into mice by colleagues at the LCMCP research group (Chimie Paristech). Using a sensitive camera, the biodistribution of the particles 15 minutes after tail vain injection can be clearly detected. Finally, cytotoxicity experiments show a low acute toxicity ($\lesssim$ 10-20%) of the $Ca_2Si_5N_8$:Eu,Tm nanoparticles, based on LDH and MTT measurements.

The search for new and better persistent luminescent phosphors continues, mainly driven by the potential applications, especially in the red and near-infrared range, such as medical imaging or safety signage. It remains a difficult task to *a priori* predict the emission and afterglow properties of a certain combination of host lattice and activator. However, by the intelligent use and combination of simulations, novel and common experimental techniques, a lot of information on the underlying kinetics and trap system can be derived. In this way, our knowledge about the persistent luminescence mechanism continues to expand, opening up the way for increasingly challenging and promising applications.

Introduction

Luminescent materials convert energy into light. This energy can come from a variety of sources such as chemical reactions, electron beams, pressure, or incoming photons. In the latter case, the phenomenon is called photoluminescence. In other words, photoluminescent materials convert incoming photons into emitted photons, usually with a different wavelength. They have numerous applications including light emitting diodes (LEDs), fluorescent lamps and displays [1].

Persistent luminescent materials, more commonly known as glow-in-the-dark materials, have the ability to continue emitting light for minutes or hours after the excitation. This remarkable phenomenon has been known to mankind since ancient times, and is still widely used today. The most well-known applications are decoration, toys, safety signage, dials and displays.

All of these applications are based on the same persistent luminescent materials: europium-doped strontium aluminates. For that reason, they all share the same bright green emission color. Other emission colors, especially orange and red, are much less frequently encountered, because only a handful of such materials are known. This is particularly unfortunate since red persistent phosphors are strongly desired for safety signage and medical imaging [2].

The search for persistent luminescent compounds with different emission colours and with a brighter and long-lasting afterglow is mainly hampered by the limited knowledge about the persistent luminescence mechanism. Even though the general role of trap levels and capture of charge carriers is well known, many important details remain unresolved. These include:

- the type of charge carriers: electrons or holes

- the mechanism of trapping and detrapping: through the conduction band or through localized transitions
- the origin of the trap levels: defects, vacancies, codopants,...
- the nature of the trap depths: discrete energy levels or depth distributions
- the number of traps, relative to the number of luminescent centers

Because of these uncertainties, the search for better persistent phosphors remains a matter of *trial and error*.

In this dissertation, we will combine two approaches to unravel some of these mysteries of persistent luminescence. On one hand, we have studied the details of the kinetics and the trap structure in some well-known persistent luminescent materials. On the other hand, we have developed our own orange-emitting family of persistent phosphors, the europium-doped nitrido-silicates.

Structure of the dissertation

The first chapter of this text offers some background information on persistent luminescence, and defines some of the commonly encountered terminology. The concept of trap levels and trapped charge carriers is briefly introduced.

The second and third chapter provide a thorough review of the state of the art of the persistent luminescence research, since such an overview was not yet available in literature. Chapter 2 lists, to the best of our knowledge, all the compounds where persistent luminescence has been reported, together with some of their most important properties. Chapter 3 reviews some of the models that have been suggested during the past two decades to describe the phenomenon of persistent luminescence.

In the second part of this dissertation, we take a look under the hood of some well-known persistent luminescent compounds. In chapter 4, we briefly address some techniques to learn more about the kinetics of the charge carriers in the material, both during the trapping phase and during the afterglow phase. In chapter 5, we present a procedure based on a combination of thermoluminescence measurements and the initial rise analysis method. Using this procedure, we can probe the trap level system in a persistent phosphor. As an example, we apply this technique on the blue-emitting phosphor $CaAl_2O_4$:Eu,Nd, and show that it has a continuous distribution of trap depths with a Gaussian shape.

The third and final part of this text describes how we developed an orange-emitting persistent phosphor, $Ca_2Si_5N_8$:Eu,Tm. We investigate the persistent luminescent properties of the europium-doped nitrido-silicate family, and optimize the afterglow brightness and duration by changing the preparation conditions, the starting materials, and the dopant concentrations. We study how the codopant influences the trap system, and compare this with the information obtained in the preceding chapters. Finally, we show that this material is a promising candidate for application in *in vivo* medical imaging techniques.

References

[1] Yen, W. M., Shionoya, S., and Yamamoto, H. *Phosphor Handbook*, chapter 1.3: Applications of phosphors. CRC Press, Boca Raton (2007).

[2] le Masne de Chermont, Q., Chanéac, C., Seguin, J., Pellé, F., Maîtrejean, S., Jolivet, J.-P., Gourier, D., Bessodes, M., and Scherman, D. *Proceedings of the National Academy of Sciences* **104**, 9266–9271 (2007).

Part I

Theoretical background

1 Persistent luminescence

This first chapter provides an overview of terminology encountered in the field of luminescence, and explains some of the key concepts used in the remainder of this text. It also provides a definition of persistent luminescence and gives a short introduction to its mechanism and applications.

1.1 Luminescence in inorganic compounds

Light emission by materials can be divided into two groups: blackbody radiation and luminescence. In the case of blackbody radiation, the light emission is caused by the (elevated) temperature of the material, and the emission spectrum is defined by Planck's law. Well-known examples are flames, filaments in incandescent light bulbs, and hot metal rods. In all other cases, the phenomenon is termed **luminescence**. To produce light, luminescent materials (also known as **phosphors**) absorb energy from external sources.

Depending on the origin of the absorbed energy, many types of luminescence can be distinguished. In this study, we focus almost exclusively on **photoluminescent** materials, which use incident photons as their energy source for the production of light. Other commonly encountered types are electroluminescence (electrical current), cathodoluminescence (electron beams), chemiluminescence (chemical reactions) and bioluminescence (chemiluminescence in living organisms), but many other, more exotic types of luminescence exist.

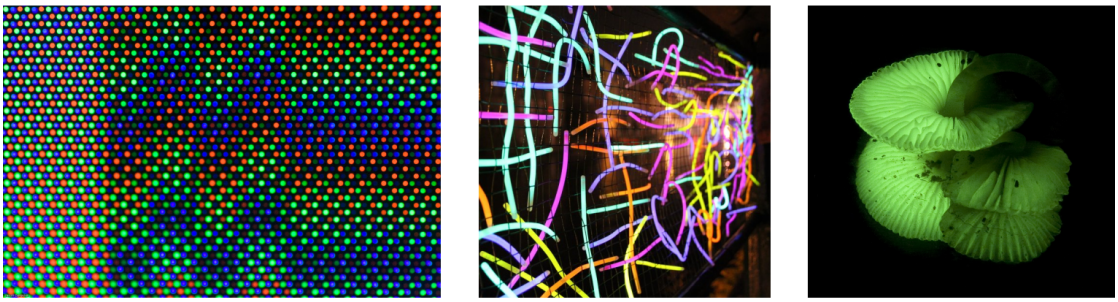

Figure 1.1: Some well-known examples of luminescence: cathodoluminescent pixels in a CRT display [1], chemiluminescent glowsticks, and bioluminescence in mushrooms [2].

At this point, it is important to stress that the word *thermoluminescence* is not used to describe materials that use heat as their source of energy for light production. In a thermoluminescence experiment, thermal energy is provided to a material to facilitate the release of *previously absorbed* energy in the form of light. A more elaborate explanation of thermoluminescence can be found in section 5.1.1.

1.1.1 Photoluminescence

Most inorganic photoluminescent materials consist of a **host lattice** in which a small amount of luminescent centers or **activators** is present. The host itself is not responsible for the light production. Instead, the incoming photons excite the luminescent centers, which subsequently return to the ground state by emitting photons (figure 1.2). In general, the energy of the emitted photons is lower than that of the absorbed ones. The energy difference is transferred to the host material in the form of heat (lattice vibrations).

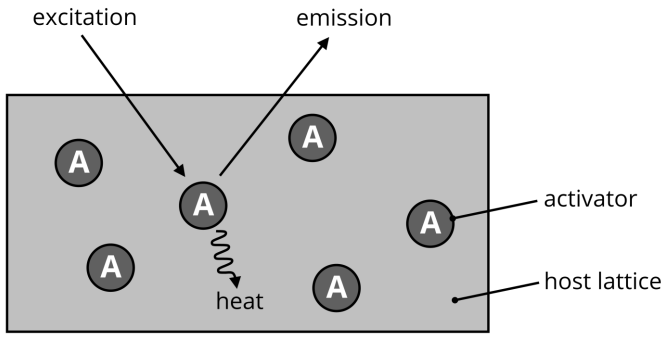

Figure 1.2: Simplified representation of a photoluminescent material where activators transform the energy of incoming photons into emitted photons and lattice vibrations [3].

In some materials, the incident photons are not absorbed by the activators themselves, but by other impurities present in the lattice (**sensitizers**), or even by the host lattice itself. The absorbed excitation energy is then transported through the material towards the activator, a process called **energy transfer**.

In the remainder of this text, a combination of a host lattice X with activator Y will be referred to as **X:Y**, for example $SrAl_2O_4$:Eu where $SrAl_2O_4$ is the host lattice and Eu is the activator.

1.1.2 Thermal quenching

The **quantum efficiency** (QE) of a luminescent material is defined as the ratio between the number of emitted and the number of absorbed photons. Therefore, if every absorbed photon leads to the emission of another photon, the material has a QE of exactly 100%. If a large fraction of the luminescent centers return to the ground state without emission of a photon (**non-radiative transitions**), the QE will be much lower than 100%.

At higher temperatures, the quantum efficiency of a phosphor drops significantly, due to an increasing fraction of non-radiative transitions. As a consequence, the intensity of the emitted light also decreases with temperature. A schematic representation is shown in figure 1.3. The temperature region in which the intensity drops is different for every luminescent material. At the **thermal quenching temperature** $T_{1/2}$, the emission intensity is exactly 50% of the original intensity.

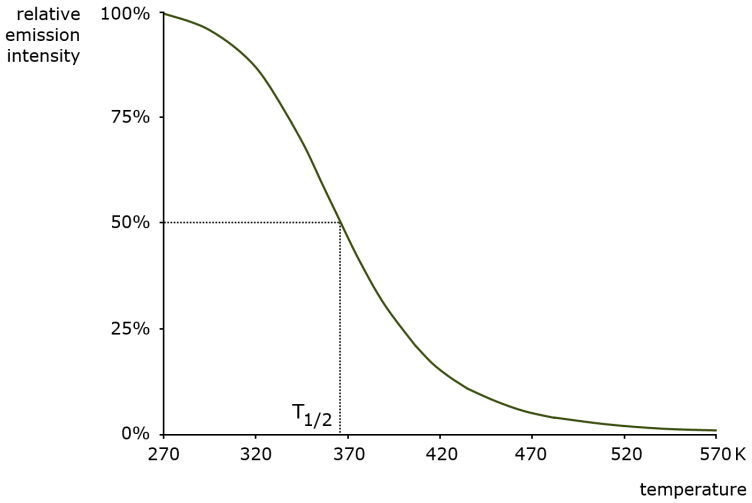

Figure 1.3: Typical thermal quenching behaviour in a luminescent material. Example for $CaAl_2O_4$:Eu,Nd [4].

The origin of the thermal quenching is in many cases not entirely clear. According to Dorenbos, the quenching is due to thermal ionization of the luminescent centers, because of the relative proximity of the excited level to the conduction band of the host lattice [5]. Others assume that a cross-over between the ground and excited level causes the increase of non-radiative transitions [6].

1.1.3 Decay of luminescence

Luminescent materials can be classified according to their behaviour after the end of the excitation. A lot of confusion exists about the correct terminology and definitions. Therefore, an attempt is made to visualize the classification in figure 1.4.

For organic molecules, the return to the ground state can be either an allowed or a forbidden transition. In the first case, the term *fluorescence* is used, while the latter type is called *phosphorescence*. For inorganic materials the terminology is different. Here, the term *fluorescence* is used for any normal radiative return to the ground state, either allowed or forbidden. In this case, the decay of the luminescence follows an exponential behaviour and ceases in a very short period of time, usually less than 10 ms.

The term *phosphorescence* is used when normal return to the ground state is delayed, either by the presence of quasi-stable excited states, or by trap levels. In the first case, the luminescence decay is also exponential, and usually lasts no longer than a second. If trap levels are present, the decay can take many shapes, and can last up to several seconds,

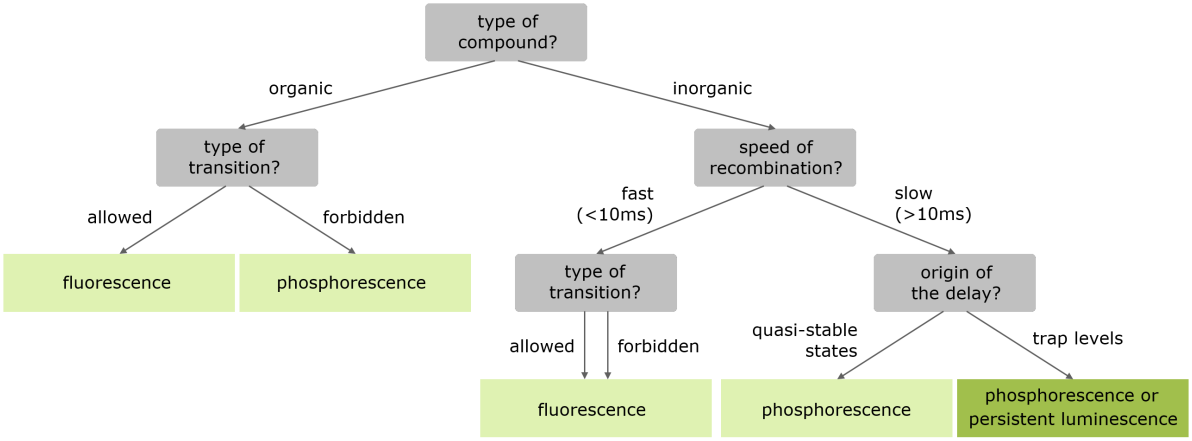

Figure 1.4: Classification of phosphors according to their behaviour after the end of the excitation.

minutes, or hours. In this text, we will focus almost exclusively on this latter group of phosphors. In order to avoid confusion, we will not use the term *phosphorescence*, but rather talk about **persistent luminescence** and persistent phosphors.

1.2 Fundamentals of persistent luminescence

Unlike the majority of phosphors, persistent luminescent materials continue emitting light for several seconds, minutes, or hours after the end of the excitation. This light emission, frequently called **afterglow**, is the most notable feature of a persistent phosphor. As mentioned previously, it is caused by the presence of trap levels in the band gap of a luminescent material.

1.2.1 Trap levels

Any imperfection of a perfect crystal lattice (lattice defects, impurity ions, surfaces,...) can give rise to the presence of additional energy levels, which can be located in the band gap of the material. After the excitation of a luminescent center (or excitation directly over the bandgap), the excited electron has a certain chance to escape and get caught by such a trap level. The trapped electron cannot recombine directly from the trap level, and thermal energy is required to release it. Therefore, the trapped electrons are released only very slowly, and the luminescence process (due to the recombination of the electron at the luminescent center) will be delayed. This trapping and detrapping process can occur either via the conduction band, or directly by localized transitions. Such localized transitions have been observed in e.g. YPO_4:Ce,R [7].

The speed with which the traps are emptied depends on the trap depth and the temperature. If the trap level is located far below the conduction band (a **deep trap**), a considerable amount of thermal energy is required to release the electrons. Therefore, at room temperature, it will take a long time before such a trap level will be emptied. For trap levels located close to the conduction band (a **shallow trap**), very little thermal energy is required. In this case, the trap level will be emptied in a matter of seconds,

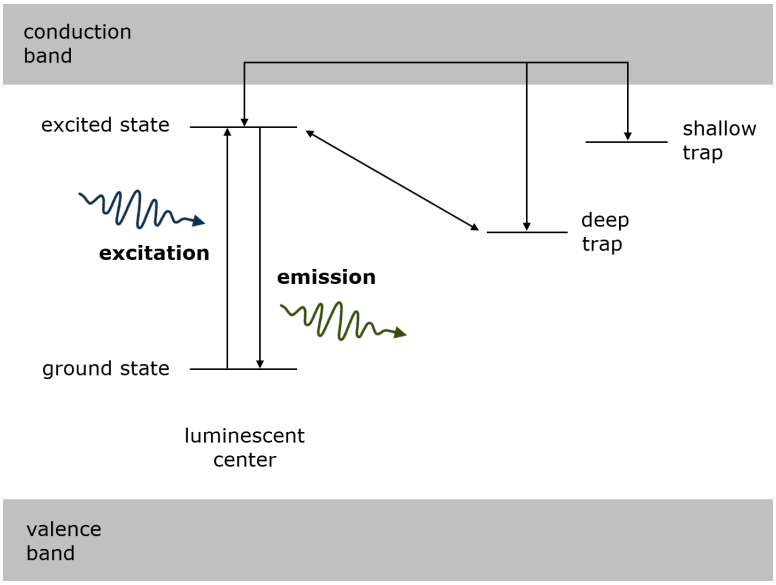

Figure 1.5: Trap levels in the band gap of the host lattice can capture electrons from the excited luminescent centers. Since thermal energy is required to escape these trap levels, the luminescence is delayed. The trapping and detrapping process can occur via the conduction band or directly by localized transitions.

or even faster. The trap depth is usually expressed in eV below the bottom of the conduction band, and the temperature most commonly in K.

A third factor that influences the speed of release is the escape frequency, or **frequency factor** s. This factor can be interpreted as the number of attempts a captured electron will undertake to escape the trap level. Even though it strongly affects the emptying of the traps, and hence the duration of the afterglow, it is one of the most difficult factors to determine. It depends heavily on the type of trap, but usually lies somewhere between 10^{10} and 10^{14} s^{-1}. If the exact value is unknown, it is common to choose $s = 10^{12}$ s^{-1}.

If a trap level has a certain depth E_T, the escape frequency is s, and the ambient temperature is T, the probability that a trapped electron escapes is defined by a Boltzmann factor:

$$p = s \cdot \exp\left(-\frac{E_T}{kT}\right) \tag{1.1}$$

where k is the Boltzmann constant. Therefore, the average lifetime of such a trapped electron becomes

$$\tau = \frac{1}{s} \cdot \exp\left(\frac{E_T}{kT}\right) \tag{1.2}$$

This lifetime at room temperature is shown in figure 1.6 as a function of trap depth. As can be seen, the lifetime dramatically increases for deeper traps. For a trap depth of 1.2 eV, and assuming an average frequency factor of $s = 10^{12}$, the average lifetime is longer than 6 years!

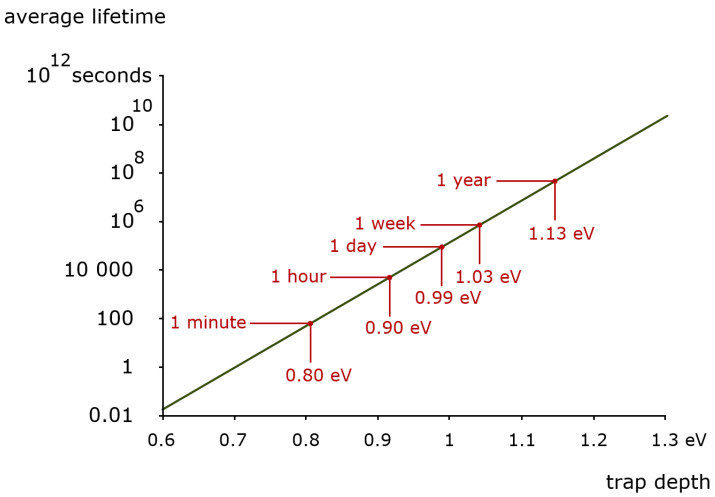

Figure 1.6: Average lifetime of an electron caught by a trap level, at room temperature and with an escape frequency of $s = 10^{12}$ s^{-1} (after [8]).

To achieve efficient persistent luminescence at room temperature, the trap should have a specific depth which is neither too shallow nor too deep. If the trap is too shallow, the electrons will easily escape from it and the afterglow will cease in a matter of seconds or less. If the trap is too deep, the thermal energy available at room temperature is not sufficient to release any trapped electron. A trap depth of around 0.6-0.7 eV is often stated as ideal to achieve efficient persistent luminescence at room temperature [9].

Luminescent materials with very deep traps can be used as **storage phosphors**, and are applied in medical imaging [10] or geochronology [11]. In these phosphors, additional stimulation (e.g. by photons or by heat) is required to empty the traps. The amount of luminescence produced in this way can then give information about the amount of radiation these materials were subjected to. Similar read-out techniques can be employed in persistent phosphors, and are the subject of chapter 5.

While the persistent luminescent mechanism described above is based on electrons moving through the conduction band and getting caught at electron traps, the same reasoning can be repeated using holes as the main charge carriers. In this case, holes can escape from the luminescent centers, travel through the valence band, and get caught at hole trap levels located close to the valence band. It should be noted that this does not affect the generic properties of a persistent phosphor. In fact, some models for persistent luminescence assign a crucial role to holes (see also chapter 3), and the exact charge carrier type remains the subject of an ongoing discussion.

1.2.2 Characteristics of persistent luminescence

A typical intensity profile of a persistent luminescent material during and after the excitation is shown in figure 1.7. During the excitation phase, the luminescence intensity does not immediately reach its maximum value. Rather, it increases gradually during several seconds or minutes until a saturation value is reached. During this initial phase, which we will address as the **charging phase**, there is a competition between recombi-

nation of the excited luminescent centers on one hand, and capturing of electrons by the traps on the other hand. Initially, when all traps are still empty, the trapping process is much more common than the recombination process. Over time, when the traps are becoming filled, the trapping and recombination will gradually find a balance. This behaviour explains the typical shape of the intensity profile during the excitation.

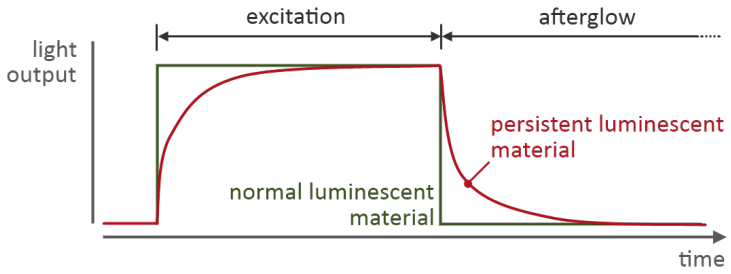

Figure 1.7: Typical profile of the emission intensity in a normal and a persistent luminescent material during and after the excitation. While this is not clear from the figure, time constants of charging and decay can be totally different.

When the excitation light is switched off, no more activators are being excited by incoming photons. However, the luminescence does not vanish completely, since traps are still being emptied, leading to recombination at the luminescent centers. As the number of filled traps continues to decrease, this 'residual' luminescence - or **afterglow** - decreases as well. This leads to a specific shape of the afterglow decay, which can be exponential, multi-exponential, hyperbolic, or even more complex.

The exact shape of the charging profile and the afterglow decay depends on a multitude of parameters: the trap depth, the temperature, the excitation intensity, the escape frequency, the concentration of traps, and the kinetics of the detrapping mechanism. This shape is difficult to predict or to model, which will be the main subject of chapter 4.

From a phenomenological point of view, the afterglow decay can be characterized by its **initial intensity** and **afterglow duration**. The former is rather straightforward, it is simply the intensity just after the excitation light has been switched off. The afterglow duration is much more difficult to define. For persistent phosphors emitting in the visible range of the electromagnetic spectrum, one can choose to define the afterglow duration as the time between the end of the excitation and the moment the photopic intensity drops below 0.32 mcd/m^2. This is about 100 times the sensitivity of the dark-adapted human eye, and a value often used in safety signage industry [12]. However, not all research groups are able to measure photopic intensities of phosphors, in which case the reported afterglow is simply the time the phosphor remains visible with the naked eye, making afterglow times difficult to compare. Furthermore, this definition cannot be applied to persistent phosphors emitting in the near-UV or near-IR region of the spectrum, where the photopic intensity is zero by definition. In that case, one must resort to radiometric units [13].

1.2.3 Applications of persistent luminescence

The phenomenon of persistent luminescence has some obvious and well-known applications, especially in decoration and safety signage. However, several new and potentially interesting fields of application have recently emerged, which has intensified the search for new and more efficient persistent luminescent materials.

Decoration and toys

Decoration is the oldest known application of persistent luminescence. Descriptions have been found of ancient Chinese paintings, where persistent phosphors were used to obtain a different scene when looking at the picture in daylight or at night [14]. Nowadays, luminous paint is widely available, and persistent luminescent toys can be found in many stores. Bedroom ceilings are sometimes decorated with persistent luminescent stars. Most of these applications are based on the greenish emission of $SrAl_2O_4$:Eu,Dy.

Watch dials

Since the end of the 19th century, watch dials have been painted with persistent luminescent material in order to make them visibly glow during the night. Originally, it was common to add radium to copper-doped zinc sulfide, in order to sustain the luminescence through beta radiation. However, this caused serious health issues. A well-known example is the radiation sickness of the 'Radium Girls', the female factory employees who painted the glow-in-the-dark watch dials, and commonly licked the tips of their paintbrushes to keep them sharp [15].

Later, the radium was replaced by smaller and less harmful amounts of tritium or promethium isotopes. Nowadays, nearly all dial paints are based on the much brighter afterglow of $SrAl_2O_4$:Eu,Dy (known under the brand name 'Super-Luminova'), which requires no radioactive isotopes at all. However, after approximately 1 hour, the afterglow of $SrAl_2O_4$:Eu,Dy drops below that of tritium-doped ZnS:Cu (see figure 1.8).

Safety signage

In the case of a power failure during an emergency, the evacuation route should be indicated by signs which do not require electrical power to be visible in the dark. Therefore, persistent luminescent safety signs are becoming increasingly important. They are commonly employed in airplanes to indicate the route towards the emergency exits, but also in buildings, particularly in staircases. Plans are being developed to incorporate persistent luminescent materials into the markings on the sides of the road. However, it is not clear if the afterglow from these strips will actually be visible, because of the relatively long time between the excitation (in daylight) and actual darkness.

Medical imaging

The most important recent development in persistent luminescence applications is the possibility of *in vivo* medical imaging using persistent luminescent nanoparticles [17–

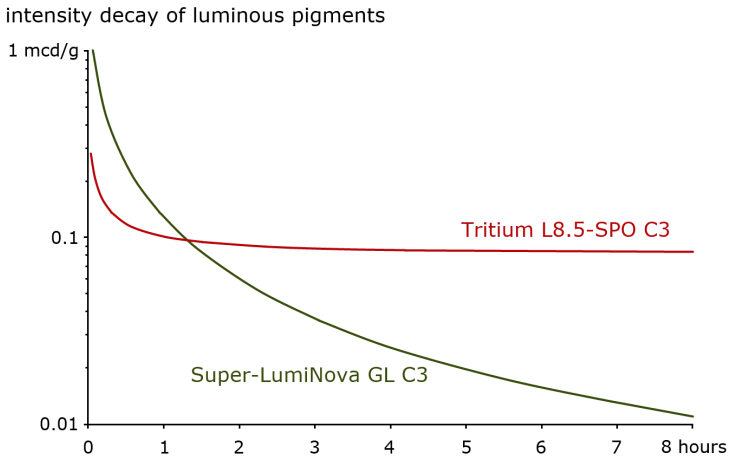

Figure 1.8: Comparison between the afterglow emission of $SrAl_2O_4$:Eu,Dy and tritium-doped ZnS:Cu. Due to the presence of tritium, the latter approaches a saturation value (data obtained from [16]).

20]. Nowadays, it is common to attach radioactive isotopes to drugs or molecules before injection into a patient, in order to trace them as they flow through the body. However, this subjects the patient to a certain amount of radioactivity. By using persistent luminescent nanoparticles instead of radioactive tracers, it is possible to excite the particles before injection, and follow their movement through the body with a very sensitive camera. The feasibility of this principle has already been demonstrated at the stage of mouse imaging. The scaling-up to human patients will require several additional steps, including severe toxicity tests. Also, this application requires rather intense red or near-IR light emission, since human tissue is only transparant for these wavelengths. Section 6.3 is entirely devoted to this specific application.

Further applications

Some other applications for persistent luminescence have been suggested, such as counterfeit detection, night-vision surveillance, or improvement of solar panel efficiency [21]. However, most of these applications have not been fully explored, and it is unsure if the expected results can also be achieved in practice.

1.2.4 The lack of red persistent phosphors

Today, nearly all of the above applications are based on Eu-doped strontium aluminates, since these are the only persistent phosphors with an afterglow which is bright enough to remain visible for an appreciable time. As a result, the emission color is always the same bright green. This is unfortunate, since several applications would benefit from other emission colors.

Specifically, efficient red-emitting phosphors are highly desired. Safety signage is mostly based on the colors red and green, however, only green persistent luminescent signs can be developed. For *in vivo* medical imaging, red or near-IR light is required for detection outside of the body.

Unfortunately, it proves to be very difficult to produce efficient red-emitting persistent phosphors. The reason for this is twofold.

- Firstly, it is difficult to obtain a red emission color using a combination of Eu^{2+} (the most efficient luminescent ion) and an oxide host compound (by far the most common type of host, see chapter 2). Therefore, it is necessary to look for more uncommon combinations of host compounds and activators. However, up to now it is not straightforward to predict the emission color and afterglow efficiency for such novel combinations, making this search a trial-and-error process.

- A second important reason for the lack of efficient red persistent phosphors is the Purkinje effect. In dark environments, the human eye sensitivity shifts to shorter wavelengths, as the rods in the retina are taking over [22–24]. Therefore, if we have a green and a red phosphor emitting the same number of photons, the green one will be perceived much brighter than the red one. A red-emitting persistent phosphor needs to be extremely efficient before it can be used for practical applications.

Currently the search for new persistent phosphors is mainly driven by this lack of red-emitting materials. Chapter 6 describes how we developed and optimized the Eu^{2+}-doped $M_2Si_5N_8$ family, a group of orange-red-emitting persistent luminescent compounds.

References

[1] Gerecke, J. http://www.flickr.com/photos/82805519@N00/, (2007). Released under Creative Commons license BY-NC-SA 2.0.
[2] Veitch, A. http://www.flickr.com/photos/gusveitch/, (2010). Released under Creative Commons license BY-NC 2.0.
[3] Blasse, G. and Grabmaier, B. C. *Luminescent materials*. Springer-Verlag, Berlin, Germany, (1994).
[4] Van den Eeckhout, K., Bos, A. J. J., Poelman, D., and Smet, P. F. *Physical Review B* **87**, 045126 (2013).
[5] Dorenbos, P. *Journal of Physics: Condensed Matter* **17**, 8103–8111 (2005).
[6] Yen, W. M., Shionoya, S., and Yamamoto, H. *Phosphor Handbook*, chapter 2.7.1: Decay of fluorescence. CRC Press, Boca Raton, FL, USA, 2nd edition (2007).
[7] Lecointre, A., Bessière, A., Bos, A. J. J., Dorenbos, P., Viana, B., and Jacquart, S. *The Journal of Physical Chemistry C* **115**, 4217–4227 (2011).
[8] Clabau, F. *Phosphorescence: Mécanismes et nouveaux matériaux*. PhD thesis, Institut des Matériaux Jean Rouxel, Nantes, (2005).
[9] Matsuzawa, T., Aoki, Y., Takeuchi, N., and Murayama, Y. *Journal of the Electrochemical Society* **143**, 2670–2673 (1996).
[10] Leblans, P., Vandenbroucke, D., and Willems, P. *Materials* **4**, 1034–1086 (2011).
[11] McKeever, S. W. S. *Thermoluminescence of solids*. Cambridge University Press, Cambridge, UK, (1985).

[12] Clabau, F., Rocquefelte, X., Jobic, S., Deniard, P., Whangbo, M. H., Garcia, A., and Le Mercier, T. *Solid State Sciences* **9**, 608–612 (2007).
[13] Pan, Z., Lu, Y.-Y., and Liu, F. *Nature Materials* **11**, 58–63 (2012).
[14] Harvey, E. N. *A history of persistent luminescence from the earliest times until 1900*. American Philosophical Society, Philadelphia, PA, USA, (1957).
[15] Carter, L. L. *American History* **42**, 32–37 (2007).
[16] `http://www.mwrforum.net/forums/showthread.php?t=20572`, (2008).
[17] le Masne de Chermont, Q., Chanéac, C., Seguin, J., Pellé, F., Maîtrejean, S., Jolivet, J.-P., Gourier, D., Bessodes, M., and Scherman, D. *Proceedings of the National Academy of Sciences* **104**, 9266–9271 (2007).
[18] Maldiney, T., Lecointre, A., Viana, B., Bessière, A., Bessodes, M., Gourier, D., Richard, C., and Scherman, D. *Journal of the American Chemical Society* **133**, 11810–11815 (2011).
[19] Maldiney, T., Richard, C., Seguin, J., Wattier, N., Bessodes, M., and Scherman, D. *ACS Nano* **5**, 854–862 (2011).
[20] Maldiney, T., Sraiki, G., Viana, B., Gourier, D., Richard, C., Scherman, D., Bessodes, M., Van den Eeckhout, K., Poelman, D., and Smet, P. F. *Optical Materials Express* **2**, 261–268 (2012).
[21] Pan, Z., Lu, Y.-Y., and Liu, F. *Nature Materials* **11**, 58–63 (2012).
[22] Poelman, D., Avci, N., and Smet, P. F. *Optics Express* **17**, 358–364 (2009).
[23] Poelman, D. and Smet, P. F. *Optics Express* **18**, 26293–26299 (2010).
[24] Poelman, D. and Smet, P. F. *Optics Express* **19**, 18808–18809 (2011).

2 State of the art

The findings in this chapter have been published in:

- **Persistent luminescence in Eu^{2+}-doped compounds: A review**
  Koen Van den Eeckhout, Philippe F. Smet and Dirk Poelman
  Materials **3** (2010) 2536-2566
- **Persistent luminescence in non-Eu^{2+}-doped compounds: A review**
  Koen Van den Eeckhout, Dirk Poelman and Philippe F. Smet
  Materials **6** (2013) 2789-2818

The phenomenon of persistent luminescence has been known to mankind for over a thousand years [1]. The first scientifically described observation dates back to 1602, when Vincenzo Casciarolo discovered the famous Bologna Stone, a persistent luminescent rock containing barium sulfide [2]. The sulfides remained at the center of attention as host compounds, and until the end of the 20th century, the majority of applications was based on ZnS doped with copper and cobalt [3, 4]. This material emits a greenish broad-band spectrum centered around 540 nm which remains visible for several hours after the end of the excitation. However, its afterglow is relatively weak, and it was common to add small amounts of radioactive radium, tritium or promethium in order to sustain the luminescence [4, 5].

In August 1996, Matsuzawa *et al.* published an article [3] that sent a shockwave through the until then relatively unpopular field of persistent luminescence. By codoping the green-emitting phosphor $SrAl_2O_4$:Eu (already showing a relatively strong and long-lasting afterglow by itself [6, 7]) with dysprosium (Dy^{3+}), they were able to create a material that emitted bright light for hours after ending the excitation. Simultaneously and independently, Takasaki *et al.* reported similar results [8]. Both groups found an afterglow with both a far higher initial intensity and a much longer lifetime compared to ZnS:Cu,Co.

This discovery marked the beginning of a renewed search for different and better persistent luminescent materials. Initially, this research was concentrated on other Eu^{2+}-doped alkaline earth aluminates, and it took a few years before other types of host materials and activators came into view. The number of materials where persistent luminescence has been observed has grown continuously over time. By now, over 200 combinations of host materials and activating ions have been described. This chapter provides an overview of these compounds and their luminescent properties.

2.1 Overview of persistent luminescent compounds

After the discovery of $SrAl_2O_4$:Eu,Dy, the persistent luminescence research remained focussed on Eu^{2+}-doped alkaline earth aluminates. It took a few years before other types of host materials and activators came into view. By now, only 15% of all known persistent phosphors uses aluminates as a host compound, and about 20% is based on Eu^{2+} as the luminescent ion (figure 2.1).

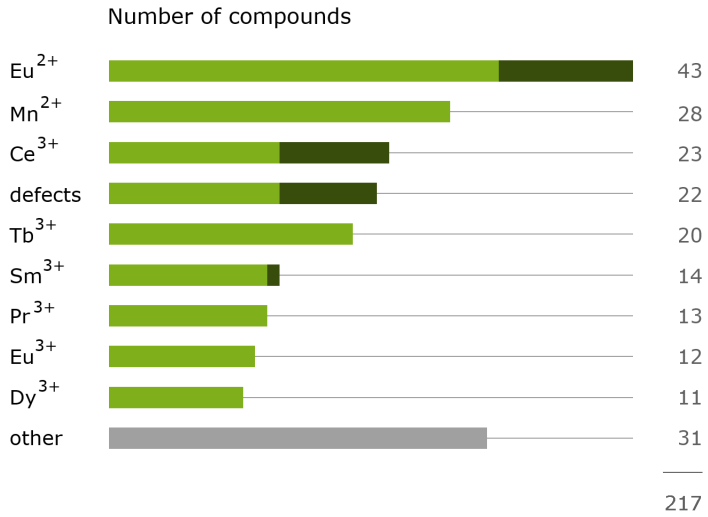

Figure 2.1: Number of known persistent luminescent compounds grouped by luminescent center. The darker areas indicate afterglow based on energy transfer during the afterglow. Eu^{2+} is the most common activator, used in about 20% of the reported compounds.

The popularity of Eu^{2+} as activator is not only based on historical reasons. It shows excellent afterglow properties in a large number of host lattices, with an afterglow duration which is often longer than 5 hours. Additionaly, its broadband emission depends strongly on the host lattice, more precisely on the nephelauxetic effect (or the centroid shift) and the strength of the crystal field acting on the ion [9]. Therefore, its emission color can be modified by changing the composition of the host lattice or the local coordination of the ion.

The research on persistent luminescent materials not based on Eu^{2+} is mainly driven by the lack of efficient red persistent phosphors. While it is quite common to obtain a blue or green afterglow using oxide hosts, it is much more difficult to find a suitable host material with sufficient red-shift in order to obtain red (persistent) luminescence. Although there are a number of red-emitting Eu^{2+}-doped persistent phosphors, such as CaS:Eu [10–12] and $Ca_2Si_5N_8$:Eu [13, 14], the choice is limited and the host lattices are chemically unstable, or difficult to prepare. This is especially unfortunate since red afterglow phosphors are strongly desired for applications in safety signage, paints, and as tracer particles for *in vivo* medical imaging (see section 1.2.3). Therefore, many research groups have focussed on different luminescent ions in order to obtain an efficient red-emitting persistent phosphor.

The most obvious and popular choice for long-wavelength luminescence is Mn^{2+}, known for its typical yellow-red emission in octahedral sites [15]. In several compounds, an energy transfer from Eu^{2+} to Mn^{2+} has been observed, leading to a red afterglow color originating from Mn^{2+}, but with a long afterglow duration defined by Eu^{2+}.

Not only red-emitting activators are being explored. Other common choices are the different trivalent rare earth ions such as Ce^{3+} and Tb^{3+}. An interesting case is Dy^{3+}, which shows a white emission color due to three different emissions around 480, 575 and 665 nm. Such a white emission is very difficult to obtain with only Eu^{2+} doping. Finally, several compounds are known to exhibit an afterglow without the addition of (co)dopants, purely based on the intrinsic luminescence of the host material.

An enormous variety of host materials are used as luminescent compounds, but when it comes to persistent luminescence, the number of known hosts is relatively low. The majority of research is concentrated around the silicates, with $Sr_2MgSi_2O_7$ as most famous representative, and the aluminates, represented by $SrAl_2O_4$. These two main classes of materials add up to about one third of all host compounds where persistent luminescence has been observed. All together, the oxides represent more than 85% of all host lattices (figure 2.2). The sulfides, having the longest recorded history of all persistent luminescent compounds, form the largest group of non-oxide hosts.

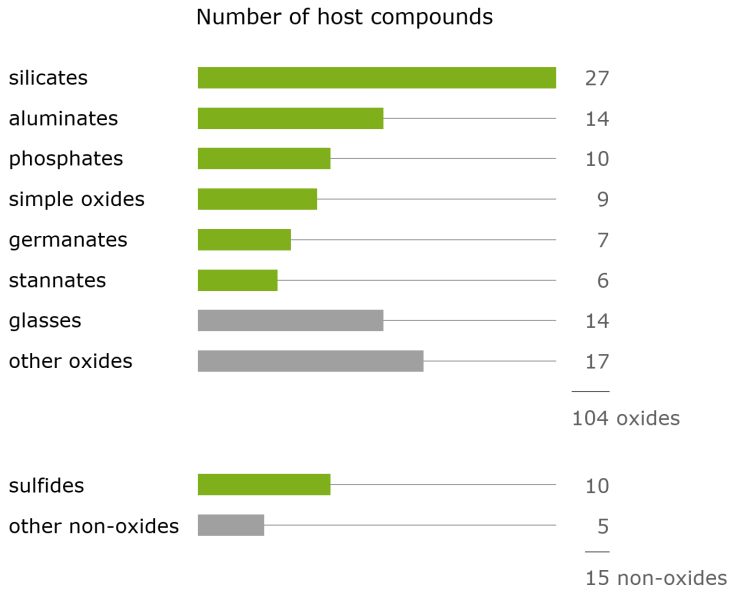

Figure 2.2: Number of known host compounds where persistent luminescence has been observed. More than 85% of all host lattices are oxides.

The following sections provide an extensive overview of all compounds where persistent luminescence has been reported. For every combination of host compound and activator relevant references are indicated in the last column. In the case of energy transfer between two different dopants or luminescent centers both the sensitizer and the activator are indicated. We use the symbol "≫" for efficient energy transfer and ">" for partial energy transfer, as derived from the emission spectra. For clarity, the materials are divided into five groups: silicates, aluminates, other oxides, non-oxides,

and glasses. If a property was not mentioned explicitly in the text of the reference, but inferred from it or from a figure, it is put between parentheses.

Only materials with an afterglow longer than a few seconds were taken into account, since only in this case the effect can be termed persistent luminescence. Some publications on phosphors, often using trivalent rare earth elements as dopants, claim to describe persistent luminescence, but only show an effective decay time of the order of milliseconds. In these cases, probably only the intrinsic decay of the forbidden transition within the rare earth ion is observed. Hence, these compounds and publications are deliberately not included in the tables.

The afterglow durations were taken directly from the mentioned references. However, not all of these were measured in a single, clearly defined way. The most common criterion is the visibility by the naked, dark-adapted eye. Only a few authors use the threshold value of 0.32 mcd/m^2 (see section 1.2.2). Also, the exact excitation conditions (wavelength, duration) are not always clear, although 254 nm is a common excitation wavelength. For details on the excitation conditions, we refer to the mentioned references. A more thorough discussion on these issues can be found in section 2.2.

2.1.1 Silicates

The silicates are used as the host crystal for a large part of the reported persistent luminescent compounds, both with Eu^{2+} and other luminescent ions. Especially the alkaline earth aluminum and magnesium silicates have been studied extensively. Some of the longest afterglow times (>5-10 hours) have been observed in $Sr_2MgSi_2O_7$:Eu^{2+},Dy^{3+} [16] and in rare-earth doped $CdSiO_3$, although the role of host and self-trapped excition (STE) luminescence remain the subject of discussion in this latter compound [17, 18]. A full list of persistent luminescent silicates can be found in table 2.1.

2.1.2 Aluminates

Ever since the discovery of $SrAl_2O_4$:Eu,Dy, the aluminates have been at the center of attention in persistent luminescent research, especially the Eu^{2+}-based materials. The aluminate compounds that are known to exhibit persistent luminescent properties are listed in table 2.2.

The alkaline earth aluminates MAl_2O_4 (M = Ca, Sr, Ba) are by far the most studied family of persistent luminescent materials. It is interesting to note that, as mentioned before, even the non-codoped $SrAl_2O_4$:Eu shows a considerable afterglow, indicating that the presence of codopants is not imperative to obtain persistent luminescence.

2.1.3 Other oxides

As shown in figure 2.2, the oxides make up the majority of persistent luminescent compounds. Besides the silicates and the aluminates, many more types have been explored, also those in which Eu^{2+} cannot be stabilized. This includes, for example, the stannates, titanates and germanates. An exceptional case is the near-IR afterglow of Cr^{3+} in $LiGa_5O_8$ and $Zn_3Ga_2Ge_2O_{10}$, which lasts several weeks and could be used for night-vision surveillance or *in vivo* bio-imaging [19, 20]. Allix *et al.* found that the latter

compound is a variant of the solid solution, $Zn_{1+x}Ga_{2-2x}Ge_xO_4:Cr^{3+}$, for $x = 0.5$. They report even better afterglow properties for the composition with $x = 0.1$ [21].

It should be noted again that there is no agreed definition of the afterglow duration for wavelengths which cannot be detected by the human eye. This makes it difficult to compare the various reported afterglow durations. A full list of persistent luminescent oxides, other than silicates and aluminates, can be found in table 2.3.

2.1.4 Other compounds

The sulfides are the most important non-oxide compounds in persistent luminescence. In fact, the famous Bologna Stone consisted mainly of copper-doped BaS [2]. Nowadays, the use of ZnS:Cu has much decreased in favor of $SrAl_2O_4$:Eu,Dy. The focus has mainly shifted to the oxysulfides, especially $Y_2O_2S:Eu^{3+},Ti^{4+},Mg^{2+}$ which is currently one of the best red-emitting phosphors. Nevertheless, the afterglow intensity is much weaker than the Eu^{2+}-doped aluminates or silicates [22]. An interesting case of persistent luminescence is observed in carbon- and oxygen-doped BN, where the emission wavelength can be shifted from blue to orange purely by changing the preparation conditions [23, 24]. All the non-oxide persistent luminescent compounds are summarized in table 2.4.

2.1.5 Glasses

A final group of persistent luminescent compounds are the glasses. Although it is sometimes difficult to accurately infer the composition of these glasses from the publications, some clear trends can be observed. Especially the calcium aluminum silicate and zinc boron silicate glasses have a long afterglow of more than one hour. A full list of persistent luminescent glasses can be found in table 2.5.

Table 2.1: Known persistent luminescent silicates

Host material	Activators	Emission maximum (nm)	Afterglow emission	Afterglow duration	refs.
$Ca_2Al_2SiO_7$	Ce^{3+}	400-417 (blue)	identical	> 1 hour	[25–28]
	$Ce^{3+} \gg Mn^{2+}$	550 (yellow)	identical	> 10 hours	[29]
$Ca_{0.5}Sr_{1.5}Al_2SiO_7$	$Ce^{3+} > Tb^{3+}$	386, 483+542+591 (white)	bluish white	> 1 min	[30]
$Sr_2Al_2SiO_7$	Ce^{3+}	400 (near UV)	identical	(> 2 mins)	[31]
	$Ce^{3+} > Dy^{3+}$	408, 491+573 (white)	(identical)	± 1 hour	[32]
	$Ce^{3+} > Tb^{3+}$	410, 482+543+588 (white)	(identical)	(> 1 min)	[33]
	Eu^{2+}	485 (blue/green)	identical	> 2 hours	[34]
$Sr_3Al_{10}SiO_{20}$	Eu^{2+}	465 (blue)	identical	> 6 hours	[35, 36]
$CaAl_2Si_2O_8$	Eu^{2+}	435 (blue)	435/510 (blue)	> 3 hours	[37, 38]
	$Eu^{2+} > Mn^{2+}$	418, 580 (blue)	identical	> 1 hour	[39]
	Mn^{2+}	?	?	± 20 mins	[40]
$CaMgSi_2O_6$	Dy^{3+}	480+575+667 (white)	identical	± 2 hours	[41]
	Eu^{2+}	445 (blue)	identical	> 4 hours	[42, 43]
	$Eu^{2+} > Mn^{2+}$	450, 580+680 (?)	identical	(± 30 mins)	[44]
	Mn^{2+}	580+680 (red)	680 nm (red)	> 1 hour	[44–48]
$SrMgSi_2O_6$	Dy^{3+}	455, 576 (blue)	identical	> 5 mins	[49]
	Mn^{2+}	455, 612 (pink)	(identical)	(± 15 mins)	[49]
$BaMg_2Si_2O_7$	$Ce^{3+} > Mn^{2+}$	408, 680 (red)	(identical)	> 2 hours	[50]
	$Eu^{2+} > Mn^{2+}$	400, 630-680 (reddish)	(identical)	> 2 mins	[51–53]
	Mn^{2+}	630-680 (red)	(identical)	> 30 mins	[50, 54]
$Ba_2MgSi_2O_7$	Eu^{2+}	505 (green)	identical	> 5 hours	[55, 56]
$Ca_2MgSi_2O_7$	Dy^{3+}	480+575+667 (white)	identical	> 3 hours	[41, 57]
	Eu^{2+}	515-535 (green)	identical	> 5 hours	[42, 58, 59]
$Sr_2MgSi_2O_7$	Dy^{3+}	441, 480+575+668 (white)	only Dy^{3+}	± 40 mins	[60]
	Eu^{2+}	470 (blue)	identical	> 10 hours	[16, 61, 62]
$Ba_3MgSi_2O_8$	Eu^{2+}	440 (blue)	identical	> 1 hour	[63]
$Ca_3MgSi_2O_8$	Dy^{3+}	480+575+667 (white)	identical	> 5 mins	[41]
	Eu^{2+}	470 (blue)	identical	> 5 hours	[63, 64]
$Sr_3MgSi_2O_8$	Eu^{2+}	460 (blue)	identical	> 10 hours	[63, 65]

	$Eu^{2+} > Mn^{2+}$	457, 670 (?)	identical	> 2 hours	[66]
$SrMgAl_2SiO_7$	Ce^{3+}	402 (near UV)	(identical)	> 2 mins	[31]
$Ca_3SnSi_2O_9$	defects	426 (blue)	(identical)	(± 10 mins)	[67]
	Dy^{3+}	426, 484+572+670 (white)	(identical)	(± 10 mins)	[67, 68]
	Pr^{3+}	426, 488 (greenish)	(identical)	(± 10 mins)	[67]
	Sm^{3+}	426, 565+600+650 (red)	(identical)	(± 10 mins)	[67]
	Tb^{3+}	426, 495+542+590 (green)	(identical)	(± 10 mins)	[67]
$Ca_{0.2}(ZnMg)_{0.9}Si_2O_6$	$Eu^{2+} \gg Mn^{2+}$	450, 580+680 (near IR)	identical	± 1 hour	[69, 70]
$Sr_2ZnSi_2O_7$	Eu^{2+}	460 (blue)	identical	> 5 mins	[43, 71]
	Eu^{3+}	617 (red)	identical	> 20 s	[72]
$CdSiO_3$	intrinsic/STE	380+467+560 (?)	±420 (blue)	± 5 hours	[17, 18]
	Dy^{3+}	410, 486+580 (white)	(identical)	> 5 hours	[73, 74]
	Eu^{3+}, Mn^{2+}	587, 610 (orange)	(identical)	> 1 hour	[75]
	Mn^{2+}	575-587 (orange)	identical	± 1-5 hours	[76–79]
	Mn^{2+}, Tb^{3+}	486+548, 587 (orange)	(identical)	> 1 hour	[80]
	Pb^{2+}	498 (green)	identical	> 2 hours	[81]
	STE > Dy^{3+}	420, 480+575 (white)	identical	± 5 hours	[17]
	STE > Eu^{3+}	420, 615 (red)	identical	± 5 hours	[17]
	STE > Pr^{3+}	420, 600 (red)	identical	± 5 hours	[17, 82]
	STE > Sm^{3+}	420, 565+600 (pink)	identical	± 5 hours	[17, 83]
	STE > Tb^{3+}	420, 485+540 (green)	identical	± 5 hours	[17]
	Tb^{3+}	495+545+590 (green)	identical	?	[84]
Lu_2SiO_5	Ce^{3+}	400+430 (blue)	(identical)	> 3 hours	[85, 86]
$MgSiO_3$	$Eu^{2+} \gg Mn^{2+}$	(456), 660-665 (?)	665 (red)	± 4 hours	[29, 87]
Mg_2SiO_4	Mn^{2+}	650 (red)	(identical)	± 20 mins	[88]
$SrSiO_3$	Dy^{3+}	480+572+664 (white)	identical	± 1 hour	[89]
Sr_2SiO_4	Dy^{3+}	480+575+665 (white)	identical	> 1 hour	[90]
	Eu^{2+}	480 (green)	identical	> 5 mins	[91]
Zn_2SiO_4	Mn^{2+}	? (green)	?	(> 5 mins)	[92, 93]
$BaZrSi_3O_9$	intrinsic/Ti^{4+}	460-470 (blue)	identical	> 20 s	[94, 95]

Table 2.2: Known persistent luminescent aluminates

Host material	Activators	Emission maximum (nm)	Afterglow emission	Afterglow duration	refs.
$BaAl_2O_4$	Ce^{3+}	402+450 (blue)	(identical)	> 10 hours	[96]
	Eu^{2+}	500 (green)	identical	> 2 hours	[97, 98]
$CaAl_2O_4$	Ce^{3+}	400 (blue)	± 413	> 10 hours	[99–101]
	$Ce^{3+} \gg Mn^{2+}$	525 (green)	(identical)	> 10 hours	[29]
	$Ce^{3+} \gg Tb^{3+}$	543 (green)	identical	> 10 hours	[99, 100]
	Dy^{3+}	477+491+577+668 (white)	identical	> 30 mins	[102]
	Eu^{2+}	440 (blue)	430	> 5 hours	[103–105]
	$Eu^{2+} > Mn^{2+}$	440, 545 (green)	± 440 (blue)	(> 3 hours)	[106]
	Tb^{3+}	493+543+590+621 (green)	identical	± 1 hour	[99, 107]
$MgAl_2O_4$	defects	520 (green)	identical	± 1 hour	[108]
	Cr^{3+}	260, 520, 710 (?)	520, 710 (?)	(> 2 hours)	[109]
	Tb^{3+}	(green)	?	± 1 hour	[110]
$SrAl_2O_4$	Ce^{3+}	375-385+427 (blue)	only 385	> 10 hours	[111–113]
	$Ce^{3+} > Mn^{2+}$	375, 515 (green)	identical	(± 5 hours)	[113]
	Eu^{2+}	520 (green)	identical	> 30 hours	[3, 114]
	$Eu^{2+} > Er^{3+}$	525, 1530 (green/IR)	mainly 525	± 10 mins	[115]
	$Eu^{2+} > Nd^{3+}$	515, 882 (green/NIR)	mainly 515	> 15 mins	[116]
$CaAl_4O_7$	Ce^{3+}	325, 420 (blue)	only 420	> 10 hours	[111]
$SrAl_4O_7$	Eu^{2+}	480 (blue)	identical	> 3 hours	[117, 118]
$Ca_{12}Al_{14}O_{33}$	Eu^{2+}	440 (indigo)	identical	> 10 mins	[119]
$SrAl_{12}O_{19}$	Eu^{2+}	400 (blue)	identical	> 3 hours	[117]
$Sr_3Al_2O_6$	Eu^{2+}	510/610 (disputed)	identical	(disputed)	[120, 121]
$Sr_4Al_{14}O_{25}$	Ce^{3+}	472+511 (blue/green)	(identical)	± 10 mins	[122]
	Eu^{2+}	490 (blue)	identical	> 20 hours	[123–125]
	$Eu^{2+} > Cr^{3+}$	490, 693 (blue/red)	mainly 490	> 2 hours	[126–128]
	Tb^{3+}	542 (green)	± 380 (blue)	?	[129]
$BaMgAl_{10}O_{17}$	Eu^{2+}	450 (blue)	identical	> 5 mins	[130]
$SrMgAl_{10}O_{17}$	Eu^{2+}	460 (blue)	515 (green)	> 3 mins	[131]

$Y_3Al_5O_{12}$	Ce^{3+}	525 (yellow)	identical	± 2 mins	[132, 133]
	Mn^{2+}	580 (yellow/orange)	585 (orange)	± 18 mins	[134]
	defects, Pr^{3+}	300-460, 490+610	380, 490+610	?	[135]
$CaYAl_3O_7$	Ce^{3+}	425 (blue)	(identical)	± mins	[25]

Table 2.3: Other known persistent luminescent oxides

Host material	Activators	Emission maximum (nm)	Afterglow emission	Afterglow duration	refs.
CaO	Eu^{3+}	594+616 (red)	(orange)	> 2 hours	[136, 137]
	Tb^{3+}	550 (green)	(identical)	?	[138]
Ga_2O_3	Cr^{3+}	720 (near-IR)	identical	> 4 hours	[139]
HfO_2	defects	480 (bluish white)	identical	> 1 min	[140, 141]
Lu_2O_3	Eu^{3+}	611 (red)	583+594+611	> 3 mins	[142]
	Tb^{3+}	490+550 (green)	identical	± 5-7 hours	[143–146]
SnO_2	Sm^{3+}	567+607+625 (red)	identical	± 40 mins	[147]
SrO	Eu^{3+}	594+616 (orange)	identical	> 1 hour	[137]
	Pb^{2+}	390 (violet)	identical	> 1 hour	[137]
	Tb^{3+}	543 (green)	(identical)	?	[138]
Y_2O_3	Eu^{3+}	612 (red)	(identical)	± 90 mins	[148, 149]
(Zn,Mg)O	unknown	520 (orange)	(identical)	± 10 mins	[150, 151]
ZrO_2	Sm^{3+}	570+614 (red)	(identical)	± 15 mins	[152]
	Ti (?)	(353+)470-500 (blue)	only 470-500	± 1 hour	[153–157]
Ba_2SnO_4	Sm^{3+}	580+611+623 (red)	(identical)	± 20 mins	[158, 159]
Ca_2SnO_4	Eu^{3+}	585+618+633 (red)	(identical)	± 50 mins	[160, 161]
	STE	410+466 (blue)	(identical)	± 3 hours	[161]
	STE $\gg$ Eu^{3+}	585+618+633 (red)	(identical)	± 100 mins	[161]
	Sm^{3+}	566+609+653 (red)	identical	> 1-7 hours	[158, 162–164]
	Tb^{3+}	435, 483+545 (blue/green)	483+545 (green)	± 3 hours	[165]
Mg_2SnO_4	defects	490-495 (green)	identical	± 5 hours	[166–168]
	Mn^{2+}	500 (green)	identical	> 5 hours	[169]
Sr_2SnO_4	Sb^{3+}	550 (yellowish white)	identical	> 2 mins	[170]
	Sm^{3+}	582+624+672 (red)	identical	> 1 hour	[158, 171–173]
	Tb^{3+}	542 (green)	(identical)	± 8 mins	[174]
$CaSnO_3$	Pr^{3+}	488+541+620+653 (white)	identical	> 3 hours	[175]
	Sm^{3+}	566+601+649+716 (red)	(identical)	?	[176]
	Tb^{3+}	491+545+588+622 (green)	identical	± 4 hours	[175, 177, 178]
$Sr_3Sn_2O_7$	Sm^{3+}	580+621+665+735 (red)	identical	> 1 hour	[179]

$Ca_9Gd(PO_4)_7$	Mn^{2+}	602+628, 660 (red)	only 660 (red)	(> 20 mins)	[180]
$Ca_9Lu(PO_4)_7$	Mn^{2+}	660 (red)	identical	(> 20 mins)	[180]
$Ca_9Tb(PO_4)_7$	Tb^{3+}	490+545 (green)	(identical)	(> 20 mins)	[180]
$Ca_3(PO_4)_2$	Mn^{2+}	645-660 (red)	identical	± 1 hour	[181, 182]
$SrMg_2(PO_4)_2$	Eu^{2+}	400 (blue)	identical	> 2 hours	[183]
	Eu^{3+}, Zr^{4+}	500, 588 (white)	(identical)	± 1.5 hours	[184]
$SrZn_2(PO_4)_2$	$Eu^{2+} > Mn^{2+}$	421, 547 (white)	(identical)	± 1 min	[185]
	Mn^{2+}	547 (green)	(identical)	± 1 min	[185]
$Zn_3(PO_4)_2$	Hf^{4+}	470 (blue)	identical	> 40 mins	[186]
	Mn^{2+}	616 (red)	identical	> 2 hours	[187–190]
	Mn^{2+}, Zr^{4-}	475, 616 (blue/red)	mainly 616	± 3 hours	[191]
YPO_4	Pr^{3+}	600+620 (orange/red)	(identical)	> 30 mins	[192]
$Ca_2P_2O_7$	Eu^{2+}	415 (blue)	identical	> 6 hours	[193]
$Sr_2P_2O_7$	Eu^{2+}	420 (blue)	identical	> 8 hours	[194]
$Ca_{0.8}Mg_{0.2}TiO3$	Pr^{3+}	613 (red)	(identical)	?	[195]
$CaTiO_3$	Pr^{3+}	612 (red)	identical	> 2 hours	[196–200]
$(CaZn)TiO_3$	Pr^{3+}	612 (red)	(identical)	± 20 mins	[201–203]
$Ca_2Zn_4Ti_{16}O_{38}$	Pr^{3+}	614+644 (red)	mainly 614	?	[204, 205]
$La_2Ti_2O_7$	Pr^{3+}	611 (red)	identical	> 1 hour	[206]
$CaAl_2B_2O$	Eu^{2+}	465 (blue)	identical	> 1 hour	[207]
$Gd_3Ga_5O_{12}$	Ce^{3+}	697+716 (red)	(identical)	?	[208, 209]
$MgGa_2O_4$	Mn^{2+}	506 (green)	(identical)	?	[210]
$LiGa_5O_8$	Cr^{3+}	716 (near-IR)	identical	> 1000 hours	[20]
$ZnGa_2O_4$	defects	410+540 (white)	identical	± 40 mins	[211]
	Cr^{3+}	650-750 (red)	identical	± 1 hour	[21, 212]
	Mn^{2+}	504 (green)	(identical)	> 15 mins	[213]
$(ZnMg)Ga_2O_4$	Mn^{2+}	505 (green)	(identical)	> 15 mins	[213]
$Cd_2Ge_7O_{16}$	Mn^{2+}	585 (orange)	identical	> 3 hours	[214]
	Pb^{2+}	352+497 (blue)	only 497	± 10 mins	[215]
$MgGeO_3$	Mn^{2+}	650-670 (red)	identical	± 30 mins	[216, 217]
Zn_2GeO_4	Mn^{2+}	528 (green)	(identical)	> 2 hours	[218]

$CaZnGe_2O_6$	Dy^{3+}	(white)	(identical)	> 3 hours	[219]
	Mn^{2+}	648 (red)	identical	> 3 hours	[220]
	Tb^{3+}	488+552+583+622 (green)	identical	± 4 hours	[221, 222]
$Cd_3Al_2Ge_3O_{12}$	defects > Dy^{3+}	437, 485+580 (?)	(identical)	± 1 hour	[223]
$La_3Ga_5GeO_{14}$	Cr^{3+}	785, 960-1030 (near-IR)	only 960-1030	> 1-8 hours	[224, 225]
$Zn_3Ga_2Ge_2O_{10}$	Cr^{3+}	696+713 (near-IR)	identical	> 360 hours	[19, 21]
$CaMoO_4$	Eu^{3+}	616 (red)	identical	> 5 mins	[226]
$NaNbO_3$	Pr^{3+}	620 (red)	identical	?	[227]
$YTaO_4$	Tb^{3+}	492+543+590+624 (green)	(identical)	± 2 hours	[228]
$CaWO_4$	defects > Pr^{3+}	415, 490+650 (blue/white)	identical	> 10 mins	[229]
	Eu^{3+}	592+616 (red)	identical	± 40 mins	[230–232]
	$Sm^{3+} \gg Eu^{3+}$	592+616 (red)	(identical)	> 35 mins	[233]
	Tb^{3+}	490+546 (green)	identical	(> 10 mins)	[234]
$BaZrO_3$	defects (F_A)	408 (blue)	identical	± 30 mins	[235]
	Eu^{3+}	574+596+614 (red)	(identical)	(± 10 mins)	[236]
	$Ti \gg Eu^{3+}$	574+596+614 (red)	(identical)	(± 10 mins)	[236]

Table 2.4: Other known persistent luminescent compounds

Host material	Activators	Emission maximum (nm)	Afterglow emission	Afterglow duration	refs.
BaS	Cu^{+}	610 (orange)	(identical)	> 30 mins	[2]
CaS	Bi^{3+}	448 (blue)	(identical)	(± 20 mins)	[11, 237–239]
	Ce^{3+}	508+568 (green)	(identical)	± 5 mins	[240]
	Eu^{2+}	650 (red)	identical	> 1 hour	[10–12]
	Sm^{3+}	569 (green)	?	(± 3 hours)	[241]
(Ca,Sr)S	Bi^{3+}	453 (blue)	(identical)	(> 15 mins)	[242]
SrS	defects	517 (green)	(identical)	(± 20 mins)	[243]
ZnS	Cu^{+}	540 (green)	(identical)	(> 3 hours)	[4, 92, 244, 245]
Gd_2O_2S	Ti/defects	590 (orange)	identical	± 2 hours	[246, 247]
	Ti > Er^{3+}	555+675 (green)	555+675, 590	> 1 hour	[247, 248]
	Ti ≫ Eu^{3+}	504+536+620 (red)	identical	(> 5 mins)	[247, 249, 250]
	Ti > Sm^{3+}	607 (red)	590, 607	?	[247]
	Ti > Tm^{3+}	513+800 (?)	590, 800	?	[247]
La_2O_2S	Sm^{3+}	605+645+656 (red)	(identical)	(> 1 min)	[251]
Y_2O_2S	Ti/defects	540-594 (orange)	identical	> 5 hours	[252–256]
	Eu^{3+}	590+614+627+710 (red)	identical	± 3 hours	[257–260]
	Sm^{3+}	570+606+659 (red)	(identical)	> 1 hour	[261–263]
	Tb^{3+}	417+546 (green)	(identical)	> 20 mins	[264]
	Ti > Eu^{3+}	616+625 (red)	565, 616+625	± 10 mins - 5 h	[265, 266]
	Tm^{3+}	495+545+588 (orange)	identical	± 1 hour	[267]
$CaGa_2S_4$	Eu^{2+}	555 (yellow)	identical	> 30 mins	[268–270]
Ca_2SiS_4	Eu^{2+}	660 (red)	identical	> 30 mins	[271]
BN	C, O	520 (green)	identical	> 2 hours	[23, 24]
$Ba_5(PO_4)_3Cl$	Ce^{3+} ≫ Eu^{2+}	350, 435 (blue)	only 435	(> 5 mins)	[272]
KY_3F_{10}	Sm^{3+}	558+597+651 (red)	(identical)	(> 2 mins)	[273]
$Ca_2Si_5N_8$	Eu^{2+}	610 (orange)	620	> 1 hour	[13, 14]
$ZnSiN_2$	Mn^{2+}	620 (red)	(identical)	± mins	[274]

Table 2.5: Known persistent luminescent glasses

Host material	Activators	Emission maximum (nm)	Afterglow emission	Afterglow duration	refs.
$Ca_4Al_6Si_3O_{19}$	Ce^{3+}	? (blue)	(identical)	> 1 hour	[275]
	Pr^{3+}	? (red)	(identical)	> 1 hour	[275]
	Tb^{3+}	350-600 (green)	identical	> 1 hour	[275]
$Ca_{59}Al_{54}Si_7Mg_7O_{161}$	Mn^{2+}	540 (yellow)	(identical)	> 1 hour	[276]
	Pr^{3+}	493+610 (red)	(identical)	> 1 hour	[276]
	Tb^{3+}	543 (green)	(identical)	> 2 hours	[276–278]
GeO_2	defects	465 (blue)	identical	(± 20 mins)	[279, 280]
SiO_2	defects	290+390 (blue)	identical	± 1 hour	[281]
$Na_2AlB_{15}O_{25}$	Mn^{2+}	590 (reddish)	identical	± 5 mins	[282]
$Na_4CaGa_8Si_3O_{21}$	Tb^{3+}	542 (green)	identical	± 1 hour	[283]
$Na_4CaSi_7O_{17}$	Cu^{+}/Cu^{2+}	510 (blue/green)	identical	> 30 mins	[284]
SrB_2O_4	Eu^{2+}	430 (blue)	identical	?	[285]
$Sr_7B_{26}O_{46}$	Eu^{2+}, Ce^{3+}	350, 430 (blue)	mainly 430	(> 2 mins)	[285]
$ZnGe_3O_7$	Mn^{2+}	534 (green)	identical	> 1 hour	[286]
Zn_2GeO_4	Mn^{2+}	540 (green)	identical	(> 10 s)	[287]
$Zn_3B_2SiO_8$	Pr^{3+}	495+603 (reddish)	identical	(> 30 mins)	[288]
	Tb^{3+}	542 (green)	identical	± 1 hour	[289, 290]
$Zn_{11}B_8Si_5O_{33}$	Mn^{2+}	525-606 (green/yellow)	identical	± 12 hours	[291]
$Zn_{11}B_{10}Si_4O_{34}$	Mn^{2+}	590 (red)	identical	(± 20 mins)	[292]
	Mn^{2+}, Sm^{3+}	600 (red)	identical	± 10 hours	[293, 294]
	Mn^{2+}, Yb^{3+}	605, 980 (red/IR)	identical	(± 10 mins)	[295]
$Zn_{60}B_{40}Si_{17}Ge_3Al_{14}O_{160}$	defects	410 (blue)	identical	± 2 hours	[296]

2.2 General remarks

It is not easy to draw general conclusions from the above tables. If we look at the activators, two of them perform exceptionally well: Eu^{2+} and Cr^{3+}. While Eu^{2+} is the best-known and most commonly employed activator (figure 2.1), Cr^{3+} is much less commonly used. However, it shows some excellent afterglow properties as a red/near-IR luminescent center. This might be especially useful for *in vivo* medical imaging applications. Unfortunately, even though the excitation spectrum of Cr^{3+} for steady-state luminescence extends to about 650 nm, it is inefficient to fill the traps, necessary to obtain afterglow, using visible light [19] (figure 2.3).

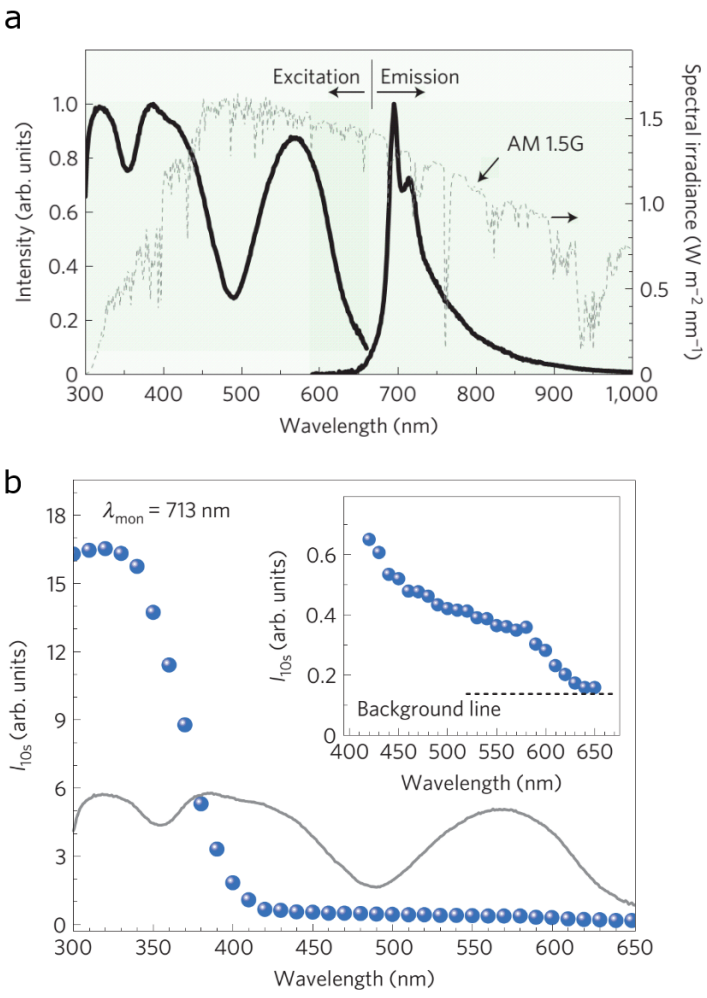

Figure 2.3: (a) Excitation and emission spectrum of $Zn_3Ga_2Ge_2O_{10}$:0.5%Cr^{3+}. (b) Effectiveness of excitation wavelength (energy) for persistent luminescence of $Zn_3Ga_2Ge_2O_{10}$:0.5%Cr^{3+}; afterglow intensity after 10s monitored as a function of the excitation wavelength (reprinted from [19], with permission).

2.2.1 Excitation difficulties

From figure 2.3, it is immediately clear that the steady-state excitation spectrum and afterglow excitation spectrum are not always the same. In many persistent luminescent materials, it is much easier to fill traps using higher energy photons (i.e. using shorter excitation wavelengths) [19, 297]. This implies that direct bandgap excitation is much more efficient to fill the traps than excitation of the luminescent centers. Even more problematic, the latter type of excitation might require a certain thermal activation barrier to be surpassed before traps can be filled [297], making the use of visible light even less favorable.

This effect appears to be even more profound in persistent phosphors which are not based on Eu^{2+}. Here, in general, only UV light is able to effectively fill the traps in the material. This implies that the role of the host compound is much larger than in Eu^{2+}-based materials. While it has been shown that in Eu^{2+}-based persistent phosphors the activator is a main source of trapped electrons [298], in non-Eu^{2+}-based compounds the trapped charge carriers are created mainly after band gap excitation. The luminescent center is subsequently excited by energy transferred from the traps when the trapped electron and hole recombine. The same phenomenon is illustrated by the fact that the afterglow duration is influenced much more by the host compound than by the actual luminescent center. Indeed, by looking at the tables presented in section 2.1, it is not uncommon to see certain host compounds with very similar afterglow durations irrespective of the activator being e.g. Pr^{3+}, Sm^{3+} or Tb^{3+}.

The fact that UV excitation is required for trap filling is especially unfortunate for persistent phosphors based on Dy^{3+}, which could be an excellent activator for white persistent luminescence, e.g. in paints, signage, and displays. However, since indoor lighting contains little to no UV (especially with the advent of LED lighting [299]), these compounds are not suited for practical indoor applications.

2.2.2 Afterglow duration

In the tables in section 2.1, the afterglow durations are taken directly from the text of the mentioned references. This makes it rather difficult to compare the various compounds with each other, since no single definition of 'afterglow duration' exists. This gives authors quite some liberty in describing the observed afterglow (see also section 1.2.2).

The afterglow duration also strongly depends on the excitation conditions, which are not always mentioned. According to DIN 67510-1, the sample should be excited for 5 minutes by 1000 lx light of an unfiltered Xe arc lamp. However, the emission spectrum of a Xe lamp is very broad and contains UV, visible as well as infrared light. This makes it hard to draw conclusions on the excitability, based on such a measurement. It does not give a good prediction of how the persistent luminescent material will behave when excited by artificial light or sunlight. It might be more interesting to excite with monochromatic light at different wavelengths and compare the afterglow in each situation. For persistent phosphors which can only be charged by UV-light, 254 nm is a common choice as the excitation wavelength.

2.2.3 Energy transfer

In several persistent luminescent compounds, energy transfer has been reported. Two types of energy transfer can be distinguished in this case. The first type is the transfer of excitation energy between a sensitizer and an activator. However, we are more interested in the second type, where energy is transferred during the afterglow phase, after the end of the excitation. When the first activating ion recombines, instead of emitting a photon, it can transfer this recombination energy to a second activating ion. This makes it possible to see or extend the afterglow emission from activators which usually have little to no persistent luminescent properties. If the energy transfer is very efficient, only emission from the second activator, receiving the recombination energy, can be observed. In the other case, luminescence from both kinds of activators can be seen simultaneously in the afterglow spectrum.

It is not always immediately clear if energy transfer is present or not. The afterglow spectrum can consist of the emission of two different kinds of activators even when no energy is transferred between them. It is therefore necessary to carefully inspect the decay behavior of both kinds of activators. If the decay rates of both are the same, this indicates that one of them is transferring its recombination energy to the other. If no energy transfer is present, it is likely that both kinds of activators will have a (slightly) different decay behavior, and the shape of the afterglow spectrum might change over time.

2.3 Some important examples

To conclude this chapter, we will highlight some of the most important persistent luminescent compounds, based on the number of publications, their exceptional properties, and their historical and future importance. For clarity, they are grouped by emission color. Only a short summary of their luminescent properties is provided. Further details can be found in the appropriate references.

2.3.1 Blue persistent phosphors

CaS:Bi^{3+}

$CaS:Bi^{3+}$ is one of the oldest known persistent phosphors, described already early in the 20th century by Lenard *et al.* [300]. It has blue, rather narrow band emission centered at 448 nm (figure 2.4) due to the $^3P_1 \rightarrow {}^1S_0$ transition of Bi^{3+} [11]. The afterglow lasts about 20 minutes, and is due to V^{2+}-defects created as a result of charge compensation upon incorporation of Bi^{3+} on Ca^{2+} sites. By addition of Na^+ ions, Jia *et al.* were able to reduce the number of vacancies, which considerably shortened the afterglow [11].

$CaAl_2O_4$:Eu^{2+}

$CaAl_2O_4:Eu^{2+}$ is closely related to the well-known $SrAl_2O_4:Eu^{2+}$, and has a long-lasting afterglow in the violet-blue region of the visible spectrum, centered around 440 nm. Its luminescent properties were first described by Blasse and Bril [302] and Palilla *et al.* [6] in 1968, but only in 1996 Matsuzawa *et al.* mentioned its persistent luminescence

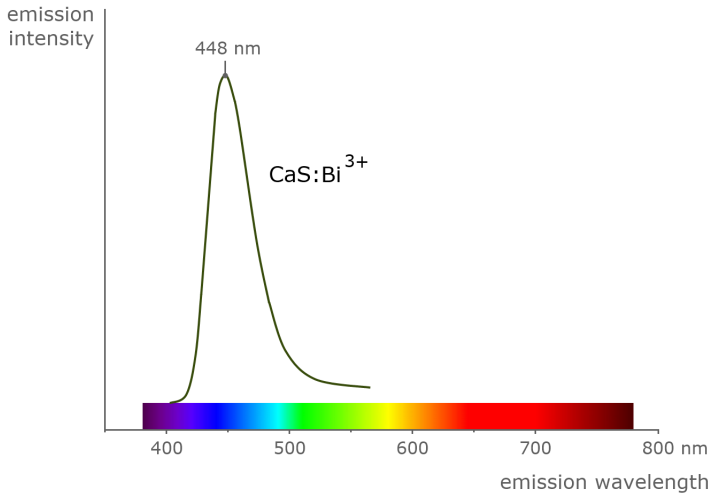

Figure 2.4: Emission spectrum of CaS:Bi^{3+} excited at 300 nm [301].

[3]. After co-doping with Nd^{3+} and e-beam annealing, the afterglow can last up to 11 hours before the photopic intensity drops below the 0.32 mcd/m^2 threshold [303], but remains visible with the unaided dark-adapted eye for at least 72 hours [304].

The presence of only a single europium site simplifies the analysis of the luminescence data (as compared to e.g. $SrAl_2O_4$:Eu^{2+} which has two possible europium sites [305]). For this reason, $CaAl_2O_4$:Eu^{2+} is often chosen as a standard material for persistent luminescence investigations, and it will play an important role in chapter 5.

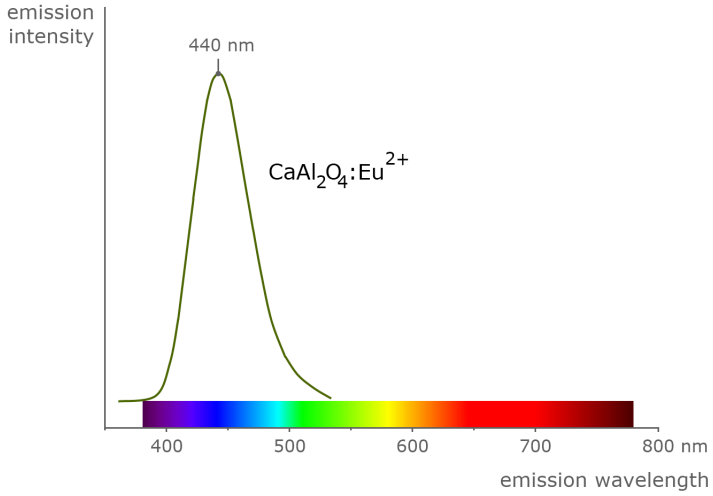

Figure 2.5: Emission spectrum of $CaAl_2O_4$:Eu^{2+} excited at 350 nm [104].

$Sr_2MgSi_2O_7$:Eu^{2+}

The longest afterglow in silicate-based persistent phosphors is achieved by codoping $Sr_2MgSi_2O_7$:Eu^{2+} with Dy^{3+}, with a blue emission around 470-480 nm. The brightness and duration of the afterglow are comparable to $SrAl_2O_4$:Eu^{2+},Dy^{3+}. It was first re-

ported by Lin *et al.* in 2001 [16], and because of the presence of only a single Sr site, it is often used as an example material in DFT calculations on persistent luminescent compounds (e.g. [306]).

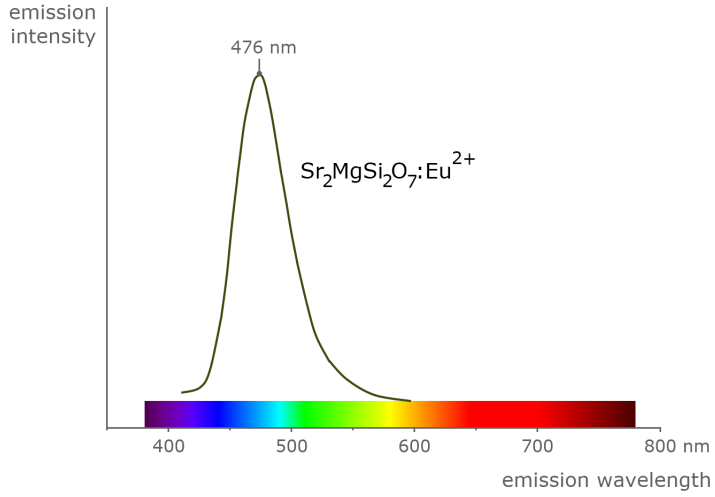

Figure 2.6: Emission spectrum of $Sr_2MgSi_2O_7:Eu^{2+}$ [16].

$Sr_4Al_{14}O_{25}:Eu^{2+}$

$Sr_4Al_{14}O_{25}:Eu^{2+}$ is very closely related to $SrAl_2O_4:Eu^{2+}$, and sometimes even appears as an unwanted phase during its preparation. The emission is greenish blue, centered around 490 nm, with - upon codoping with Dy^{3+}- an afterglow duration and brightness sometimes claimed to be better than that of $SrAl_2O_4:Eu^{2+},^{3+}$. Therefore, it is possibly the most effective persistent phosphor emitting in the visible region known today.

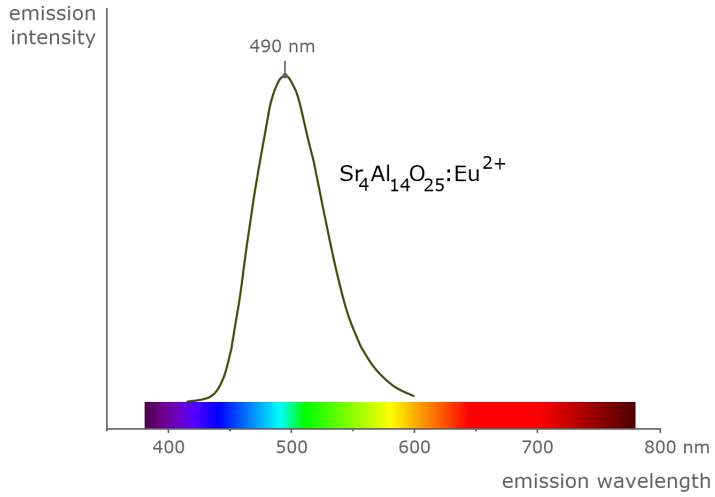

Figure 2.7: Emission spectrum of $Sr_4Al_{14}O_{25}:Eu^{2+}$ [124].

2.3.2 Green persistent phosphors

ZnS:Cu^{+}

Until 1996, ZnS:Cu^{+} (often co-doped with cobalt) was the most widely (and probably only) used material for persistent luminescent applications. Its broad greenish emission is centered around 540 nm. Since the afterglow is relatively weak, it was common to add radioactive ions to the compound, in order to sustain the luminescence. As of today, it is rendered obsolete by the Eu^{2+}-based aluminate and silicate phosphors.

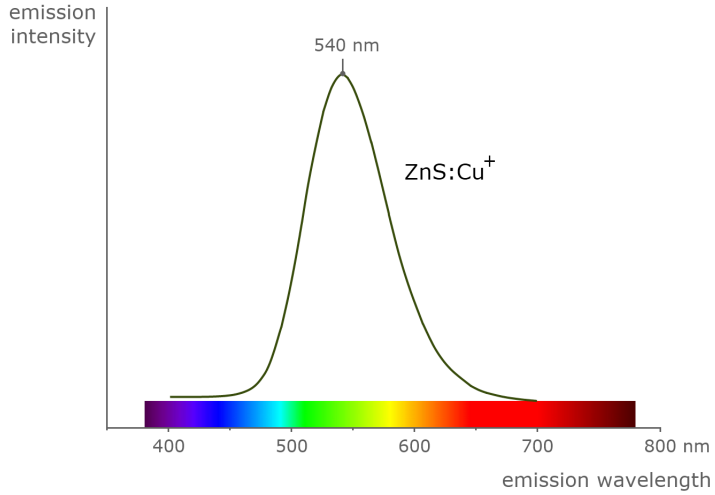

Figure 2.8: Emission spectrum of ZnS:Cu^{+}.

$SrAl_2O_4$:Eu^{2+}

The bright green luminescence of the monoclinic $SrAl_2O_4$:Eu^{2+} was discovered in 1966 and described by Blasse and Bril two years later [307], together with $CaAl_2O_4$:Eu^{2+} and $BaAl_2O_4$:Eu^{2+}. Palilla *et al.* [6] and Abbruscato [7] mentioned the presence of an afterglow, but only in 1996, Matsuzawa *et al.* reported the spectacular enhancement of the afterglow after codoping with Dy^{3+} [3]. This effectively increased the afterglow brightness by more than one order of magnitude. Today, $SrAl_2O_4$:Eu it is the most widely studied persistent luminescent compound, with over 150 entries in the Web of Knowledge.

2.3.3 Red and near-IR persistent phosphors

Y_2O_2S:Eu^{3+},Ti^{4+},Mg^{2+}

The afterglow of Y_2O_2S:Eu^{3+},Ti^{4+},Mg^{2+} lasts for about 3 hours, making it the most efficient red-emitting phosphor known today. The emission spectrum is the typical line emission of Eu^{3+}, with the most intense peak located at 627 nm. While it is known that the addition of Ti^{4+} strongly enhances the afterglow, the exact mechanism behind this enhancement is unknown and remains the subject of discussion.

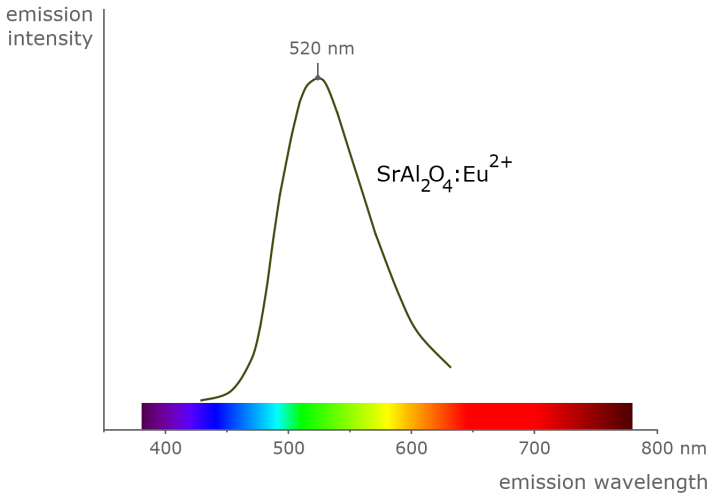

Figure 2.9: Emission spectrum of $SrAl_2O_4:Eu^{2+}$ [3].

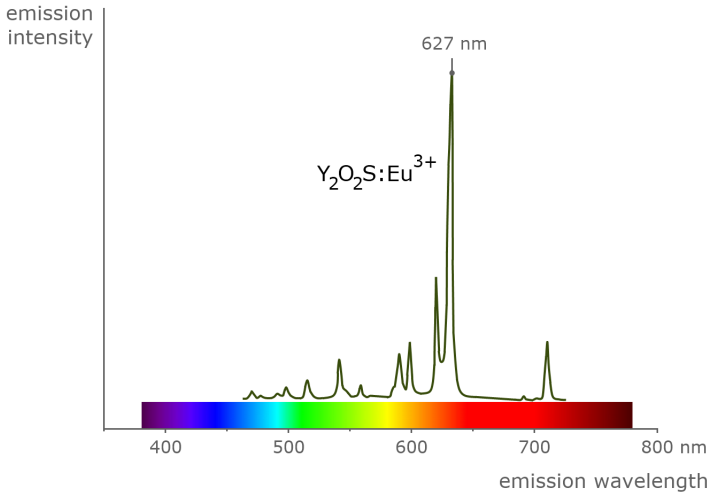

Figure 2.10: Emission spectrum of $Y_2O_2S:Eu^{3+}$ [257].

$Zn_3Ga_2Ge_2O_{10}:Cr^{3+}$

By doping $Zn_3Ga_2Ge_2O_{10}$ with Cr^{3+}, Pan *et al.* obtained a persistent phosphor with a remarkably long afterglow duration [19]. The near-IR emission of Cr^{3+}, located around 700 nm with a tail towards longer wavelengths, lasts up to two weeks. This might prove very promising for *in vivo* bio-imaging applications, where these near-IR wavelengths are strongly desired (see also section 6.3). However, it should be noted that there exists no definition to exactly determine the afterglow duration at these long wavelengths, almost invisible to the human eye. This makes it difficult to compare the afterglow duration to other known persistent phosphors.

Recently, Allix *et al.* found that $Zn_3Ga_2Ge_2O_{10}$ is not the correct formula for the compound described by Pan *et al.* [21]. In stead, it is a mixture of $Zn_{1+x}Ga_{2-2x}Ge_xO_4$ (where $x = 0.5$) with excess of GeO_2. They found even better afterglow properties for

the compound with $x = 0.1$.

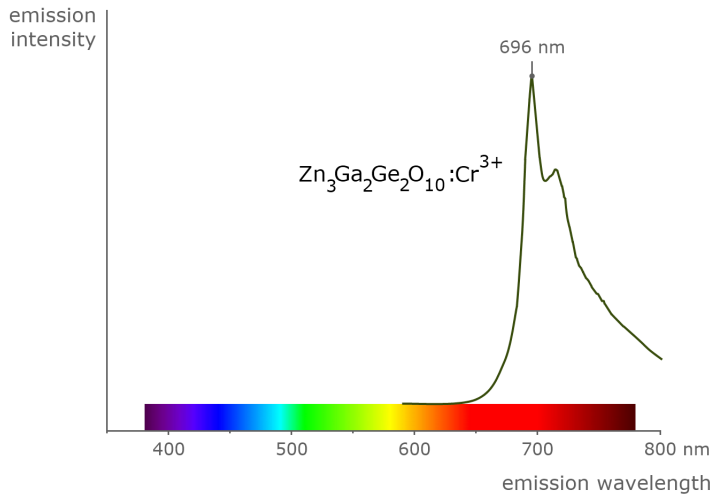

Figure 2.11: Emission spectrum of $Zn_3Ga_2Ge_2O_{10}:Cr^{3+}$ [19].

References

[1] Harvey, E. N. *A history of persistent luminescence from the earliest times until 1900*. American Philosophical Society, Philadelphia, PA, USA, (1957).

[2] Lastusaari, M., Laamanen, T., Malkamäki, M., Eskola, K. O., Kotlov, A., Carlson, S., Welter, E., Brito, H. F., Bettinelli, M., Jungner, H., and Hölsä, J. *European Journal of Mineralogy* **24**, 885–890 (2012).

[3] Matsuzawa, T., Aoki, Y., Takeuchi, N., and Murayama, Y. *Journal of the Electrochemical Society* **143**, 2670–2673 (1996).

[4] Yen, W. M., Shionoya, S., and Yamamoto, H. *Phosphor Handbook*, chapter 12: Other phosphors. CRC Press, Boca Raton, FL, USA, 2nd edition (2007).

[5] Wang, D., Yin, Q., Li, Y., and Wang, M. *Journal of Luminescence* **97**, 1–6 (2002).

[6] Palilla, F. C., Levine, A. K., and Tomkus, M. R. *Journal of The Electrochemical Society* **115**, 642–644 (1968).

[7] Abbruscato, V. *Journal of the Electrochemical Society* **118**, 930–933 (1971).

[8] Takasaki, H., Tanabe, S., and Hanada, T. *Journal of the Ceramic Society of Japan* **104**, 322–326 (1996).

[9] Dorenbos, P. *Journal of Luminescence* **104**, 239–260 (2003).

[10] Jia, D., Jia, W., Evans, D. R., Dennis, W. M., Liu, H., Zhu, J., and Yen, W. M. *Journal of Applied Physics* **88**, 3402–3407 (2000).

[11] Jia, D., Zhu, J., and Wu, B. *Journal of the Electrochemical Society* **147**, 386–389 (2000).

[12] Jia, D. *Journal of the Electrochemical Society* **153**, H198–H201 (2006).

[13] Miyamoto, Y., Kato, H., Honna, Y., Yamamoto, H., and Ohmi, K. *Journal of the Electrochemical Society* **156**, J235–J241 (2009).

[14] Van den Eeckhout, K., Smet, P. F., and Poelman, D. *Journal of Luminescence* **129**, 1140–1143 (2009).
[15] Yen, W. M., Shionoya, S., and Yamamoto, H. *Phosphor Handbook*, chapter 3: Principal phosphor materials and their optical properties. CRC Press, Boca Raton, FL, USA, 2nd edition (2007).
[16] Lin, Y., Tang, Z., Zhang, Z., Wang, X., and Zhang, J. *Journal of Materials Science Letters* **20**, 1505–1506 (2001).
[17] Liu, Y., Kuang, J., Lei, B., and Shi, C. *Journal of Materials Chemistry* **15**, 4025–4031 (2005).
[18] Kuang, J. Y. and Liu, Y. L. *Chinese Physics Letters* **23**, 204–206 (2006).
[19] Pan, Z., Lu, Y.-Y., and Liu, F. *Nature Materials* **11**, 58–63 (2012).
[20] Liu, F., Yan, W., Chuang, Y.-J., Zhen, Z., Xie, J., and Pan, Z. *Scientific Reports* **3**, 1554 (2013).
[21] Allix, M., Chenu, S., Véron, E., Poumeyrol, T., Kouadri-Boudjelthia, E. A., Alahraché, S., Porcher, F., Massiot, D., and Fayon, F. *Chemistry of Materials* **25**, 1600–1606 (2013).
[22] Poelman, D., Avci, N., and Smet, P. F. *Optics Express* **17**, 358–364 (2009).
[23] Liu, X., Qiao, Y., Dong, G., Ye, S., Zhu, B., Zhuang, Y., and Qiu, J. *Journal of the Electrochemical Society* **156**, P81–P84 (2009).
[24] Wang, W.-N., Ogi, T., Kaihatsu, Y., Iskandar, F., and Okuyama, K. *Journal of Materials Chemistry* **21**, 5183–5189 (2011).
[25] Kodama, N., Takahashi, T., Yamaga, M., Tanii, Y., Qiu, J., and Hirao, K. *Applied Physics Letters* **75**, 1715–1717 (1999).
[26] Kodama, N., Tanii, Y., and Yamaga, M. *Journal of Luminescence* **87-89**, 1076–1078 (2000).
[27] Yamaga, M., Tanii, Y., Kodama, N., Takahashi, T., and Honda, M. *Physical Review B* **65**, 235108 (2002).
[28] Wu, H., Hu, Y., Ju, G., Chen, L., Wang, X., and Yang, Z. *Journal of Luminescence* **131**, 2441–2445 (2011).
[29] Wang, X.-J., Jia, D., and Yen, W. M. *Journal of Luminescence* **102-103**, 34–37 (2003).
[30] Ito, Y., Komeno, A., Uematsu, K., Toda, K., and Sato, M. *Journal of Alloys and Compounds* **408-412**, 907–910 (2006).
[31] Gutiérrez-Martín, F., Fernández-Martinez, F., Díaz, P., Colón, C., and Alonso-Medina, A. *Journal of Alloys and Compounds* **501**, 193–197 (2010).
[32] Gong, Y., Wang, Y., Li, Y., and Xu, X. *Journal of the Electrochemical Society* **157**, J208–J211 (2010).
[33] Pan, W., Ning, G., Lin, Y., and Yang, X. *Journal of Rare Earths* **26**, 207–210 (2008).
[34] Ding, Y., Zhang, Y., Wang, Z., Li, W., Mao, D., Han, H., and Chang, C. *Journal of Luminescence* **129**, 294–299 (2009).
[35] Kuang, J., Liu, Y., Zhang, J., Huang, L., Rong, J., and Yuan, D. *Solid State Communications* **136**, 6–10 (2005).
[36] Kuang, J. Y., Liu, Y. L., and Zhang, J. X. *Journal of Materials Science* **41**, 5500–5503 (2006).
[37] Wang, Y., Wang, Z., Zhang, P., Hong, Z., Fan, X., and Qian, G. *Materials Letters*

58, 3308–3311 (2004).

[38] Clabau, F., Garcia, A., Bonville, P., Gonbeau, D., Le Mercier, T., Deniard, P., and Jobic, S. *Journal of Solid State Chemistry* **181**, 1456–1461 (2008).

[39] Zhang, J., Chen, B., Sun, J., Li, X., Cheng, L., and Zhong, H. *Journal of Physics D: Applied Physics* **45**, 325105 (2012).

[40] Chen, B. S., Zheng, Z. S., Lin, Y. M., Chen, G. L., Zhou, L., Guo, H. X., and Huang, L. F. *Preparation of a novel red long lasting phosphorescent material $CaAl_2Si_2O_8$:Mn^{2+} and investigation of its luminescent properties*, volume 71-78 of *Applied Mechanics and Materials*, 3151–3155. Trans Tech Publications Ltd, Stafa-Zurich (2011).

[41] Chen, Y., Cheng, X., Liu, M., Qi, Z., and Shi, C. *Journal of Luminescence* **129**, 531–535 (2009).

[42] Jiang, L., Chang, C., and Mao, D. *Journal of Alloys and Compounds* **360**, 193–197 (2003).

[43] Jiang, L., Chang, C., Mao, D., and Feng, C. *Journal of Alloys and Compounds* **377**, 211–215 (2004).

[44] Lecointre, A., Bessière, A., Viana, B., and Gourier, D. *Radiation Measurements* **45**, 497–499 (2010).

[45] Maldiney, T., Lecointre, A., Viana, B., Bessière, A., Bessodes, M., Gourier, D., Richard, C., and Scherman, D. *Journal of the American Chemical Society* **133**, 11810–11815 (2011).

[46] Bessière, A., Lecointre, A., Priolkar, K. R., and Gourier, D. *Journal of Materials Chemistry* **22**, 19039–19046 (2012).

[47] Maldiney, T., Lecointre, A., Viana, B., Bessiere, A., Gourier, D., Bessodes, M., Richard, C., and Scherman, D. *Trap depth optimization to improve optical properties of diopside-based nanophosphors for medical imaging*, volume 8263 of *Proceedings of SPIE*, 826318. Spie-Int Soc Optical Engineering, Bellingham (2012).

[48] Lecointre, A., Bessière, A., Priolkar, K. R., Gourier, D., Wallez, G., and Viana, B. *Materials Research Bulletin* **48**, 1898–1905 (2013).

[49] He, Z., Wang, X.-j., and Yen, W. M. *Journal of Luminescence* **122-123**, 381–384 (2007).

[50] Gong, Y., Xu, X. H., Zeng, W., Wu, C. J., and Wang, Y. H. *Ce^{3+}, Mn^{2+} co-doped red-light long-lasting phosphor: $BaMg_2Si_2O_7$ through energy transfer*, volume 29 of *Physics Procedia*, 86–90. Elsevier Science Bv, Amsterdam (2012).

[51] Abe, S., Uematsu, K., Toda, K., and Sato, M. *Journal of Alloys and Compounds* **408**, 911–914 (2006).

[52] Ye, S., Zhang, J., Zhang, X., Lu, S., Ren, X., and Wang, X.-j. *Journal of Applied Physics* **101**, 063545–1 (2007).

[53] Aitasalo, T., Hietikko, A., Hreniak, D., Hölsä, J., Lastusaari, M., Niittykoski, J., and Stręk, W. *Journal of Alloys and Compounds* **451**, 229–231 (2008).

[54] Ye, S., Zhang, J., Zhang, X., and Wang, X. *Journal of Luminescence* **122-123**, 914–916 (2007).

[55] Aitasalo, T., Hölsä, J., Laamanen, T., Lastusaari, M., Lehto, L., Niittykoski, J., and Pellé, F. *Ceramics-Silikáty* **49**, 58–62 (2005).

[56] Aitasalo, T., Hreniak, D., Hölsä, J., Laamanen, T., Lastusaari, M., Niittykoski, J., Pellé, F., and Stręk, W. *Journal of Luminescence* **122-123**, 110–112 (2007).

[57] Lin, L., Zhao, Z., Zhang, W., Zheng, Z., and Yin, M. *Journal of Rare Earths* **27**, 749–752 (2009).

[58] Blasse, G., Wanmaker, W. L., ter Vrugt, J. W., and Bril, A. *Philips Research Reports* **23**, 189–200 (1968).

[59] Aitasalo, T., Hölsä, J., Kirm, M., Laamanen, T., Lastusaari, M., Niittykoski, J., Raud, J., and Valtonen, R. *Radiation Measurements* **42**, 644–647 (2007).

[60] Liu, B., Kong, L., and Shi, C. *Journal of Luminescence* **122Ű123**, 121–124 (2007).

[61] Lin, Y., Nan, C. W., Zhou, X., Wu, J., Wang, H., Chen, D., and Xu, S. *Materials Chemistry and Physics* **82**, 860–863 (2003).

[62] Liu, B., Shi, C., Yin, M., Dong, L., and Xiao, Z. *Journal of Alloys and Compounds* **387**, 65–69 (2005).

[63] Lin, Y., Tang, Z., Zhang, Z., and Nan, C. W. *Journal of Alloys and Compounds* **348**, 76–79 (2003).

[64] Lin, Y., Zhang, Z., Tang, Z., Wang, X., Zhang, J., and Zheng, Z. *Journal of the European Ceramic Society* **21**, 683–685 (2001).

[65] Sabbagh Alvani, A. A., Moztarzadeh, F., and Sarabi, A. A. *Journal of Luminescence* **114**, 131–136 (2005).

[66] Gong, Y., Wang, Y., Xu, X., Li, Y., Xin, S., and Shi, L. *Optical Materials* **33**, 1781–1785 (2011).

[67] Xu, X., Wang, Y., Zeng, W., Gong, Y., and Liu, B. *Journal of the American Ceramic Society* **94**, 3632–3635 (2011).

[68] Wei, R.-P., Ju, Z.-H., Ma, J.-X., Zhang, D., Zang, Z.-P., and Liu, W.-S. *Journal of Alloys and Compounds* **486**, L17–L20 (2009).

[69] le Masne de Chermont, Q., Chanéac, C., Seguin, J., Pellé, F., Maîtrejean, S., Jolivet, J.-P., Gourier, D., Bessodes, M., and Scherman, D. *Proceedings of the National Academy of Sciences* **104**, 9266–9271 (2007).

[70] Lecointre, A., Viana, B., LeMasne, Q., Bessière, A., Chanéac, C., and Gourier, D. *Journal of Luminescence* **129**, 1527–1530 (2009).

[71] Wang, X. J., He, Z., Jia, D., Strek, W., Pazik, R., Hreniak, D., and Yen, W. M. *Microelectronics Journal* **36**, 546–548 (2005).

[72] Lin, H., Xu, A. X., Chen, G. L., Zheng, Z. S., Lin, H., Chen, B. S., Huang, L. F., Guo, H. X., and Xu, Y. *Synthesis of a new red long persistent phosphor $Sr_2ZnSi_2O_7$: Eu^{3+}, Lu^{3+} via sol-gel method and investigation of its luminescence*, volume 393-395 of *Advanced Materials Research*, 362–365. Trans Tech Publications Ltd, Stafa-Zurich (2012).

[73] Lei, B. F., Liu, Y. L., Ye, Z. R., and Shi, C. S. *Chinese Chemical Letters* **15**, 335–338 (2004).

[74] Liu, Y. L., Lei, B., and Shi, C. H. *Chemistry of Materials* **17**, 2108–2113 (2005).

[75] Qu, X., Cao, L., Liu, W., Su, G., and Wang, P. *Journal of Alloys and Compounds* **487**, 387–390 (2009).

[76] Lei, B., Liu, Y., Ye, Z., and Shi, C. *Journal of Luminescence* **109**, 215–219 (2004).

[77] Kuang, J. Y., Liu, Y. L., and Zhang, J. X. *Journal of Materials Science* **41**, 5500–5503 (2006).

[78] Qu, X., Cao, L., Liu, W., Su, G., Xu, C., and Wang, P. *Journal of Alloys and Compounds* **494**, 196–198 (2010).
[79] Qu, X. F., Cao, L. X., Liu, W., and Su, G. *Journal of Alloys and Compounds* **533**, 83–87 (2012).
[80] Qu, X., Cao, L., Liu, W., and Su, G. *Ceramics International* **38**, 1765–1769 (2012).
[81] Kuang, J. and Liu, Y. *Journal of the Electrochemical Society* **153**, G245–G247 (2006).
[82] Kuang, J. and Liu, Y. *Chemical Physics Letters* **424**, 58–62 (2006).
[83] Lei, B., Liu, Y., Liu, J., Ye, Z., and Shi, C. *Journal of Solid State Chemistry* **177**, 1333–1337 (2004).
[84] Rodrigues, L. C. V., Brito, H. F., Hölsä, J., Stefani, R., Felinto, M. C. F. C., Lastusaari, M., Laamanen, T., and Nunes, L. A. O. *The Journal of Physical Chemistry C* **116**, 11232–11240 (2012).
[85] Dorenbos, P., Vaneijk, C. W. E., Bos, A. J. J., and Melcher, C. L. *Journal of Physics-Condensed Matter* **6**, 4167–4180 (1994).
[86] Yamaga, M., Ohsumi, Y., Nakayama, T., and Han, T. P. J. *Optical Materials Express* **2**, 413–419 (2012).
[87] Lin, L., Shi, C., Wang, Z., Zhang, W., and Yin, M. *Journal of Alloys and Compounds* **466**, 546–550 (2008).
[88] Lin, L., Yin, M., Shi, C., and Zhang, W. *Journal of Alloys and Compounds* **455**, 327–330 (2008).
[89] Kuang, J., Liu, Y., and Zhang, J. *Journal of Solid State Chemistry* **179**, 266–269 (2006).
[90] Kuang, J. and Liu, Y. *Chemistry Letters* **34**, 598–599 (2005).
[91] Lakshminarasimhan, N. and Varadaraju, U. V. *Materials Research Bulletin* **43**, 2946–2953 (2008).
[92] Garlick, G. F. J. and Gibson, A. F. *Proceedings of the Physical Society* **60**, 574–590 (1948).
[93] Avouris, P. and Morgan, T. N. *The Journal of Chemical Physics* **74**, 4347–4355 (1981).
[94] Takahashi, Y., Masai, H., Fujiwara, T., Kitamura, K., and Inoue, S. *Journal of the Ceramic Society of Japan* **116**, 357–360 (2008).
[95] Iwasaki, K., Takahashi, Y., Masai, H., and Fujiwara, T. *Optics Express* **17**, 18054–18062 (2009).
[96] Jia, D., Wang, X.-j., van der Kolk, E., and Yen, W. M. *Optics Communications* **204**, 247–251 (2002).
[97] Sakai, R., Katsumata, T., Komuro, S., and Morikawa, T. *Journal of Luminescence* **85**, 149–154 (1999).
[98] Lin, Y., Zhang, Z., Tang, Z., Zhang, J., Zheng, Z., and Lu, X. *Materials Chemistry and Physics* **70**, 156–159 (2001).
[99] Jia, D., Meltzer, R. S., Yen, W. M., Jia, W., and Wang, X. *Applied Physics Letters* **80**, 1535 (2002).
[100] Jia, D., Wang, X. J., Jia, W., and Yen, W. M. *Journal of Applied Physics* **93**, 148–152 (2003).
[101] Jia, D. and Yen, W. M. *Journal of the Electrochemical Society* **150**, H61–H65 (2003).

[102] Liu, B., Shi, C., and Qi, Z. *Applied Physics Letters* **86**, 191111 (2005).
[103] Katsumata, T., Nabae, T., Sasajima, K., and Matsuzawa, T. *Journal of Crystal Growth* **183**, 361–365 (1998).
[104] Hölsä, J., Jungner, H., Lastusaari, M., and Niittykoski, J. *Journal of Alloys and Compounds* **323-324**, 326–330 (2001).
[105] Lin, Y., Tang, Z., Zhang, Z., and Nan, C. *Journal of the European Ceramic Society* **23**, 175–178 (2003).
[106] Xu, X., Wang, Y., Li, Y., and Gong, Y. *Journal of Applied Physics* **105**, 083502–083506 (2009).
[107] Jia, D., Wang, X.-j., and Yen, W. M. *Chemical Physics Letters* **363**, 241–244 (2002).
[108] Jia, D. and Yen, W. M. *Journal of Luminescence* **101**, 115–121 (2003).
[109] Lorincz, A., Puma, M., James, F. J., and Crawford, J. H. J. *Journal of Applied Physics* **53**, 927–932 (1982).
[110] Nakagawa, H., Ebisu, K., Zhang, M., and Kitaura, M. *Journal of Luminescence* **102-103**, 590–596 (2003).
[111] Jia, D. *Journal of Luminescence* **117**, 170–178 (2006).
[112] Jia, D., Wang, X.-j., Jia, W., and Yen, W. M. *Journal of Luminescence* **122-123**, 311–314 (2007).
[113] Xu, X., Wang, Y., Yu, X., Li, Y., and Gong, Y. *Journal of the American Ceramic Society* **94**, 160–163 (2011).
[114] Katsumata, T., Nabae, T., Sasajima, K., Komuro, S., and Morikawa, T. *Journal of the Electrochemical Society* **144**, L243–L245 (1997).
[115] Yu, N., Liu, F., Li, X., and Pan, Z. *Applied Physics Letters* **95**, 231110 (2009).
[116] Teng, Y., Zhou, J., Ma, Z., Smedskjaer, M. M., and Qiu, J. *Journal of the Electrochemical Society* **158**, K17–K19 (2011).
[117] Katsumata, T., Sasajima, K., Nabae, T., Komuro, S., and Morikawa, T. *Journal of the American Ceramic Society* **81**, 413–416 (1998).
[118] Preethi, K. R. S., Lu, C. H., Thirumalai, J., Jagannathan, R., Natarajan, T. S., Nayak, N. U., Radhakrishna, I., Jayachandran, M., and Trivedi, D. C. *Journal of Physics D: Applied Physics* **37**, 2664–2669 (2004).
[119] Zhang, J., Zhang, Z., Wang, T., and Hao, W. *Materials Letters* **57**, 4315–4318 (2003).
[120] Zhang, P., Xu, M., Zheng, Z., Sun, B., and Zhang, Y. *Materials Science and Engineering B* **136**, 159–164 (2007).
[121] Chang, C., Li, W., Huang, X., Wang, Z., Chen, X., Qian, X., Guo, R., Ding, Y., and Mao, D. *Journal of Luminescence* **130**, 347–350 (2010).
[122] Sharma, S. K., Pitale, S. S., Manzar Malik, M., Dubey, R. N., and Qureshi, M. S. *Journal of Luminescence* **129**, 140–147 (2009).
[123] Lin, Y., Tang, Z., and Zhang, Z. *Materials Letters* **51**, 14–18 (2001).
[124] Lin, Y., Tang, Z., Zhang, Z., and Nan, C. W. *Applied Physics Letters* **81**, 996–998 (2002).
[125] Nakazawa, E., Murazaki, Y., and Saito, S. *Journal of Applied Physics* **100**, 113113 (2006).
[126] Zhong, R., Zhang, J., Zhang, X., Lu, S., and Wang, X.-j. *Applied Physics Letters* **88**, 201916 (2006).

[127] Zhong, R., Zhang, J., Zhang, X., Lu, S., and Wang, X.-j. *Journal of Luminescence* **119-120**, 327–331 (2006).
[128] Luitel, H. N., Watari, T., Torikai, T., and Yada, M. *Optical Materials* **31**, 1200–1204 (2009).
[129] Zhang, S., Pang, R., Li, C., and Su, Q. *Journal of Luminescence* **130**, 2223–2225 (2010).
[130] Jüstel, T., Bechtel, H., Mayr, W., and Wiechert, D. U. *Journal of Luminescence* **104**, 137–143 (2003).
[131] Wanjun, T., Donghua, C., and Ming, W. *Optics & Laser Technology* **41**, 81–84 (2009).
[132] Mu, Z. F., Wang, Y. H., Hu, Y. H., Wu, H. Y., Deng, L. Y., Xie, W., Fu, C. J., and Liao, C. X. *Acta Physica Sinica* **60**, 013201 (2011).
[133] Zhang, S., Li, C., Pang, R., Jiang, L., Shi, L., and Su, Q. *Journal of Rare Earths* **29**, 426–430 (2011).
[134] Mu, Z., Hu, Y., Wang, Y., Wu, H., Fu, C., and Kang, F. *Journal of Luminescence* **131**, 676–681 (2011).
[135] Zhang, S., Li, C., Pang, R., Jiang, L., Shi, L., and Su, Q. *Journal of Luminescence* **131**, 2730–2734 (2011).
[136] Fu, J. *Electrochemical and Solid-State Letters* **3**, 350–351 (2000).
[137] Fu, J. *Journal of the American Ceramic Society* **85**, 255–257 (2002).
[138] Kuang, J. Y., Liu, Y. L., Zhang, J. X., Yuan, D. S., Huang, L. H., and Rong, J. H. *Chinese Journal of Inorganic Chemistry* **21**, 1383–1385 (2005).
[139] Lu, Y.-Y., Liu, F., Gu, Z., and Pan, Z. *Journal of Luminescence* **131**, 2784–2787 (2011).
[140] Pejakovic, D. A. *Journal of Luminescence* **130**, 1048–1054 (2010).
[141] Wiatrowska, A., Zych, E., and Kepinski, L. *Radiation Measurements* **45**, 493–496 (2010).
[142] Zych, E. and Trojan-Piegza, J. *Journal of Luminescence* **122-123**, 335–338 (2007).
[143] Zych, E., Trojan-Piegza, J., Hreniak, D., and Strek, W. *Journal of Applied Physics* **94**, 1318 (2003).
[144] Trojan-Piegza, J., Niittykoski, J., Hölsä, J., and Zych, E. *Chemistry of Materials* **20**, 2252–2261 (2008).
[145] Trojan-Piegza, J., Zych, E., Holsa, J., and Niittykoski, J. *Journal of Physical Chemistry C* **113**, 20493–20498 (2009).
[146] Chen, S., Yang, Y., Zhou, G., Wu, Y., Liu, P., Zhang, F., Wang, S., Trojan-Piegza, J., and Zych, E. *Optical Materials* **35**, 240–243 (2012).
[147] Zhang, J., Ma, X., Qin, Q., Shi, L., Sun, J., Zhou, M., Liu, B., and Wang, Y. *Materials Chemistry and Physics* **136**, 320–324 (2012).
[148] Lin, Y., Nan, C.-W., Cai, N., Zhou, X., Wang, H., and Chen, D. *Journal of Alloys and Compounds* **361**, 92–95 (2003).
[149] Xie, W., Wang, Y. H., Hu, Y. H., Luo, L., Wu, H. Y., and Deng, L. Y. *Acta Physica Sinica* **59**, 3344–3349 (2010).
[150] Zhang, J., Zhang, Z., and Wang, T. *Chemistry of Materials* **16**, 768–770 (2004).
[151] Zhang, J., Pan, F., Hao, W., and Wang, T. *Materials Science and Engineering B* **129**, 93–95 (2006).

[152] Zhao, Z. and Wang, Y. *Journal of Luminescence* **132**, 2842–2846 (2012).
[153] Cong, Y., Li, B., Lei, B., and Li, W. *Journal of Luminescence* **126**, 822–826 (2007).
[154] Cong, Y., Li, B., Wang, X.-J., Lei, B., and Li, W. *Journal of the Electrochemical Society* **155**, K195–K198 (2008).
[155] Liu, Y.-h., Li, B., and Cong, Y. *Spectroscopy and Spectral Analysis* **30**, 887–891 (2010).
[156] Wang, Z., Zhang, J., Zheng, G., Liu, Y., and Zhao, Y. *Journal of Luminescence* **132**, 2817–2821 (2012).
[157] Carvalho, J. M., Rodrigues, L. C. V., Holsa, J., Lastusaari, M., Nunes, L. A. O., Felinto, M. C. F. C., Malta, O. L., and Brito, H. F. *Optical Materials Express* **2**, 331–340 (2012).
[158] Xu, X., Wang, Y., Zeng, W., and Gong, Y. *Journal of the Electrochemical Society* **158**, J305–J309 (2011).
[159] Zhang, J., Hu, R., Qin, Q., Wang, D., Liu, B., Wen, Y., Zhou, M., and Wang, Y. *Journal of Luminescence* **132**, 2590–2594 (2012).
[160] Lei, B. F., Man, S. Q., Liu, Y. L., and Yue, S. *Chinese Journal of Inorganic Chemistry* **26**, 1259–1263 (2010).
[161] Gao, X., Zhang, Z., Wang, C., Xu, J., Ju, Z., An, Y., and Liu, W. *Journal of the Electrochemical Society* **158**, J405–J408 (2011).
[162] Ju, Z. H., Wei, R. P., Zheng, J. R., Gao, X. P., Zhang, S. H., and Liu, W. S. *Applied Physics Letters* **98**, 121906 (2011).
[163] Ju, Z.-H., Zhang, S.-H., Gao, X.-P., Tang, X.-L., and Liu, W.-S. *Journal of Alloys and Compounds* **509**, 8082–8087 (2011).
[164] Lei, B., Zhang, H., Mai, W., Yue, S., Liu, Y., and Man, S.-q. *Solid State Sciences* **13**, 525–528 (2011).
[165] Jin, Y., Hu, Y., Chen, L., Wang, X., Ju, G., and Mu, Z. *Journal of Luminescence* **138**, 83–88 (2013).
[166] Jiachi, Z., Minghui, Y., Qingsong, Q., Hongliang, Z., Meijiao, Z., Xuhui, X., and Yuhua, W. *Journal of Applied Physics* **108**, 123518 (2010).
[167] Zhang, J.-C., Qin, Q.-S., Yu, M.-H., Zhou, H.-L., and Zhou, M.-J. *Chinese Physics B* **20**, 094211 (2011).
[168] Zhang, J., Qin, Q., Yu, M., Zhou, M., and Wang, Y. *Journal of Luminescence* **132**, 23–26 (2012).
[169] Lei, B., Li, B., Wang, X., and Li, W. *Journal of Luminescence* **118**, 173–178 (2006).
[170] Wang, Z.-L., Zheng, G.-S., Wang, S.-Q., Qin, Q.-S., Zhou, H.-L., and Zhang, J.-C. *Acta Physica Sinica* **61**, 127805–127805 (2012).
[171] Lei, B.-F., Yue, S., Zhang, Y.-Z., and Liu, Y.-L. *Chinese Physics Letters* **27**, 037201 (2010).
[172] Xu, X., Wang, Y., Gong, Y., Zeng, W., and Li, Y. *Optics Express* **18**, 16989–16994 (2010).
[173] Yu, X., Xu, X., and Qiu, J. *Materials Research Bulletin* **46**, 627–629 (2011).
[174] Qin, Q. S., Ma, X. L., Shao, Y., Yang, X. Y., Sheng, H. F., Yang, J. Z., Yin, Y., and Zhang, J. C. *Acta Physica Sinica* **61**, 097804 (2012).
[175] Lei, B., Li, B., Zhang, H., Zhang, L., Cong, Y., and Li, W. *Journal of the Electrochemical Society* **154**, H623–H630 (2007).

[176] Lei, B., Li, B., Zhang, H., and Li, W. *Optical Materials* **29**, 1491–1494 (2007).
[177] Liu, Z. and Liu, Y. *Materials Chemistry and Physics* **93**, 129–132 (2005).
[178] Liang, Z., Zhang, J., Sun, J., Li, X., Cheng, L., Zhong, H., Fu, S., Tian, Y., and Chen, B. *Physica B: Condensed Matter* **412**, 36–40 (2013).
[179] Lei, B., Man, S.-Q., Liu, Y., and Yue, S. *Materials Chemistry and Physics* **124**, 912–915 (2010).
[180] Bessière, A., Benhamou, R. A., Wallez, G., Lecointre, A., and Viana, B. *Acta Materialia* **60**, 6641–6649 (2012).
[181] Lecointre, A., Ait Benhamou, R., Bessière, A., Wallez, G., Elaatmani, M., and Viana, B. *Optical Materials* **34**, 376–380 (2011).
[182] Bessière, A., Lecointre, A., Benhamou, R. A., Suard, E., Wallez, G., and Viana, B. *Journal of Materials Chemistry C* **1**, 1252–1259 (2013).
[183] Liu, L., Li, C., Wang, S., and Su, Q. *Applied Physics Letters* **88**, 241107 (2006).
[184] Wang, X., Du, F., Wei, D., Huang, Y., and Seo, H. J. *Sensors and Actuators B: Chemical* **158**, 171–175 (2011).
[185] Jeong, J., Jayasimhadri, M., Lee, H. S., Jang, K., Yi, S. S., Jeong, J. H., and Kim, C. *Physica B: Condensed Matter* **404**, 2016–2019 (2009).
[186] Peng, Z., Xu, Z., Luo, C., Yu, J., and Zhang, G. *Luminescence* **23**, 14–16 (2008).
[187] Wang, J., Wang, S., and Su, Q. *Journal of Solid State Chemistry* **177**, 895–900 (2004).
[188] Wang, J., Wang, S. B., and Su, Q. *Journal of Materials Chemistry* **14**, 2569–2574 (2004).
[189] Wang, J., Su, Q., and Wang, S. B. *Materials Research Bulletin* **40**, 590–598 (2005).
[190] Song, Y. H., Zou, H. F., Gan, S. C., Deng, Y. F., Hong, G. Y., and Meng, J. *Journal of Materials Science* **42**, 4899–4904 (2007).
[191] Wang, J., Su, Q., and Wang, S. B. *Journal of Physics and Chemistry of Solids* **66**, 1171–1176 (2005).
[192] Lecointre, A., Bessière, A., Bos, A. J. J., Dorenbos, P., Viana, B., and Jacquart, S. *The Journal of Physical Chemistry C* **115**, 4217–4227 (2011).
[193] Pang, R., Li, C., Zhang, S., and Su, Q. *Materials Chemistry and Physics* **113**, 215–218 (2009).
[194] Pang, R., Li, C., Shi, L., and Su, Q. *Journal of Physics and Chemistry of Solids* **70**, 303–306 (2009).
[195] Zhang, X. Y., Cheng, G., Mi, X. Y., Xiao, Z. Y., Jiang, W. W., and Hujingjie. *Journal of Rare Earths* **22**, 137–139 (2004).
[196] Pan, Y. X., Su, Q., Xu, H. F., Chen, T. H., Ge, W. K., Yang, C. L., and Wu, M. M. *Journal of Solid State Chemistry* **174**, 69–73 (2003).
[197] Jia, W., Jia, D., Rodriguez, T., Evans, D. R., Meltzer, R. S., and Yen, W. M. *Journal of Luminescence* **119-120**, 13–18 (2006).
[198] Zhang, X., Zhang, J., Nie, Z., Wang, M., Ren, X., and Wang, X.-j. *Applied Physics Letters* **90**, 151911–3 (2007).
[199] Zhang, X., Zhang, J., Zhang, X., Chen, L., Lu, S., and Wang, X.-J. *Journal of Luminescence* **122-123**, 958–960 (2007).
[200] Boutinaud, P., Sarakha, L., Cavalli, E., Bettinelli, M., Dorenbos, P., and Mahiou, R. *Journal of Physics D: Applied Physics* **42**, 045106 (2009).

[201] Haranath, D., Khan, A. F., and Chander, H. *Journal of Physics D: Applied Physics* **39**, 4956–4960 (2006).
[202] Wanjun, T. and Donghua, C. *Journal of the American Ceramic Society* **90**, 3156–3159 (2007).
[203] Yuan, X., Shi, X., Shen, M., Wang, W., Fang, L., Zheng, F., and Wu, X. *Journal of Alloys and Compounds* **485**, 831–836 (2009).
[204] Qi, Y., Lian, S. X., Yu, L. P., Zhou, W., and Yin, D. L. *Chinese Journal of Inorganic Chemistry* **25**, 218–222 (2009).
[205] Lian, S. X., Qi, Y., Rong, C. Y., Yu, L. P., Zhu, A. L., Yin, D. L., and Liu, S. B. *Journal of Physical Chemistry C* **114**, 7196–7204 (2010).
[206] Chu, M.-H., Jiang, D.-P., Zhao, C.-J., and Li, B. *Chinese Physics Letters* **27**, 047203 (2010).
[207] Li, C. and Su, Q. *Journal of Alloys and Compounds* **408-412**, 875–878 (2006).
[208] Blasse, G., Grabmaier, B. C., and Ostertag, M. *Journal of Alloys and Compounds* **200**, 17–18 (1993).
[209] Kostyk, L., Luchechko, A., Zakharko, Y., Tsvetkova, O., and Kuklin'ski, B. *Journal of Luminescence* **129**, 312–316 (2009).
[210] Matsui, H., Xu, C.-N., Akiyama, M., and Watanabe, T. *Japanese Journal of Applied Physics* **39**, 6582 (2000).
[211] Zhuang, Y., Ueda, J., and Tanabe, S. *Optical Materials Express* **2**, 1378–1383 (2012).
[212] Bessière, A., Jacquart, S., Priolkar, K., Lecointre, A., Viana, B., and Gourier, D. *Optics Express* **19**, 10131–10137 (2011).
[213] Uheda, K., Maruyama, T., Takizawa, H., and Endo, T. *Journal of Alloys and Compounds* **262-263**, 60–64 (1997).
[214] Che, G., Li, X., Liu, C., Wang, H., Liu, Y., and Xu, Z. *physica status solidi (a)* **205**, 194–198 (2008).
[215] Yi Shou-Jun, Liu Ying-Liang, Z. J.-X. Y. D.-S. *Chemical Journal of Chinese Universities* **25**, 1400–1402 (2004).
[216] Iwasaki, M., Kim, D. N., Tanaka, K., Murata, T., and Morinaga, K. *Science and Technology of Advanced Materials* **4**, 137–142 (2003).
[217] Cong, Y., Li, B., Yue, S., Zhang, L., Li, W., and Wang, X.-j. *Journal of the Electrochemical Society* **156**, H272–H275 (2009).
[218] Sun, Z. X. *Chinese Journal of Inorganic Chemistry* **28**, 1229–1233 (2012).
[219] Che, G. B., Liu, C. B., Wang, Q. W., and Xu, Z. L. *Chemistry Letters* **37**, 136–137 (2008).
[220] Che, G., Liu, C., Li, X., Xu, Z., Liu, Y., and Wang, H. *Journal of Physics and Chemistry of Solids* **69**, 2091–2095 (2008).
[221] Liu, C., Che, G., Xu, Z., and Wang, Q. *Journal of Alloys and Compounds* **474**, 250–253 (2009).
[222] Woo, B. K., Luo, Z., Li, Y., Singh, S. P., Joly, A. G., Hossu, M., Liu, Z., and Chen, W. *Optical Materials* **33**, 1283–1290 (2011).
[223] Liu, Z. and Liu, L. Y. *physica status solidi (a)* **202**, 1814–1817 (2005).
[224] Jia, D., Lewis, L. A., and Wang, X.-j. *Electrochemical and Solid-State Letters* **13**, J32–J34 (2010).

[225] Yan, W., Liu, F., Lu, Y.-Y., Wang, X.-J., Yin, M., and Pan, Z. *Optics Express* **18**, 20215–20221 (2010).
[226] Kang, F.-W., Hu, Y.-H., Wu, H.-Y., and Ju, G.-F. *Chinese Physics Letters* **28**, 107201 (2011).
[227] Boutinaud, P., Sarakha, L., and Mahiou, R. *Journal of Physics-Condensed Matter* **21**, 025901 (2009).
[228] Takayama, T., Katsumata, T., Komuro, S., and Morikawa, T. *Journal of Crystal Growth* **275**, e2013–e2017 (2005).
[229] Wu, H., Hu, Y., Kang, F., Li, N., Ju, G., Mu, Z., and Yang, Z. *Journal of the American Ceramic Society* **95**, 3214–3219 (2012).
[230] Liu, Z. W., Liu, Y. L., Yuan, D. S., Zhang, J. X., Rong, J. H., and Huang, L. H. *Chinese Journal of Inorganic Chemistry* **20**, 1433–1436 (2004).
[231] Wu, H. Y., Hu, Y. H., Kang, F. W., and Li, N. N. *Journal of Materials Research* **27**, 959–964 (2012).
[232] Kang, F., Hu, Y., Chen, L., Wang, X., Mu, Z., Wu, H., and Ju, G. *Applied Physics B* **107**, 833–837 (2012).
[233] Kang, F., Hu, Y., Wu, H., Mu, Z., Ju, G., Fu, C., and Li, N. *Journal of Luminescence* **132**, 887–894 (2012).
[234] Wu, H., Hu, Y., Kang, F., Chen, L., Wang, X., Ju, G., and Mu, Z. *Materials Research Bulletin* **46**, 2489–2493 (2011).
[235] Moon, C., Nishi, M., Miura, K., and Hirao, K. *Journal of Luminescence* **129**, 817–819 (2009).
[236] Sun, D., Li, D., Zhu, Z., Xiao, J., Tao, Z., and Liu, W. *Optical Materials* **34**, 1890–1896 (2012).
[237] Garlick, G. F. J. and Mason, D. E. *Journal of the Electrochemical Society* **96**, 90–113 (1949).
[238] Lawangar, R. D., Shalgaonkar, C. S., Pawar, S. H., and Narlikar, A. V. *Solid State Communications* **10**, 1241–1246 (1972).
[239] Pawar, S. H. and Narlikar, A. V. *Materials Research Bulletin* **11**, 821–826 (1976).
[240] Jia, D., Meltzer, R. S., and Yen, W. M. *Journal of Luminescence* **99**, 1–6 (2002).
[241] Paulose, P. I., Joseph, J., Rudra Warrier, M. K., Jose, G., and Unnikrishnan, N. V. *Journal of Luminescence* **127**, 583–588 (2007).
[242] Jia, D., Zhu, J., and Wu, B. *Journal of Luminescence* **91**, 59–65 (2000).
[243] Pitale, S. S., Sharma, S. K., Dubey, R. N., Qureshi, M. S., and Malik, M. M. *Journal of Luminescence* **128**, 1587–1594 (2008).
[244] Clabau, F., Rocquefelte, X., Le Mercier, T., Deniard, P., Jobic, S., and Whangbo, M. H. *Chemistry of Materials* **18**, 3212–3220 (2006).
[245] Ma, L. and Chen, W. *The Journal of Physical Chemistry C* **115**, 8940–8944 (2011).
[246] Zhang, J. W., Liu, Y. L., Zhang, J. X., Yuan, D. S., Rong, J. H., and Huang, L. H. *Rare Metal Materials and Engineering* **35**, 766–769 (2006).
[247] Lei, B., Liu, Y., Zhang, J., Meng, J., Man, S., and Tan, S. *Journal of Alloys and Compounds* **495**, 247–253 (2010).
[248] Zhang, J., Liu, Y.-L., and Man, S.-q. *Journal of Luminescence* **117**, 141–146 (2006).
[249] Hang, T., Liu, Q., Mao, D., and Chang, C. *Materials Chemistry and Physics* **107**, 142–147 (2008).

[250] Mao, S., Liu, Q., Gu, M., Mao, D., and Chang, C. *Journal of Alloys and Compounds* **465**, 367–374 (2008).
[251] Liu, G., Zhang, Q., Wang, H., and Li, Y. *Materials Science and Engineering B* **177**, 316–320 (2012).
[252] Kang, C.-C., Liu, R.-S., Chang, J.-C., and Lee, B.-J. *Chemistry of Materials* **15**, 3966–3968 (2003).
[253] Zhang, P. Y., Wang, M. Q., Hong, Z. L., Fang, X. P., Qian, G. D., and Wang, Z. Y. *Journal of Rare Earths* **22**, 75–78 (2004).
[254] Zhang, P., Hong, Z., Wang, M., Fang, X., Qian, G., and Wang, Z. *Journal of Luminescence* **113**, 89–93 (2005).
[255] Liu, C. B. and Che, G. B. *physica status solidi (a)* **203**, 558–564 (2006).
[256] Wang, L., Zhang, L., Huang, Y., Jia, D., and Lu, J. *Journal of Luminescence* **129**, 1032–1035 (2009).
[257] Wang, X., Zhang, Z., Tang, Z., and Lin, Y. *Materials Chemistry and Physics* **80**, 1–5 (2003).
[258] Zhang, J. Y., Zhang, Z. T., Tang, Z. L., and Wang, T. M. *Ceramics International* **30**, 225–228 (2004).
[259] Wang, Y. H. and Wang, Z. L. *Journal of Rare Earths* **24**, 25–28 (2006).
[260] Yuan, S., Yang, Y., Fang, B., and Chen, G. *Optical Materials* **30**, 535–538 (2007).
[261] Lei, B. F., Liu, Y. L., Tang, G. B., Ye, Z. R., and Shi, C. S. *Chemical Journal of Chinese Universities* **24**, 208–210 (2003).
[262] Lei, B., Liu, Y., Tang, G., Ye, Z., and Shi, C. *Materials Chemistry and Physics* **87**, 227–232 (2004).
[263] Yao, K., Wang, M., Liu, S., Zhang, L., and Li, W. *Journal of Rare Earths* **24**, 524–528 (2006).
[264] Liu, B., Shi, C., and Qi, Z. *Journal of Physics and Chemistry of Solids* **67**, 1674–1677 (2006).
[265] Hong, Z., Zhang, P., Fan, X., and Wang, M. *Journal of Luminescence* **124**, 127–132 (2007).
[266] Holsa, J., Laamanen, T., Lastusaari, M., Malkamaki, M., Niittykoski, J., and Zych, E. *Optical Materials* **31**, 1791–1793 (2009).
[267] Lei, B.-F., Liu, Y.-L., Tang, G.-B., Ye, Z.-R., and Shi, C.-S. *Chemical Journal of Chinese Universities* **24**, 782–784 (2003).
[268] Najafov, H., Kato, A., Toyota, H., Iwai, K., Bayramov, A., and Iida, S. *Japanese Journal of Applied Physics* **41**, 2058–2065 (2002).
[269] Guo, C., Zhang, C., Lü, Y., Tang, Q., and Su, Q. *physica status solidi (a)* **201**, 1588–1593 (2004).
[270] Guo, C., Tang, Q., Huang, D., Zhang, C., and Su, Q. *Journal of Physics and Chemistry of Solids* **68**, 217–223 (2007).
[271] Smet, P. F., Avci, N., and Poelman, D. *Journal of the Electrochemical Society* **156**, H243–H248 (2009).
[272] Ju, G., Hu, Y., Chen, L., and Wang, X. *Journal of Applied Physics* **111**, 113508–6 (2012).
[273] Zhang, J.-S., Zhong, H.-Y., Sun, J.-S., Cheng, L.-H., Li, X.-P., and Chen, B.-J. *Chinese Physics Letters* **29**, 017101 (2012).

[274] Uheda, K., Takizawa, H., Endo, T., Miura, C., Shimomura, Y., Kijima, N., and Shimada, M. *Journal of Materials Science Letters* **20**, 1753–1755 (2001).
[275] Qiu, J., Miura, K., Inouye, H., Kondo, Y., Mitsuyu, T., and Hirao, K. *Applied Physics Letters* **73**, 1763–1765 (1998).
[276] Kinoshita, T. and Hosono, H. *Journal of Non-Crystalline Solids* **274**, 257–263 (2000).
[277] Hosono, H., Kinoshita, T., Kawazoe, H., Yamazaki, M., Yamamoto, Y., and Sawanobori, N. *Journal of Physics: Condensed Matter* **10**, 9541 (1998).
[278] Kinoshita, T. and Yamazaki, M. *Journal of Applied Physics* **86**, 3729 (1999).
[279] Qiu, J., Wada, N., Ogura, F., Kojima, K., and Hirao, K. *Journal of Physics: Condensed Matter* **14**, 2561–2567 (2002).
[280] Wada, N., Ogura, F., Yamamoto, K., and Kojima, K. *Glass Technology* **46**, 163–170 (2005).
[281] Qiu, J., Gaeta, A. L., and Hirao, K. *Chemical Physics Letters* **333**, 236–241 (2001).
[282] Qiu, J., Kondo, Y., Miura, K., Mitsuyu, T., and Hirao, K. *Japanese Journal of Applied Physics* **38**, L649 (1999).
[283] Yamazaki, M. and Kojima, K. *Solid State Communications* **130**, 637–639 (2004).
[284] Qiu, J., Miyauchi, K., Kawamoto, Y., Kitamura, N., Qiu, J., and Hirao, K. *Applied Physics Letters* **81**, 394–396 (2002).
[285] Zhang, L., Li, C., and Su, Q. *Journal of Rare Earths* **24**, 196–198 (2006).
[286] Sanada, T., Seto, H., Morimoto, Y., Yamamoto, K., Wada, N., and Kojima, K. *Journal of Sol-Gel Science and Technology* **56**, 82–86 (2010).
[287] Takahashi, Y., Ando, M., Ihara, R., and Fujiwara, T. *Optical Materials Express* **1**, 372–378 (2011).
[288] Jiang, X.-W., Qiu, J.-R., Zeng, H.-D., and Zhu, C.-S. *Chinese Physics* **12**, 1386 (2003).
[289] Yamazaki, M., Yamamoto, Y., Nagahama, S., Sawanobori, N., Mizuguchi, M., and Hosono, H. *Journal of Non-Crystalline Solids* **241**, 71–73 (1998).
[290] Wang, Z.-y., Zhang, F.-a., Guo, X.-r., Wang, Y.-h., Fan, X.-p., and Qian, G.-d. *Journal of Zhejiang University* **40**, 1454–7, 14727, 1472 (2006).
[291] Li, C., Su, Q., and Wang, S. *Materials Research Bulletin* **37**, 1443–1449 (2002).
[292] Li, C., Yu, Y., Wang, S., and Su, Q. *Journal of Non-Crystalline Solids* **321**, 191–196 (2003).
[293] Li, C. and Su, Q. *Applied Physics Letters* **85**, 2190–2192 (2004).
[294] Li, C. and Su, Q. *Journal of Rare Earths* **24**, 506–508 (2006).
[295] Li, C., Wang, J., Liang, H., and Su, Q. *Journal of Applied Physics* **101**, 113304 (2007).
[296] Lin, G., Dong, G., Tan, D., Liu, X., Zhang, Q., Chen, D., Qiu, J., Zhao, Q., and Xu, Z. *Journal of Alloys and Compounds* **504**, 177–180 (2010).
[297] Smet, P. F., Van den Eeckhout, K., Bos, A. J. J., van der Kolk, E., and Dorenbos, P. *Journal of Luminescence* **132**, 682–689 (2012).
[298] Korthout, K., Van den Eeckhout, K., Botterman, J., Nikitenko, S., Poelman, D., and Smet, P. F. *Physical Review B* **84**, 085140 (2011).
[299] Smet, P. F., Parmentier, A. B., and Poelman, D. *Journal of the Electrochemical Society* **158**, R37–R54 (2011).

[300] Lenard, P., Schmidt, F., and Tomascheck, R. *Phosphoreszenz und Fluoreszenz*, volume 23 of *Handbuch der Experimentalphysik*. Akademische Verlagsgesellschaft, Leipzig, (1928).
[301] Jia, D., Zhu, J., and Wu, B. *Journal of Luminescence* **90**, 33–37 (2000).
[302] Blasse, G., Wanmaker, W. L., and ter Vrugt, J. W. *Journal of The Electrochemical Society* **115**, 673–673 (1968).
[303] Smet, P. F., Avci, N., Van den Eeckhout, K., and Poelman, D. *Optical Materials Express* **2**, 1306–1313 (2012).
[304] Van den Eeckhout, K., Bos, A. J. J., Poelman, D., and Smet, P. F. *Physical Review B* **87**, 045126 (2013).
[305] Nakamura, T., Matsuzawa, T., Rowlands, C. C., Beltran-Lopez, V., Smith, G. M., and Riedi, P. C. *Journal of the Chemical Society, Faraday Transactions* **94**, 3009–3012 (1998).
[306] Hölsä, J., Laamanen, T., Lastusaari, M., and Novák, P. *Journal of Rare Earths* **29**, 1130–1136 (2011).
[307] Blasse, G. and Bril, A. *Philips Research Reports* **23**, 201–206 (1968).

3 Suggested mechanisms

The findings in this chapter have been published in:

- **Persistent luminescence in Eu^{2+}-doped compounds: A review**
  Koen Van den Eeckhout, Philippe F. Smet and Dirk Poelman
  Materials **3** (2010) 2536-2566

The discovery of the persistent luminescent properties of $SrAl_2O_4$:Eu,Dy also marked the beginning of a renewed search for the underlying mechanisms. Until then, relatively little research had been done on this subject. It was generally agreed that after excitation, charge carriers could get caught by trap levels inside the band gap. To study these trap levels, quite some research had been done on thermoluminescence glow curves and how to extract information about trap depth from them (see section 5.1.1 for a description of thermoluminescence). However, details such as the nature and origin of the traps and the charge carriers were still unclear.

However, since 1996, different mechanisms have been suggested, ranging from very basic conceptual models to complex systems with multiple charge traps of various types and depths. In this chapter, we give a brief overview of the most important ones, how they were conceived and how they were justified or disproved by experimental results.

3.1 The Matsuzawa model

In the same famous article announcing the discovery of $SrAl_2O_4$:Eu,Dy, Matsuzawa *et al.* tried to explain the origins of the extraordinary persistent luminescence. A schematic picture of their model is shown in figure 3.1.

In the Matsuzawa model, holes are assumed to be the main charge carriers. This assumption is based on earlier measurements by Abbruscato on non co-doped $SrAl_2O_4$:Eu, which also shows a weak afterglow. From his results obtained by Hall measurements, Abbruscato concluded that holes in the valence band had to be the main charge carriers [1]. He suspected that Sr^{2+} vacancies acted as traps for these holes. Additionally, Matsuzawa *et al.* performed non-uniform illumination photoconductivity measurements, which also suggested that holes are the main charge carriers [2].

The Matsuzawa model modified Abbruscato's assumptions in order to explain the influence of rare earth codoping. When an Eu^{2+} ion is excited by an incident photon, there is a possibility that a hole escapes to the valence band, thereby leaving behind

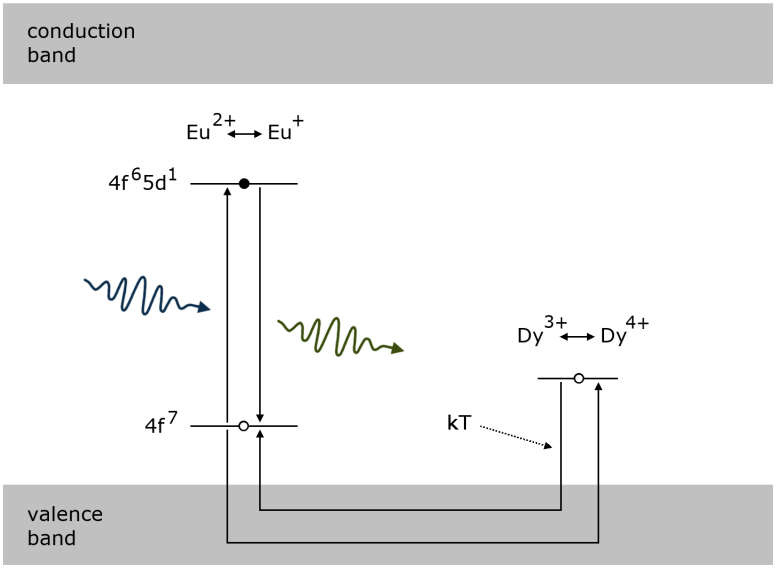

Figure 3.1: Persistent luminescence mechanism proposed by Matsuzawa *et al.* for $SrAl_2O_4$:Eu,Dy [2].

a Eu^+ ion. The hole is then captured by a trivalent rare earth ion, such as Dy^{3+}, thus creating a Dy^{4+} ion. After a while, thermal energy causes the trapped hole to be released into the valence band again. From there it can move back to a Eu^+ ion, allowing it to return to the Eu^{2+} ground state with emission of a photon [2].

The Matsuzawa model quickly gained popularity [3–7], and was used frequently to explain observed afterglow in newly discovered compounds [8–10]. Various thermoluminescence [11–14], photoconductivity [6] and electron paramagnetic resonance [15–17] measurements were performed to confirm the validity of the model. However, the results of these experiments were often inconclusive and no hard evidence for the model could be found. It was inevitable that certain researchers started to raise questions about the Matsuzawa mechanism.

3.2 The Aitasalo model

In 2003, Aitasalo *et al.* suggested a model that differed considerably from the Matsuzawa model (figure 3.2) [18]. In this model, electrons are excited directly from the valence band into trap levels of unspecified origin. The hole that is created in this way migrates towards a calcium vacancy (V''_{Ca} in the Kröger-Vink notation [19]) where it is caught. The electron is removed from the trap level by thermal energy and ends up at an oxygen vacancy level.

Since the conduction band is located too high above the energy level of the oxygen vacancy trap to enable a thermally assisted transition to the conduction band, they assumed that the energy released on recombination of the electron and the hole was delivered directly to the europium ions, by means of energy transfer. This assumption requires close proximity of the vacancies to the luminescent centers. The transferred

energy excites an electron of europium to a 5d level, followed by recombination and emission of the persistent luminescent light [18]. It should be noted that only holes are present as free charge carriers (in the valence band), which explains the previous observations by Abbruscato and Matsuzawa.

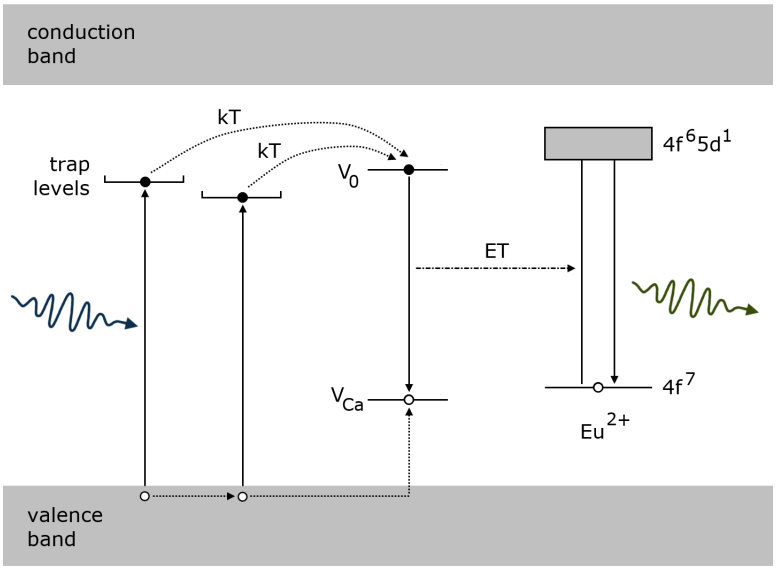

Figure 3.2: Persistent luminescence mechanism proposed by Aitasalo *et al.* for $CaAl_2O_4$:Eu [18].

Hölsä and coworkers introduced this model for several reasons. Firstly, the Matsuzawa model ignores the afterglow observed in non-codoped $SrAl_2O_4$:Eu [20]. Therefore, a model avoiding the explicit use of the trivalent rare earth codopants needed to be developed. Aitasalo *et al.* explained the influence of the codopants by suggesting that they increased the number of lattice defects, because the trivalent lanthanide ions occupy the divalent alkaline earth sites, leading to spontaneous defect creation for charge compensation. This also explains why adding Sm to the material is detrimental for the persistent luminescence, since it is reduced to Sm^{2+} during preparation, thereby removing the cation vacancies acting as hole traps [18].

A second reason for rejecting the original Matsuzawa model was the implausibility of the occurrence of monovalent europium and tetravalent dysprosium ions in the material. Aitasalo *et al.* argued that the reduction of Eu^{2+} to Eu^{+} and the oxidation of Dy^{3+} to Dy^{4+} would result in chemically unstable ions [18]. This reasoning was later supported by other authors such as Dorenbos [21].

A final observation that encouraged Aitasalo *et al.* to suggest a new persistent luminescence mechanism was the observation that the blue persistent luminescence of $CaAl_2O_4$:Eu,Nd could be induced by excitation with wavelengths as large as 530 nm [22]. They concluded that the absorption of two photons had to occur in the process, through direct excitation of an electron from the valence band into a long-lived intermediate trap level, followed by an excited state absorption. Since the Matsuzawa model assumed that the trapped charge carriers originated from the Eu^{2+} ions, it could not explain how these could be created with such low-energy photons.

3.3 The Dorenbos model

Dorenbos has put great effort into the determination of lanthanide energy levels in inorganic compounds, with applications in scintillator physics and persistent luminescence [23]. As previously mentioned, he agreed with Aitasalo *et al.* that the existence of Eu^{+} and Dy^{4+} in aluminate or silicate compounds is highly improbable [21]. Secondly, he pointed out that the assumed hole on the ground state of Eu^{2+} after excitation is based on faulty reasoning. The energy levels of the lanthanides are localized, in contrast to the delocalized Bloch states of the valence and conduction band. Therefore, the 4f state of europium after the excitation should not be interpreted as a "real hole" that can accept an electron. He was not convinced by the observation of hole conduction by Abbruscato and Matsuzawa, and noted that more detailed research was required [21].

These problems with the Matsuzawa model encouraged Dorenbos to present a different model in 2005, depicted in figure 3.3. As in Matsuzawa's model, electrons are excited in divalent europium ions. Since the 5d level of divalent europium lies very close to the conduction band [21], these excited electrons can easily be released into the conduction band and subsequently caught by a trivalent rare earth codopant, creating a divalent ion. Thermal energy can then release the trapped electron, after which it recombines upon reaching a luminescent center [21, 24]. The suggestion that the rare earth codopants act as traps is similar to Matsuzawa's, but it does not require the existence of Eu^{+} and RE^{4+}. It can, however, not explain the existence of intrinsic persistent luminescence in non-codoped materials.

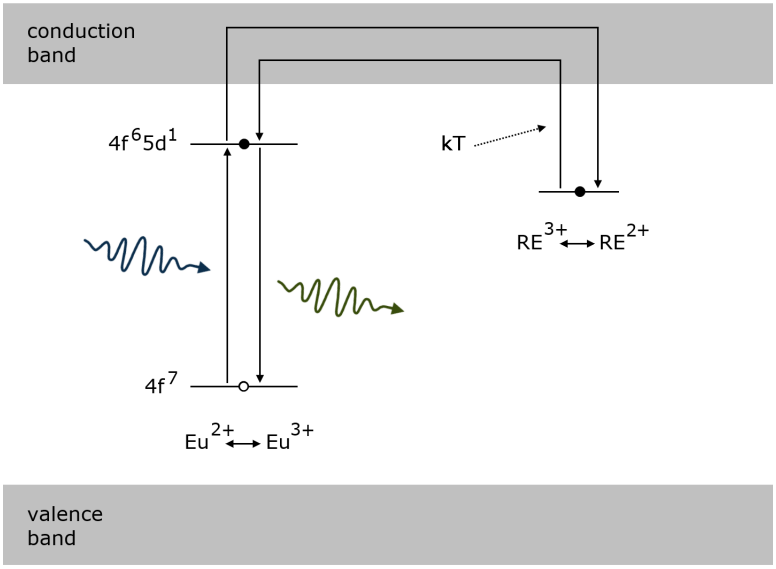

Figure 3.3: Persistent luminescence mechanism proposed by Dorenbos for aluminate and silicate compounds [21].

Based on his previous research on the location of lanthanide levels in inorganic compounds, Dorenbos derived that the energy level of Dy^{2+} (i.e., Dy^{3+} after capture of an electron) in $SrAl_2O_4$ lies approximately 0.9 eV below the conduction band [21], which is of the same order as the trap depth found in $SrAl_2O_4$:Eu,Dy [2, 11, 25]. The

Dorenbos model also explains why adding Sm or Yb strongly reduces the afterglow. Previous work revealed that the relevant levels of Sm^{2+} and Yb^{2+} are located much lower than those of the other divalent rare earth ions such as Dy^{2+} and Nd^{2+} [26]. This results in traps that are too deep to be emptied at room temperature.

3.4 The Clabau model

Around the same time as Dorenbos, Clabau *et al.* reviewed the existing mechanisms for persistent luminescence and found that a revision was needed. For the same reasons as Dorenbos, these authors did not accept the Matsuzawa model. Furthermore, they mention EPR measurements that show a decrease in the Eu^{2+} concentration during excitation, followed by an increase as soon as the excitation is terminated, continuing until the afterglow ends. They concluded that Eu^{2+} must participate in the trapping process, which contradicted the idea of energy transfer to Eu^{2+} after the trapping, as suggested by Aitasalo [27–29].

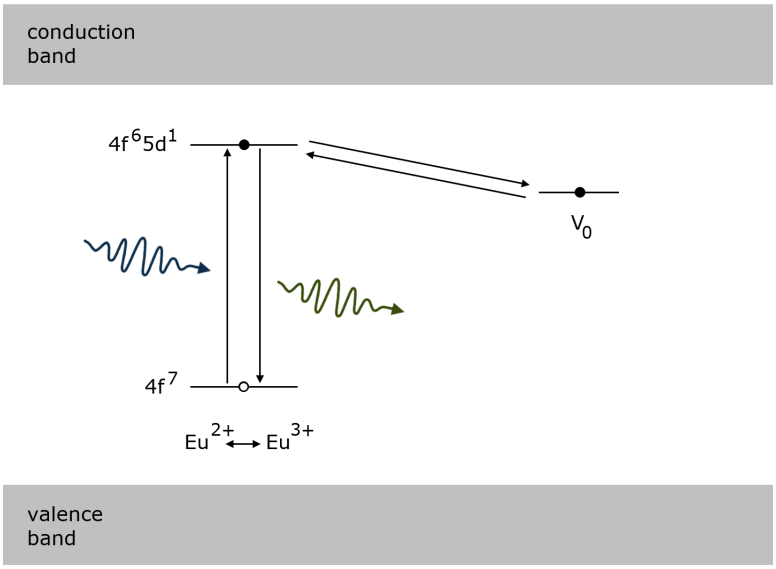

Figure 3.4: Persistent luminescence mechanism proposed by Clabau *et al.* for $SrAl_2O_4$:Eu,Dy [27].

The model proposed by Clabau *et al.* is shown in figure 3.4. It is similar to the Dorenbos model, but differs on some important points. Firstly, there is no migration of electrons through the conduction band. The transport of electrons between the traps and the luminescent centers is believed to occur through direct transfer, which requires close proximity between the europium ions and the lattice defects [27]. This assumption is based on measurements of the temperature dependence of the photoconductivity in $SrAl_2O_4$:Eu,Dy under UV excitation, which increases up to 250 K, and subsequently enters a plateau phase until 300 K, indicating that no free charge carriers are released around this temperature. However, thermoluminescence measurements around 300 K clearly show the presence of de-trapping processes at this temperature (figure 3.5). From

this, Clabau *et al.* concluded that the interaction between the traps and the luminescent centers could not occur via the conduction band.

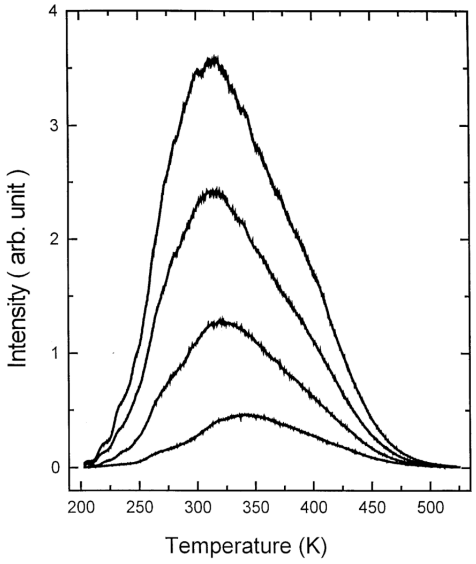

Figure 3.5: The glow curve for $SrAl_2O_4$:Eu,Dy after UV excitation at 200K for different periods of time. From bottom to top: 10, 30, 60 and 120 s. The heating rate is 16 K/min. Reprinted with permission from [14].

A second difference to the Dorenbos mechanism is the nature of the traps. By comparing glow curves of non-codoped and Dy^{3+}-codoped $SrAl_2O_4$:Eu, Clabau *et al.* noticed that the relevant peaks differed in size and location, but were very similar in shape. From this, they concluded that the chemical nature of the trap was not influenced under codoping. This led them to the idea that lattice defects, namely oxygen vacancies, must act as traps in $SrAl_2O_4$:Eu,Dy [29].

The influence of the lanthanides as codopants is explained by their stabilizing influence on the oxygen vacancies. The ionization potentials of the rare earths can be used as a measure for the extent of this stabilization, since a lower ionization potential will cause the codopant to attract oxygen vacancies more strongly, hereby increasing the trap depth [28]. Indeed, when codoping $SrAl_2O_4$:Eu with different rare earths with an increasing ionization potential, the duration of the afterglow is shortened [27].

3.5 Recent developments

In 2006, Aitasalo et al. described a mechanism for persistent luminescence that incorporates suggestions from both Clabau and Dorenbos (figure 3.6) [30]. Electrons that are excited in the Eu^{2+} luminescent centers can easily escape into the conduction band. Both oxygen vacancies and trivalent codopant ions introduce trap levels, but the exact nature was not clarified, since these defects can interact with each other and form complex aggregates [30]. When enough thermal energy is available, the captured electrons can escape again into the conduction band and recombine in a luminescent center.

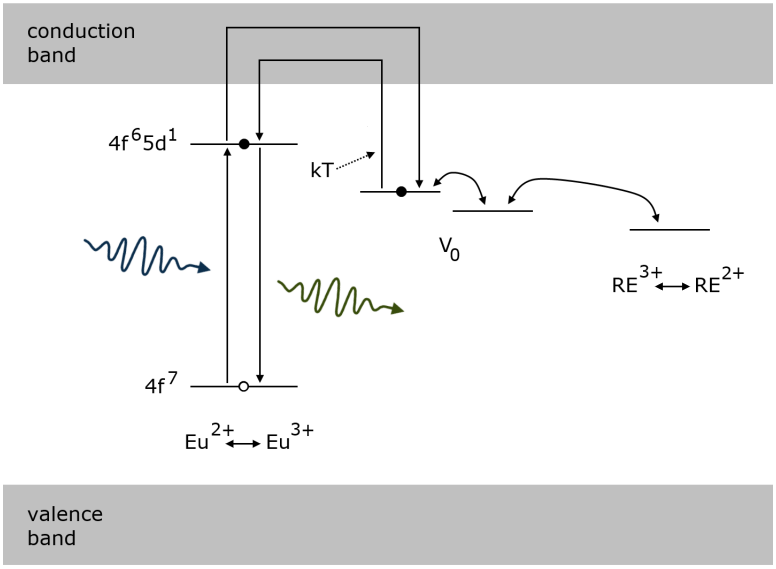

Figure 3.6: Persistent luminescence mechanism proposed in 2006 by Aitasalo *et al.* for $CaAl_2O_4$:Eu,Nd [30].

3.6 Experimental evidence

Synchrotron radiation measurements offer interesting new ways to study persistent luminescence, and were not always fully appreciated until recently. Qiu *et al.* [31], Qi *et al.* [32], and more recently Carlson *et al.* [33] and Hölsä *et al.* [34] performed X-ray absorption near edge structure (XANES) measurements to uncover the valence of the rare earth ions in $Sr_2MgSi_2O_7$:Eu,RE and $CaAl_2O_4$:Eu,Nd. Both divalent and trivalent europium were encountered, but for the rare earth codopants only the trivalent form could be detected. They could not identify the divalent form predicted by Dorenbos. Also, no monovalent europium or tetravalent codopant ions, as would be expected in the Matsuzawa model, were observed. This could indicate that the Matsuzawa and Dorenbos models are not suitable. However, the lack of direct experimental evidence could also be due to a low concentration of filled trap levels in these materials, which makes it hard to detect these specific valence states. Indeed, none of the models described above gives information about the actual number or concentration of trap levels and trapped charge carriers involved in the afterglow.

Since 2010, we have also performed XANES measurements on $SrAl_2O_4$:Eu,Dy and $CaAl_2O_4$:Eu,Nd to verify the suggestions by Dorenbos and Clabau. We were able to prove that the trapped charge carriers are indeed electrons originating from the Eu^{2+} activators, and we could follow the valence state changes of Eu during the charging phase. However, the low concentrations of the dopant and codopant ions (typically of the order of 1%) make it very difficult to detect these subtle changes. These results will be discussed more thoroughly in chapter 4 on kinetics.

Electron paramagnetic resonance (EPR) measurements are another suitable way to study traps in the investigated materials. Hölsä *et al.* used EPR to prove the existence of electrons in anion vacancies (i.e., F^+ colour centers) in non-codoped and even non-

Eu^{2+}-doped $CaAl_2O_4$ [35].

Dorenbos showed that the 4f levels of the lanthanide series follow a characteristic pattern relative to each other, independent of the host material (figure 3.7) [26]. If the trivalent codopants indeed act as traps, as the Dorenbos model claims, it is reasonable to expect that this pattern can be recognized by studying the trap depth for different codopants. Unfortunately, results on this matter are scarce and rather ambiguous. Aitasalo *et al.* estimated the trap depth in $CaAl_2O_4$:Eu,RE^{3+} for the entire lanthanide series as codopant, but did not find a clear trend (figure 3.8) [18]. In chapter 6, we will compare the Dorenbos pattern with the thermoluminescence measurements in $Ca_2Si_5N_8$:Eu,RE^{3+} to look for additional experimental evidence.

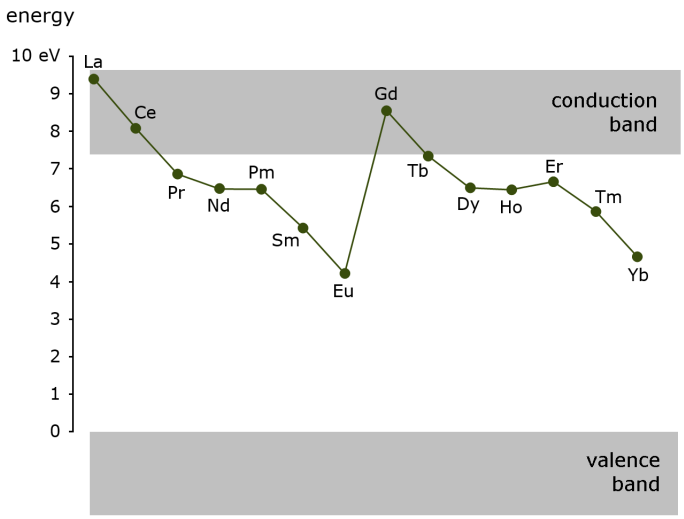

Figure 3.7: Typical energy level pattern for the divalent lanthanide series in $SrAl_2O_4$:Eu,RE^{3+}, as suggested by Dorenbos [21].

For the case of YPO_4:Ce^{3+},RE^{3+}, a material commonly used in thermoluminescence dosimetry, Bos *et al.* measured glow curves for different lanthanide codopants [36]. The trap depths obtained in this way (estimated using the different analysis techniques discussed in chapter 5) are shown in figure 3.9, together with the predicted depth using the energy level scheme by Dorenbos. Although this is not a Eu^{2+}-based compound, these results seem to confirm that the codopant ions play the role of traps in at least some materials. We can conclude that experimental backup for the different suggested models is very scarce and often indecisive. Further measurements are vital to unravel the mysteries surrounding the persistent luminescence mechanism.

3.7 Concluding remarks

The exact mechanisms governing persistent luminescence in materials have yet to be clarified. Intense research by several groups has produced different models, but none of these have enough experimental backup to be identified as the true afterglow mechanism. Further research, both theoretical and experimental, remains vital. The Matsuzawa model has by now lost a lot of its popularity, because of some flaws pointed out

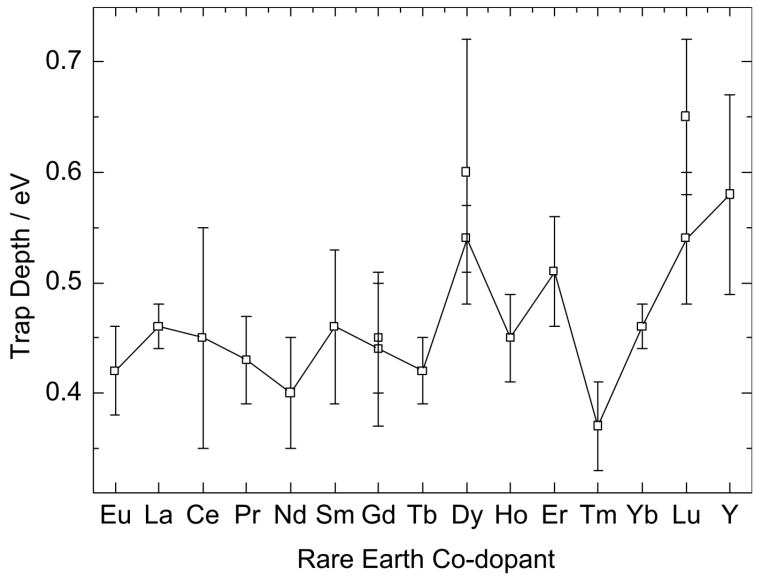

Figure 3.8: Trap depth for different codopants in $CaAl_2O_4$:Eu,RE^{3+}, estimated from thermoluminescence experiments using the Hoogenstraaten method. Reprinted with permission from [18].

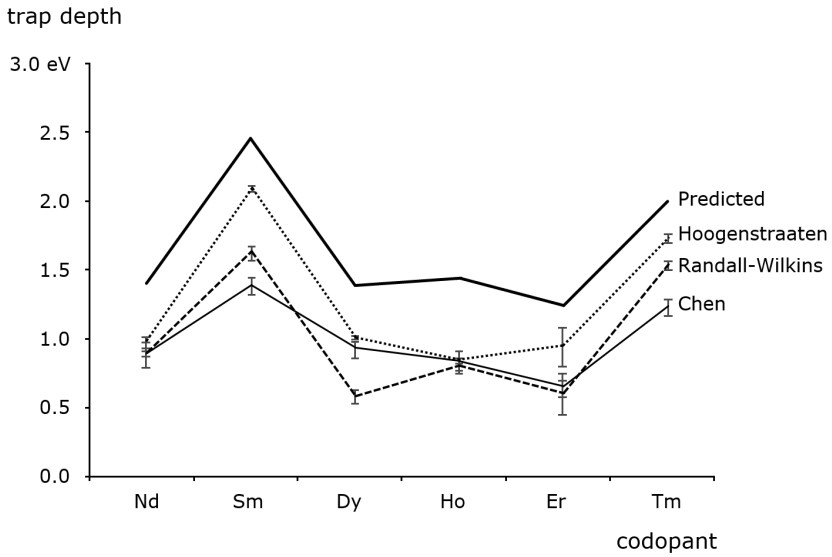

Figure 3.9: Trap depths in YPO_4:Ce^{3+} codoped with various lanthanides, as predicted by the Dorenbos energy level scheme and estimated from thermoluminescence measurements (data taken from [36]).

by several authors. The influence of lattice defects such as oxygen vacancies cannot be neglected, given the afterglow in non-codoped compounds, but it remains unclear if a similar reasoning can be used to explain persistent luminescence in other host materials such as the sulfides or nitrides.

It is nowadays generally assumed that the main charge carriers in Eu^{2+}-based compounds are electrons. This is similar to earlier models developed for binary sulfides

such as ZnS:Cu [37]. The afterglow mechanism of other sulfides was also interpreted with electron trapping, for example in $CaGa_2S_4$:Eu^{2+},Ce^{3+} [38] and CaS:Eu^{2+},Tm^{3+} [39], although for the latter a hole trapping mechanism has also been suggested [40]. However, it remains unclear how one should interpret the results found by Abbruscato and Matsuzawa that point in the direction of holes as the main charge carriers in $SrAl_2O_4$:Eu,Dy.

References

[1] Abbruscato, V. *Journal of the Electrochemical Society* **118**, 930–933 (1971).

[2] Matsuzawa, T., Aoki, Y., Takeuchi, N., and Murayama, Y. *Journal of the Electrochemical Society* **143**, 2670–2673 (1996).

[3] Jia, W., Yuan, H., Lu, L., Liu, H., and Yen, W. M. *Journal of Luminescence* **76-77**, 424–428 (1998).

[4] Sakai, R., Katsumata, T., Komuro, S., and Morikawa, T. *Journal of Luminescence* **85**, 149–154 (1999).

[5] Jia, W., Yuan, H., Holmstrom, S., Liu, H., and Yen, W. M. *Journal of Luminescence* **83-84**, 465–469 (1999).

[6] Yuan, H., Jia, W., Basun, S. A., Lu, L., Meltzer, R. S., and Yen, W. M. *Journal of The Electrochemical Society* **147**, 3154–3156 (2000).

[7] Nag, A. and Kutty, T. R. N. *Journal of Alloys and Compounds* **354**, 221–231 (2003).

[8] Lin, Y., Tang, Z., and Zhang, Z. *Materials Letters* **51**, 14–18 (2001).

[9] Lin, Y., Zhang, Z., Tang, Z., Wang, X., Zhang, J., and Zheng, Z. *Journal of the European Ceramic Society* **21**, 683–685 (2001).

[10] Jiang, L., Chang, C., and Mao, D. *Journal of Alloys and Compounds* **360**, 193–197 (2003).

[11] Nakazawa, E. and Mochida, T. *Journal of Luminescence* **72-74**, 236–237 (1997).

[12] Yamamoto, H. and Matsuzawa, T. *Journal of Luminescence* **72-74**, 287–289 (1997).

[13] Kato, K., Tsutai, I., Kamimura, T., Kaneko, F., Shinbo, K., Ohta, M., and Kawakami, T. *Journal of Luminescence* **82**, 213–220 (1999).

[14] Jia, W., Yuan, H., Lu, L., Liu, H., and Yen, W. M. *Journal of Crystal Growth* **200**, 179–184 (1999).

[15] Nakamura, T., Matsuzawa, T., Rowlands, C. C., Beltran-Lopez, V., Smith, G. M., and Riedi, P. C. *Journal of the Chemical Society, Faraday Transactions* **94**, 3009–3012 (1998).

[16] Nakamura, T., Kaiya, K., Takahashi, N., Matsuzawa, T., Rowlands, C. C., Beltran-Lopez, V., Smith, G. M., and Riedi, P. C. *Journal of Materials Chemistry* **10**, 2566–2569 (2000).

[17] Nakamura, T., Kaiya, K., Takahashi, N., Matsuzawa, T., Ohta, M., Rowlands, C. C., Smith, G. M., and Riedi, P. C. *Physical Chemistry Chemical Physics* **3**, 1721–1723 (2001).

[18] Aitasalo, T., Deren, P., Hölsä, J., Jungner, H., Krupa, J.-C., Lastusaari, M., Legendziewicz, J., Niittykoski, J., and Stręk, W. *Journal of Solid State Chemistry* **171**, 114–122 (2003).

[19] Kröger, F. A. and Vink, H. H. *Relations between the concentrations of imperfections in crystalline solids*. Academic Press, San Diego, CA, USA (1956).
[20] Palilla, F. C., Levine, A. K., and Tomkus, M. R. *Journal of The Electrochemical Society* **115**, 642–644 (1968).
[21] Dorenbos, P. *Journal of The Electrochemical Society* **152**, H107–H110 (2005).
[22] Aitasalo, T., Hölsä, J., Jungner, H., Lastusaari, M., and Niittykoski, J. *Journal of Luminescence* **94-95**, 59–63 (2001).
[23] Dorenbos, P. *Journal of Luminescence* **108**, 301–305 (2004).
[24] Dorenbos, P. *physica status solidi (b)* **242**, R7–R9 (2005).
[25] Aitasalo, T., Hölsä, J., Jungner, H., Krupa, J.-C., Lastusaari, M., Legendziewicz, J., and Niittykoski, J. *Radiation Measurements* **38**, 727–730 (2004).
[26] Dorenbos, P. *Journal of Physics: Condensed Matter* **15**, 8417–8434 (2003).
[27] Clabau, F., Rocquefelte, X., Jobic, S., Deniard, P., Whangbo, M. H., Garcia, A., and Le Mercier, T. *Chemistry of Materials* **17**, 3904–3912 (2005).
[28] Clabau, F., Rocquefelte, X., Le Mercier, T., Deniard, P., Jobic, S., and Whangbo, M. H. *Chemistry of Materials* **18**, 3212–3220 (2006).
[29] Clabau, F., Rocquefelte, X., Jobic, S., Deniard, P., Whangbo, M. H., Garcia, A., and Le Mercier, T. *Solid State Sciences* **9**, 608–612 (2007).
[30] Aitasalo, T., Hölsä, J., Jungner, H., Lastusaari, M., and Niittykoski, J. *The Journal of Physical Chemistry B* **110**, 4589–4598 (2006).
[31] Qiu, J., Kawasaki, M., Tanaka, K., Shimizugawa, Y., and Hirao, K. *Journal of Physics and Chemistry of Solids* **59**, 1521–1525 (1998).
[32] Qi, Z., Shi, C., Liu, M., Zhou, D., Luo, X., Zhang, J., and Xie, Y. *physica status solidi (a)* **201**, 3109–3112 (2004).
[33] Carlson, S., Hölsä, J., Laamanen, T., Lastusaari, M., Malkamäki, M., Niittykoski, J., and Valtonen, R. *Optical Materials* **31**, 1877–1879 (2009).
[34] Hölsä, J., Laamanen, T., Lastusaari, M., Malkamäki, M., Welter, E., and Zajac, D. A. *Spectrochimica Acta Part B: Atomic Spectroscopy* **65**, 301–305 (2010).
[35] Hölsä, J., Aitasalo, T., Jungner, H., Lastusaari, M., Niittykoski, J., and Spano, G. *Journal of Alloys and Compounds* **374**, 56–59 (2004).
[36] Bos, A. J. J., Dorenbos, P., Bessière, A., and Viana, B. *Radiation Measurements* **43**, 222–226 (2008).
[37] Hoogenstraaten, W. *Philips Research Reports* **13**, 515–693 (1958).
[38] Najafov, H., Kato, A., Toyota, H., Iwai, K., Bayramov, A., and Iida, S. *Japanese Journal of Applied Physics* **41**, 2058–2065 (2002).
[39] Jia, D., Jia, W., Evans, D. R., Dennis, W. M., Liu, H., Zhu, J., and Yen, W. M. *Journal of Applied Physics* **88**, 3402–3407 (2000).
[40] Jia, D., Zhu, J., and Wu, B. *Journal of the Electrochemical Society* **147**, 386–389 (2000).

Part II

Mechanism of persistent luminescence

4 Trapping and detrapping kinetics

Some of the results of this chapter have been published in:

- **Luminescence and x-ray absorption measurements of persistent $SrAl_2O_4$:Eu,Dy powders: Evidence for valence state changes**
  Katleen Korthout, Koen Van den Eeckhout, Jonas Botterman, Sergey Nikitenko, Dirk Poelman and Philippe F. Smet
  Physical Review B **84** (2011) 085140

- **Temperature and wavelength dependent trap filling in $M_2Si_5N_8$:Eu (M = Ca, Sr, Ba) persistent phosphors**
  Philippe F. Smet, Koen Van den Eeckhout, Adrie J.J. Bos, Erik van der Kolk and Pieter Dorenbos
  Journal of Luminescence **132** (2012) 682-689

The XANES analysis in this chapter (section 4.2.4) is part of the PhD research: "Site selective spectroscopy of rare earth doped luminescent materials", conducted by Katleen Korthout (LumiLab research group) and was performed at the DUBBLE beamline BM26 at the ESRF in Grenoble, France.

To unravel the mechanism of persistent luminescence, we need to know what is happening inside the material during the afterglow, and also during the excitation phase. We want to know how charge carriers escape from the activators, how they move throughout the material to get caught by trap levels, and how they can be released again under the influence of thermal energy. In short, we want to know more about the kinetics of the charge carriers inside the persistent phosphor.

There are two complementary ways to find out more about these kinetics. On one hand, we can look at the behaviour of the luminescent intensity, both during and after the excitation. From the shape of these curves, and from the way this shape changes under various circumstances, we can draw conclusions on the behaviour of the charge carriers.

On the other hand, we can test our assumptions on the kinetics by building a basic model, and predicting how the associated charging and decay will behave. We can then try to modify our assumptions in order to obtain the best possible accordance between the expected and the observed behaviour.

In this chapter, these *bottom-up* and *top-down* approaches are closely intertwined. We will start by looking at the detrapping kinetics, and see how retrapping can influence

the shape of the afterglow decay. We will build some basic models to mimic the trapping kinetics and predict the shape of the emission intensity during excitation. We will probe the valence state changes of the luminescent centers during the excitation phase. Finally, we will try to make an estimate on the number of traps present in a persistent luminescent material.

4.1 Detrapping kinetics

First, we will consider the detrapping process. During the afterglow phase, there is no excitation of luminescent centers. The only charge carriers involved are those that were previously trapped, and are escaping from the trap levels they were caught at.

Even though we can describe this behaviour with a very basic three-level model, the related equations can become complicated very quickly, and it is necessary to make several assumptions in order to keep the problem manageable.

4.1.1 One trap/one center model

In the most basic model, known as the **one trap/one center** model, we only take three levels into account: the *ground state* of the luminescent center, the *trap level*, and an *excited state* which acts as an intermediate stage for the charge carriers. In practice, this excited state is a simplification of the conduction band, allowing transport between the luminescent centers and the traps. Only three processes are possible: *detrapping* (from the trap level into the excited state), *recombination* (from the excited to the ground state), and *retrapping* (from the excited state into a trap level). These three levels and three processes are shown schematically in figure 4.1.

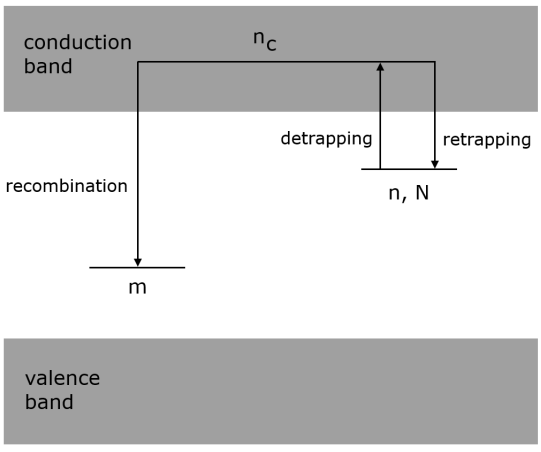

Figure 4.1: In a simple one trap/one center model, only three levels are taken into account and only three transitions are allowed: detrapping, retrapping and recombination.

The model in figure 4.1 assumes that electrons are the charge carriers, and that the transport to the traps occurs through the conduction band. However, all the equations

derived below are equally valid in the case of hole transport, and the transport does not necessarily have to happen through the conduction band.

We can write down rate equations for each of these three energy levels, based on the probability for each of the processes to occur and the occupation of each level. The details of these calculations are beyond the scope of this text, but an excellent explanation can be found in [1]. By assuming charge neutrality, time and temperature independence of the charge carriers concentrations and quasi-equilibrium (the free electron concentration in the excited level is quasi-stationary), we can derive the **General One Trap** (GOT) expression for the emission intensity:

$$I(t,T) = ns\exp\left(-\frac{E_T}{kT}\right)\left[1 - \frac{(N-n)\sigma_n}{(N-n)\sigma_n + m\sigma_{mn}}\right] \tag{4.1}$$

In this equation, σ_{mn} is the cross section for recombination, and σ_n that for retrapping. It is the ratio between these two cross sections that will mainly influence the shape of the afterglow decay. n is the concentration of filled traps, N the total concentration of traps (both filled and unfilled), and m the concentration of ionized luminescent centers, available for recombination (hole states). As usual, s is the frequency factor, E_T is the trap depth, k is the Boltzmann constant and T is the temperature.

Since n in equation 4.1 depends on the time and temperature, the GOT expression is a rather complex differential equation. At this point, it is common to introduce approximations in order to make solving the equation more manageable.

4.1.2 First and second order kinetics

As early as 1945, Randall and Wilkins [2] made the assumption that the retrapping probability is negligible. In other words, every escaped charge carrier will recombine, and $\sigma_n = 0$. This assumption is known as **first order kinetics**, and greatly simplifies the GOT expression to

$$I = ns\exp\left(-\frac{E_T}{kT}\right) \tag{4.2}$$

If we assume a constant temperature, we can predict the shape of the afterglow decay, which in this case will have an exponential shape:

$$I(t) = I_0\exp\left[-s\exp\left(-\frac{E_T}{kT}\right)t\right] \tag{4.3}$$

The expected exponential decay is shown in figure 4.2 for various trap depths.

In practice, a simple exponential decay is rarely observed in actual persistent luminescent materials. In fact, a power-law like behaviour is much more common [3]. This means that a simple one trap/one center model without retrapping is not sufficient.

Garlick and Gibson [4] therefore explored the possibility of recombination and retrapping having an equal probability. In other words, they assumed $\sigma_n = \sigma_{mn}$. Now, the GOT expression becomes

$$I = s\cdot\frac{n^2}{N}\cdot\exp\left(-\frac{E_T}{kT}\right) \tag{4.4}$$

The fact that the intensity is now proportional to the square of the density of filled traps n is the main reason that this assumption is known as **second order kinetics**. Now,

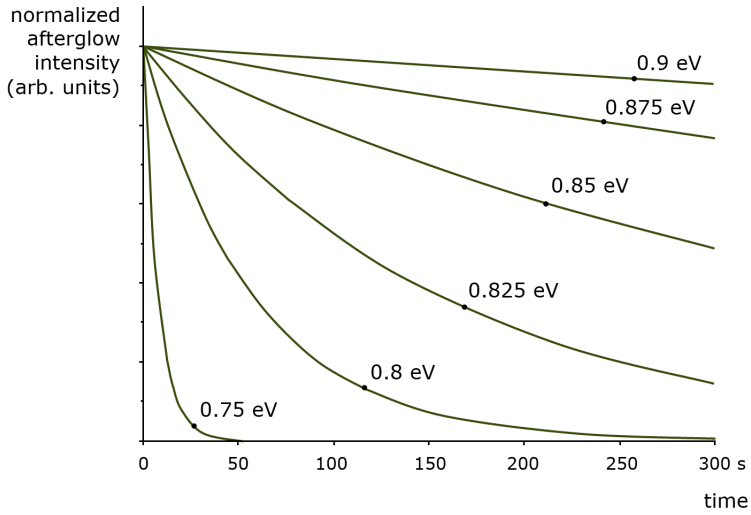

Figure 4.2: Afterglow decay in the case of first order kinetics for several different trap depths. The shape of the decay is exponential, the decay speed is determined by the trap depth. In this figure, $s = 10^{12}$ s^{-1} and T = 293 K. The curves are normalized for easy comparison.

the afterglow decay is no longer expontial, but has a power-law like behaviour:

$$I(t) = I_0 \left[1 + \frac{n_0}{N} s \exp\left(-\frac{E_T}{kT} \right) t \right]^{-2} \tag{4.5}$$

This means that, when plotted in a double-logarithmic diagram, the afterglow decay will approach a straight line with a slope of -2. The second order decay shape is shown in figure 4.3 for various trap depths. Upon comparison with the exponential first order decay (figure 4.2), we can see that the intensity approaches zero much more slowly and gradually.

4.1.3 General order kinetics

It is clear from the above discussion that first and second order kinetics refer to two very specific cases: when the retrapping probability is negligable, or when it is exactly the same as the recombination probability. For intermediate situations, May and Partridge [5] and Rasheedy [6] developed an empirical expression based on equations 4.2 and 4.4:

$$I = s \cdot \frac{n^b}{N^{b-1}} \cdot \exp\left(-\frac{E_T}{kT} \right) \tag{4.6}$$

where b is the order of kinetics.

This expression, known as **general order kinetics**, leads to a smooth transition between the decay shapes of first ($b = 1$) and second ($b = 2$) order kinetics (and beyond). This is illustrated in figure 4.4 for various orders of kinetics b.

It should be noted that the general order kinetics expression is a purely mathematical interpolation between the cases of first and second order kinetics, and that a certain order b has no direct physical meaning.

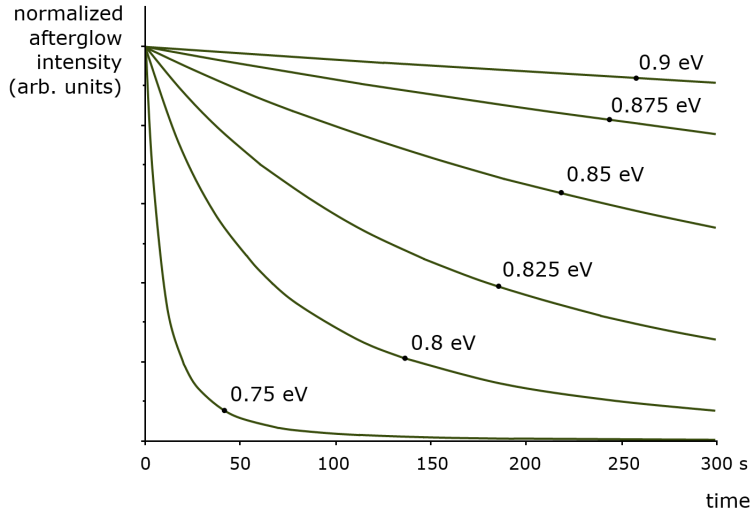

Figure 4.3: Afterglow decay in the case of second order kinetics for several different trap depths. The decay has a power-law like behaviour. On longer timescales, the decay drops to zero much slower than in the case of first order kinetics. In this figure, $s = 10^{12}$ s^{-1}, T = 293 K and $n_0/N = 1/2$. The curves are normalized for easy comparison.

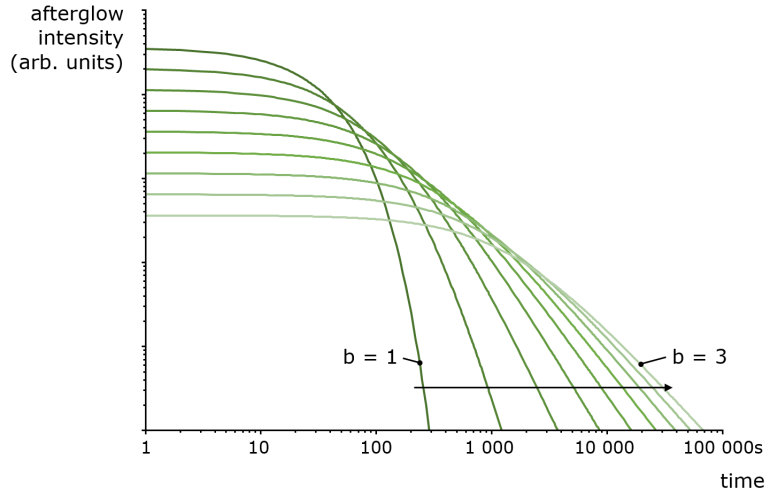

Figure 4.4: Afterglow decay for different orders of kinetics ranging from 1 to 3, assuming general order kinetics. The decay is plotted on a log-log scale. For $b = 1$, an exponential decay is obtained.

It is interesting to verify how well the general order kinetics expression compares to a more physical interpolation between the first and second order expressions. For this purpose, let us introduce the parameter R as the ratio between the retrapping and the recombination probability:

$$R = \frac{\sigma_n}{\sigma_{mn}} \tag{4.7}$$

which leads to the following simplification of the GOT expression:

$$I = s \cdot \frac{n^2}{(N-n)\cdot R + n} \cdot \exp\left(-\frac{E_T}{kT}\right) \tag{4.8}$$

If retrapping can be neglected, $R = 0$ and equation 4.8 reduces to the first order case. For equal probabilities of retrapping and recombination, $R = 1$ and the second order case is obtained.

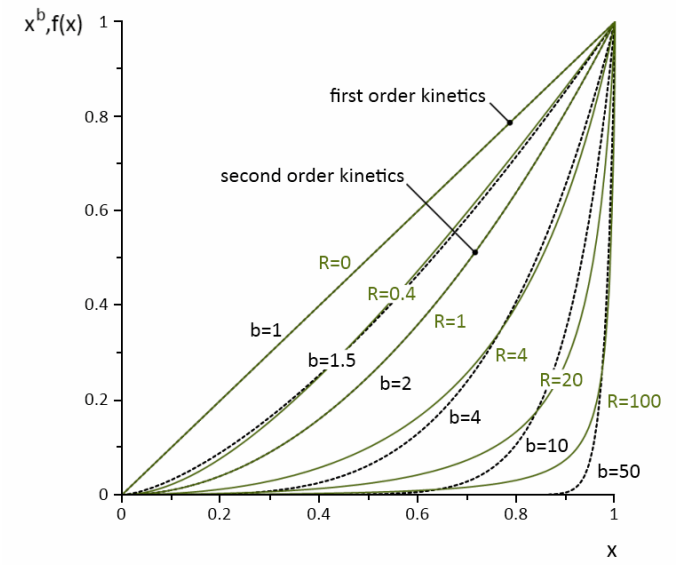

Figure 4.5: Comparison between the functions x^b and $f(x) = x^2/(R - Rx + x)$ for various values of b and R. In the case of first ($b = 1$, $R = 0$) and second ($b = 2$, $R = 1$) order kinetics, the curves overlap.

Even though equation 4.8 is difficult to solve analytically, we can make a comparison with the general order case by comparing the functions x^b (for the general order case) and $f(x) = x^2/(R - Rx + x)$ (for the more physical expression). This comparison is made in figure 4.5. The value $x = 0$ corresponds to empty traps ($n = 0$), $x = 1$ is the situation where all traps are completely filled ($n = N$).

In the case of first ($b = 1$, $R = 0$) and second ($b = 2$, $R = 1$) order kinetics the curves for x^b and $f(x)$ overlap, but for intermediate values of b, and even more for high b values, there is a clear difference between both options. In this region, fitting an experimentally obtained afterglow decay or glow peak to a curve predicted by general order kinetics will yield less accurate results.

4.1.4 Influence of the excitation intensity

Figure 4.6 shows how the afterglow decay in $SrAl_2O_4$:Eu,Dy is influenced by the excitation intensity. The sample was excited by a Xe arc lamp for 1 minute, with intensities varying from 10 to 1000 lux.

The decay profiles are not exponential, but approach a straight line in a double-logarithmic diagram, indicating at least some influence of retrapping, the presence of a continuous trap distribution, or the possibility of tunneling processes. As could be

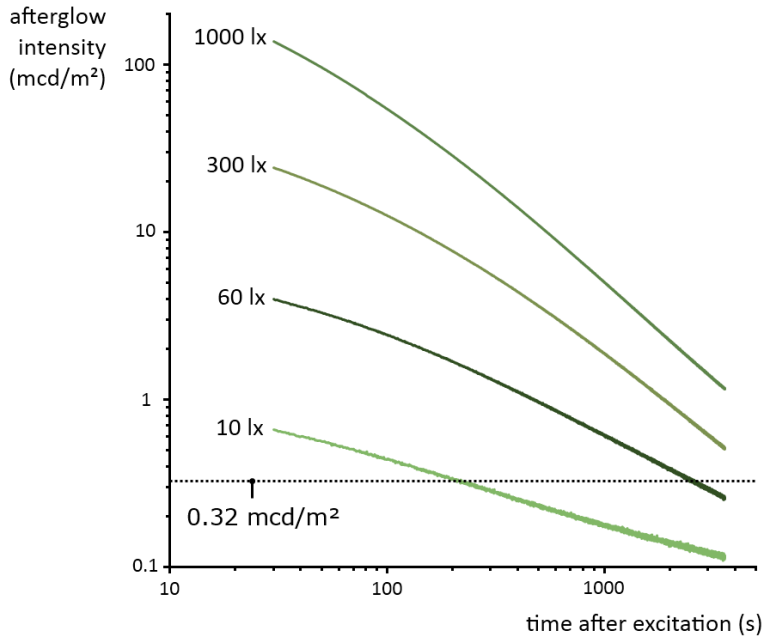

Figure 4.6: Afterglow decay in $SrAl_2O_4$:Eu,Dy for various excitation intensities of a Xe arc lamp (excited for 1 minute). At higher excitation intensities, the light output during the afterglow increases, but the decay becomes faster.

expected, the total light output increases with increasing excitation intensity, because more traps are being filled. However, a second phenomenon can also be discerned. At higher excitation intensities, the slope of the afterglow decay also increases. In other words, the decay of the luminescence becomes faster for higher excitation intensities.

To investigate this more accurately, the evolution of the light output versus the excitation intensity is plotted in figure 4.7, and the evolution of the afterglow duration, defined as the time between the end of the excitation and the moment the intensity drops below 0.32 mcd/m^2, in figure 4.8.

From figure 4.7, we can see that the light output is proportional to the excitation intensity. In other words, the number of filled traps increases linearly with increasing excitation intensity. However, the afterglow duration does not follow this trend. At around 600 lux, it reaches a saturation value of approximately 4 hours (figure 4.8).

The increasing slope of the decay tells us that the detrapping rate is increasing after excitation with higher intensities. This might mean that either shallower traps are being filled at higher excitation intensities, or that the larger number of filled traps leads to a faster detrapping.

The first explanation assumes that multiple trap levels, or even a continuous distribution of trap levels exist in the material. At low intensity, only the deeper levels would be filled, which explains the slower decay of the afterglow. However, in chapter 5 we will see that the excitation duration does not influence the depth of the traps that are filled, even in the presence of a continuous trap depth distribution. Of course, it is possible that increasing the excitation duration has a different effect on the trap filling

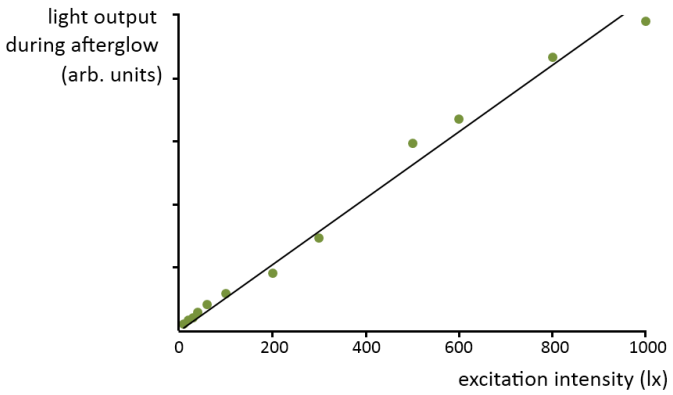

Figure 4.7: Integrated light output during the afterglow in $SrAl_2O_4$:Eu,Dy for various excitation intensities of a Xe arc lamp (excited for 1 minute). For increasing excitation intensities, the light output increases proportionally.

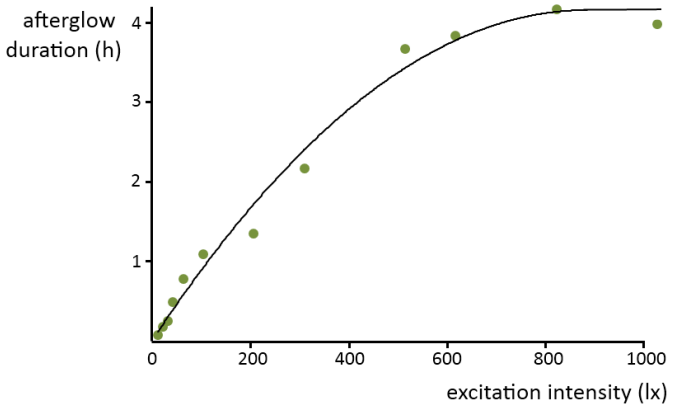

Figure 4.8: The afterglow duration in $SrAl_2O_4$:Eu,Dy for various excitation intensities of a Xe arc lamp (excited for 1 minute). For higher excitation intensities, a saturation value is reached.

than increasing the excitation intensity.

To conclude this section, it is interesting to remark that even for very low excitation intensities, charge carriers can be trapped. In figure 4.9, the emission intensity is shown for a (previously thermally emptied) $CaAl_2O_4$:Eu,Nd sample subjected to a very low excitation intensity. Even though no emission from the sample is observed during the excitation phase, thermoluminescence (TL) reveals a glow peak, indicating that at least some traps were filled by the excitation light (see section 5.1.1 for an explanation of thermoluminescence). This observation indicates a remarkably high trapping probability in $CaAl_2O_4$:Eu,Nd, which will be confirmed in section 4.2.1.

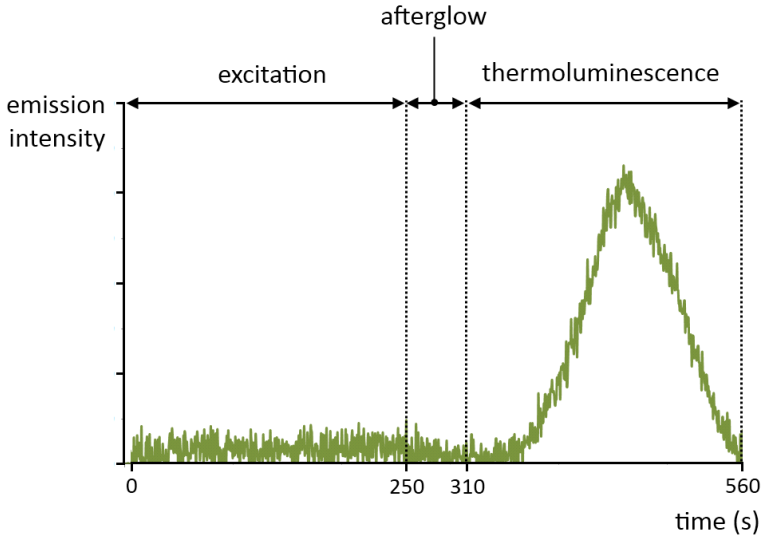

Figure 4.9: Emission intensity of $CaAl_2O_4$:Eu,Nd during and after the excitation with very low intensity, and during a subsequent thermoluminescence measurement. Even at these very low intensities, when no emission is visible during the excitation, some of the traps in $CaAl_2O_4$:Eu,Nd can be filled, as can be seen from the TL emission. The TL was measured from room temperature to 550 K with a heating rate of 1 K/s.

4.2 Trapping kinetics

In this section, we will look at the behaviour of the emission intensity during the excitation phase. As discussed in section 1.2.2, the emission intensity does not immediately jump to a constant value. Instead, it slowly increases until a saturation value is reached.

If we want to describe this behaviour, the same principles apply as in the case of detrapping. However, we have an additional factor that greatly complicates the analysis: the excitation intensity. Solving the rate equations becomes impractical, and it is more useful to turn to some simulations to explain the observed charging behaviour.

4.2.1 Simulating trapping processes

The emission intensity during the excitation of the persistent luminescent materials in the following section was measured using an Ocean Optics QE65000 portable spectrometer equipped with an optical fiber. The samples were excited by filtered Xe-lamp light (the wavelengths between 400 and 700 nm were filtered out). The intensity of the light could be varied by using suitable quartz grey filters.

Compared to the study of the afterglow intensity, the rate equations necessary to describe the emission intensity during the excitation contain an additional term, the excitation strength. Because of this term, it quickly becomes extremely difficult (if not impossible) to analytically solve the system of rate equations. For that reason, we chose to simulate the behaviour of the emission intensity during the excitation numerically, rather than calculating it mathematically.

The simulation results were obtained by converting the presented models to a Microsoft Excel® worksheet. At $t = 0$, all traps are supposed to be empty, and all Eu ions are in the divalent, non-excited ground state. For each discrete time step, the electrons are assumed to have a certain probability to undergo either excitation, trapping, detrapping, or recombination. Using this information, the number of electrons in each state (ground state, excited state, trapped state) is calculated based on the information from the previous time step. The number of recombining electrons at each time step is a measure for the emission intensity, since only these transitions can give rise to the emission of a photon (non-radiative transitions are not taken into account).

By varying the excitation, (de)trapping and recombination probabilities, the simulated emission intensity behaviour can be fitted to the experimentally observed emission intensity. This was done using the built-in 'solver' function of Microsoft Excel®.

Trapping in $Sr_2MgSi_2O_7$:Eu,Dy

Figure 4.10 shows the emission intensity of a $Sr_2MgSi_2O_7$:Eu,Dy sample during excitation with filtered Xe-lamp light. Initially, when the first photons hit the sample and all traps are still empty, the trapping process dominates the normal luminescence. Only after a few minutes the traps are largely filled. The trapping and detrapping will now balance each other, and the normal luminescence will dominate over the trap filling.

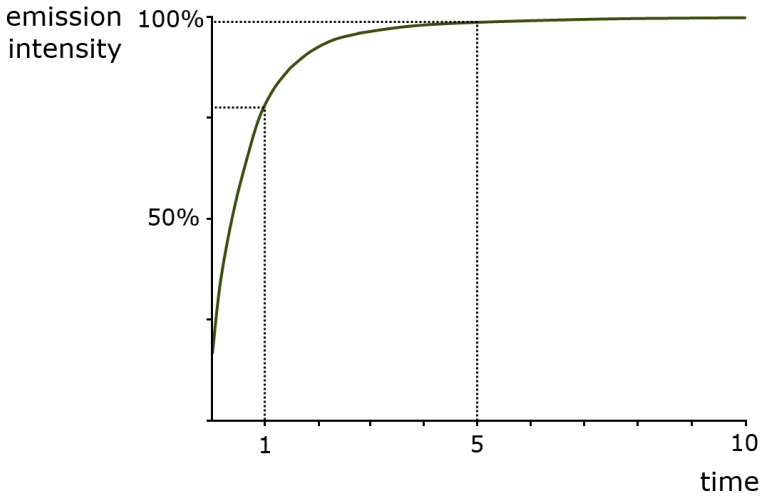

Figure 4.10: Emission intensity of $Sr_2MgSi_2O_7$:Eu,Dy during the excitation by filtered Xe-lamp light. The emission intensity increases as a function of the excitation intensity until a saturation value is reached.

We can use the simple model in figure 4.11 to explain this behaviour. It is basically the same as the one trap/one center model, but with the addition of a possible transition from the ground state of the luminescent ion to the excited state. Once an electron is excited, it can either get caught by a trap level, or recombine by returning to the ground state.

Only a few parameters are required in this model. The trapping probability p is assumed to depend on the fraction of filled traps. If all traps are empty, it will have

its maximum value of p_0. If all traps are filled, $p = 0$. The detrapping probability p' is assumed to be independent of the fraction of filled traps. In this way, the trapping probability will continuously decrease as the traps are getting filled, until it finally reaches a balance with the (small) detrapping probability. Note that the trap depth is not explicitly introduced into this model, but that it is integrated in the detrapping probability p'. A deeper trap will have a much lower detrapping probability than a shallower trap. Besides p and p', we will also need a parameter describing the excitation strength.

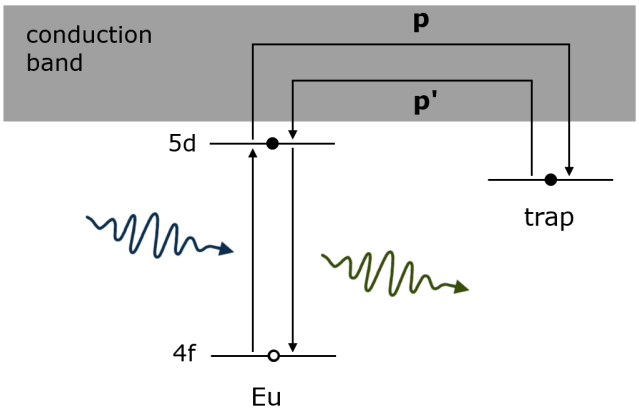

Figure 4.11: Simplified model with one trap level used to simulate the emission intensity of $Sr_2MgSi_2O_7$:Eu,Dy during excitation. The trapping probability p depends on the fraction of filled traps, the detrapping probability p' doesn't.

The shape of the emission intensity that is obtained using this simple model is in good agreement with the measured intensity in figure 4.10. Figure 4.12a shows a comparison between the experimental data and a simulated emission intensity fitted to these data. From this, we find a maximum trapping probability p_0 of around 80.3%, and a negligible detrapping probability p' of only 0.06%.

Even at lower excitation intensity (about 50% of the original intensity), using these same trapping and detrapping parameters obtained from our first fit, we find an excellent agreement between the observed and simulated emission intensity during excitation (figure 4.12b).

In figure 4.12b, and also to a lesser extent in figure 4.12a, it can be seen that the emission intensity does not start from zero at the start of the excitation. Instead, an initial 'jump' of about 20% of the saturation value is observed. In fact, this intial jump is present for all excitation intensities, and always has this same value of 20% (figure 4.13).

The explanation of this 'initial jump' is straightforward and intuitive. At the start of the excitation, when all traps are still empty, the first photons hitting the sample have a chance of $p_0 \approx 80\%$ to induce trapping. Therefore, there is a chance of $1 - p_0 \approx 20\%$ that the excited electron will simply recombine instead of getting trapped (figure 4.14). This does not necessarily mean that every single excited ion has an 80% chance to lead to

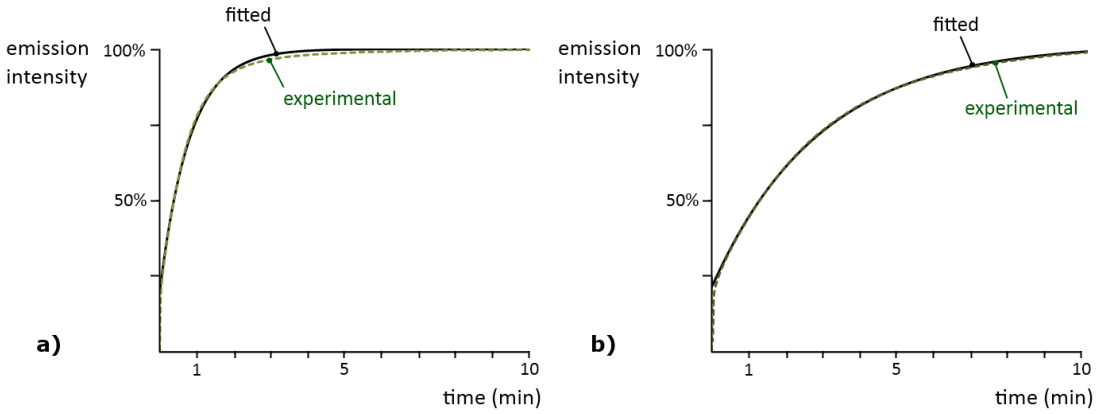

Figure 4.12: (a) Comparison between the observed and simulated emission intensity in $Sr_2MgSi_2O_7$:Eu,Dy during excitation. (b) Even at lower excitation intensity, and assuming the same fitting parameters, the agreement is very good.

trapping and a 20% chance to lead to recombination. It could be possible that different sites for the activating ions exist in the material, some of which always participate to the trapping process while others don't. Then, the combined effect of all activators also leads to a certain trapping probability. In $Sr_2MgSi_2O_7$:Eu,Dy, we found a maximum trapping probability of $p \approx 80\%$, which is perfectly consistent with the observed initial jump of about 20%.

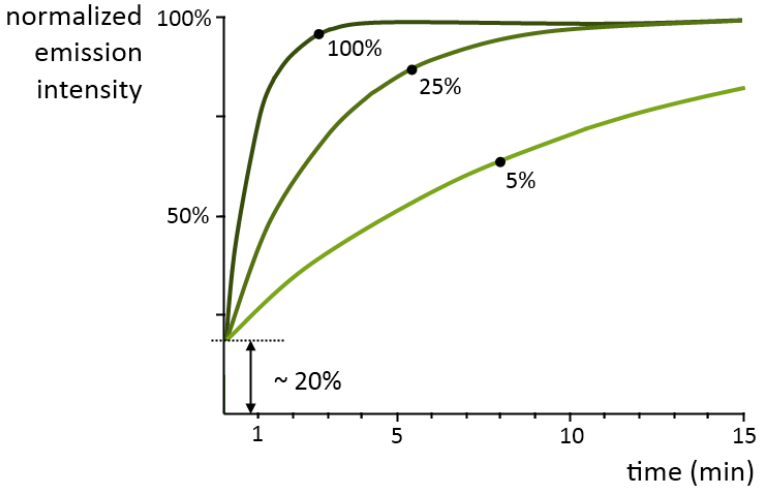

Figure 4.13: Emission intensity of $Sr_2MgSi_2O_7$:Eu,Dy for increasing excitation intensity (5%, 25% or 100% of the maximum intensity). Independant of the excitation strength, the emission shows an initial 'jump' of about 20%.

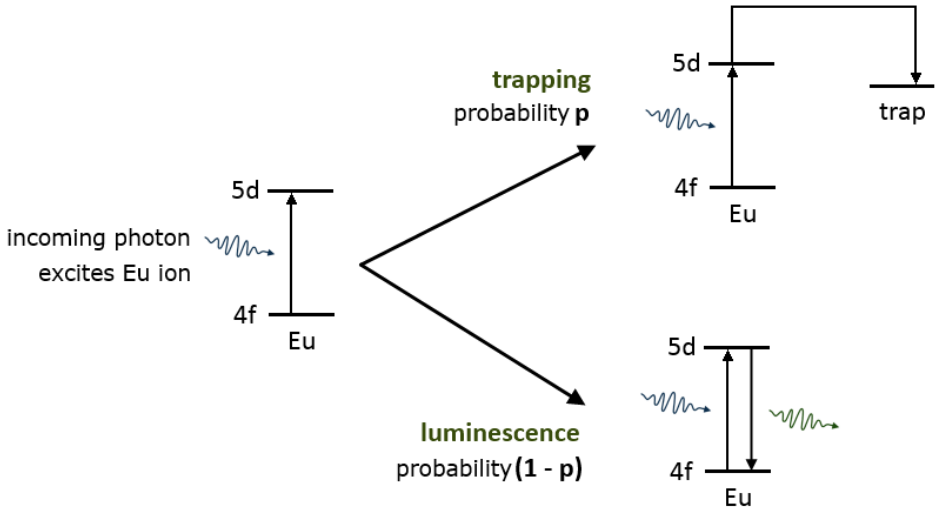

Figure 4.14: Explanation for the initial jump observed in the emission intensity of $Sr_2MgSi_2O_7$:Eu,Dy during excitation. From the very start of the excitation, every incoming photon has a certain chance to lead to trapping and a certain chance to lead to recombination.

Trapping in $CaAl_2O_4$:Eu,Nd

If we look at the emission intensity during excitation in a $CaAl_2O_4$:Eu,Nd sample, shown in figure 4.15, we see a more complicated shape. Rather than a steep increase of the luminescence, we observe an S-like behaviour at the start of the excitation. Also, the initial jump is much smaller than in the $Sr_2MgSi_2O_7$:Eu,Dy sample.

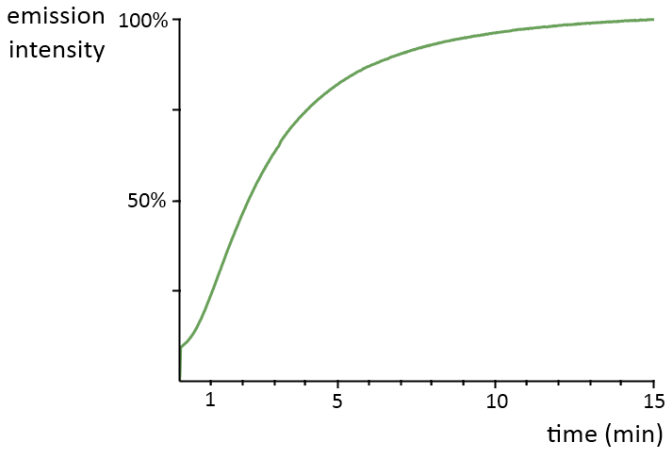

Figure 4.15: Emission intensity of $CaAl_2O_4$:Eu,Nd during the excitation by filtered Xe-lamp light. The emission intensity shows an S-like shape with only a small initial jump.

This S-shape cannot be simulated with our basic model from figure 4.11. However, we can introduce a second trap level at a different depth, as depicted in figure 4.16. Now, we need a separate detrapping probability p_1' and p_2' for each of the trap levels. For the

deeper trap, the detrapping probability will be much lower than for the shallower trap, since less thermal energy is required to escape. The trapping probability p is assumed to be the same for both trap levels, but it still depends on the fraction of traps that is filled.

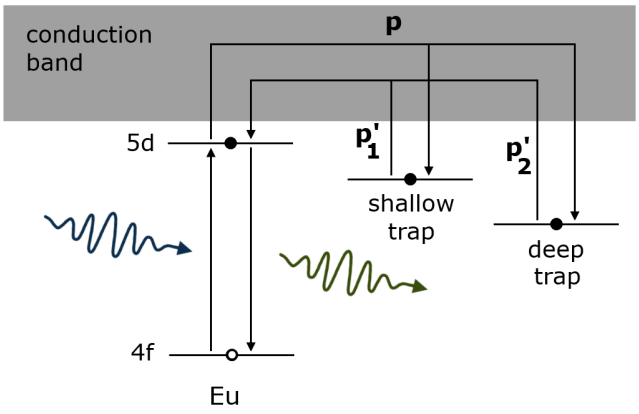

Figure 4.16: Simplified model with two trap levels used to simulate the emission intensity of $CaAl_2O_4$:Eu,Nd during excitation.

The emission intensity can again be fitted very accurately (figure 4.17a). Interestingly enough, the trapping probability in this case is nearly 100%, which explains the very small initial jump at the start of the excitation. The detrapping probability of the shallow trap is again very small, around 0.11%. The deeper trap has a detrapping probability of 0%. In practice, no charge carriers can escape from these deeper traps in a reasonable amount of time, at least not at room temperature.

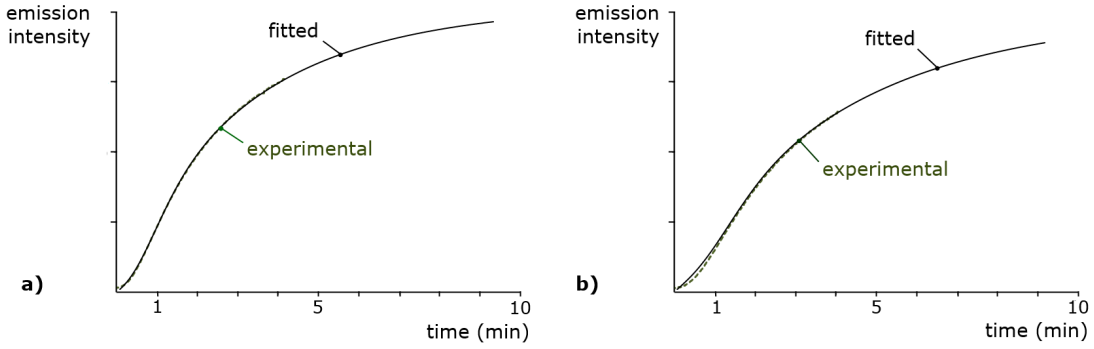

Figure 4.17: (a) Observed and simulated emission intensity in $CaAl_2O_4$:Eu,Nd during excitation. (b) Even at lower excitation intensity, and assuming the same fitting parameters, the agreement is very good.

Again, using the same parameters, we can also accurately fit the emission during excitation at lower intensity (about 50% of the original intensity, figure 4.17b). Only at the very start of the excitation, the simulated emission intensity is a bit higher than the observed one.

The simulation also gives us the number of filled shallow and deep traps at each moment. This is depicted in figure 4.18 as a percentage of the final number of filled

traps for each level. While the filling of the deep traps continues for several minutes until saturation is reached, the shallow traps reach their saturation value relatively quickly. After reaching a maximum, the number of filled shallow traps starts to drop again, as charge carriers are released and trapped again by the deeper traps, from which they cannot escape.

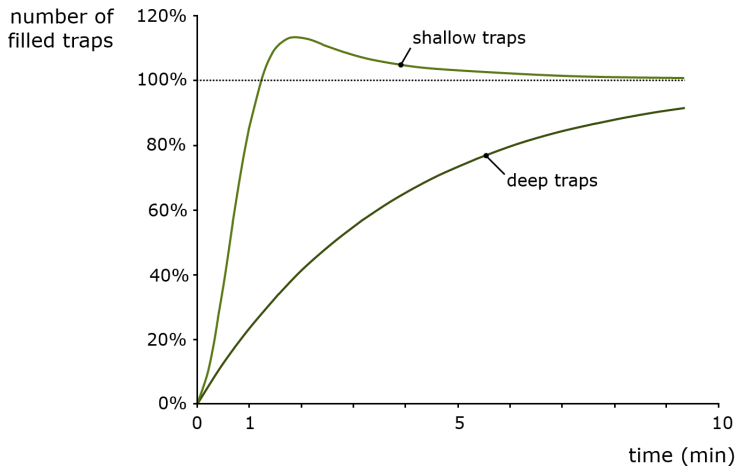

Figure 4.18: Fraction of filled shallow and deep traps (compared to their saturation value) simulated using the simple two-trap model from figure 4.16. The shallow traps reach their saturation value much faster than the deep traps.

Although figure 4.18 might suggest that the trap filling rate of the shallow traps is initially much higher than that of the deep traps, this is not the case. In fact, the simulation results show that the final number of filled deep traps is much higher than the final number of filled shallow traps (about 60 times higher). Therefore, the number of charge carriers per second being trapped in a deep trap is much higher than those being trapped in a shallow trap level.

We can conclude that even with very simple models, it is possible to accurately simulate the observed emission intensity behaviour. These simulations can give us an idea of the rates at which different traps inside the material are filled. In the next section, we will attempt to derive the same information by looking at only the measured emission intensity.

4.2.2 Radioluminescence and x-ray absorption

For the experiments described in the following two sections, $SrAl_2O_4$:Eu,Dy samples were subjected to x-ray radiation. Therefore, it might be instructive to explain what we can learn by exciting a persistent phosphor with x-ray radiation.

On one hand, the exposure of a persistent phosphor to an x-ray beam will induce the emission of light in a way very simular to normal photoluminescence. This phenomenon is called **radioluminescence** (RL). The energy of the x-ray photons is considerably larger than that of UV or visible light, and also leads to the trapping of charge carriers. Indeed,

the radioluminescent intensity during the excitation shows the same typical behaviour as the photoluminescent intensity during the trap filling.

On the other hand, by varying the energy of the x-ray irradiation, the internal structure of the persistent luminescent material can be investigated. In a XANES (X-ray Absorption Near-Edge Structure) measurement, the exact shape and location of the absorption edge of a certain element are studied in detail. This is especially useful if we are interested in the valence state of certain elements, since the absorption edge has a slightly different location for the different valences.

The x-ray measurements in the following sections were carried out at the Dutch-Belgian beam line (DUBBLE, BM26A) of the European Synchrotron Radiation Facility (ESRF) in Grenoble, France operating with a 160-200-mA electron current.

4.2.3 Measuring the trap filling rate under x-ray irradiation

Figure 4.19 shows the RL intensity of an $SrAl_2O_4$:Eu,Dy sample under x-ray irradiation at 120 K. The shape of the emission intensity is comparable to that under normal UV excitation. The inset shows the radioluminescence for consecutive cycles of irradiation, thermal cleaning of the traps, and cooling. Since the intensity is identical for each measurement, this proves that the optical properties of the sample are not damaged by the x-ray irradiation.

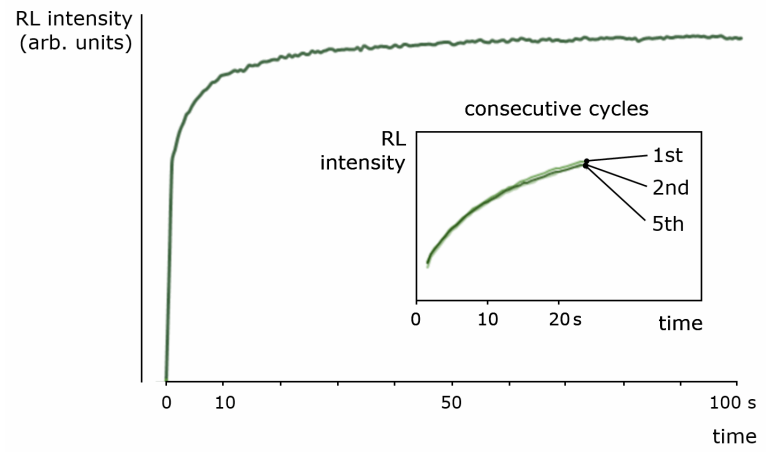

Figure 4.19: Luminescence intensity of $SrAl_2O_4$:Eu,Dy as a function of the x-ray irradiation time at 120 K, after the sample was thermally emptied and kept in the dark prior to the irradiation.

As in the case of UV excitation, the emission intensity increases rapidly and continues to grow until a stationary regime is reached after approximately two minutes. At this moment the maximum number of charge traps is filled. The measurement temperature of 120 K is sufficiently low to keep all trap levels filled due to the lack of thermal energy to induce the detrapping leading to the afterglow.

The time evolution of the RL intensity $I_{RL}(t)$ can be expressed as a function of the final $I_{RL,f}$ when all traps are filled and the RL intensity reaches a constant value

$$I_{RL}(t) = I_{RL,f}\,(1 - F(t)) \tag{4.9}$$

The function $F(t)$, as derived from the RL-intensity profile, is shown in figure 4.20. It describes how many excitations in the phosphor are *not* used for luminescence, but instead lead to the filling of trap states. It can be approximated by two exponentially decaying components, so that

$$F(t) = A_1 \exp\left(-\frac{t}{\tau_1}\right) + A_2 \exp\left(-\frac{t}{\tau_2}\right) \tag{4.10}$$

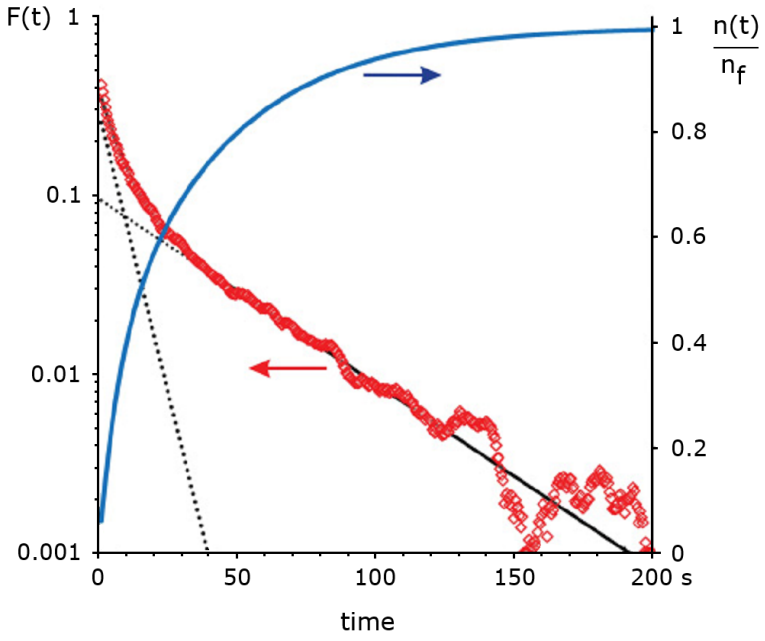

Figure 4.20: Evolution of the trap filling rate $F(t)$ in $SrAl_2O_4$:Eu,Dy as a function of x-ray irradiation time at 120 K, obtained from the RL intensity profile. Two exponentials (dotted lines) were fit to the experimental data points (red diamonds). The blue curve shows the fraction $n(t)/n_f$ of filled traps.

The origin of these two exponential components is probably related to two different types of trap centers. Fitting $F(t)$ to the trap-filling profile yields values of 7 and 42 s for τ_1 and τ_2. The total number n of trapped charge carriers at a given time t is proportional to

$$n(t) \approx \int_0^t \left[A_1 \exp\left(-\frac{\theta}{\tau_1}\right) + A_2 \exp\left(-\frac{\theta}{\tau_2}\right)\right] \mathrm{d}\theta = \tau_1 A_1 \left[1 - \exp\left(-\frac{t}{\tau_1}\right)\right] + \tau_2 A_2 \left[1 - \exp\left(-\frac{t}{\tau_2}\right)\right] \tag{4.11}$$

This is only valid on the condition that (i) there is no thermal emptying of the traps during the illumination and (ii) no tunneling, or other nonradiative recombination occurs. The former is ensured by the low measurement temperature, while the latter losses are negligible due to the short time scale of the measurements, certainly in comparison to the long-lasting afterglow of $SrAl_2O_4$:Eu,Dy. The time dependency of $n(t)$ is shown in figure 4.20. After sufficiently long illumination (i.e., $t \gg \tau_1, \tau_2$) all traps are filled and we find

$$n(t) \to n_f = \tau_1 A_1 + \tau_2 A_2 \tag{4.12}$$

From the trap filling profile, we can derive that half of the traps are filled after only 15 seconds of x-ray illumination. After 80 seconds 90% of all available traps are filled. These short time scales have important implications if one wants to use x-ray absorption techniques for studying the charge carrier dynamics in persistent phosphors, as will be discussed in the following section.

4.2.4 In situ monitoring of valence state changes using XANES

To determine the valence state of the Eu activators in $SrAl_2O_4$:Eu,Dy, XANES measurements were performed at the L_{III} absorption edge of Eu, which is located roughly around 6970 eV. The spectra were recorded in the energy range 6.78-7.03 keV, with an energy step of typically 1 eV. They were collected in fluorescence mode (because of the low dopant concentration) by monitoring the Eu Lα_1 peak fluorescence lines (centered around 5.85 keV) using a 9-element monolithic Ge detector.

The Eu L_{III} edge shows a double peak, because the white lines for divalent and trivalent Eu ions are slightly shifted relative to each other. The L_{III} edge for Eu^{2+} is located at about 6972 eV, while that of Eu^{3+} is located around 6980 eV. Therefore, if we look at the shape of the absorption edge and the relative intensity of both absorption peaks we can study the valence states of the Eu ions present in the sample.

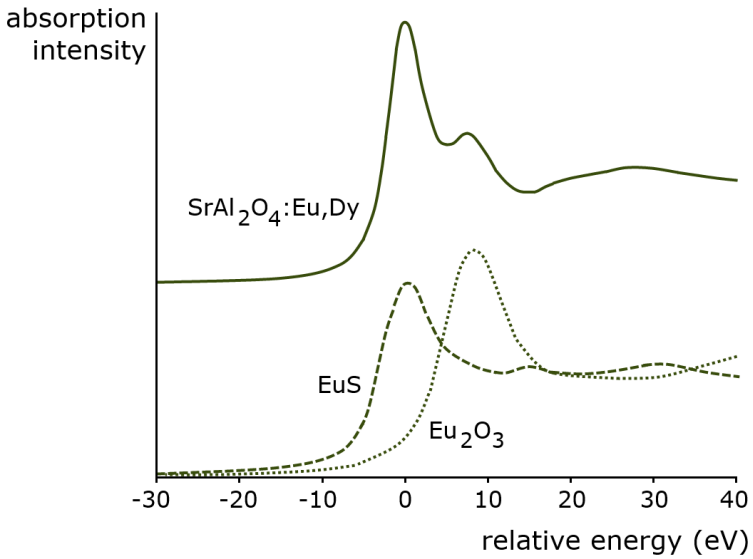

Figure 4.21: Eu L_{III} XANES spectrum of $SrAl_2O_4$:Eu,Dy at 120 K. EuS and Eu_2O_3 were measured as reference compounds. Zero of the relative energy scale is set at the position of the Eu^{2+} resonance. The spectra are shifted vertically for clarity. These spectra show that $SrAl_2O_4$:Eu,Dy contains both divalent and trivalent Eu ions.

An example of such a XANES spectrum for $SrAl_2O_4$:Eu,Dy is shown in figure 4.21, together with the XANES spectrum of two reference samples EuS and Eu_2O_3. As can be seen, the EuS sample contains purely divalent Eu, while the Eu_2O_3 sample contains

almost exclusively trivalent Eu. The $SrAl_2O_4$:Eu,Dy sample contains a mixture of both valence states.

We can now study how the ratio between these two peaks changes as a result of the excitation. If it is true that the trapped charge carriers are electrons, coming from the Eu luminescent centers, we should be able to see a decrease in the amount of Eu^{2+} during the excitation phase. Figure 4.22 shows two averaged XANES spectra of $SrAl_2O_4$:Eu,Dy. The solid line indicates an average of a collection of XANES spectra started within 10 seconds of exposure to the x-ray beam. The dotted line is an average of spectra started after 120 seconds of exposure to the beam. Even though the differences between both spectra are subtle, it can be seen that the ratio of both peaks has changed. After 120 seconds of excitation, the peak related to Eu^{3+} has increased in favor of the Eu^{2+} peak, confirming our expectations.

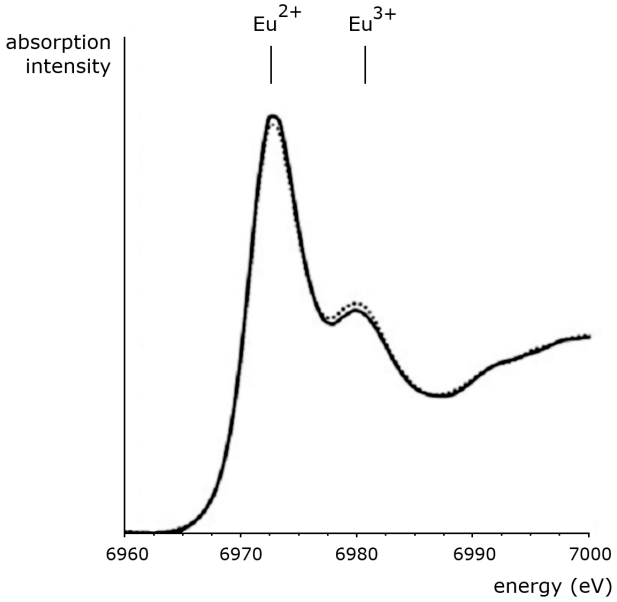

Figure 4.22: Averaged XANES spectra for Eu in $SrAl_2O_4$:Eu,Dy at 120 K started within 10 seconds (full line) and after 120 seconds (dotted line) of exposure to the x-ray beam. After 120 s excitation, the Eu^{3+} has increased in favor of the Eu^{2+} peak.

If we perform the XANES measurements very quickly, we are able to monitor the changes in the ratio between both peaks *in situ*, during the excitation phase. However, we need to be careful when performing such experiments, since the x-ray beam is both our 'pump' (to excite the sample) and our 'probe' (to monitor the valence state through XANES). We need to make sure that the sample is subjected to as little x-ray irradiation as possible, to slow down the trap filling process. Therefore, we need to perform our XANES scans as quickly as possible, on a time scale as fast as several seconds at most. Unfortunately, this comes at the expense of spectral quality and a strongly decreased signal-to-noise ratio.

We performed about 130 short measurements with varying exposure time to the x-ray beam after the thermally emptying of all traps. The exact procedure for these

measurements is beyond the scope of this text, but can be found in reference [7]. The ratio of the peak areas for both valence states is shown in figure 4.23 as a function of excitation time.

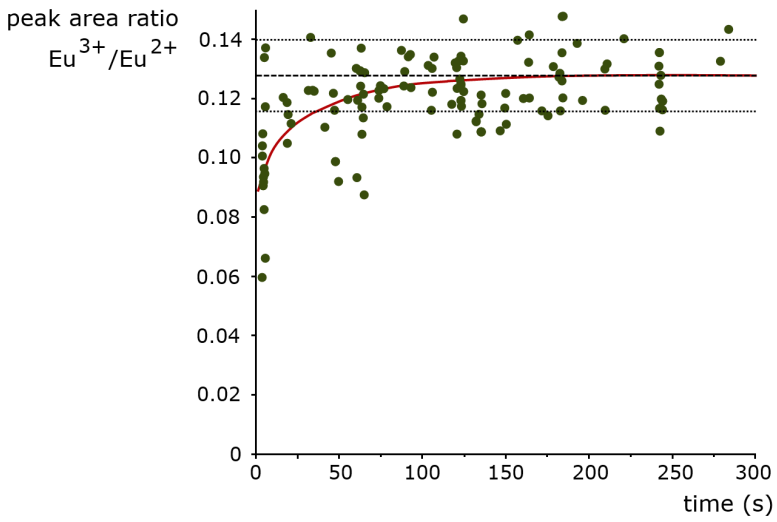

Figure 4.23: XANES peak area ratio between Eu^{3+} and Eu^{2+} as a function of x-ray irradiation time at 120 K for all separate experiments . The dashed line is the best fit assuming a constant ratio, based on all data points with t > 85 s, the dotted lines show the standard deviation (σ). The full red line is a fitted line based on the number of trapped charges as derived from the RL data.

The low signal-to-noise ratio of the measurements leads to large scatter on the data points, but an increasing trend is nevertheless visible. To disprove the hypothesis of having a constant ratio, the average peak area ratio for all data points with $t > 85$ s was calculated, along with the standard deviation σ. This is shown as a black line in figure 4.23. Despite the large scatter on the data points, the peak area ratios for the measurements with the shortest x-ray exposure time are well below this average, even when taking the large variability in the position of the data points into account. Hence, the change in peak area ratio, or alternatively, the change in valence state for a fraction of the Eu ions, can be confirmed.

For completeness, we should note that a similar change of the valence state could not be observed for other, non-persistent luminescent materials such as SrS:Eu. Also, the reproducibility of our observations during several experimental cycles show that the oxidations is not caused by irreversible degradation of the phosphor by the x-ray irradiation, as suggested by Rodrigues *et al.* [8].

The red line is a fit of equation 4.11, the function that describes the number of filled traps as a function of time, through the data points. A good agreement is found, which confirms our expectation that the Eu ions are the source for the electrons being trapped during the excitation phase.

4.2.5 Thermal activation of the trapping process

A final important property of the trapping kinetics that we will discuss is the thermal activation of the trapping process. Figure 4.24 shows the thermoluminescence (TL) glow curves of the persistent phosphor $Ba_2Si_5N_8$:Eu, excited with 285 nm light and 420 nm light. The exact details of the TL measurement will be discussed in the following chapter, but for now it suffices to understand that the area under the TL glow curve is a measure for the number of trapped charge carriers.

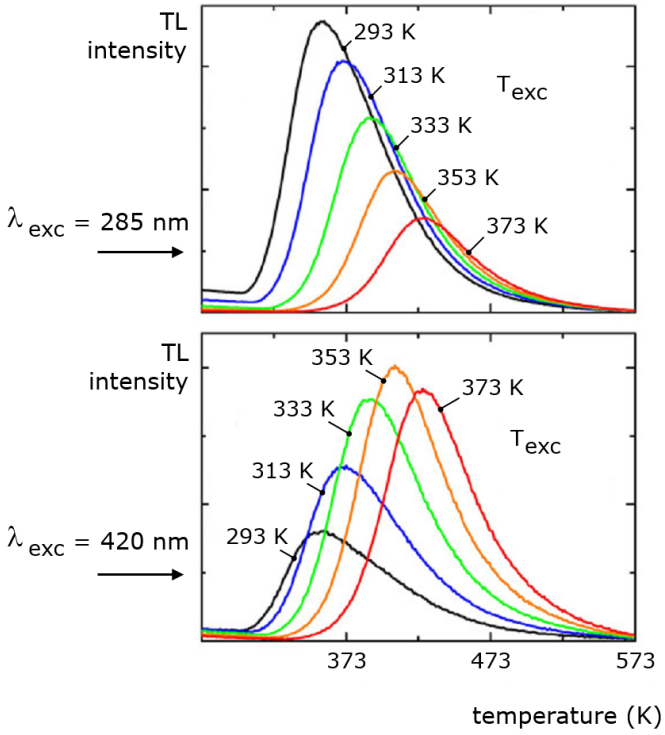

Figure 4.24: After excitation by 285 nm light, the TL intensity in $Ba_2Si_5N_8$:Eu decreases for increasing excitation temperature. After excitation by 420 nm light, this intensity first increases, and then decreases again. The heating rate in all measurements was 5 K/s.

After excitation with 285 nm, i.e. directly from the Eu ground state into the (optical) band gap, the trapping is not thermally activated. If we compare the different TL curves in figure 4.24, we see that the total number of filled traps decreases if we excite the sample at higher temperatures. This is exactly what we expect: at higher excitation temperature, more thermal energy is available, and trapped electrons will have a higher chance to escape.

If we excite the $Ba_2Si_5N_8$:Eu sample with 420 nm light, i.e. into the 5d level of Eu, the situation is different. Now, if we excite at higher temperatures, the total number of filled traps will first increase. Only at excitation temperatures above 353K, the total TL intensity will start to drop again. This means that an increase in thermal energy is beneficial for the trapping process. In other words, when exciting at longer wavelengths, the trapping process is thermally activated. Figure 4.25 gives a rudimentary representation

of this thermal activation process in $Ba_2Si_5N_8$:Eu and $CaAl_2O_4$:Eu,Nd. To construct this figure, the location of the energy levels was estimated by measuring the thermal quenching and the energy of the fd-absorption, as suggested by Dorenbos [9].

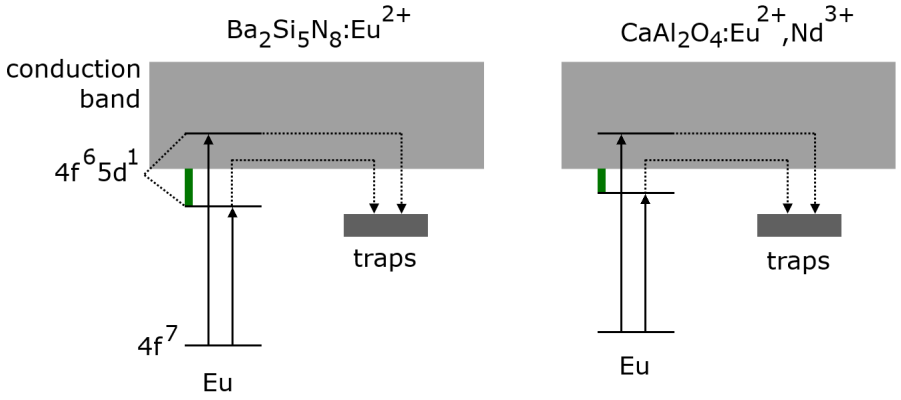

Figure 4.25: Energy level scheme for $Ba_2Si_5N_8$:Eu and $CaAl_2O_4$:Eu,Nd. The distance between the lowest 5d level and the conduction band (indicated in green) determines the thermal barrier for trapping after excitation with long wavelengths.

The main factor that determines the thermal activation of the trapping is the distance between the lowest 5d level of Eu and the conduction band. As shown in figure 4.25, this distance is much larger for $Ba_2Si_5N_8$:Eu than for $CaAl_2O_4$:Eu,Nd. For this reason, no thermal activation of the trapping is observed in the latter material (see also chapter 5). The distance between the 5d level and the conduction band also determines the thermal quenching behaviour of a luminescent material, at least according to Dorenbos [10]. Therefore, phosphors with a high quenching temperature, such as $Ba_2Si_5N_8$:Eu, will have a higher chance of having a trapping process that is thermally activated.

The presence of thermal activation for charging in persistent phosphors is undesired, since it hinders the trapping of charge carriers upon excitation with long wavelengths, i.e. visible light. Hence, when searching for Eu^{2+}-based long-wavelength persistent phosphors, we should focus on those compounds having a relatively low thermal quenching temperature, as this facilitates trap filling of the phosphors with visible light.

4.3 Number of traps

Now that we know the origin of the charge carriers and the rate at which they are trapped and detrapped, we also want to estimate their total number. More specifically, we want to estimate the number of available traps, relative to the number of available luminescent centers.

4.3.1 Increasing the excitation energy

In section 4.1.4, we saw how the light output in $SrAl_2O_4$:Eu,Dy during the afterglow is proportional to the excitation intensity. This total light output during the afterglow is a direct measure for the total number of trapped charge carriers, since (if we assume a QE of 100%) every escaped charge carriers leads to the emission of exactly one photon.

If we continue increasing the excitation intensity, by using e.g. a laser excitation source, the light output during the afterglow will eventually start saturating at a certain excitation intensity. This is shown in figure 4.26 for a sample consisting of a thin layer of $SrAl_2O_4$:Eu,Dy on a plastic substrate.

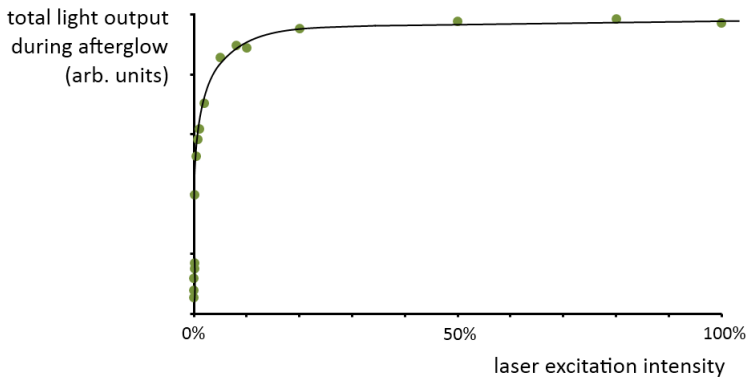

Figure 4.26: Integrated light output during the afterglow as a function of increasing excitation intensity by a 40 mW Ar laser (457 nm; spot size of 0.4 mm^2). The total light output during the afterglow reaches a saturation value at around 10% of the maximum excitation strength.

The total light output saturates because the total available number of traps has been filled. The moment where this light output starts saturating is crucial in estimating the total number of traps available in the material.

4.3.2 Estimating the number of activators

We will first calculate the number of activators in the sample. For that, we need to know the number of europium ions being excited by the laser beam (figure 4.27).

The doping ratio of the sample is 1%, which means that 1% of the Sr ions has been replaced by a Eu ion. From the material data of $SrAl_2O_4$ [11], we know that it contains 1.04×10^{19} Sr ions per mm^3. The laser spot size was measured to be 0.4 mm^2, and the layer thickness was verified by SEM to be 100 μm. We assume that the laser penetrates sufficiently far into the material at this wavelength (457 nm) to excite the entire thickness of the $SrAl_2O_4$:Eu,Dy layer.

Consequently, the volume of material excited by the laser is about 0.04 mm^3. Therefore, we can assume that a total number of 4.2×10^{15} Eu ions is present in the volume excited by the laser beam.

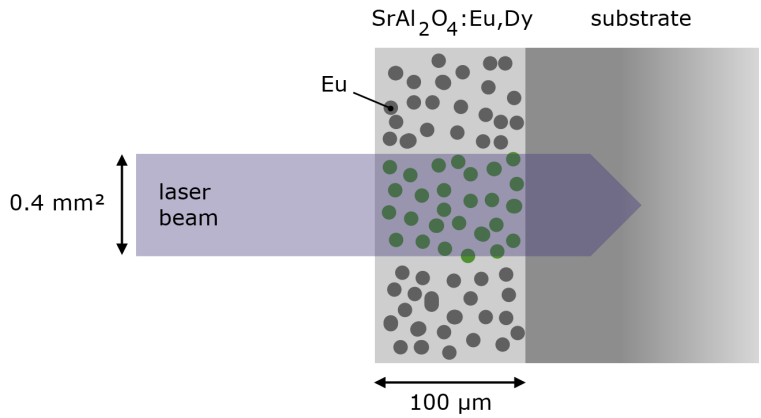

Figure 4.27: Geometry of the laser-excited sample of $SrAl_2O_4$:Eu,Dy used to determine the number of available traps in the material.

4.3.3 Estimating the number of traps

From the data of the laser excitation, we can also determine the number of photons hitting our sample. Since we used a 40 mW laser at a wavelength of 457 nm, we can estimate the number of incoming photons as 9.2×10^{16} per second.

From figure 4.26, we see that saturation of the number of traps is reached already at about 10% of the maximum laser intensity or, in other words, at 9.2×10^{15} photons per second. Since we excited the material for 30 seconds, this gives us a total number of 2.8×10^{17} photons.

We also need to take into account the quantum efficiency of the material. For this specific sample, the external QE was determined using an integrating sphere to be approximately 24%. This means that only 24% of the incoming photons will eventually lead to a radiative transition, or a total of 6.7×10^{16} photons.

Finally, we have to realize that only a fraction of these incoming photons will actually lead to trapping. Indeed, most of the photons will simply lead to excitation followed by recombination of a Eu ion, without creating a trapped charge carrier. This fraction can be estimated by looking at the emission intensity during laser excitation, as shown in figure 4.28.

The fraction of incoming photons leading to a trapped charge carrier is given by the grey area in figure 4.28, which is about 0.97% of the total number of incoming photons. In other words, 6.7×10^{14} photons will create a trapped electron. Since we know that saturation of the number of traps is reached at this excitation intensity, we can assume that this number is also the maximum number of traps available in the material. We can therefore conclude:

- **Number of activators:** 4.2×10^{15}
- **Number of available traps:** 6.7×10^{14}

Hence, we can estimate that the number of traps is about 16% of the number of luminescent centers. Of course, this is not an exact value but rather an approximation.

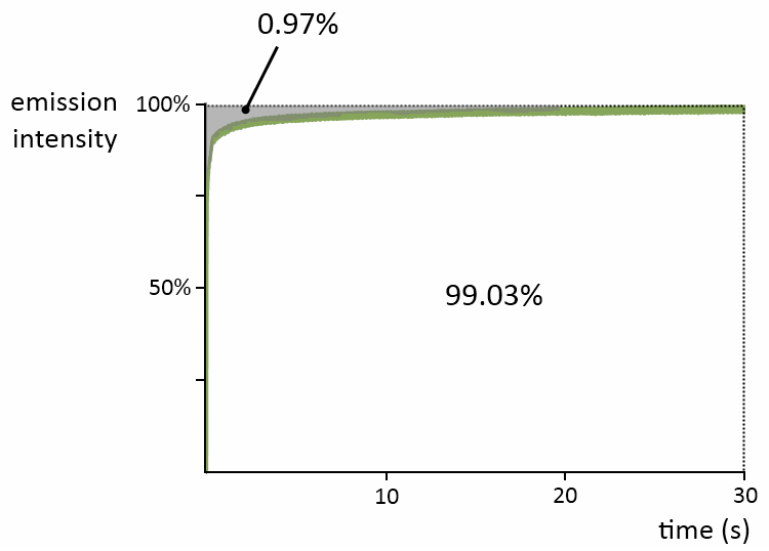

Figure 4.28: The fraction of incoming photons that lead to a trapped electron can be estimated by looking at the area above the intensity curve during excitation (the gray area). In this case (for 10% of the maximum excitation power), it is nearly 1%.

For example, we overlooked the influence of non-radiative transitions in the material. In this way, a trapped electron can be released without the emission of a photon, and the number of traps will be slightly underestimated. On the other hand, figure 4.28 calculates the number of trapping processes as a fraction of only the radiative transitions, which could lead to a slight overestimation of the number of traps.

More advanced experiments are needed to take these additional factors into account and improve our estimation of the number of trap levels. As a first important step, the internal and external quantum efficiency of the materials should be determined by measuring the number of incoming and outgoing photons. However, it is difficult - if not impossible - to distinguish between luminescence produced by detrapping electrons, and luminescence caused by immediate recombination of excited Eu ions. Furthermore, it is unknown if the influence of the quantum efficiency (*i.e.*, the fraction of non-radiative transitions) is equally large for normal recombination and for detrapping. Also, absorption measurements are essential to obtain a better estimate of the penetration depth of the light in the material. Ideally, this should be performed on a single crystal, to avoid the influence of grain boundaries on the light penetration.

Since the estimated number of traps is already very comparable to the number of activating ions, one can wonder how far this persistent phosphor is off from the 'theoretical limit'. In this limit, every excited ion gives rise to a trapped charge carrier, and hence contributes to the afterglow. For that, more accurate measurements - as described above - are indispensable. However, even if this theoretical limit is reached, it might still be possible to engineer the trap system in such a way that the intensity and duration of the afterglow can be optimized, depending on the required application (e.g. a short but very intense afterglow, or a very long afterglow with only moderate intensity).

4.4 Summary and remaining challenges

In this chapter, we have briefly described some experiments and simulations that can teach us more about the kinetics of the persistent luminescent process. We have investigated how the excitation intensity influences the total light output and duration of the afterglow, and how this can help us in estimating the number of trap levels in a persistent phosphor. However, more precise investigations might be required, to take into account both the intrinsic and extrinsic quantum efficiency, and to accurately determine the number of excited luminescent centers and the number of trapped charge carriers (e.g. by measuring the number of emitted photons).

Furthermore, we have developed some simple simulation models to mimic the behaviour of the luminescence intensity during the excitation phase. With only a few parameters, a good agreement can be found between the simulated and the measured intensity. These models can be further extended to account for other observed phenomena, however, this increases the number of necessary parameters. More specifically, the possibility of a continuous trap depth distribution might be included in the model. In the next chapter, we will prove that such a continuous distribution exists in e.g. $CaAl_2O_4$:Eu,Nd.

Using x-ray irradiation and XANES measurements, we were able to determine the trap filling rate in $SrAl_2O_4$:Eu,Dy during excitation, and to *in situ* monitor the change of (part of) the Eu valence from the divalent to trivalent state. Follow-up experiments are planned to measure similar valence state changes in the codopant ions (e.g. Dy), as predicted by - among others - Dorenbos [12] and Aitasalo *et al.* [13]. However, preliminary measurements show that if such a valence state change occurs, the changes in the Dy XANES spectra are even more subtle than those of Eu.

Finally, we have shown that trapping in persistent phosphors is sometimes thermally activated - at least upon excitation with long wavelength light. To avoid this, we should focus our attention on phosphors having a low thermal quenching temperature, such as $CaAl_2O_4$:Eu,Nd.

References

[1] Chen, R. and McKeever, S. W. S. *Theory of thermoluminescence and related phenomena*. World Scientific, Singapore, (1997).

[2] Randall, J. T. and Wilkins, M. H. F. *Proceedings of the Royal Society of London. Series A: Mathematical and Physical Sciences* **184**, 390–407 (1945).

[3] Hornyak, W. F. and Chen, R. *Journal of Luminescence* **44**, 73–81 (1989).

[4] Garlick, G. F. J. and Gibson, A. F. *Proceedings of the Physical Society* **60**, 574–590 (1948).

[5] May, C. E. and Partridge, J. A. *The Journal of Chemical Physics* **40**, 1401–1409 (1964).

[6] Rasheedy, M. S. *Journal of Physics: Condensed Matter* **5**, 633 (1993).

[7] Korthout, K., Van den Eeckhout, K., Botterman, J., Nikitenko, S., Poelman, D., and Smet, P. F. *Physical Review B* **84**, 085140 (2011).

[8] Rodrigues, L. C. V., Stefani, R., Brito, H. F. d., Felinto, M. C. F. C., Hölsä, J., Lastusaari, M., Laamanen, T., and Malkamäki, M. *Journal of Solid State Chemistry* **183**, 2365–2371 (2010).

[9] Dorenbos, P. *Journal of Solid State Science and Technology* **2**, R3001–R3011 (2013).

[10] Dorenbos, P. *Journal of Physics: Condensed Matter* **17**, 8103–8111 (2005).

[11] Schulze, A. R. and Buschbaum, H. M. *Zeitschrift für anorganische und allgemeine chemie* **475**, 205–210 (1981).

[12] Dorenbos, P. *Journal of The Electrochemical Society* **152**, H107–H110 (2005).

[13] Aitasalo, T., Hölsä, J., Jungner, H., Lastusaari, M., and Niittykoski, J. *The Journal of Physical Chemistry B* **110**, 4589–4598 (2006).

5 Estimating trap depths

The results of this chapter have been published in:

- **Revealing trap depth distributions in persistent phosphors**
  Koen Van den Eeckhout, Adrie J.J. Bos, Dirk Poelman and Philippe F. Smet
  Physical Review B **87** (2013) 045126

The energy needed to release trapped charge carriers is determined by the depth of the trap levels. Knowledge of these trap depths is therefore crucial in the understanding of the persistent luminescence mechanism. Unfortunately, the trap depths in persistent phosphors are often difficult to evaluate in an accurate and reliable way.

This chapter is devoted to the estimation of trap depths through thermoluminescence experiments. By heating a previously excited sample and monitoring the emitted light, we can learn more about the trap system of the persistent phosphor. We will describe a technique to accurately probe the trap system even in the presence of a continuous trap distribution, and we will apply this technique to the well-known persistent phosphor $CaAl_2O_4$:Eu,Nd.

5.1 Determining trap depths

During the past decades, several methods for estimating trap depths in persistent phosphors have been developed [1, 2]. Most of these start from glow curves obtained through thermoluminescence (TL) experiments. Roughly, they can be divided in five broad categories:

- **initial rise** methods, based on the initial fraction of the glow curve
- **area** methods, based on the area under the glow curve
- **peak position** methods, based on the location of the maximum
- **shape** methods, based on the shape and symmetry of the curve
- **curve fitting** methods, computerized or using a series expansion

The best known and most used of these are the Hoogenstraaten method [3], based on the shift of the peak position under variable heating rates, the shape method developed by Chen [4], and the computerized fitting of the glow curve using specialized software [5, 6].

5.1.1 Principle of thermoluminescence

Thermoluminescence is a powerful and versatile tool to investigate the depth of the trap(s) present in persistent phosphors. It is frequently used in storage phosphors for dosimetry and geological dating purposes [1], but is also becoming increasingly common in persistent luminescence research.

The principle is as follows. First, the material of interest is heated to ensure that all the charge carrier traps are empty. Subsequently, the sample is excited for a certain time using UV-radiation (or X-ray or β-radiation in the case of scintillators or storage phosphors) at low temperature (commonly room temperature, but liquid nitrogen or helium temperature are also used). The material is then heated in a controlled way, usually with a constant heating rate, while the light output is continuously measured. A schematic representation of this procedure is shown in figure 5.1.

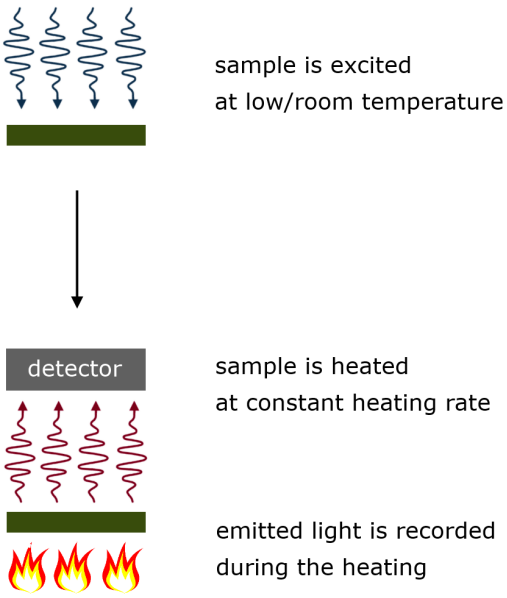

Figure 5.1: In a thermoluminescence experiment, a previously excited sample is heated in a controlled way, while the emission intensity is monitored.

The appearance of a peak in the emitted light intensity (**glow peak**) indicates the presence of a charge carrier trap in the material. The temperature at which this peak is located is a measure of the trap depth, since it is the temperature at which enough thermal energy is available for the trapped charge carriers to be released and recombine at luminescent centers. A shallow trap will give rise to a glow peak at low temperature, while a deep trap will cause a glow peak at higher temperatures (figure 5.2). The shape, height and location of the peak all contain information on the number and depth of the traps and the kinetics of the trapping and detrapping process.

A factor which should not be overlooked when analyzing TL glow curves is the thermal quenching of the material. At higher temperatures, non-radiative decay processes become increasingly important and start dominating the radiative transitions. Hence,

the emitted light intensity starts to drop upon increasing temperature. In the present case we are not interested in the radiative transitions only, but in the total number of charge carriers released from the traps. As previously pointed out by various authors, the glow curves measured during a TL experiment should therefore be corrected for thermal quenching in order to represent the actual number of released charge carriers [1, 7, 8].

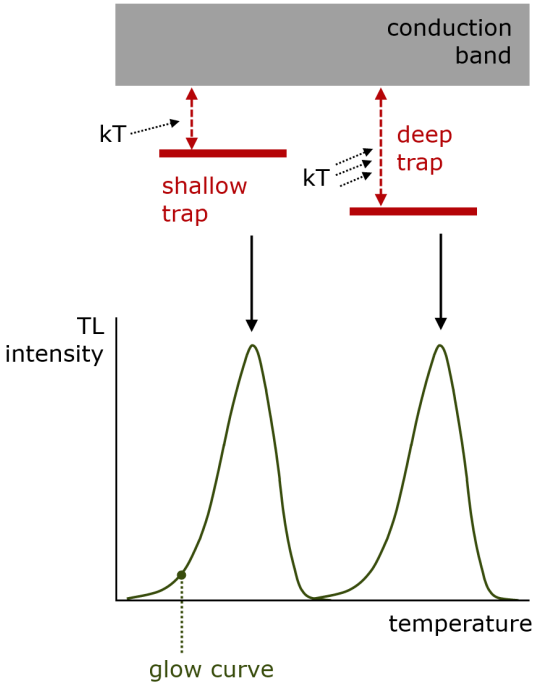

Figure 5.2: In general, shallow traps give rise to glow peaks at low temperature, while deep traps cause glow peaks at higher temperatures.

5.1.2 First, second, and general order kinetics

The different types of kinetics, discussed in chapter 4, also have their effect on the glow curve. In the case of first order kinetics, as described by Randall and Wilkins in 1941 [9], the possibility of retrapping is assumed to be negligible. This leads not only to an exponential afterglow decay profile, but also to an asymmetric TL glow peak with a negative skew, as depicted in figure 5.3.

The shape of the first order glow peak can be described mathematically as:

$$I(T) = \frac{s}{\beta} \cdot n_0 \cdot \exp\left(-\frac{E_T}{kT}\right) \cdot \exp\left[-\frac{s}{\beta} \cdot \int_{T_0}^{T} \exp\left(-\frac{E_T}{k\theta}\right) \mathrm{d}\theta\right] \tag{5.1}$$

where s is the frequency factor, n_0 is the initial concentration of trapped electrons, E_T is the trap depth, and β is the constant heating rate during the experiment.

Function 5.1 illustrates the competition between the increased recombination during heating on the one hand (the Boltzmann factor) and the progressive emptying of the traps on the other hand (described by the integral).

In 1948, Garlick and Gibson derived expressions for the glow peak in the case of second order kinetics, when recombination and retrapping have the same probability [10]. The peak in this case is much more symmetrical compared to the first order case (figure 5.3).

The mathematical expression for a second order glow peak is given by:

$$I(T) = \frac{s}{\beta} \cdot \frac{n_0^2}{N} \cdot \exp\left(-\frac{E_T}{kT}\right) \cdot \left[1 + \frac{s}{\beta} \cdot \frac{n_0}{N} \cdot \int_{T_0}^{T} \exp\left(-\frac{E_T}{k\theta}\right) \mathrm{d}\theta\right]^{-2} \tag{5.2}$$

The expressions for first and second order kinetics are only valid in ideal situations, i.e. when the retrapping probability is negligible or when it is equal to the recombination probability. For intermediate situations, described by May and Partridge as general order kinetics [11], the glow curve is given by:

$$I(T) = \frac{s}{\beta} \cdot \frac{n_0^b}{N^{b-1}} \cdot \exp\left(-\frac{E_T}{kT}\right) \cdot \left[1 + \frac{s}{\beta} \cdot \left(\frac{n_0}{N}\right)^{b-1} \cdot (b-1) \cdot \int_{T_0}^{T} \exp\left(-\frac{E_T}{k\theta}\right) \mathrm{d}\theta\right]^{\frac{-b}{b-1}} \tag{5.3}$$

The expressions 5.1 to 5.3 are nowadays commonly employed, especially since the introduction and profusion of software for TL glow curve fitting. However, it must be kept in mind that the general order approach is a purely mathematical interpolation between the simplified cases of first and second order kinetics, and therefore lacks a straightforward physical meaning.

Figure 5.3 summarizes how the order of kinetics influences the shape of a glow peak. In the case of first order kinetics ($b = 1$), the peak is asymmetric with a strongly negative skew, while for second order kinetics ($b = 2$) the peak is almost symmetric. For general order kinetics, the curve lies in between these two extremes.

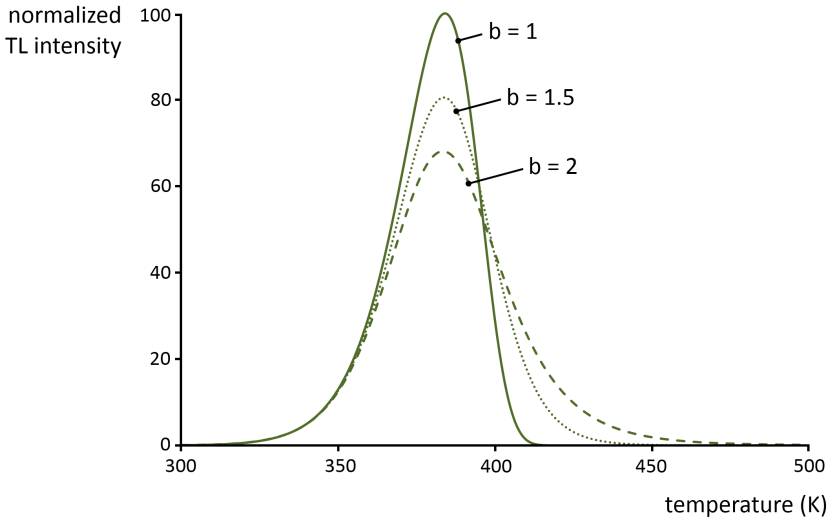

Figure 5.3: Typical glow curve shape for first, second, and general order kinetics. While a first order kinetics peak has a strongly negative skew, a second order peak is much more symmetric. $E_T = 1$ eV, $n_0 = N$, $s = 10^{12}$ s^{-1}, and $\beta = 1$ K/s. (Adapted from [7].)

5.2 Continuous trap depth distributions

Most afterglow decay curves, as well as glow curves obtained in a TL experiment, cannot be explained by the simplest model of a single discrete energy level with first, second, or even general order kinetics. Afterglow decay curves often follow a t^{-1} behaviour [12], which cannot be understood by any of these models. The same is true for many TL glow peaks, which are often too broad - especially on the high temperature side - to be described by a single first, second, or general order glow peak.

A common approach is therefore to assume the presence of multiple discrete energy levels obeying first order kinetics. The decay curve is then decomposed into multiple (three or more) exponential components [13–16], frequently called 'fast', 'intermediate' and 'slow', however, the time constants obtained in this way are difficult to interpret physically and the large number of parameters involved can make the fitting procedure unreliable.

Similarly, broad TL glow peaks are often fitted to three or more individual glow peaks obeying general order kinetics. Again, since each glow peak has five independent parameters (the trap depth E_T, the frequency factor s, the trap concentration N, the initial concentration of filled traps n_0, and the order of kinetics b) 15 or more parameters are needed for fitting, making a physical interpretation impossible. This is especially the case if only a single TL experiment is taken into account, as opposed to a series of experiments performed on a single sample.

5.2.1 Existence of continuous trap depth distributions

Another approach to explain the broadness of the TL peaks is assuming the presence of a **trap depth distribution**. In this case, the trap level is not regarded as a discrete energy level located in the band gap of the host material, but rather as a continuum of energy levels around a certain mean value. This possibility has been explored by various authors [12, 17–32] and three main types of trap distributions have been considered: uniform, exponential and Gaussian profiles.

An example of these different profiles is shown in figure 5.4. For a uniform profile, every trap depth has the same density of traps. An exponential trap profile has a small number of deep traps and a large number of shallow traps. A Gaussian profile is centered around a mean trap depth value, with tails extending to deeper and shallower regions.

The advantage of this approach is twofold. Firstly, a distribution of trap depths requires less parameters to be accurately described than a multitude of discrete energy levels. Secondly, it is believed that a continuous distribution of trap depths is a more intuitively acceptable description of the actual defect situation in inorganic phosphors since the structure of the lattice surrounding the trapping center may exhibit random variations in the nearest neighbor bond angles and bond lengths. Also, association of the trapping centers with other defects in the vicinity is possible. In this case, small variations in the spatial configurations of the defect aggregates can cause a broadening of the trap depth distribution. Another possible origin for variations in trap depths is the distance from the traps to the luminescent centers, as has been shown in e.g.

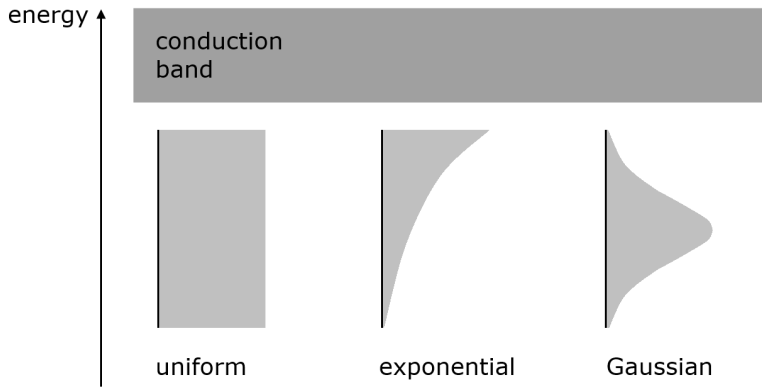

Figure 5.4: Some examples of continuous trap depth distribution profiles: uniform, exponential and Gaussian profiles.

$Lu_xY_{2-x}SiO_5$ [8].

The presence of such a continuous trap distribution directly influences the shape of the TL glow peaks by broadening them, and can also explain the observed t^{-1} decay behaviour of the afterglow [17], although other authors suggest that this behaviour could be due to a trapping mechanism governed by tunneling [33]. In principle, these two explanations could be experimentally distinguished, since the t^{-1} behaviour in the case of a continuous trap depth distribution is dependent on the temperature (at different temperatures greater or smaller parts of the distribution are filled), while tunneling is temperature independent. However, such an experimental verificiation is beyond the scope of our study.

The first order kinetics formula (equation 5.1) can be modified to incorporate such a continuous distribution of traps by integrating over the trap depth [1]:

$$I(T) = \int_0^\infty \frac{s}{\beta} \cdot N(E_T) \cdot f_0(E_T) \cdot \exp\left(-\frac{E_T}{kT}\right) \cdot \exp\left[-\frac{s}{\beta} \cdot \int_{T_0}^{T} \exp\left(-\frac{E_T}{k\theta}\right) \mathrm{d}\theta\right] \mathrm{d}E_T \qquad (5.4)$$

where $N(E_T)$ is the distribution of available trap depths (this can be uniform, exponential, Gaussian,...) and $f_0(E_T)$ describes which fraction of the traps is filled at $t = 0$. k is the Boltzmann constant.

It should be noted that integrating over the energy range of the distribution is only valid for first order kinetics. In the case of higher order kinetics, the presence of retrapping seriously complicates the process, since the escaped charge carriers can be captured by neighboring traps with different activation energies than the one they escaped from. This complex interaction between trap levels with various trap depths makes the simple integration over the energy range invalid.

For practical purposes, this glow curve behaviour in the presence of a trap depth distribution can be simulated numerically. For this purpose, it suffices to divide the continuous distribution into a large number of small intervals, calculate the glow curve for each of these intervals, and adding these glow curves to obtain the curve for the entire trap distribution. An example of this procedure and its result is shown in figure

5.5. It was shown by Rudlof *et al.* [34] and Hornyak and Chen [12] that the results of such a numerical approach agree very well with the analytical expression.

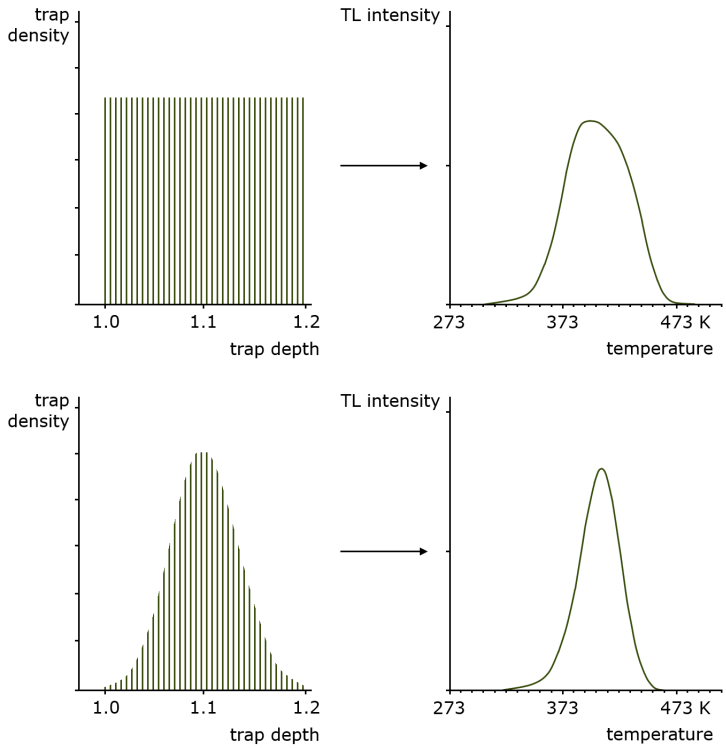

Figure 5.5: The glow curve of a continuous trap distribution can be simulated by dividing the distribution into a large number of small intervals and summing the glow curves for each of these intervals. (After Rudlof *et al.* [34])

5.2.2 Series of TL measurements

Compared to a single glow curve, a series of TL experiments on the same sample yields a lot more information than a single experiment. Firstly, more data is available to analyze, making the final result more accurate and more reliable. Secondly, performing a series of subsequent TL experiments while changing only a single parameter between each measurement can yield additional information which cannot be extracted from only one glow curve.

To study trap depth distributions in persistent phosphors, two parameters are particularly interesting: the **duration of the excitation** and the **temperature during the excitation** of the sample. Varying the excitation duration provides insight into the kinetics of the trapping and detrapping process. Indeed, in the case of first order kinetics we expect the location of the peak maximum to be independent of the excitation dose (and hence the excitation duration), while for higher order kinetics a shift of the maximum is expected [7].

To study the presence of a trap depth distribution it is interesting to vary the temperature at which the sample is excited. The reason for this is graphically explained in figure 5.6. If a phosphor with a continuous trap depth distribution is excited at a higher temperature, only deeper fractions of the distribution are (kept) filled. The shallower traps are immediately bleached because of the increased thermal energy available. If we then estimate the trap depth, the resulting value will increase (become deeper) with increasing excitation temperature.

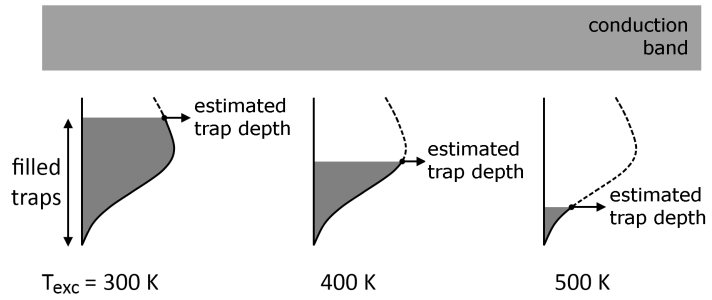

Figure 5.6: Schematic representation of the fractions of a trap distribution that are filled, as a function of increasing excitation temperatures. For higher excitation temperature, only the deepest fraction of the distribution is filled, and the estimated trap depth will be much deeper than at lower excitation temperatures.

5.3 Initial rise analysis

Most of the methods to analyze glow curves, described at the start of section 5.1 have their shortcomings. Often, the presence of discrete trap depths is assumed, and the possibility of a continuous trap depth distribution is not considered. Furthermore, many of these methods are applied to the glow curve acquired during a single TL measurement. This makes the interpretation of the obtained results physically less sound.

One of the most useful analysis techniques is the initial rise method. This approach for estimating trap depths starts from the assumption that on the low-temperature side of a TL glow curve, the concentration of trapped charge carriers is relatively constant. Only a tiny fraction of the charge carriers can escape given the small amount of thermal energy available. We can therefore approximate the equations for first, second and general order kinetics to

$$I(T) \propto C \cdot \exp\left(-\frac{E_T}{kT}\right) \tag{5.5}$$

The constant C includes the frequency factor s which is assumed to be independent of the temperature. If we now plot the glow curve as $\ln(I)$ versus $1/T$, i.e. in an Arrhenius plot, the low-temperature side of the peak will resemble a straight line, from which the trap depth can be readily estimated. This is illustrated in figure 5.7, which shows a simulated glow curve for a uniform trap distribution stretching from 0.9 to 1.1

eV, assuming first order kinetics and $\beta = 5$ K/s. Note that even in the case of a relatively broad continuous distribution a straight section in the Arrhenius plot can be clearly resolved. For an accurate result, typically only the fraction where $I < 0.15\ I_{max}$ should be considered [2, 35].

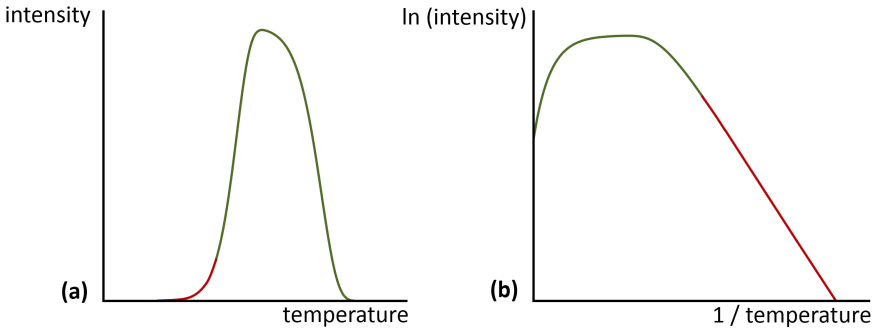

Figure 5.7: The initial rise analysis for estimating trap depths, illustrated for a simulated glow curve of a continuous trap depth distribution. (a) TL glow curve. (b) Glow curve in Arrhenius diagram. The slope of the straight section on the low-temperature side is determined only by the trap depth, and equal to $-E_T/k$.

The initial rise method has two major advantages. Firstly, it is independent of the order of kinetics involved in the trapping and detrapping processes. Secondly, since only a part of the glow peak is considered (the low-temperature side), the problem of overlapping TL peaks is greatly reduced. However, for two largely overlapping peaks, the initial part of the highest-temperature peak might be obscured by the tail of the low-temperature peak. In this case, it is possible that no straight section can be resolved in the Arrhenius plot, and the initial rise analysis cannot be employed. Thermal cleaning of the traps [36] might partially resolve this problem.

In the case of a continuous trap depth distribution, the initial rise analysis is expected to yield the depth of the shallowest occupied traps in the distribution. Indeed, we look only at the low-temperature region of the glow peak, where only the charge carriers in the shallowest traps are involved. The deeper traps remain filled because not enough thermal energy is available for the charge carriers to escape.

This expectation can be verified by simulations. In a first step, a trap depth distribution is created and the glow curve is simulated using the procedure described in the final paragraph of section 5.2.1, by dividing the continuous distribution into a large number of discrete intervals. Secondly, this simulated glow curve is analyzed using the initial rise procedure and the obtained estimation for the trap depth is compared to the actual trap distribution used. Such simulations were performed for both uniform and Gaussian trap depth distributions.

An overview of the simulation results is presented in figure 5.8. The created trap depth distributions are indicated in green, and the estimated trap depths are shown in red. As can be seen, the initial rise procedure always produces a value at the shallowest end of the distribution. For uniform distributions, the estimation is within 2.1% of the low energy edge. For a Gaussian distribution, the estimated value lies around the $E_0 - 3\sigma$

mark, within a 3.9% error margin. Only for very broad distributions the estimated trap depth is somewhat lower, around the $E_0 - 4\sigma$ mark (0.65 eV for a distribution around 1 eV with $\sigma = 0.08$ eV).

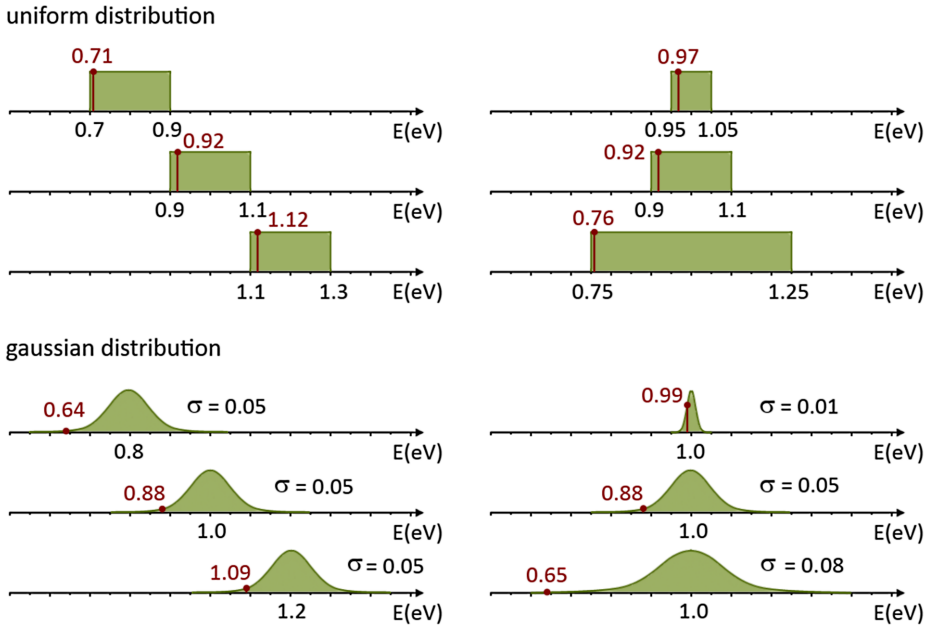

Figure 5.8: Simulation of trap depth estimations (indicated in red, in eV) using the initial rise method, for various (artificial) uniform and Gaussian distributions (indicated in green). The estimated trap depth is always situated at the shallowest end of the distribution.

From these results, we can conclude that the initial rise analysis indeed gives a good estimation for the trap depth of the shallowest occupied trap levels. No influence of the frequency factor s or the heating rate β was found.

5.4 Combining TL and initial rise analysis for trap depth spectroscopy

As discussed above, the presence of a trap depth distribution can be proven by performing a series of TL experiments at varying excitation temperatures and performing the initial rise analysis. If the estimated trap depth increases continuously with increasing excitation temperature, there is a strong indication for the presence of a continuous trap distribution, rather than one or more discrete energy levels. The obtained trap depth value is a good estimate for the shallowest edge of this distribution.

Information on the shape of the continuous trap depth distribution can also be obtained. In other words, it can be estimated how many trap levels are available at each depth for charge carriers to be trapped in. From a statistical point of view, a Gaussian distribution of traps is the most probable option. Sakurai *et al.* [26] found proof for an

exponential trap profile in brown microcline, but later showed that this exponential profile was in fact only the deeper side of a Gaussian distribution [28].

This information on the shape of the distribution can be obtained by integrating the glow curves for various excitation temperatures. The surface under the glow curve is a measure for the total number of luminescent ions returning to the ground state during the TL experiment, and hence for the total number of trapped charge carriers. As shown in figure 5.6, only the deeper fraction of the trap depth distribution - the trap depth deeper than the value estimated using the initial rise analysis - is filled. Therefore, at each excitation temperature, the integrated TL intensity is directly related to the total number of traps *below* the estimated trap depth. This means that the difference between the integrated TL intensities at two different excitation temperatures is a measure for the number of available traps *between* the depths estimated for these two measurements. In this way, the density of traps at various depths can be derived. This is shown schematically in figure 5.9.

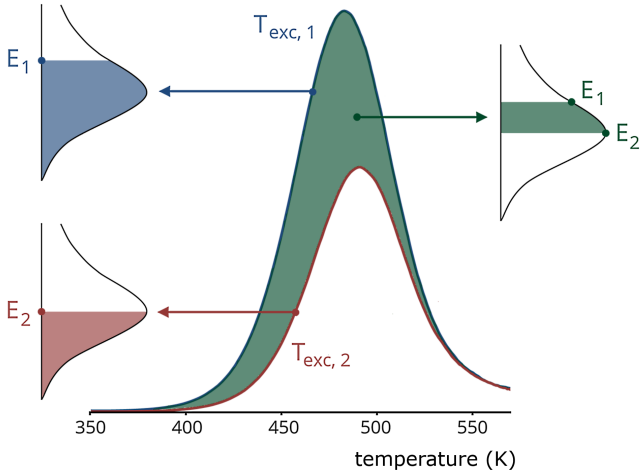

Figure 5.9: The density of the continuous trap depth distribution at a certain depth can be estimated from the difference between the integrated intensities at two different excitation temperatures.

The presented procedure is in a way comparable to the so-called 'preheating' or 'thermal cleaning' technique, in which the sample is heated to a temperature T_{stop} after the excitation and before the TL experiment [24, 36–38]. In this way, the continuous distribution of trap depths is also emptied up to a certain depth, depending on T_{stop}. However, care should be taken that the preheating phase in each experiment has the same duration, to avoid the effects of fading. For clarity, the temperature profiles of both procedures (our procedure and the preheating technique) are shown in figure 5.10.

An extension to the preheating technique is known as the 'fractional glow' technique, in which the temperature is repeatedly increased and decreased during the TL measurement [18]. Although this technique is also able to estimate the shape of the continuous trap depth distribution, the setup and data analysis are much more demanding [36].

In principle, a fading experiment, where the duration between the excitation and the

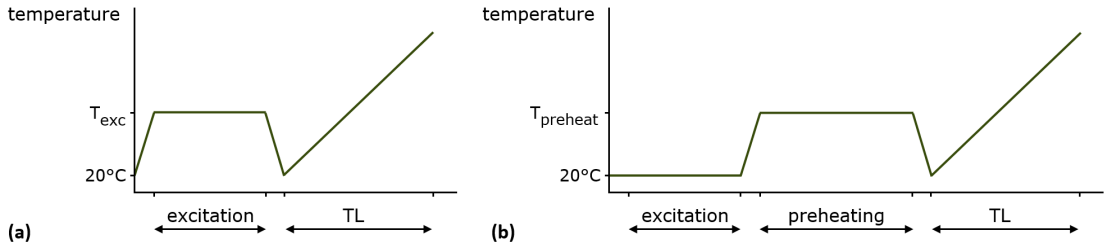

Figure 5.10: (a) In our presented procedure, the sample is excited at elevated temperature, after which the TL experiment starts. (b) In the preheating technique, the sample is heated after the excitation and before the TL measurement.

actual TL experiment is varied, could provide similar information about the presence of a trap depth distribution. However, for long fading times it is more difficult to accurately determine the trap depth because the edge between the filled and empty fraction of the trap distribution will be less clearly defined. Additionally, since the lifetime of the trapped charge carriers scales exponentially with the trap depth, the delay between the excitation and the TL measurement needs to be very long in order to study deeper parts of the distribution. For example, if we assume $s = 10^{12}$ s^{-1}, the average lifetime of a charge carrier in a trap with a depth of $E_T = 1.1$ eV is nearly 150 days, which gives an idea of the measurement times required (see also section 1.2.1).

5.5 Trap depth distribution in $CaAl_2O_4$:Eu,Nd

As an illustration of the concepts explained above, the well-known persistent phosphor $CaAl_2O_4$:Eu,Nd was examined. This material, closely related to $SrAl_2O_4$:Eu,Dy, has a long-lasting afterglow in the violet-blue region of the visible spectrum. Its luminescent properties were first described by Blasse and Bril [39] and Palilla *et al.* [40] in 1968, but only in 1996 Matsuzawa *et al.* mentioned its persistent luminescence [41]. An afterglow duration of up to 10 hours is mentioned in literature [42–44].

The host material has a monoclinic crystal structure [45], but when prepared with a combustion or sol-gel method, a hexagonal or orthorhombic phase is sometimes obtained [46, 47]. The monoclinic structure has three possible cation sites, but the Eu^{2+} ions, which are somewhat larger than the Ca^{2+} ions, are only incorporated in the more spacious trigonal anti-prism site [48]. The presence of only a single europium site simplifies the analysis of the luminescence data (as compared to e.g. $SrAl_2O_4$:Eu which has two possible europium sites [48]). For this reason, $CaAl_2O_4$:Eu is often chosen as a standard material for persistent luminescence investigations [29, 43, 49–55].

5.5.1 Experimental

The measurements in the follow sections were not performed on $CaAl_2O_4$:Eu,Nd powder, but on pellets. These were prepared via a non-aqueous sol-gel method [55] and e-beam annealing as described in reference [56]. The pellets produced using this procedure have an afterglow intensity of about three times that of commercially available

powder, and the afterglow duration extends to 10 hours. The origin of this improved afterglow duration is still being investigated, but the annealed samples show full crystallization, a white body colour, and an increased concentration of (co)dopants in the grain boundaries.

The emission and excitation spectra were measured in a fluorescence spectrometer (Edinburgh FS920) with a xenon arc lamp as a light source. Afterglow decays were obtained using a calibrated photometer (ILT 1700, International Light Technologies) which is equipped with a photopic filter (YPM) to mimic the respons of the human eye, and a xenon arc lamp for uniform excitation at 1000 lx. The thermal quenching was measured using a pulsed nitrogen laser (at λ_{exc} = 337 nm, with a pulse length of 800 ps) and a 1024-channel intensified CCD (Andor Technology) attached to a 0.5 m Ebert monochromator, in combination with a helium contact gas cryostat (Optistat, Oxford Instruments).

Thermoluminescent glow curves were obtained at Delft University of Technology, The Netherlands. Our samples were exposed to 365 nm radiation at various temperatures and for various periods of time. The emission during heating was monitored using a Risø Thermoluminescence reader (TL/OSL-DA-15) collecting the glow curves by means of a photomultiplier tube and suitable optical filters.

The thermoluminescence setup is fully automated and software controlled by a user interface written in LabVIEW® [57]. For experiments with an excitation temperature above room temperature, the TL measurement was started 5 seconds after the excitation. This means that the natural cooling of the sample continued during the initial moments of the TL measurement but, as can be seen from figure 5.15 below, this has little to no influence on the measured glow curves.

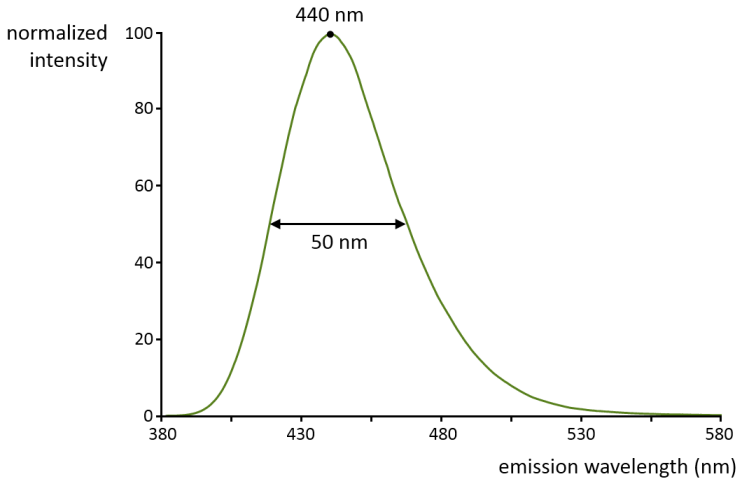

Figure 5.11: The emission spectrum of $CaAl_2O_4$:Eu,Nd (λ_{exc} = 365 nm) consists of a single broad Eu^{2+}-based peak around 440 nm.

5.5.2 Optical properties

Emission and afterglow

The emission spectrum, depicted in figure 5.11 consists of a single broad peak (50 nm FWHM) peaking around 440 nm, in the violet region of the visible spectrum. The broad peak is typical for Eu^{2+} emission. The location and shape of the spectrum is consistent with previous reports [39, 40, 58].

The decay of the afterglow after 5 min excitation by 365 nm radiation is shown in figure 5.12. During the first few minutes, the emission intensity drops rapidly, but this decrease slows down over time. As reported in [56], the photopic intensity (not shown) drops below the 0.32 mcd/m^2 threshold after 11 hours (figure 5.13), but the afterglow remains visible with the unaided dark-adapted eye for at least 72 hours.

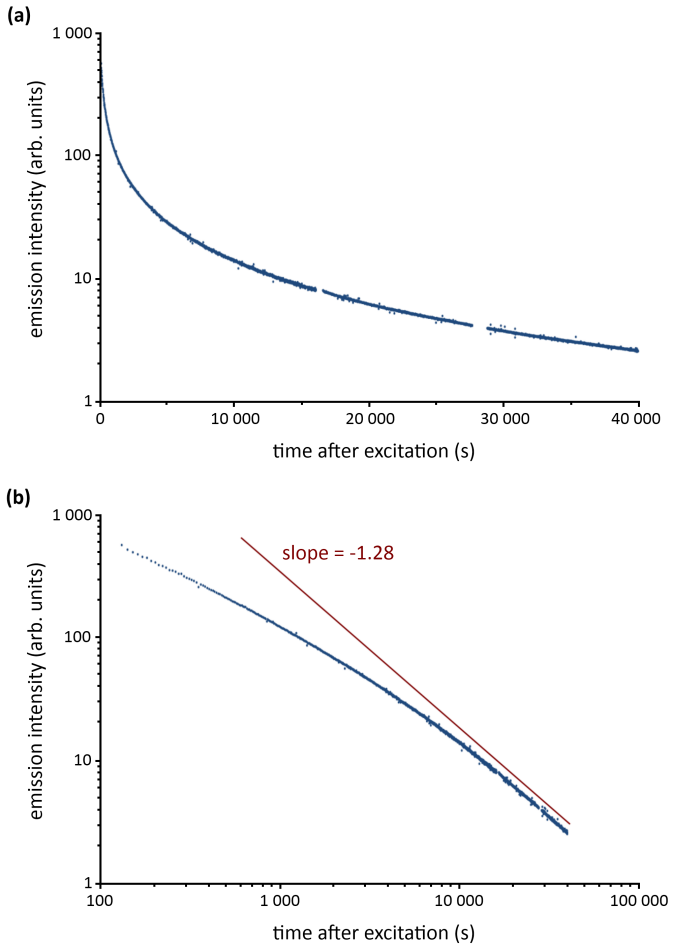

Figure 5.12: Afterglow decay of $CaAl_2O_4$:Eu,Nd after 5 minutes excitation by 365 nm radiation: (a) in a linear-logarithmic diagram; (b) in a double-logarithmic diagram.

The afterglow behaviour shown in figure 5.12a cannot be explained by assuming a single trap with first order kinetics. In that case, an exponential decay profile would be observed, following a straight line in a linear-logarithmic plot. For the case of higher

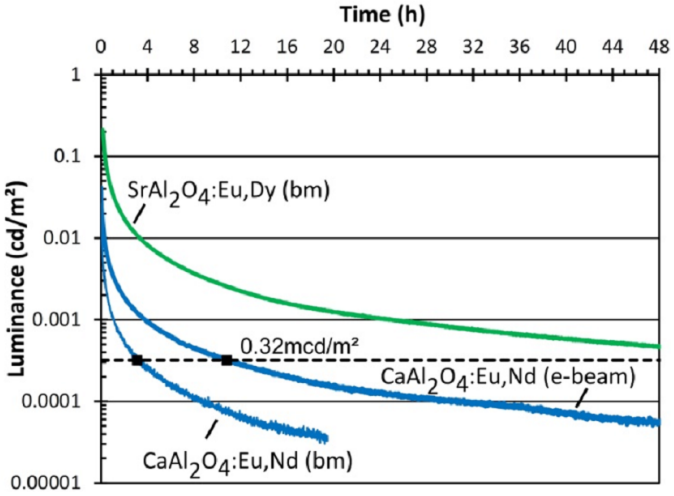

Figure 5.13: Absolute luminance of $CaAl_2O_4$:Eu,Nd and $SrAl_2O_4$:Eu,Dy persistent phosphors measured after excitation for 10 minutes with 1000 lx of unfiltered light from a Xe arc source. (bm): benchmark phosphor, (e-beam): phosphor prepared using e-beam annealing. The e-beam annealed sample reaches the threshold after about 11 hours [56].

order kinetics, the following profile is expected:

$$I(t) = \frac{I_0}{\left(1 + \frac{t}{\tau}\right)^{\frac{b}{b-1}}} \tag{5.6}$$

where b is the order of kinetics. In the limit for long time values, this should show a power law behaviour. In other words, a plot of the afterglow decay in a double-logarithmic diagram would show a straight line with a slope of $b/(1-b)$. Figure 5.12b shows that such a power law behaviour is only reached after 5 hours or more, which makes it impossible to fit the decay profile to equation 5.6. Also, the slope of -1.28 would imply a kinetic order of $b = 4.57$, a rather high value which suggests a very high importance of retrapping processes. However, such a strong influence of retrapping is not observed in TL experiments (see below).

In short, the afterglow results strongly suggest the presence of a trap distribution, which will now be verified using TL experiments.

Thermal quenching

The thermal quenching profile for $CaAl_2O_4$:Eu,Nd is given in figure 5.14. A fit to a standard 'single-barrier' model [59]

$$I(T) = \frac{I_0}{1 + \frac{\Gamma_0}{\Gamma_\nu} \exp\left(-\frac{\Delta E}{kT}\right)} \tag{5.7}$$

is used to obtain a smooth profile for correcting the TL glow curves. The quenching temperature, defined as the temperature where the emission intensity has dropped by

50%, is 367 K, a rather low value compared to other luminescent materials. Since the sample in a TL experiment is typically heated to 550 K or higher, it is essential to take the thermal quenching into account [7]. At 473 K, the intensity has already fallen by 95%. Hence, even a weak glow peak at higher temperatures can represent a considerable number of detrapping charge carriers, taking into account the large fraction of non-radiative transitions in this temperature region. All TL data in the remainder of this text has been corrected for thermal quenching.

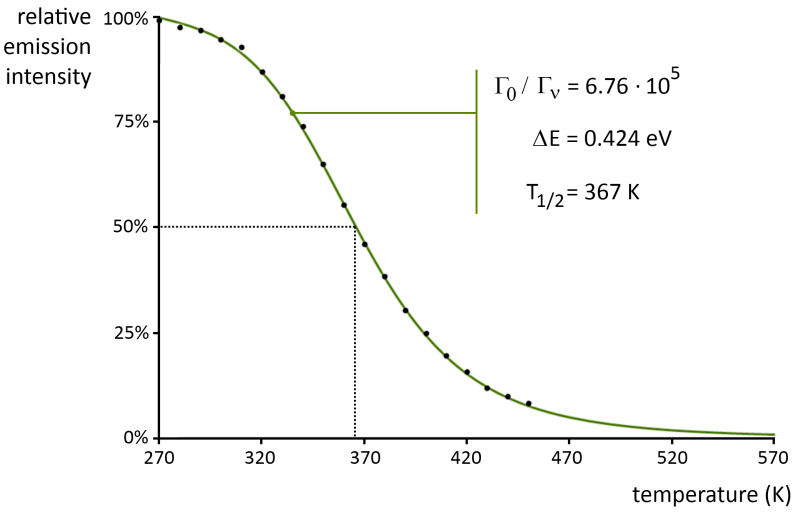

Figure 5.14: The thermal quenching temperature of $CaAl_2O_4$:Eu,Nd lies at 367 K. The data points were obtained using pulsed 337 nm radiation. The blue line represents the best fit to a standard single-barrier model.

5.5.3 Thermoluminescence experiments

Influence of the excitation duration

In figure 5.15, the influence of the excitation duration on the $CaAl_2O_4$:Eu,Nd glow curve is shown. For longer durations the total amount of emitted light increases, because a larger number of traps is filled. The location of the maximum also shows a slight shift towards lower temperatures. For 30 seconds excitation, the peak maximum is located at 483 K, while for 360 seconds excitation this has shifted to 470 K. This shift shows that the trap system is more complicated than a single trap obeying first order kinetics.

Compared to previous reports [29, 42, 51], the glow peak is located at a rather high temperature (470 K vs. 420 K). A comparison is shown in figure 5.16. Possibly, this is due to the alternative preparation technique of the sample, and it could be an explanation for the improved afterglow lifetime of the sample compared to a benchmark $CaAl_2O_4$:Eu,Nd persistent phosphor, as reported by Smet *et al.* [56].

Aitasalo *et al.* [29] found that the glow curve for $CaAl_2O_4$:Eu,Nd consists of two overlapping peaks. The main TL peak, around 350 K, was present in all $CaAl_2O_4$:Eu,R samples and is therefore assumed to be related to the lattice rather than to the codopants.

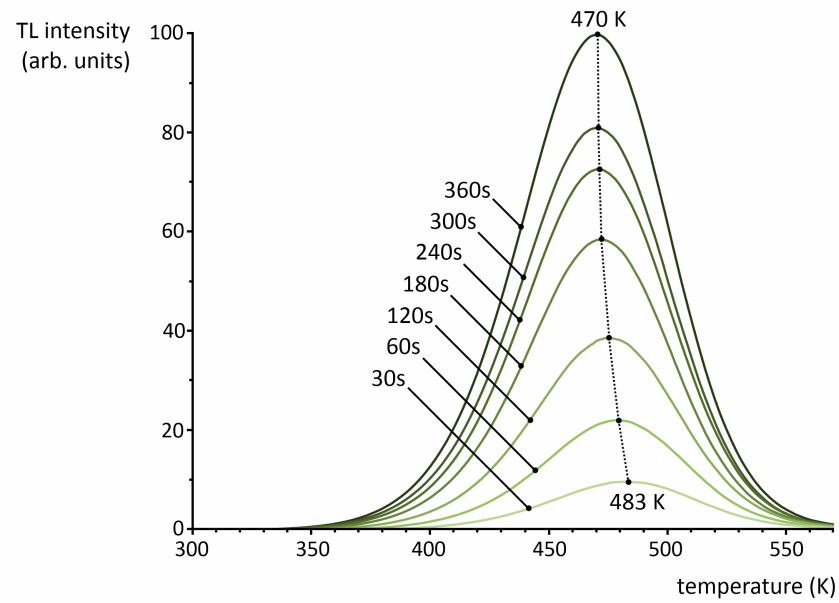

Figure 5.15: TL intensity of $CaAl_2O_4$:Eu,Nd after 365 nm excitation at room temperature with various durations (30-360 s), at a heating rate of 5 K/s.

The peak at higher temperature is attributed to Nd^{3+}-related traps which improve the afterglow decay time. The presence of only a single glow peak at relatively high temperature in our sample therefore indicates that the deeper Nd-related defects dominate the more shallow intrinsic traps in this sample [29]. It should be noted, however, that the TL experiments in reference [29] were performed at low excitation intensity, which could influence the relative trap filling of both kinds of traps (the heating rate of 5 K/s was the same in both cases).

If the trap depth for each of the curves is estimated using the initial rise method, the result shown in figure 5.17 is obtained. When plotted in an Arrhenius diagram, each curve has a straight section on the low-temperature side, indicating that the assumption made for the initial rise analysis is valid. The slope of these sections, and hence the estimated trap depth, is almost independent of the excitation duration, as shown in figure 5.18. The trap depth is located between 0.66 and 0.68 eV, which is in relatively good agreement with previous estimates by Aitasalo *et al.* [29], who found a trap at 0.67 eV, but with the additional presence of a more shallow trap around 0.55 eV (by employing the preheating technique and the initial rise analysis).

In the remainder of this text, we will prove the presence of a continuous trap depth distribution. However, the constant trap depth as seen in figure 5.18 indicates that we are looking at the same traps in each experiment (independent of the excitation time), and that the slight shift of the glow peak maximum as seen in figure 5.15 is not caused by the presence of this distribution. Rather, the shift is most probably due to some - albeit relatively minor - retrapping.

In the case of a single discrete trap level, the expected temperature shift in the

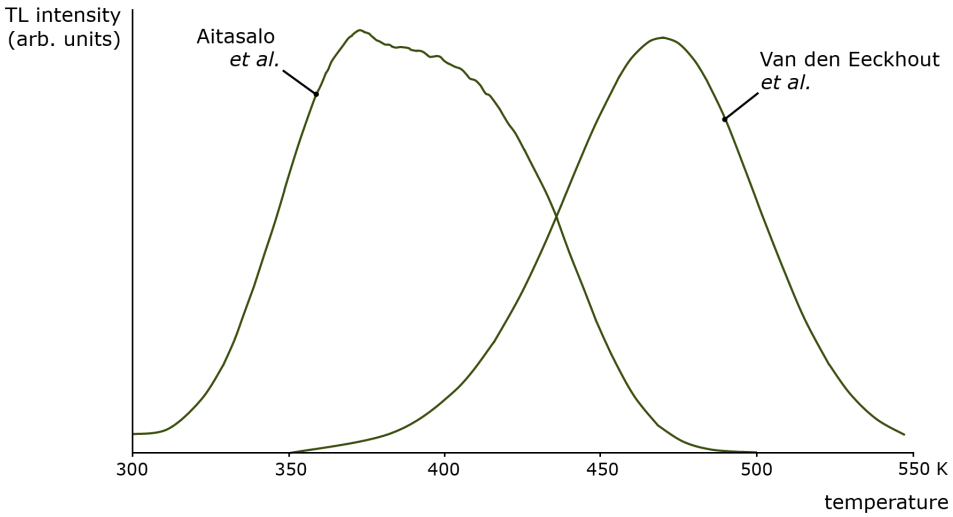

Figure 5.16: Our measured glow curve of $CaAl_2O_4$:Eu,Nd is located at a much higher temperature than reported by Aitasalo *et al.* [29]. This can be due to the different preparation technique (e-beam annealing) and the different excitation intensity.

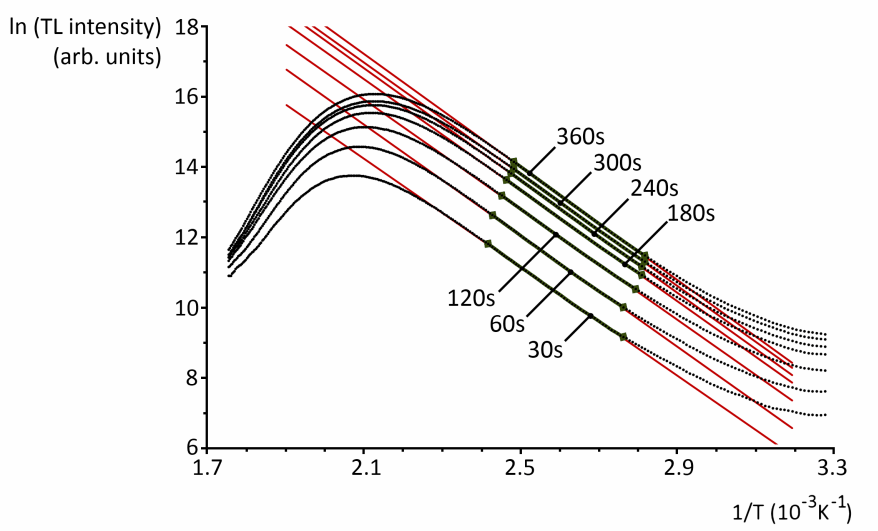

Figure 5.17: Initial rise analysis of the TL glow curves in $CaAl_2O_4$:Eu,Nd as a function of the excitation duration. The dark green lines represent the areas of the curve used for the fitting; these are the areas where the intensity is between 1% and 15% of the maximal intensity. The red lines represent the fitting results.

presence of retrapping can be approximated by [7]

$$T_1 - T_2 \approx T_1 T_2 \frac{k(b-1)}{E_T} \ln f \tag{5.8}$$

where T_1 is the temperature of maximum intensity at a certain dose and T_2 the temper-

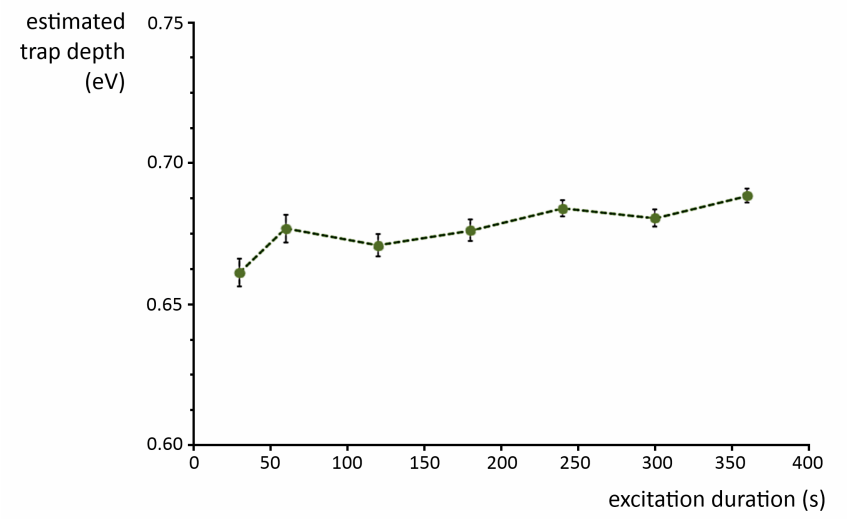

Figure 5.18: Estimated trap depth in $CaAl_2O_4$:Eu,Nd as a function of the excitation duration. The error bars indicate three times the standard deviation of the data from the fitting result.

ature of maximum intensity at an f times higher dose. b is again the order of kinetics. Assuming equation 5.8 is also approximately valid for a continuous trap depth distribution, we can estimate the value of b to be around 1.17. This indicates that some retrapping may take place.

Influence of the excitation temperature

The influence of changing the excitation temperature on the glow curves is given in figure 5.19. As expected, the total TL intensity lowers for higher excitation temperatures. Note that this also means that the trapping process is not thermally activated within the studied temperature range, as is the case for some phosphor materials e.g. the Eu-doped nitrido-silicates [60] and Pr-doped lutetium pyrosilicate [61] (see also section 4.2.5). In such phosphors, trap filling is facilitated at higher excitation temperatures, leading to more filled traps and an increase in the total TL intensity for increasing excitation temperature. This behaviour is not seen in our $CaAl_2O_4$:Eu,Nd sample for the studied range of excitation temperatures.

Again, as in figure 5.15, a shift in the location of the glow peak maximum is seen, which is much larger than in the previous case (from 475 K at T_{exc} = 303 K to 560 K at T_{exc} = 483 K), and cannot be explained by the possibility of retrapping alone. Here, the presence of a continuous trap depth distribution is strongly suggested by the data.

The initial rise analysis is shown in figure 5.20. The straight sections at the low-temperature side of the glow curves have a slope which is increasing for increasing excitation temperatures. Only at high excitation temperatures (503 K) the low emission intensity makes the data too unreliable to accurately estimate the trap depth. The resulting trap depths are given in figure 5.21. Upon excitation at room temperature, the estimated depth is 0.69 eV, as in the previous experiment, but this depth increases to over 1.2 eV for an excitation temperature of 483 K.

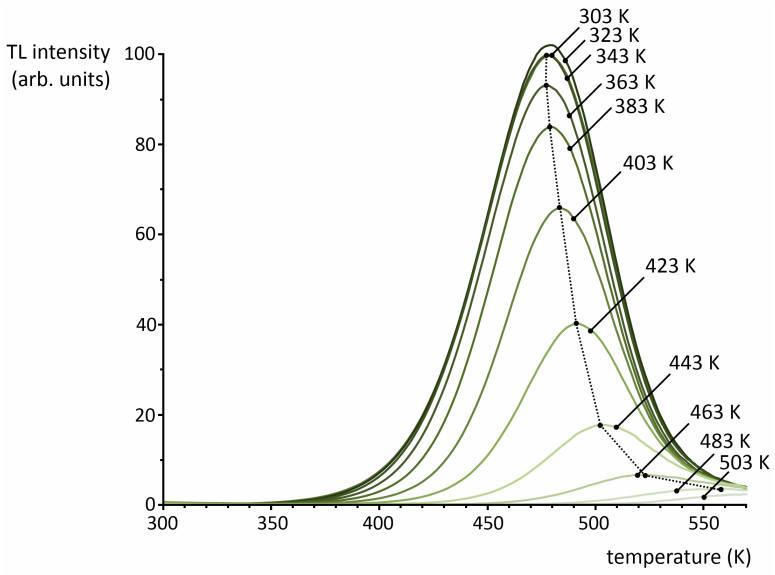

Figure 5.19: TL intensity of $CaAl_2O_4$:Eu,Nd for various excitation temperatures, T_{exc}, as indicated. Samples were excited at T_{exc} by 365 nm light for 60 s. The TL measurement started 5 s after the excitation at a heating rate of 5 K/s.

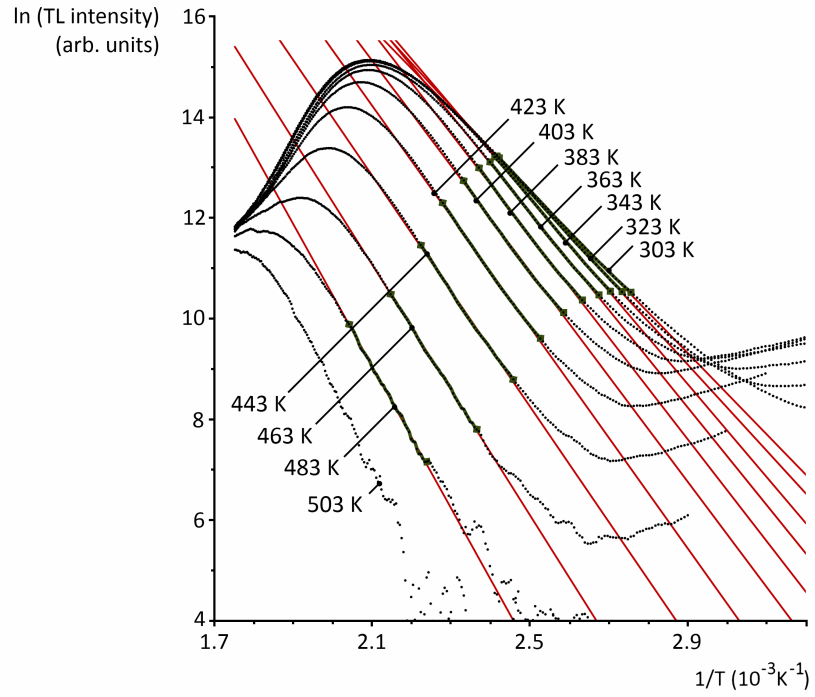

Figure 5.20: Initial rise analysis of the TL glow curves in $CaAl_2O_4$:Eu,Nd as a function of the excitation temperature.

As discussed in section 5.2.2, the gradual deepening of the trap depth for increasing excitation temperature proves the presence of a continuous trap distribution in

$CaAl_2O_4$:Eu,Nd, in this case located roughly between 0.69 and 1.2 eV.

It must be kept in mind that the continuous trap depth distribution can extend further on both ends, i.e. it is possible that even shallower and even deeper traps exist. However, these are difficult to detect experimentally. Traps which are too shallow could only be seen when exciting at temperatures below room temperature, which requires cooling of the sample. Not only does this require a more advanced experimental set-up, but it might also be more difficult to efficiently fill traps at these lower temperatures due to thermal activation of the trapping [60].

On the other hand, traps deeper than 1.2 eV are difficult to detect because of the low intensity of the involved glow peaks for these high excitation temperatures (see figure 5.19). Also, the glow peaks in this case are located at high readout temperatures (600-700 K), where the influence of thermal quenching is very high. The combination of these factors makes an analysis of possible deep traps unreliable. For applications, however, these deep traps have little to no effect on the afterglow at room temperature.

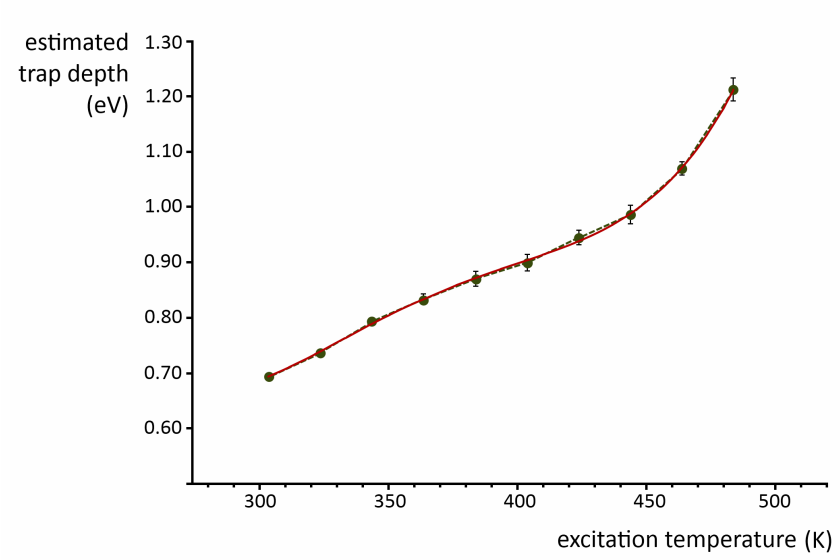

Figure 5.21: Estimated trap depth in $CaAl_2O_4$:Eu,Nd as a function of excitation temperature. The red line is a polynomial fit through the obtained results.

5.5.4 Shape of the trap depth distribution

To determine the shape of the trap depth distribution, the glow curves in figure 5.19 are integrated to obtain the total TL intensity for each measurement. As described in section 5.4, the level density can be estimated at various depths by taking the difference between each of these values. For example, when exciting at 383 K the calculated trap depth was 0.87 eV, while exciting at 403 K gave a trap depth of 0.90 eV. Hence, the difference between the integrated TL intensity of the curves at T_{exc} = 383 K and T_{exc} = 403 K is a direct measure for the number of traps between 0.87 eV and 0.90 eV.

Figure 5.22 shows the final result of this analysis. A Gaussian shape was found, with a maximum around 0.9 eV, but extending from at least 0.7 to 1.2 eV. The best fit to a

Gaussian profile is also shown (in red), from which we find a maximum around 0.91 eV, with a standard deviation of about 0.07 eV. As mentioned previously, the Gaussian shape of the profile is not unexpected from a statistical point of view. Furthermore, looking at the work of Medlin *et al.* [17], the shape and broadness of the TL glow curves and the shape of the afterglow decay are both qualitatively consistent with the presence of such a Gaussian-shaped trap depth distribution.

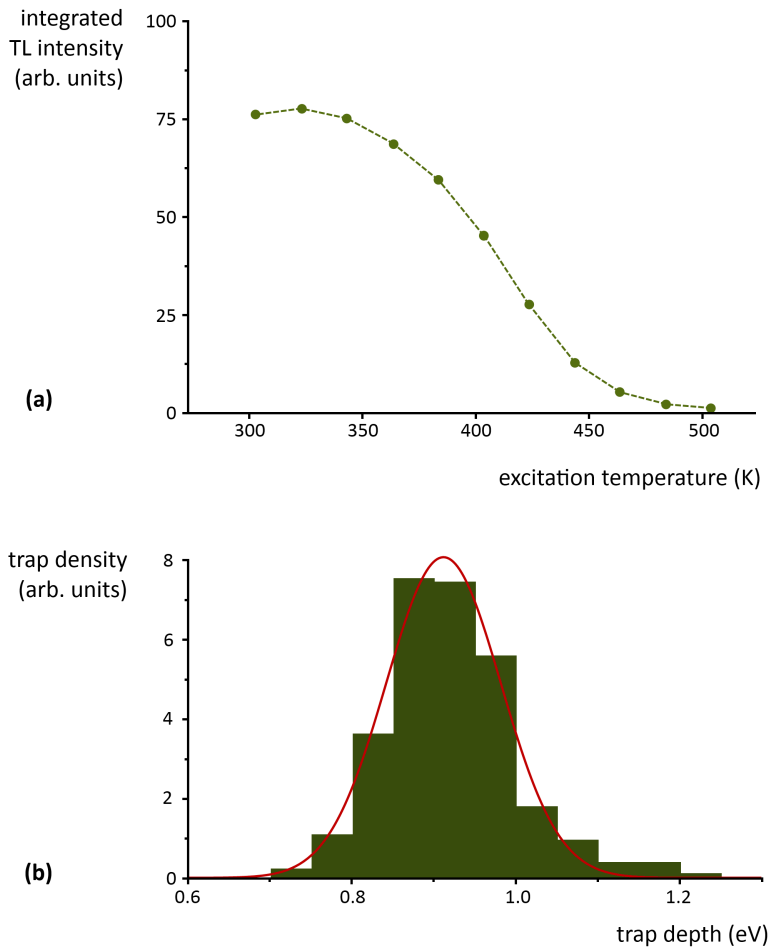

Figure 5.22: (a) Integrated TL intensity in $CaAl_2O_4$:Eu,Nd for various excitation temperatures. (b) Density of energy levels for the trap depth distribution in $CaAl_2O_4$:Eu,Nd. The red line shows the best fit to a Gaussian profile.

5.5.5 Simulation of the afterglow decay

Now that we have determined the trap depth distribution in $CaAl_2O_4$:Eu,Nd, it is interesting to calculate the expected afterglow behaviour from such a distribution. By using the numerical approach described in section 5.2.1, we can simulate the decay of the emission intensity for a Gaussian-shaped trap depth distribution centered around 0.91 eV, with a standard deviation of 0.07 eV. The best fit is obtained for a frequency factor

$s = 1.49 \cdot 10^{11} s^{-1}$ and a kinetic order of $b = 1$. A comparison between the simulated and the experimental data is shown in figure 5.23. As can be seen, the shape of the afterglow decay can be accurately modeled in this way. Nevertheless, the simulation becomes less accurate at longer time scales. This might be due to the fact that the surrounding temperature during the afterglow experiment was not always constant (due to the day and night cycle).

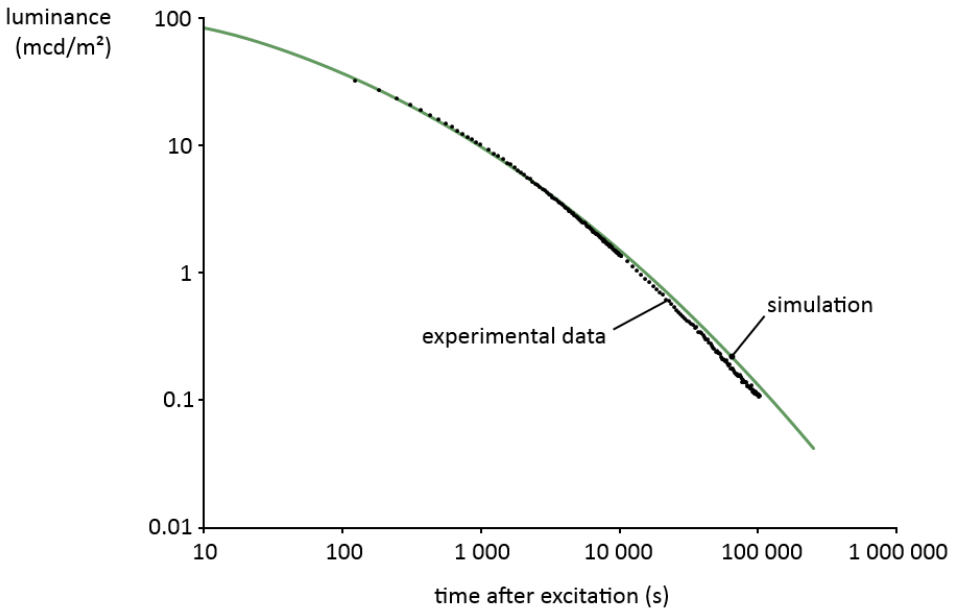

Figure 5.23: Comparison of the measured and simulated afterglow intensity in $CaAl_2O_4$:Eu,Nd. The measured data is the same as in figure 5.13. The simulated intensity is calculated by assuming a trap depth distribution centered around 0.91 eV with a standard deviation of 0.07 eV, with a frequency factor $s = 1.49 \cdot 10^{11} s^{-1}$ and a kinetic order $b = 1$.

5.6 Summary of the procedure

In the previous sections, we have described a procedure to accurately determine trap systems in persistent phosphors, even in the presence of a continuous distribution. This procedure combines a series of TL experiments at various excitation duration and temperature with the initial rise analysis. This procedure can be applied to other persistent phosphors as well, or even to storage phosphors and scintillators.

In summary, the following steps should be taken for such a trap depth probing:

1. Measuring the thermal quenching of the sample in order to properly correct the thermoluminescence data.

2. Measuring the dose dependence of the thermoluminescence glow curves to verify the presence of higher order kinetics.

3. Measuring the thermoluminescence glow curves after exciting at various temperatures T_{exc}. The initial rise analysis can be performed to estimate the trap depths. An estimated trap depth which varies continuously as a function of T_{exc} is a strong indication for the presence of a continuous trap depth distribution.

4. If the trapping process is not thermally activated, the area under the glow curves obtained in 3) can be used to estimate the shape of the continuous trap depth distribution. If thermal activation of the trapping is seen, the areas should first be corrected for this.

5.7 Conclusions and perspectives

Knowledge about the trap system in a persistent phosphor is one of the crucial steps in understanding the mechanism behind persistent luminescence. Rather than discrete energy levels, these trap systems often consist of continuous distributions of trap depths.

The activation energies in persistent phosphors can be determined in an accurate and reliable way by combining series of TL experiments at different excitation duration and with different excitation temperature with the initial rise method. In this way, it is possible to reveal the presence of a continuous distribution of trap depths and to estimate the shape and depth of this distribution.

As an example, we studied the activation energies in $CaAl_2O_4$:Eu,Nd responsible for the persistent luminescence. We found that the trap system is composed of a continuous distribution which is more or less Gaussian in shape, with the highest density of available trap depths in the region around 0.9 eV and tails extending from at least 0.7 to 1.2 eV.

The described procedure could further be applied to other persistent phosphors, storage phosphors and scintillators to obtain the crucial information on the activation energies necessary to understand the persistent luminescence mechanism.

References

[1] Chen, R. and McKeever, S. W. S. *Theory of thermoluminescence and related phenomena*. World Scientific, Singapore, (1997).

[2] Pagonis, V., Kitis, G., and Furetta, C. *Numerical and practical exercises in thermoluminescence*. Springer, New York, (2006).

[3] Hoogenstraaten, W. *Philips Research Reports* **13**, 515–693 (1958).

[4] Chen, R. *Journal of The Electrochemical Society* **116**, 1254–1257 (1969).

[5] Bos, A. J. J., Piters, T., Gómez-Ros, J., and Delgado, A. *Radiation Protection Dosimetry* **47**, 473–477 (1993).

[6] Bos, A. J. J., Piters, T., Gómez Ros, J., and Delgado, A. *Radiation Protection Dosimetry* **51**, 257–264 (1994).

[7] Bos, A. J. J. *Radiation Measurements* **41**, S45–S56 (2007).

[8] Vedda, A., Nikl, M., Fasoli, M., Mihokova, E., Pejchal, J., Dusek, M., Ren, G., Stanek, C. R., McClellan, K. J., and Byler, D. D. *Physical Review B* **78**, 195123 (2008).

[9] Randall, J. T. and Wilkins, M. H. F. *Proceedings of the Royal Society of London. Series A: Mathematical and Physical Sciences* **184**, 390–407 (1945).
[10] Garlick, G. F. J. and Gibson, A. F. *Proceedings of the Physical Society* **60**, 574–590 (1948).
[11] May, C. E. and Partridge, J. A. *The Journal of Chemical Physics* **40**, 1401–1409 (1964).
[12] Hornyak, W. F. and Chen, R. *Journal of Luminescence* **44**, 73–81 (1989).
[13] Pan, W., Ning, G., Zhang, X., Wang, J., Lin, Y., and Ye, J. *Journal of Luminescence* **128**, 1975–1979 (2008).
[14] Dejene, F. B., Bem, D. B., and Swart, H. C. *Journal of Rare Earths* **28**, 272–276 (2010).
[15] Gutiérrez-Martín, F., Fernández-Martinez, F., Díaz, P., Colón, C., and Alonso-Medina, A. *Journal of Alloys and Compounds* **501**, 193–197 (2010).
[16] Ju, Z.-H., Zhang, S.-H., Gao, X.-P., Tang, X.-L., and Liu, W.-S. *Journal of Alloys and Compounds* **509**, 8082–8087 (2011).
[17] Medlin, W. L. *Physical Review* **123**, 502–509 (1961).
[18] Gobrecht, H. and Hofmann, D. *Journal of Physics and Chemistry of Solids* **27**, 509–522 (1966).
[19] Bosacchi, A., Bosacchi, B., Franchi, S., and Hernandez, L. *Solid State Communications* **13**, 1805–1809 (1973).
[20] Bosacchi, A., Franchi, S., and Bosacchi, B. *Physical Review B* **10**, 5235–5238 (1974).
[21] Pender, L. F. and Fleming, R. J. *Journal of Physics C: Solid State Physics* **10**, 1561 (1977).
[22] Pender, L. F. and Fleming, R. J. *Journal of Physics C: Solid State Physics* **10**, 1571 (1977).
[23] Hagekyriakou, J. and Fleming, R. J. *Journal of Physics D: Applied Physics* **15**, 163 (1982).
[24] Lorincz, A., Puma, M., James, F. J., and Crawford, J. H. J. *Journal of Applied Physics* **53**, 927–932 (1982).
[25] Hornyak, W. F., Chen, R., and Franklin, A. *Physical Review B* **46**, 8036–8049 (1992).
[26] Sakurai, T. and Gartia, R. K. *Journal of Applied Physics* **82**, 5722–5727 (1997).
[27] Kitis, G. and Gomez-Ros, J. M. *Nuclear Instruments and Methods in Physics Research Section A: Accelerators, Spectrometers, Detectors and Associated Equipment* **440**, 224–231 (2000).
[28] Sakurai, T., Shoji, K., Itoh, K., and Gartia, R. K. *Journal of Applied Physics* **89**, 2208 (2001).
[29] Aitasalo, T., Hölsä, J., Jungner, H., Lastusaari, M., and Niittykoski, J. *The Journal of Physical Chemistry B* **110**, 4589–4598 (2006).
[30] Zahedifar, M., Karimi, L., and Kavianinia, M. J. *Nuclear Instruments and Methods in Physics Research Section A: Accelerators, Spectrometers, Detectors and Associated Equipment* **564**, 515–520 (2006).
[31] Zahedifar, M., Rezaeian, P., and Harooni, S. *Nuclear Instruments and Methods in Physics Research Section B: Beam Interactions with Materials and Atoms* **264**, 378–382 (2007).

[32] Zahedifar, M., Harooni, S., and Sadeghi, E. *Nuclear Instruments and Methods in Physics Research Section A: Accelerators, Spectrometers, Detectors and Associated Equipment* **654**, 569–574 (2011).
[33] Avouris, P. and Morgan, T. N. *The Journal of Chemical Physics* **74**, 4347–4355 (1981).
[34] Rudlof, G., Becherer, J., and Glaefeke, H. *physica status solidi (a)* **49**, K121–K124 (1978).
[35] Kivits, P. and Hagebeuk, H. J. L. *Journal of Luminescence* **15**, 1–27 (1977).
[36] McKeever, S. W. S. *Thermoluminescence of solids*. Cambridge University Press, Cambridge, UK, (1985).
[37] Nahum, J. and Halperin, A. *Journal of Physics and Chemistry of Solids* **24**, 823–834 (1963).
[38] Nicholas, K. H. and Woods, J. *British Journal of Applied Physics* **15**, 783 (1964).
[39] Blasse, G. and Bril, A. *Philips Research Reports* **23**, 201–206 (1968).
[40] Palilla, F. C., Levine, A. K., and Tomkus, M. R. *Journal of The Electrochemical Society* **115**, 642–644 (1968).
[41] Matsuzawa, T., Aoki, Y., Takeuchi, N., and Murayama, Y. *Journal of the Electrochemical Society* **143**, 2670–2673 (1996).
[42] Hölsä, J., Jungner, H., Lastusaari, M., and Niittykoski, J. *Journal of Alloys and Compounds* **323-324**, 326–330 (2001).
[43] Lin, Y., Tang, Z., Zhang, Z., and Nan, C. *Journal of the European Ceramic Society* **23**, 175–178 (2003).
[44] Chang, C., Xu, J., Jiang, L., Mao, D., and Ying, W. *Materials Chemistry and Physics* **98**, 509–513 (2006).
[45] Hörkner, W. and Müller-Buschbaum, H.-K. *Journal of Inorganic and Nuclear Chemistry* **38**, 983–984 (1976).
[46] Aitasalo, T., Hölsä, J., Jungner, H., Lastusaari, M., and Niittykoski, J. *Journal of Alloys and Compounds* **341**, 76–78 (2002).
[47] Aitasalo, T., Hölsä, J., Jungner, H., Lastusaari, M., Niittykoski, J., Parkkinen, M., and Valtonen, R. *Optical Materials* **26**, 113–116 (2004).
[48] Nakamura, T., Matsuzawa, T., Rowlands, C. C., Beltran-Lopez, V., Smith, G. M., and Riedi, P. C. *Journal of the Chemical Society, Faraday Transactions* **94**, 3009–3012 (1998).
[49] Yamamoto, H. and Matsuzawa, T. *Journal of Luminescence* **72-74**, 287–289 (1997).
[50] Aitasalo, T., Hölsä, J., Jungner, H., Lastusaari, M., and Niittykoski, J. *Journal of Luminescence* **94-95**, 59–63 (2001).
[51] Aitasalo, T., Deren, P., Hölsä, J., Jungner, H., Krupa, J.-C., Lastusaari, M., Legendziewicz, J., Niittykoski, J., and Stręk, W. *Journal of Solid State Chemistry* **171**, 114–122 (2003).
[52] Aitasalo, T., Deren, P., Hölsä, J., Jungner, H., Lastusaari, M., Niittykoski, J., and Stręk, W. *Radiation Measurements* **38**, 515–518 (2004).
[53] Wang, Y. and Wang, L. *Journal of Applied Physics* **101**, 053108 (2007).
[54] Hölsä, J., Laamanen, T., Lastusaari, M., Malkamäki, M., Welter, E., and Zajac, D. A. *Spectrochimica Acta Part B: Atomic Spectroscopy* **65**, 301–305 (2010).
[55] Avci, N., Korthout, K., Newton, M. A., Smet, P. F., and Poelman, D. *Optical*

Materials Express **2**, 321–330 (2012).

[56] Smet, P. F., Avci, N., Van den Eeckhout, K., and Poelman, D. *Optical Materials Express* **2**, 1306–1313 (2012).

[57] Bos, A. J. J., van Duijvenvoorde, R. M., van der Kolk, E., Drozdowski, W., and Dorenbos, P. *Journal of Luminescence* **131**, 1465–1471 (2011).

[58] Katsumata, T., Nabae, T., Sasajima, K., and Matsuzawa, T. *Journal of Crystal Growth* **183**, 361–365 (1998).

[59] Dorenbos, P. *Journal of Physics: Condensed Matter* **17**, 8103–8111 (2005).

[60] Smet, P. F., Van den Eeckhout, K., Bos, A. J. J., van der Kolk, E., and Dorenbos, P. *Journal of Luminescence* **132**, 682–689 (2012).

[61] Fasoli, M., Vedda, A., Mihokova, E., and Nikl, M. *Physical Review B* **85**, 085127 (2012).

Part III

Development of persistent phosphors

6 The nitrido-silicate family

The results of this chapter have been published in:

- **Persistent luminescence in rare-earth codoped $Ca_2Si_5N_8:Eu^{2+}$**
  Koen Van den Eeckhout, Philippe F. Smet and Dirk Poelman
  Journal of Luminescence **129** (2009) 1140-1143
- **Luminescent afterglow behaviour in the $M_2Si_5N_8$:Eu family (M = Ca, Sr, Ba)**
  Koen Van den Eeckhout, Philippe F. Smet and Dirk Poelman
  Materials **4** (2011) 980-990
- **Temperature and wavelength dependent trap filling in $M_2Si_5N_8$:Eu (M = Ca, Sr, Ba) persistent phosphors**
  Philippe F. Smet, Koen Van den Eeckhout, Adrie J.J. Bos, Erik van der Kolk and Pieter Dorenbos
  Journal of Luminescence **132** (2012) 682-689

Part of the work in this chapter, especially section 6.2.3 on flux materials and section 6.3 on medical imaging have been conducted in the framework of the Master thesis of Inge Nys (LumiLab research group) [1].

The medical imaging experiments on mice (section 6.3.4) have been performed by Thomas Maldiney and colleagues at the LCMCP research group (Chimie Paristech) in Paris, France, and have been published in:

- **In vivo optical imaging with rare earth doped $Ca_2Si_5N_8$ persistent luminescence nanoparticles**
  Thomas Maldiney, Guillaume Sraiki, Bruno Viana, Didier Gourier, Cyrille Richard, Daniel Scherman, Michel Bessodes, Koen Van den Eeckhout, Dirk Poelman and Philippe F. Smet
  Optical Materials Express **2** (2012) 261-268

An important element in persistent luminescent research is the actual development and optimization of new afterglow phosphors. Above all, efficient orange- and red-emitting persistent phosphors are very scarce, although they are strongly desired for safety signage and medical imaging applications (see also section 1.2.4).

In order to alleviate this need, we focus on the europium-doped nitrido-silicate family, known for their bright orange photoluminescence, and their high chemical and thermal stability. We investigate the influence of the lattice cations (Ca, Sr, Ba) and the addition of rare earth codopants on the afterglow, in order to develop a new, efficient, orange-emitting persistent phosphor.

In a second stage, our optimized persistent luminescent material is used as a probe for *in vivo* medical imaging. This offers a harmless alternative for real-time tracking of drugs throughout the body, or could help optimizing the effectiveness of transplantation surgery.

6.1 Orange persistent luminescence in the $M_2Si_5N_8$:Eu family

We focus our attention on three members of the alkaline earth nitrido-silicate family: $Ca_2Si_5N_8$, $Sr_2Si_5N_8$ and $Ba_2Si_5N_8$. Upon doping with europium, all of these have a bright emission in the orange-to-red region of the visible spectrum, and they are commonly employed as conversion phosphors in white LEDs. Additionally, promising afterglow properties have been reported earlier by Höppe *et al.* in $Ba_2Si_5N_8$:Eu [2]. They have a broad excitation spectrum, which is promising for the development of persistent phosphors excitable by visible light. Here, the effect of the various cations (Ca, Sr and Ba) on the afterglow has been investigated, as well as the influence of codoping with different rare earth ions (Dy, Nd, Sm and Tm).

6.1.1 Sample preparation

The host material $M_2Si_5N_8$ is made by mixing appropriate amounts of M_3N_2 (M = Ca, Sr, Ba) and α-Si_3N_4. Dopants (europium) and codopants (rare earths, R) were added to the starting mixture in oxide (R_2O_3) or fluoride (RF_3) form. Unless mentioned otherwise, the powders were prepared with 1 mol% of Eu and R. In other words, 1% of the alkaline earth ions is substituted by Eu, and 1% is substituted by R. Also, a 2.5% deficit of M_3N_2 was employed, for reasons explained in section 6.2.3. The materials were weighed, ground and mixed under a protective Ar or N_2 atmosphere in a glove box.

Unless mentioned otherwise, all powders were prepared using a solid state reaction at 1400 °C for 3 hours, under reducing atmosphere of forming gas (90% N_2, 10% H_2). This atmosphere ensures the reduction of the incorporated europium ions from Eu^{3+} to Eu^{2+}. Additionally, the nitrogen in the atmosphere can alleviate the small nitrogen deficit in the starting mixture. The preparation procedure is shown schematically in figure 6.1.

6.1.2 Structural properties

The $M_2Si_5N_8$ compounds crystallize in two different structure types. The orthorhombic $Sr_2Si_5N_8$ and $Ba_2Si_5N_8$ are isostructural, both having space group $Pmn2_1$ [3]. In contrast, $Ca_2Si_5N_8$ has a monoclinic structure of space group Cc [4], probably because of the smaller size of the Ca ion compared to Sr and Ba. Because of this, the properties of the different compounds cannot be readily compared. For example, the position of the

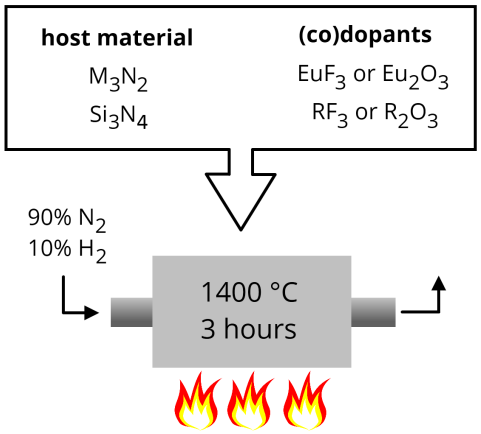

Figure 6.1: $M_2Si_5N_8$:Eu,R samples are prepared through a solid state reaction under reducing atmosphere.

emission spectrum of $M_2Si_5N_8$:Eu does not shift monotonously in the series Ca - Sr - Ba compounds. Also, the excitation spectrum of $Ca_2Si_5N_8$:Eu differs significantly from those of $Sr_2Si_5N_8$:Eu and $Ba_2Si_5N_8$:Eu [5].

Table 6.1: Comparison of experimental $Ca_{1.94}Eu_{0.02}Tm_{0.04}Si_5N_8$ lattice parameters (obtained using XRD) with literature data for $Ca_2Si_5N_8$ found in reference [4].

		experimental	**Schlieper *et al.***
a	(Å)	14.330	14.352
b	(Å)	5.604	5.610
c	(Å)	9.682	9.689
volume	($Å^3$)	777.516	780.107
β	(°)	112.07	112.06

All three of these compounds consist of a strong network of interconnected SiN_4 tetrahedra, which is the main reason for their large thermal and chemical stability. The crystal structure of $Ca_2Si_5N_8$ is shown in figure 6.2. Due to the different size of the rare earth ions, the lattice parameters slightly change upon (co)doping. For example, in $Ca_{1.94}Eu_{0.02}Tm_{0.04}Si_5N_8$ (where Eu^{2+} is somewhat larger than Ca^{2+}, and Tm^{3+} is notably smaller [6]) the volume of the unit cell is reduced by around 1.7% compared to the undoped compound (table 6.1).

Diffuse reflection spectra on undoped samples were performed to verify the band gap of the materials (figure 6.3). $Ca_2Si_5N_8$ has the largest band gap (with an optical absorption edge around 250 nm), followed by $Sr_2Si_5N_8$ (265 nm) and $Ba_2Si_5N_8$ (280 nm). These values are the same as found by Li *et al.*, except for $Ba_2Si_5N_8$ where they found a band gap at 270 nm [5].

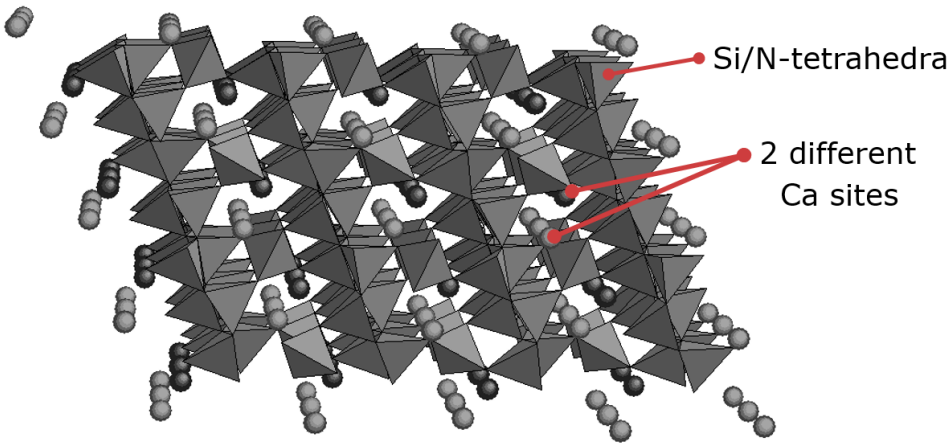

Figure 6.2: The crystal structure of $Ca_2Si_5N_8$ consists of a network of interconnected SiN_4 tetrahedra, with two lattice sites for the Ca ions.

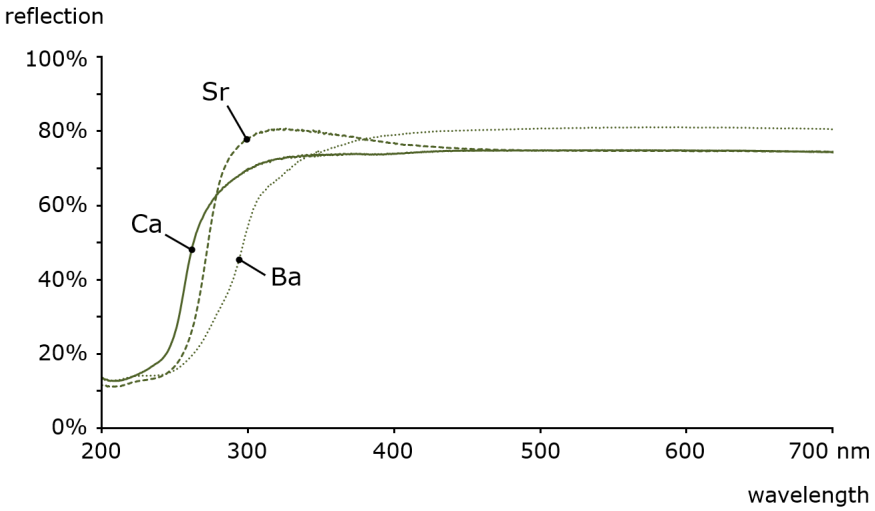

Figure 6.3: Reflection spectra of $M_2Si_5N_8$ (M = Ca, Sr, Ba). The absorption edge is determined by the band gap, which is largest for $Ca_2Si_5N_8$ (250 nm) and smallest for $Ba_2Si_5N_8$ (280 nm).

6.1.3 Photoluminescent properties

Emission

Figure 6.4 shows the steady state emission spectra (emission spectra recorded during excitation) of $Ca_2Si_5N_8$:Eu, $Sr_2Si_5N_8$:Eu and $Ba_2Si_5N_8$:Eu. In all three cases, the spectrum consists of one broad Eu^{2+}-based band (FWHM of about 100 nm). The broadness of the emission can be explained by the existence of two similar cation sites in the host lattice. Since the europium ions occupy both of these cation sites, and the position of the emission band is closely related to the europium surroundings, the spectrum will consist of two bands, in this case largely overlapping [5].

The emission maximum shifts from 585 nm (yellowish orange) for M = Ba, over 610 nm (orange) for M = Ca, to 620 nm (reddish orange) for M = Sr. It could be expected

that the position of the emission maximum shifts monotonously when changing the cation from Ca over Sr to Ba. However, $Ca_2Si_5N_8$:Eu does not follow this trend because of its different crystal structure compared to $Sr_2Si_5N_8$:Eu and $Ba_2Si_5N_8$:Eu. For dopant concentrations below 5%, the wavelength position of the maxima is in all powders only slightly dependent on the europium concentration.

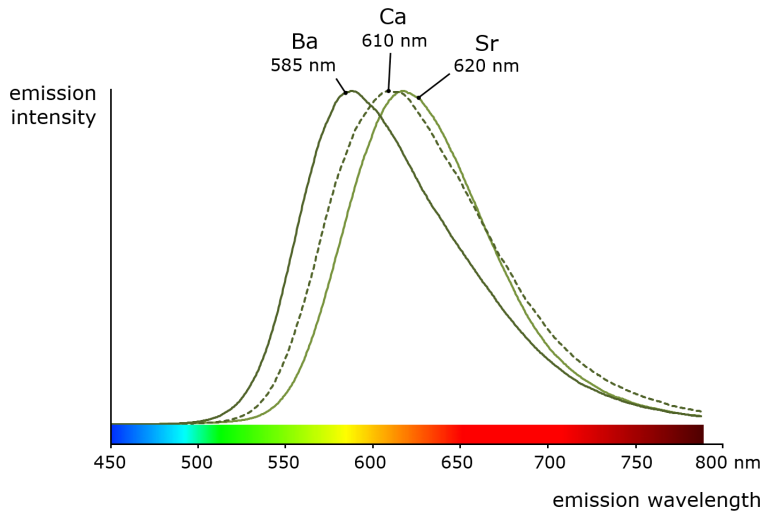

Figure 6.4: Emission spectra of $M_2Si_5N_8$:Eu (M = Ca, Sr, Ba) under 365 nm UV excitation.

If we look at the location of the samples' emission colors in a chromaticity diagram, we see that they are located near the edge, indicating that they are very saturated (figure 6.5).

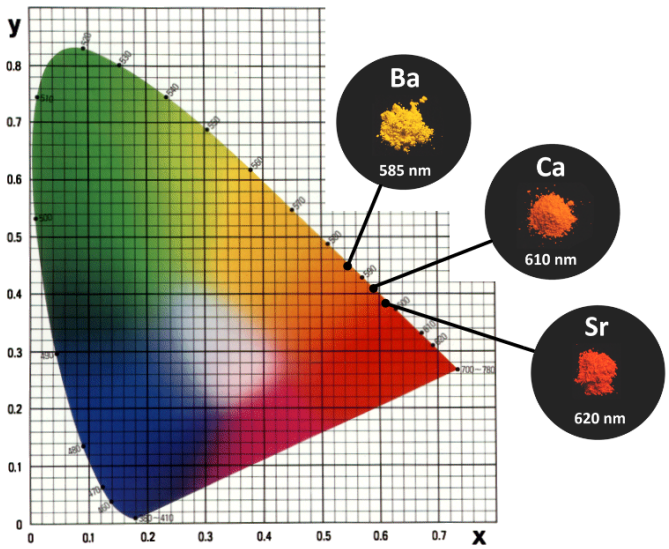

Figure 6.5: Emission color and visual appearance of $Ca_2Si_5N_8$:Eu, $Sr_2Si_5N_8$:Eu and $Ba_2Si_5N_8$:Eu under 365 nm UV excitation.

Excitation

The steady state excitation spectra are given in figure 6.6. These are very broad, and extend well into the visible region, up to 550 nm. On the short wavelength side, the samples show exciton absorption in the region just below the band gap. The remaining bands can be attributed to the $4f^7 \rightarrow 4f^6 5d^1$ transition in the Eu^{2+} ions, with a maximum in a broad region around 400 nm.

The fact that these materials can be excited with visible light is promising for indoor applications of persistent luminescence. However, it does not necessarily mean that traps can be filled efficiently at these longer wavelengths. In other words, the excitation spectrum of the persistent luminescence might be very different from the steady state excitation spectrum. This possibility is further explored in section 6.1.5.

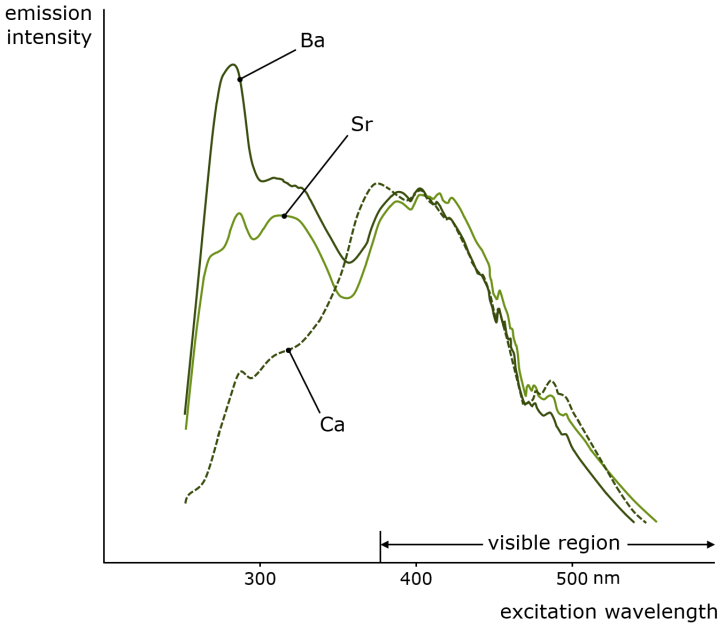

Figure 6.6: Excitation spectra of $M_2Si_5N_8$:Eu (M = Ca, Sr, Ba) measured at the emission maximum for each compound.

6.1.4 Afterglow

After excitation, all materials show some form of persistent luminescence. Figure 6.7 shows the afterglow intensity as a function of time after 1 minute excitation with an unfiltered xenon arc lamp at 1000 lux. The decay curves follow straight lines in a log-log plot, implying that they can be modeled by a power law with negative scaling exponent. Initially, the decay is very fast, dropping several orders of magnitude during the first minute. This decay gradually slows down over time, a type of behaviour which is typical for most persistent luminescent materials.

We define the afterglow duration as the time between the end of the excitation and the moment when the afterglow intensity drops below 0.32 mcd/m^2. The afterglow duration is longest for $Ba_2Si_5N_8$:Eu, around 400 seconds, followed by $Ca_2Si_5N_8$:Eu,

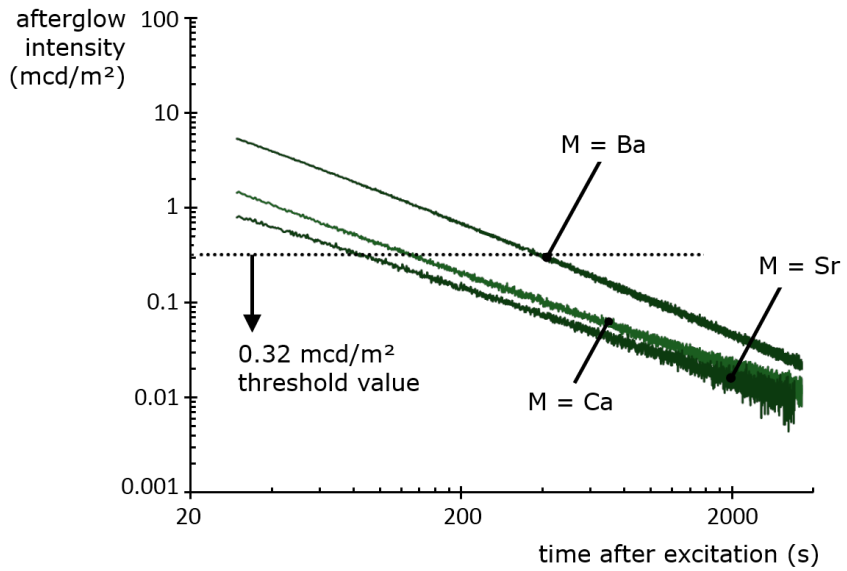

Figure 6.7: Comparison of the afterglow intensity of $M_2Si_5N_8$:Eu (M = Ca, Sr, Ba) after 1 minute excitation with a 1000 lx unfiltered Xe arc lamp. $Ba_2Si_5N_8$:Eu has the most intense afterglow lasting about 400 seconds before it drops below the 0.32 mcd/m^2 threshold.

around 150 seconds. $Sr_2Si_5N_8$:Eu has a very short afterglow duration of 80 seconds. This rapid afterglow decay is often an advantage, since $Sr_2Si_5N_8$:Eu is a popular conversion phosphor in GaN- or InGaN-based white LEDs, where a long afterglow is undesired.

The afterglow spectra of $Ca_2Si_5N_8$:Eu and $Ba_2Si_5N_8$:Eu are red-shifted about 5-10 nm compared to the steady state spectra. For $Sr_2Si_5N_8$:Eu the afterglow was too weak to measure this with sufficient accuracy. A similar red-shift in the persistent spectrum is also seen in Ca_2SiS_4:Eu,Nd [7] and in $CaAl_2Si_2O_8$:Eu [8].

Measurements of the decay behaviour of $Ca_2Si_5N_8$:Eu in the first moments after the end of the excitation show that this red-shift occurs in the first 5-10 μs after the end of the excitation (figure 6.8), after which the spectrum remains unchanged during the afterglow. This means that both crystallographic sites available for europium take part in the luminescence. If only one of the sites showed persistent luminescence, the decay time of the other would be determined solely by the lifetime of Eu^{2+} (around 1 μs), and the persistent emission spectrum would reach its final position on a much faster timescale than the observed 5-10 μs. Secondly, the integrated emission intensity in the first microseconds after the excitation does not show a clear exponential component with a lifetime of 1 μs (figure 6.9), which would be expected if one of the sites did not take part in the persistent luminescence.

Translating these observations to a defect model is not straightforward and remains somewhat speculative. A first possibility is formed by defects (which serve as trap states) near the europium ions, thus altering the local environment. This could then lead to the observed red-shift in the afterglow spectrum. Another possibility could be the affinity for traps to be dominantly coupled to only one of the europium sites. Differences in energy transfer behaviour between both sites for the steady state emission

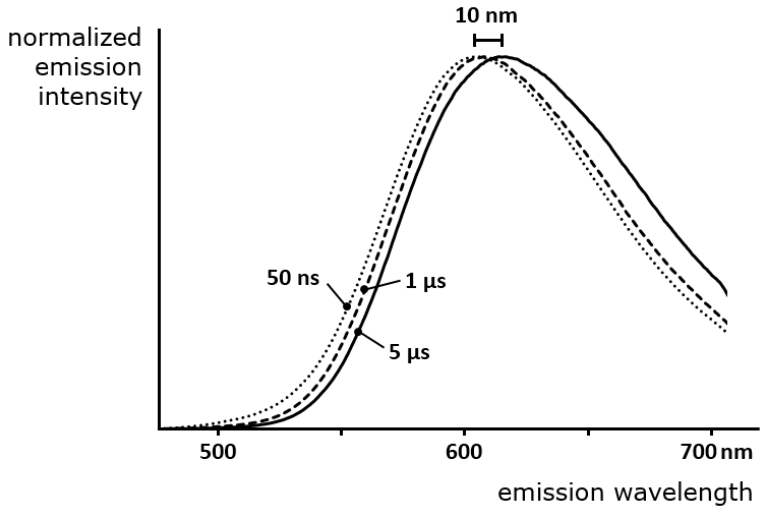

Figure 6.8: The afterglow spectrum of $Ca_2Si_5N_8$:Eu,Tm shows a red-shift of about 10 nm which occurs during the first few μs of the decay.

and the afterglow might occur also, although this is less likely given that the steady state emission spectrum of $Ca_2Si_5N_8$:Eu is invariable for changes in excitation wavelength or intensity. Clearly more in-depth research is required to fully explain these observations.

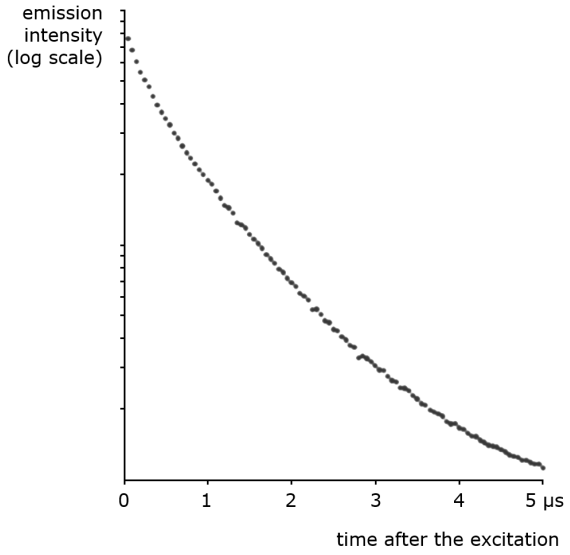

Figure 6.9: Decay of the luminescence intensity in $Ca_2Si_5N_8$:Eu,Tm during the first few μs after the excitation.

6.1.5 Trap filling

As discussed in section 6.1.3, the excitation spectra of the alkaline earth nitrido-silicates are very broad, extending well into the visible region. This could be promising for indoor persistent luminescent applications, where UV excitation is not readily avail-

able. Especially with the increase of LED-based lighting [9], the amount of indoor short-wavelength excitation light is greatly reduced. However, the broad steady state excitation spectrum does not necessarily imply an efficient excitation of the persistent luminescence at longer wavelengths.

To investigate the effectiveness of various wavelengths for inducing persistent luminescence in $M_2Si_5N_8$:Eu, the thermoluminescence excitation (**TL-excitation**) contour plots are shown in figure 6.10. In this type of experiment, the sample undergoes a series of TL measurements for a wide range of excitation wavelengths. For optimal accuracy, the set-up is fully automated and software controlled. Each horizontal line in the contour plot represents the glow curve obtained at a specific excitation wavelength. In this way, it is immediately clear which wavelengths lead to an efficient trap filling (indicated by a high intensity during the TL measurement). The exact procedure is explained in detail in reference [10].

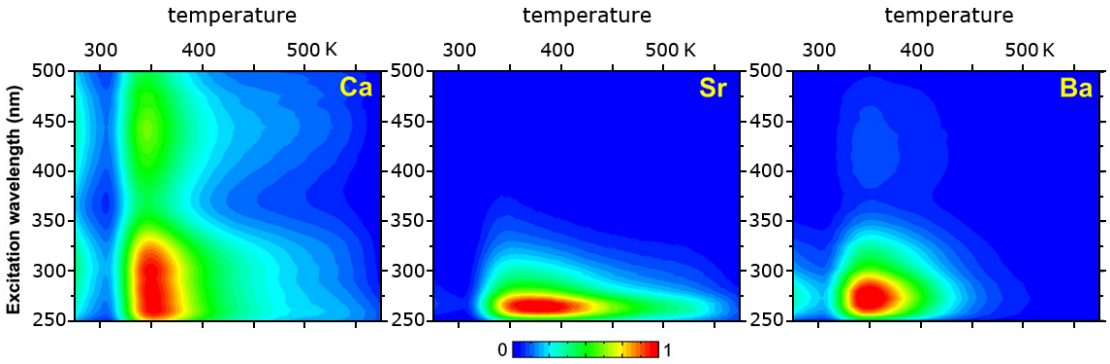

Figure 6.10: Normalized TL excitation contour plots for $M_2Si_5N_8$:Eu (M = Ca, Sr, Ba) excited at room temperature. The heating rate was 5 K/s. For $Sr_2Si_5N_8$:Eu, persistent luminescence can only be induced by excitation with short wavelengths in the order of the bandgap energy. In $Ca_2Si_5N_8$:Eu, traps can also be filled by exciting with visible light.

For all three materials, the same two regions can be discerned. Below 325-350 nm, i.e. with photon energies close to or larger than the band gap, trap filling is very efficient, possibly due to the immediate trapping of the electron. The glow curves are very broad, and extend to a relatively high temperature, indicating the presence of a complicated trap system, possibly with multiple trap levels or a continuous distribution of trap depths. For $Ca_2Si_5N_8$:Eu, the maximum of the glow peak lies around 348 K. For $Ba_2Si_5N_8$:Eu this maximum is located around 351 K, while in $Sr_2Si_5N_8$:Eu the glow curve peaks around 368 K.

For wavelengths above 350 nm, the situation is dramatically different. In this case, the electrons are excited solely into the lower levels of the 5d state. In $Sr_2Si_5N_8$:Eu, no traps can be filled using these longer wavelengths, as no TL emission was obtained after the excitation. In $Ca_2Si_5N_8$:Eu, on the other hand, this way of trap filling is rather efficient. The peak in the TL excitation map above 350 nm is clearly visible, and has the same glow curve as the peak below 350 nm, indicating that the same traps are being

accessed. In $Ba_2Si_5N_8$:Eu, an intermediate situation can be seen, with some trap filling at long wavelengths, albeit rather inefficient compared to the region below 350 nm.

If we sum the total TL intensity for each excitation wavelength, we obtain the **trap filling spectrum** for the three materials, as depicted in figure 6.11. From these spectra, we can basically draw the same conclusions. In $Ca_2Si_5N_8$:Eu, persistent luminescence can be induced by a broad range of wavelengths extending up to 500 nm. In $Ba_2Si_5N_8$:Eu, this is also possible, although excitation wavelengths above 350 nm are not very efficient. In $Sr_2Si_5N_8$:Eu, only excitation wavelengths shorter than 350 nm can lead to trap filling and thus to persistent luminescence. This makes the $Ca_2Si_5N_8$-based phosphors the most promising candidates for future persistent luminescence applications.

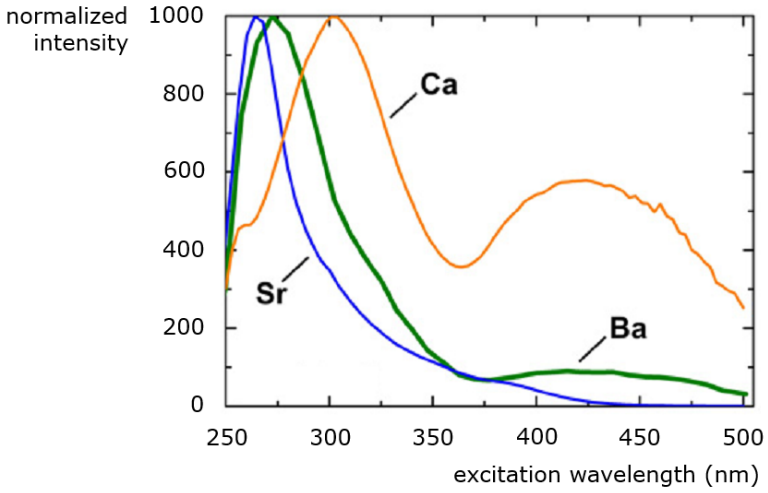

Figure 6.11: Excitation curves for the persistent luminescence of $M_2Si_5N_8$:Eu (M = Ca, Sr, Ba). These trap filling spectra were obtained from the TL excitation contour plots by integrating over the entire glow peak.

6.1.6 Rare earth codoping

To study the influence of rare earth ions on $M_2Si_5N_8$:Eu, we codoped samples with 1% of dysprosium, neodymium, samarium or thulium, and compared the persistent luminescence with the material without codoping. This codoping has no effect on the emission spectrum. Figure 6.12 shows the afterglow intensity 1 minute after excitation with 300 nm (UV) light. As can be seen, the codopant strongly influences the afterglow in $Ca_2Si_5N_8$:Eu,R and $Ba_2Si_5N_8$:Eu,R. For $Sr_2Si_5N_8$:Eu,R no afterglow of importance could be achieved with any of the codopants. For $Ba_2Si_5N_8$:Eu,R codoping with dysprosium does not considerably influence the afterglow. The other codopants have a negative effect on the afterglow in $Ba_2Si_5N_8$:Eu,R.

In $Ca_2Si_5N_8$:Eu,R a strong influence of the codopant is seen. Dysprosium and neodymium enhance the afterglow intensity considerably, while samarium reduces it by more than 40%. The most spectacular effect is obtained with thulium codoping,

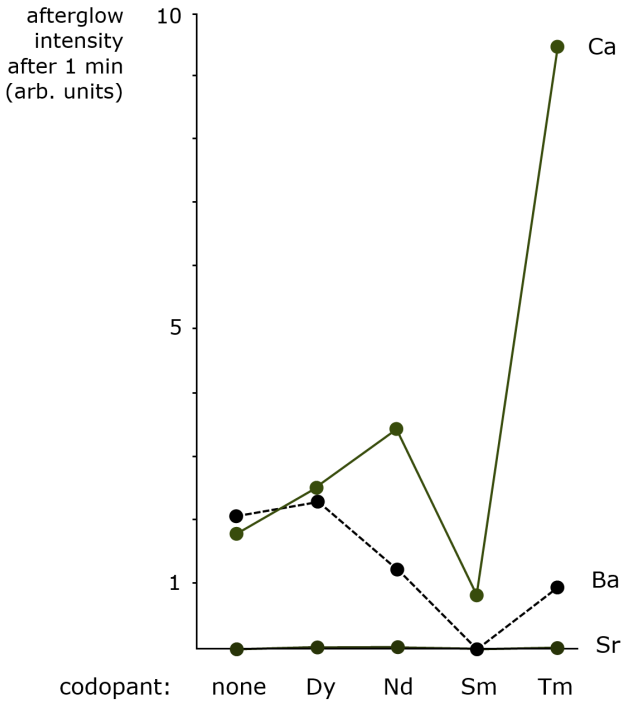

Figure 6.12: Influence of the codopant on the intensity of the afterglow in $M_2Si_5N_8$:Eu (M = Ca, Sr, Ba) recorded 1 minute after the end of the excitation by 300 nm light.

as was also noted by Miyamoto *et al.* [11] and Lei *et al.* [12]. In this case, the afterglow intensity after one minute is nearly six times as high as in the non-codoped sample. The afterglow duration after 1 minute excitation with a Xe arc lamp at 1000 lux is around 2500 s, compared to 150 s for non-codoped $Ca_2Si_5N_8$:Eu (figure 6.13). Therefore, also taking into account the results from the previous section, $Ca_2Si_5N_8$:Eu,Tm is our material of choice to continue our development of an efficient, long-lasting, orange-emitting persistent luminescent material.

The charge carrier traps, which are presumably created or affected by the codopant ions, can be investigated by TL experiments. Figure 6.14a compares the glow curves obtained during a TL measurement for $Ca_2Si_5N_8$:Eu and the thulium-codoped variant, after 300 nm excitation at room temperature for 2 minutes, with a heating rate β of 5 K/s.

The curves were analyzed with the TL Glow Curve Analyzer software [13]. Nevertheless, care should be taken when analysing these glow curves. The broadness of the peaks, especially on the high-temperature side, indicates that a single first- or second-order trap description is insufficient and multiple traps or trap distributions might be present. Therefore, the trap depths presented here are only indicative. In the non-codoped and the thulium-codoped case the shape of the peak is similar, suggesting that the same trap is responsible for the afterglow. However, upon codoping with thulium the peak location shifts to higher temperatures, around 370 K, indicating that the trap depth has increased to a more suitable depth for persistent luminescence. Assuming general order kinetics, the trap depth is estimated to shift from 0.87 eV to 0.91 eV upon codoping.

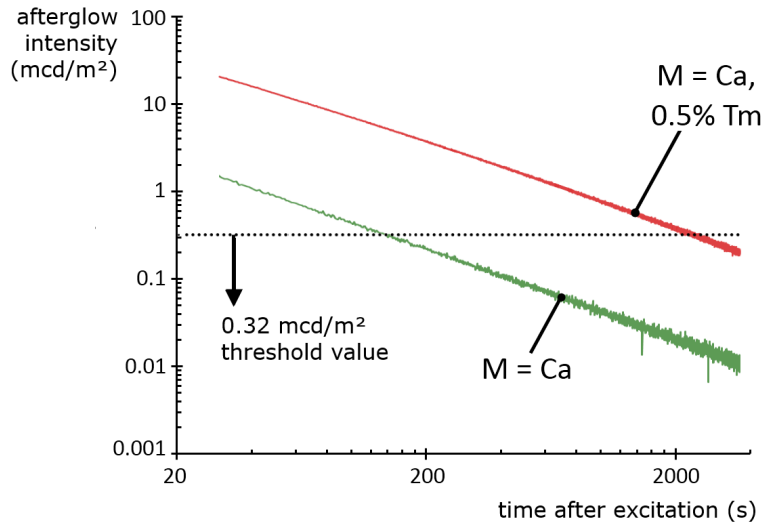

Figure 6.13: Comparison of the afterglow in $Ca_2Si_5N_8$:Eu and $Ca_2Si_5N_8$:Eu,Tm after 1 minute excitation with a 1000 lx unfiltered Xe arc lamp.

To illustrate that the same codopant can have different effects in different host crystals, the glow curves for $Ba_2Si_5N_8$:Eu and $Ba_2Si_5N_8$:Eu,Tm are shown in figure 6.14b. In this case, the glow peak shifts to lower temperatures, in other words, the charge carrier trap becomes shallower (0.71 eV in the non-codoped case, 0.68 eV in the thulium-codoped sample, again assuming general order kinetics).

6.2 The special case of $Ca_2Si_5N_8$:Eu,Tm

From the discussion above, we know that the orange afterglow in $Ca_2Si_5N_8$:Eu,Tm is exceptionally bright when compared to the other members of the nitrido-silicate family,

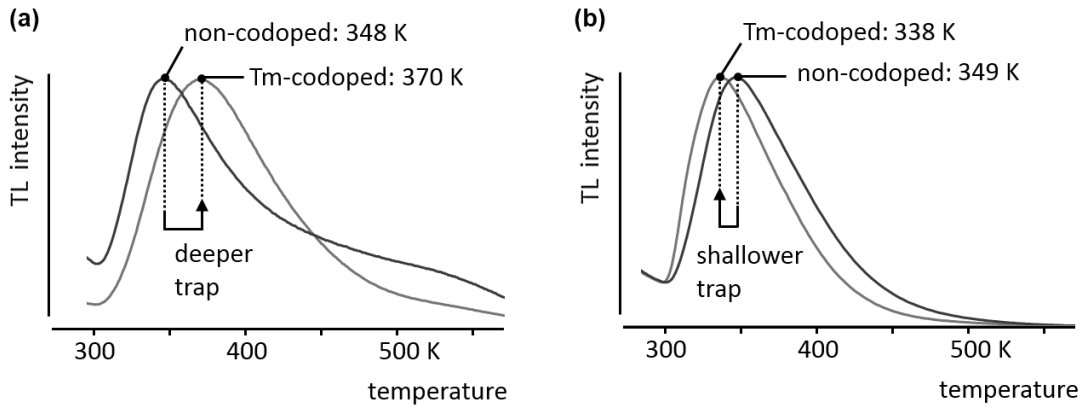

Figure 6.14: Normalized TL glow curves for (a) non-codoped $Ca_2Si_5N_8$:Eu and $Ca_2Si_5N_8$:Eu,Tm and (b) for non-codoped $Ba_2Si_5N_8$:Eu and $Ba_2Si_5N_8$:Eu,Tm. The samples were excited at room temperature for 2 minutes at 300 nm. The heating rate β was 5 K/s

lasting up to 2500 seconds after the end of the excitation. Furthermore, this persistent luminescence can be induced by a broad range of wavelengths extending from below 250 nm to over 500 nm, well into the visible region of the spectrum. In the remainder of this chapter, we will try to optimize and understand this exceptional behaviour.

6.2.1 Rare earth codoping in $Ca_2Si_5N_8$:Eu

First of all, it is important to verify if thulium is truly the best choice for the rare earth codopant in $Ca_2Si_5N_8$:Eu. Figure 6.15 compares the afterglow intensity 1 minute after 400 nm excitation for $Ca_2Si_5N_8$:Eu codoped with any of the rare earth ions, including yttrium, but excluding promethium.

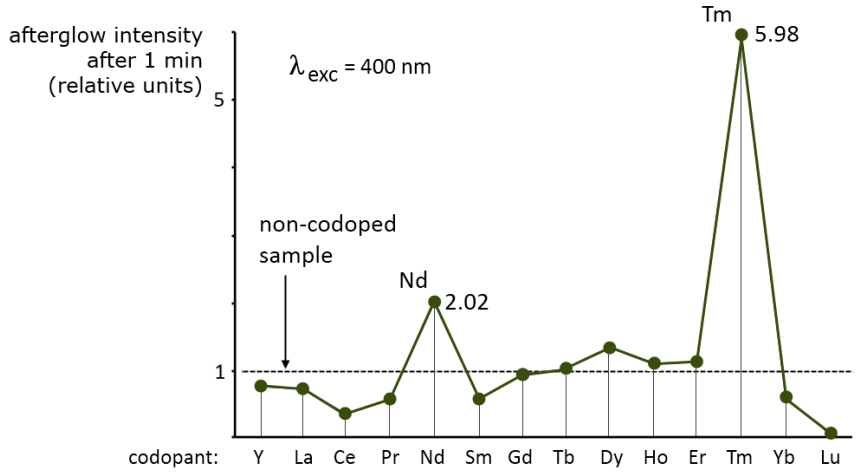

Figure 6.15: Influence of the codopant choice on the afterglow intensity in $Ca_2Si_5N_8$:Eu recorded 1 minute after the end of the excitation by 400 nm light.

There is a considerable influence of the codopant on the afterglow intensity. Only neodymium, dysprosium and thulium have a clear positive effect on the persistent luminescence, with the latter being by far the best choice. Again, as was the case after excitation with 300 nm (figure 6.12) the afterglow intensity of $Ca_2Si_5N_8$:Eu,Tm is about 6 times that of non-codoped $Ca_2Si_5N_8$:Eu. On the other hand, several rare earth codopants, such as cerium, samarium, ytterbium and lutetium have a considerable negative influence on the afterglow.

The influence of the different rare earths can be studied in more detail by measuring the TL glow curve for various codoped samples, as is shown in figure 6.16. The TL glow curve of non-codoped $Ca_2Si_5N_8$:Eu is characterized by three major peaks. The main one is situated at about 100 K, although its shape suggests multiple components. A second peak, extending beyond room temperature, peaks at 200-220 K. Beyond 450 K, a third glow peak emerges, although this peak could not be fully recorded due to the temperature limitation of the cryostat.

The addition of codopants introduces other glow peaks, superposed on the features observed for $Ca_2Si_5N_8$:Eu. Codoping with Nd, Dy and Ho yields additional peaks at approximately 175, 205 and 215 K, respectively. As these glow peaks are largely situ-

ated below room temperature, they do not contribute to the persistent luminescence observed at room temperature. When adding thulium, an additional glow peak is introduced around 340 K.

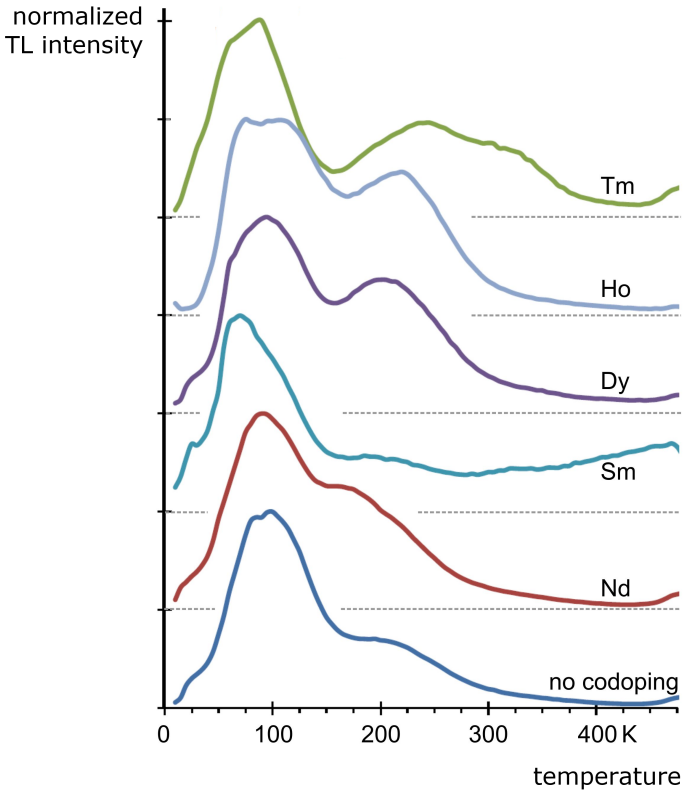

Figure 6.16: Thermoluminescence glow curves for $Ca_2Si_5N_8$:Eu codoped with various rare earths (R = Nd, Sm, Dy, Ho and Tm) after excitation by 400 nm light. The heating rate was 6.6 K/min, the emission was monitored at 620 nm.

The depth of the introduced traps is comparable in the case of Nd, Dy and Ho, while Tm causes much deeper traps. This is in line with the Dorenbos energy level scheme [14]. As can be seen from figure 6.17, the 4f energy levels of divalent Nd, Dy and Ho are located at approximately the same depth. The level of Tm is considerably deeper, and might be located at the optimal depth for persistent luminescence in $Ca_2Si_5N_8$:Eu,R. The energy level of Sm is located even deeper. In practice, the Sm^{2+} level is probably located below the Fermi level, causing the ion to exist only in its divalent form, which makes it impossible to act as a trap level. This could explain the negative influence of Sm on the persistent luminescence in all of the $M_2Si_5N_8$:Eu compounds.

6.2.2 Rare earth concentration

An important point of interest concerns the concentration of the dopant and codopant ions in the host crystal. Increasing the concentration might improve the light output of the phosphor, but it might also have a negative influence due to concentration quenching.

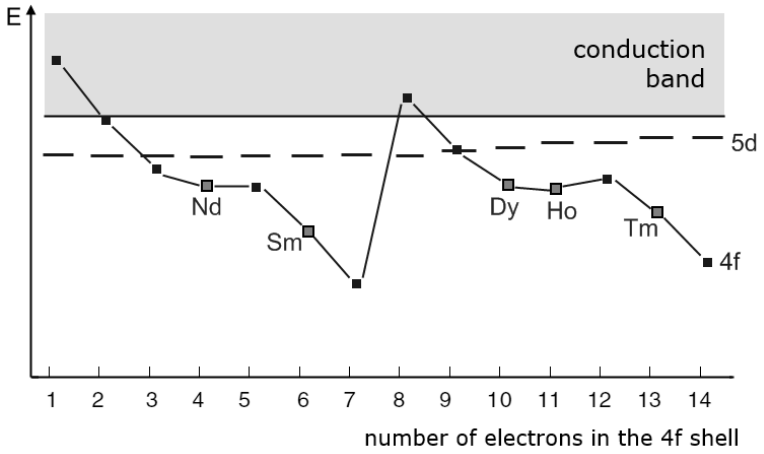

Figure 6.17: Relative location of the 4f energy levels of the divalent lanthanides, according to the Dorenbos model [14].

Dopant concentration

As with normal fluorescence, a high concentration of luminescent centers is usually undesired in persistent luminescence, due to concentration quenching. This is confirmed by figure 6.18, showing the afterglow intensity in $Ca_2Si_5N_8$:Eu,Tm after 10 minutes as a function of Eu concentration, where the Tm codopant concentration is kept at 1%. Clearly, it is best to keep the dopant concentration below 1%.

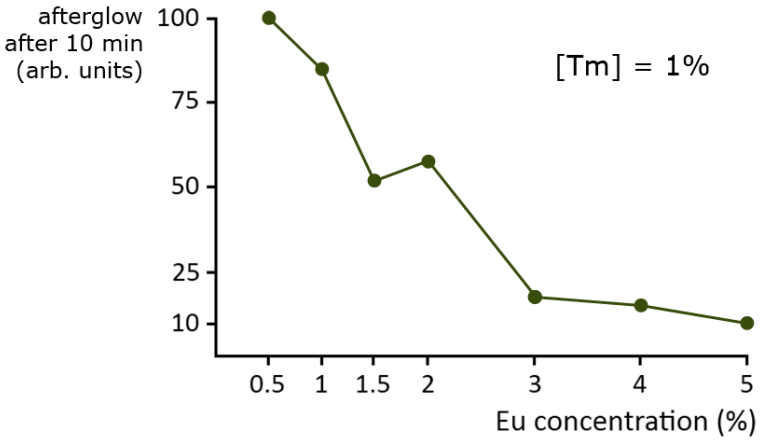

Figure 6.18: Afterglow intensity of $Ca_2Si_5N_8$:Eu,Tm 10 minutes after excitation by 365 nm light, as a function of Eu concentration. Increasing the Eu concentration has a negative influence on the afterglow intensity.

Codopant concentration

The afterglow brightness as a function of codopant concentration is shown in a similar fashion in figure 6.19, where the Eu concentration is kept constant at 1%. The effect is even more dramatic here: a Tm concentration of 2% reduces the afterglow intensity

to 10% of the value at a concentration of 0.5%. If the concentration of Tm becomes too high, this might lead to the formation of Tm-rich islands (see also section 6.2.3). In any case, a Tm concentration above 1% is undesired for persistent luminescence in $Ca_2Si_5N_8$:Eu,Tm.

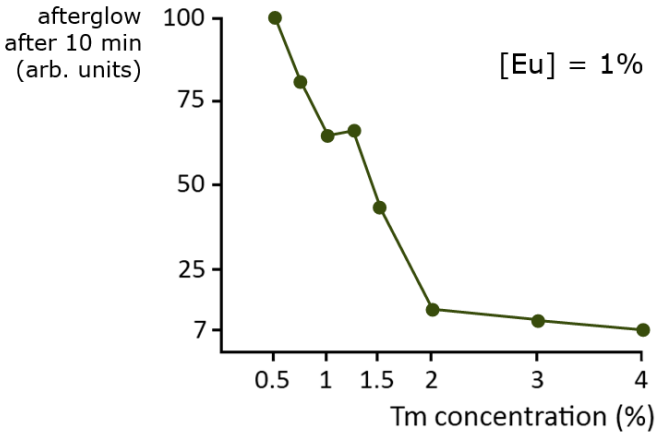

Figure 6.19: Afterglow intensity of $Ca_2Si_5N_8$:Eu,Tm 10 minutes after excitation by 365 nm light, as a function of Tm concentration. Increasing the Tm concentration has a negative influence on the afterglow intensity.

6.2.3 Optimization of the preparation

The afterglow intensity of the samples is not only influenced by the (co)dopants, but also by the starting materials chosen during the preparation and by the preparation conditions, such as temperature and duration.

Influence of the Ca vs. Sr ratio

A first important effect of the starting materials is of a stoichiometric nature. A 5% deficiency of Ca_3N_2 in the starting mixture for $Ca_2Si_5N_8$:Eu,Tm increases the afterglow intensity by nearly 300% (figure 6.20). This might be due to the fact that the dopant and codopant ions are located at Ca-sites. Hence an increase of Ca-vacancies, caused by the Ca_3N_2 deficiency, might facilitate the incorporation of rare earth ions in the host, because of charge compensation effects. However, as noted above, the nature and location of the traps that lead to persistent luminescence is still debated, and further research is necessary to study the incorporation of the rare earths and their influence on the afterglow.

At even higher deficiencies of Ca_3N_2, the brightness of the persistent luminescence decreases again. XRD measurements show that a (non-luminescent) α-Si_3N_4 phase remains in these samples, as can be seen in figure 6.21.

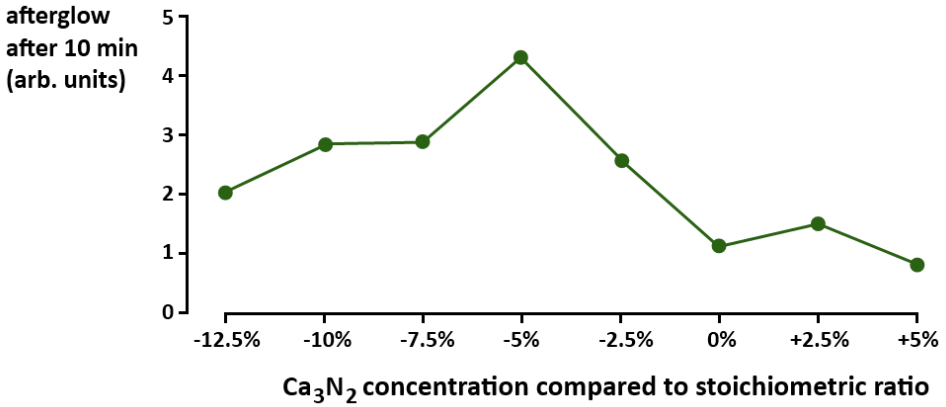

Figure 6.20: A small deficit of Ca in the starting mixture strongly increases the afterglow intensity in $Ca_2Si_5N_8$:Eu,Tm.

Formation of Tm-rich regions

SEM and EDX investigations reveal the formation of (non-luminescent) micron-sized Tm-rich aggregates in the material when the Tm concentration becomes too high. An example of such a Tm-rich island is shown in figure 6.22. This undesired phenomenon can be partially countered by increasing the preparation duration and temperature. Still, it is very difficult to get rid of these Tm-rich regions completely. It should therefore be kept in mind that the actual concentration of Tm in the bulk material might be considerably lower than the concentration of Tm added to the starting mixture during preparation.

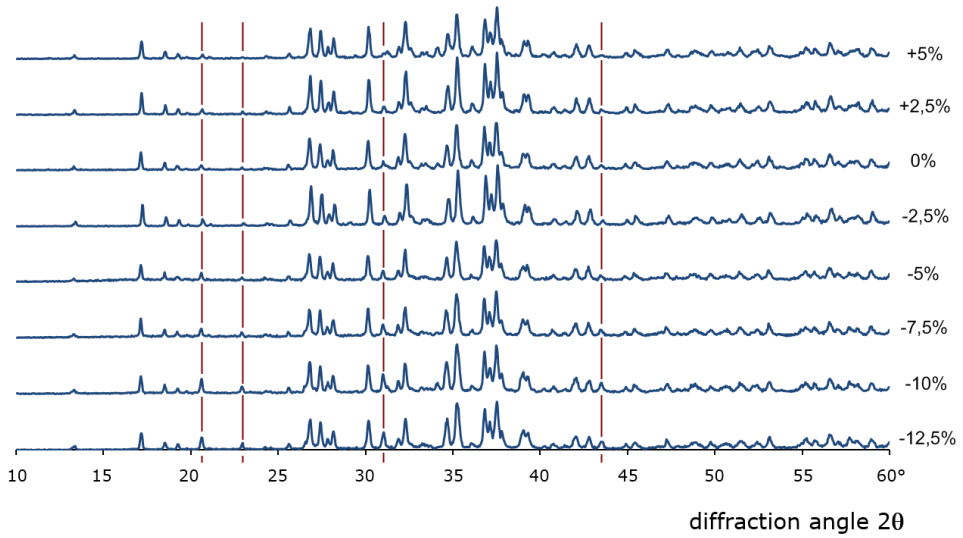

Figure 6.21: XRD spectra of $Ca_2Si_5N_8$:Eu,Tm samples with increasing Ca deficit reveal the presence of an undesired α-Si_3N_4 phase. The peaks originating from α-Si_3N_4 are indicated by the vertical red lines.

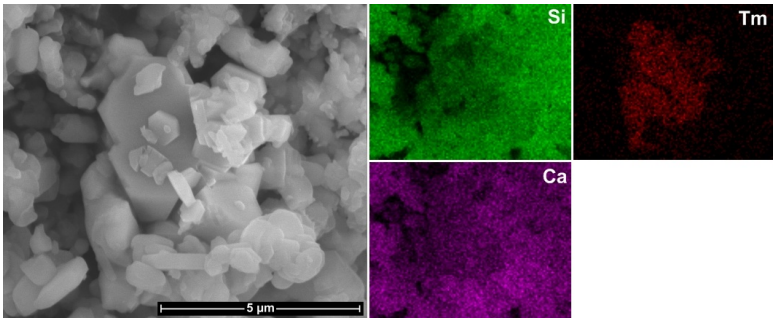

Figure 6.22: Scanning electron microscope image and elemental EDX maps of $Ca_2Si_5N_8$:Eu,Tm powder reveal the formation of Tm-rich regions.

Influence of the preparation duration

One possible solution for the removal of Tm-rich regions might be increasing the duration of the reaction. It is possible that the rare earth ions are more easily distributed through the material when the mixture is kept at high temperature for a longer period of time. Figure 6.23 shows a comparison of the afterglow intensity of two samples with a different preparation duration. After increasing the baking time from 1 hour to 3 hours, the persistent luminescent intensity is increased about 3 times.

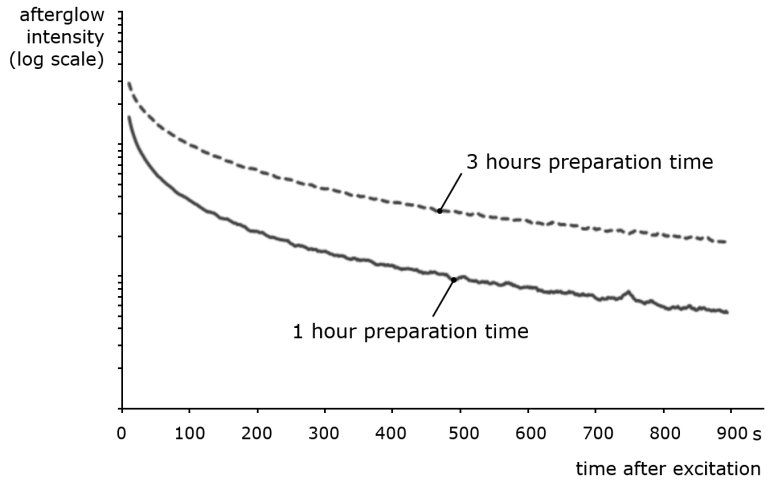

Figure 6.23: Increasing the preparation duration from 1 to 3 hours extends the afterglow in $Ca_2Si_5N_8$:Eu,Tm to approximately 2500 s.

EDX mapping reveals that Tm-rich islands are still present even after increasing the preparation time to 3 hours. Although the number and size of these islands appear to be smaller, the effect is not as big as we would expect based on the increase in afterglow brightness. Probably, the origin of the enhanced afterglow can be found on a smaller scale than detectable by EDX mapping.

Oxides and fluorides in the starting mixture

A crucial factor is the choice of starting material for the rare earth ions. When the dopant and codopant ions are added to the starting mixture in their fluoride form (EuF_3 and TmF_3), the afterglow 10 minutes after excitation is over 12 times brighter than if oxides (Eu_2O_3 and Tm_2O_3) are used (figure 6.24). This is most probably due to the more favorable chemical properties of fluorides compared to oxides, for example their lower melting point. This makes it easier for the materials to diffuse into the host crystal during the sintering phase of the preparation.

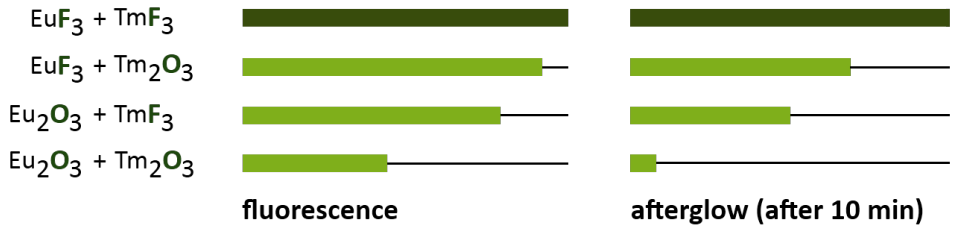

Figure 6.24: Using rare earth fluorides instead of oxides in the starting mixture can improve the afterglow intensity more than tenfold.

XRD measurements show an increased crystallinity when using fluorides, indicating that fluorine also acts as a flux material during the reaction. EDX investigations of $Ca_2Si_5N_8$:Eu,Tm have revealed the formation of multiple Tm- and O-rich aggregates upon preparation with oxides. Analysis of these aggregates indicates that they contain comparable amounts of Tm, Si and N, and almost no Ca. This suggests the formation of the non-luminescent $TmSiO_2N$ phase. When using fluorides some Tm-rich aggregates were still formed, but in a lower concentration. Here, the equal concentrations of Ca and Tm and the hexagonal structure of the aggregates suggest the formation of $CaTmSi_4N_7$. No fluorine was encountered in any of the samples.

Influence of flux materials

Besides simply adding the rare earths in their fluoride form, we might also consider the addition of other flux materials to the starting mixture, in order to improve the afterglow efficiency. A comparison of the afterglow duration for three different types of flux materials (KF, KCl and NH_4Cl) is shown in figure 6.25. While KF has only a small influence on the afterglow, the addition of KCl and NH_4Cl can make the afterglow duration up to four times as long as in a sample without flux.

While figure 6.25 might suggest that adding even more flux material might improve the afterglow duration even more, it should also be noted that the HF and HCl gases released during the preparation are starting to damage the oven equipment. Also, at higher flux concentrations, part of the fluorine or chlorine ions remain present in the sample, as shown by EDX analysis.

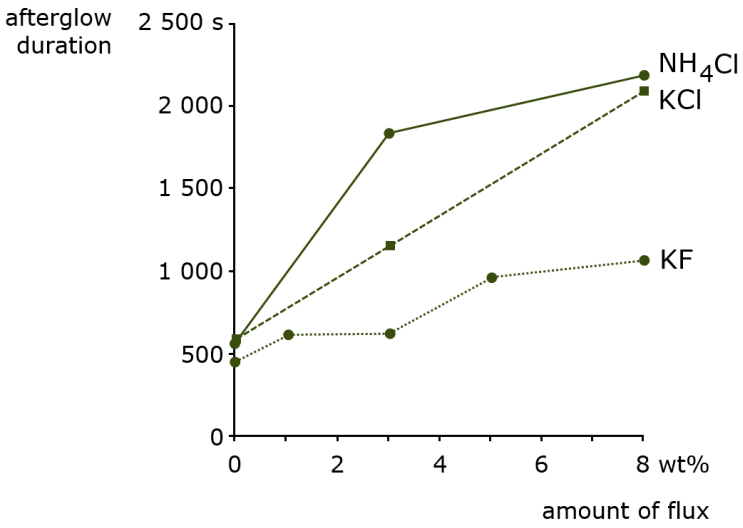

Figure 6.25: Addition of NH_4Cl or KCl as flux material can improve the afterglow duration to 4 times its initial length.

6.2.4 Stability

A final important aspect of $Ca_2Si_5N_8$:Eu,Tm is its high chemical stability, especially in view of its application for *in vivo* medical imaging. After storage in distilled water for two years, the intensity of the persistent luminescence has decreased by only 2% (figure 6.26). For other commonly encountered persistent phosphors the stability is much lower. For example, the afterglow intensity of $SrAl_2O_4$:Eu,Dy has decreased over 50% after storage in water for two years.

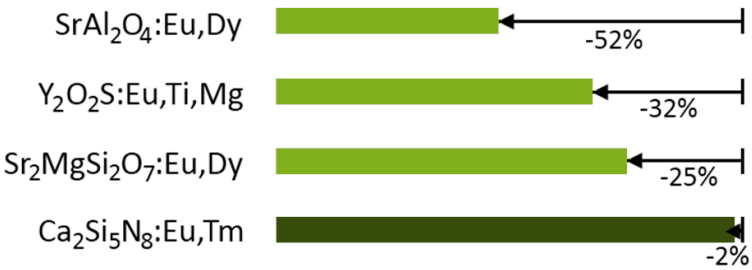

Figure 6.26: After 2 years storage in water, the intensity of the persistent luminescence in $Ca_2Si_5N_8$:Eu,Tm has decreased by only 2%, which is much less than in other well-known persistent phosphors.

6.3 Medical imaging using nitridosilicate nanoparticles

The most fascinating and important novel application of persistent luminescence is probably *in vivo* medical imaging. Using persistent luminescent nanoparticles, it is possible to track the distribution of drugs and other molecules throughout the body of a patient.

6.3.1 Principle of *in vivo* imaging

Typically, *in vivo* medical imaging is performed using radioactive isotopes, such as the metastable ^{99m}Tc isotope of technetium. These so-called **tracer particles** are attached to molecules or drugs that need to be followed as they flow through the body of a patient. After injection, the radiation of the tracers can be detected outside the body, and the location of the particles can be monitored. A simplified overview of the method is shown in figure 6.27.

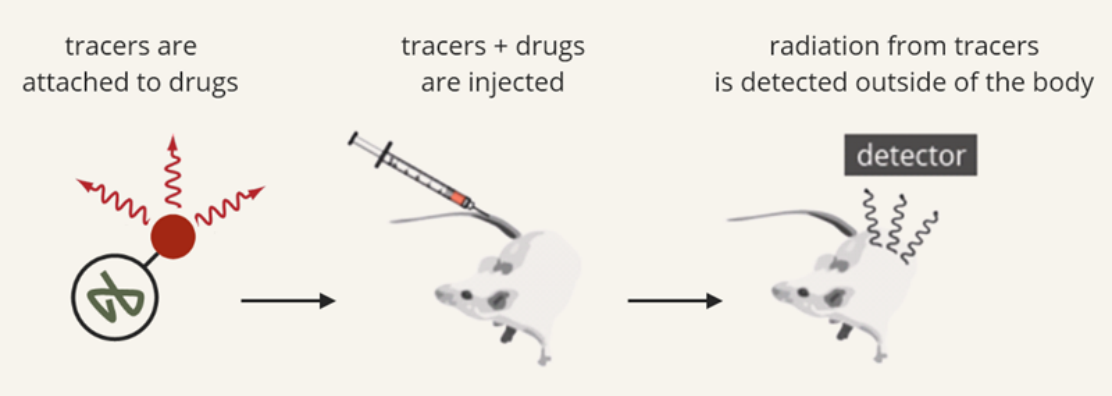

Figure 6.27: In classical *in vivo* medical imaging, radioactive tracer particles are attached to drugs or molecules that need to be followed throughout the body.

To avoid the presence of radioactive tracer particles, the molecules or drugs can also be attached to nano-sized persistent luminescent particles. These particles can be excited by UV-light before injection. As they move through the body, their emission can be detected from the outside using a very sensitive camera, e.g. a CCD camera. The principle is shown in figure 6.28.

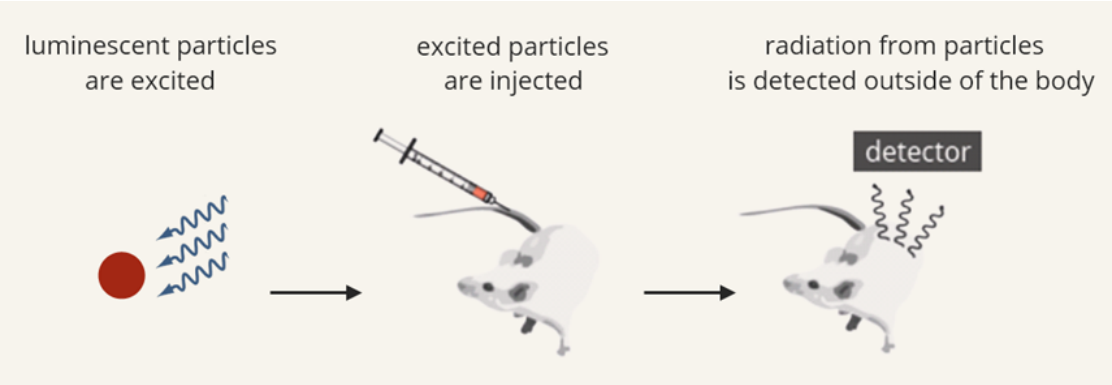

Figure 6.28: Persistent luminescent nanoparticles can be used as an alternative to radioactive tracer particles.

Of course, not all wavelengths are suited for this kind of imaging technique. Human and animal tissue contain water, blood, melanine and fat, which all have their own specific absorption behaviour. However, in a region located roughly between 600 and

1300 nm, the absorption is relatively low. This region is known as the **optical window** (figure 6.29). In other words, red and infrared light can be partially transmitted through the tissue. For the same reason, upon holding a flashlight against your hand, only the red part of the light will come through, and you will see a red glow through your hand.

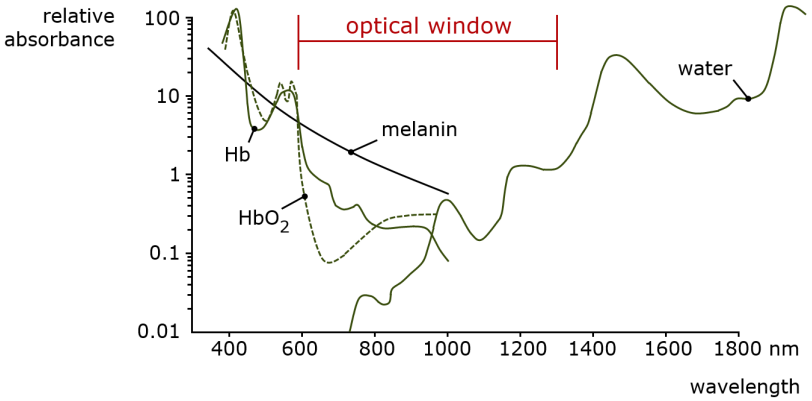

Figure 6.29: The absorption of different tissue components leads to an optical window for tissue transparancy located roughly between 600 and 1300 nm. Adapted from [15].

The position of this optical window is the main reason why we are looking for red- and near-IR-emitting persistent phosphors. The use of Cr^{3+} as a luminescent ion proves to be very interesting for these applications. However, also $Ca_2Si_5N_8$:Eu,Tm, having an orange-to-red emission and a very high stability, is a possible candidate. The fact that $Ca_2Si_5N_8$:Eu,Tm is excitable by visible light opens up the possibility for re-excitation of the tracer particles, after they have been injected into the body. However, for practical applications, we will need to produce the material as nanosized particles rather than micron-sized grains, and we will need to verify that the presence of $Ca_2Si_5N_8$:Eu,Tm nanoparticles is not harmful for a biological environment.

6.3.2 Nanoparticle preparation

After the solid state reaction described in section 6.1.1, a powder is obtained with a grain size of around 1 to 5 micron. Since the diameter of the smallest blood vessels in the human body (the capillaries) is typically in the order of 5 to 10 micron, we need smaller particles to easily penetrate the veins. Also, particles which are too large might end up in the liver instead of elsewhere. For optimal biodistribution, we require particles with a diameter of around 100 nm.

To reduce the particle size, several routes can be followed. We have applied both pulsed laser ablation (PLAL) and wet grinding in a planetary ball mill. Afterwards, the samples are centrifuged to select the smallest particles. Both techniques give satisfactory results, but the wet grinding is much less time consuming. After 10 minutes of wet grinding at 400 rpm and 5 minutes of centrifuging at 4500 rpm, a mean particle size of 114 nm is obtained, with a standard deviation of 43 nm. This particle size could also be verified with SEM measurements.

The emission spectrum of the nanoparticles is exactly the same as that of the bulk material. However, if we look at the persistent luminescent emission, we see that no red-shift is observed for the nanoparticles (figure 6.30). Therefore, the persistent emission of the particles appears to be blue-shifted by about 10 nm compared to the persistent emission of the bulk.

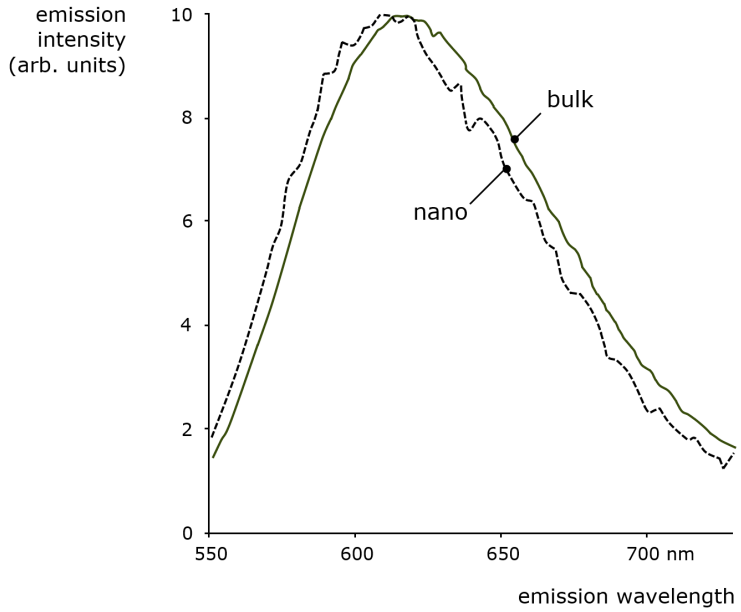

Figure 6.30: The persistent emission spectrum of $Ca_2Si_5N_8$:Eu,Tm nanoparticles is blue-shifted by about 10 nm compared to that of the bulk material.

Although it is difficult to compare the afterglow of the bulk material and the nanoparticles in solution, we can take a look at the shape of the decay in both cases (figure 6.31). During the first two minutes, the initial decay of the afterglow is stronger in the nanoparticles than in the bulk material. After this initial phase, the afterglow decay has exactly the same shape, indicating that the same kind of trap plays a role in both nanoparticles and bulk material.

6.3.3 Cytotoxicity

In order to verify the cytotoxicity of the nanoparticles, two standard *in vitro* tests were performed. In the first type of test, the release of LDH (lactate dehydrogenase) by the cells is measured. This compound is present inside the cell membrane, and is released upon cell death or membrane damage. The second type of test is based on the soluble tetrazolium dye MTT (3-(4,5-dimethylthiazol-2-yl)-2,5-diphenyltetrazolium bromide). Around living cells, this dye is reduced by the cell metabolism. Hence, the amount of MTT is a measure for the viability of the cells. In both tests, a sample without the addition of $Ca_2Si_5N_8$:Eu,Tm nanoparticles was taken as the 100% viability reference, and a sample with addition of a deadly concentration of Triton X-100 was taken as the 0% viability reference.

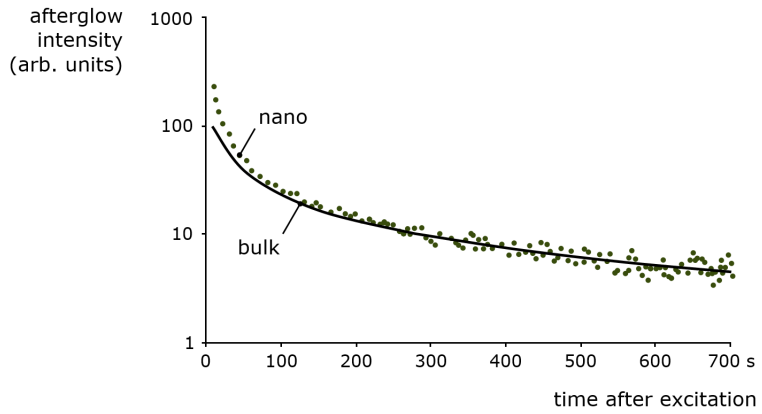

Figure 6.31: The afterglow decay of the $Ca_2Si_5N_8$:Eu,Tm nanoparticles largely coincides with that of the bulk material, although it is steeper during the first two minutes.

The results of the cytotoxicity tests are shown in figure 6.32, together with the standard deviation. Typically, the standard deviation of the MTT tests is larger than that of the LDH tests. The measured acute cytotoxicity is very low, with a viability of about 90%. Only for smaller concentrations of the nanoparticles, in the order of 1/500 of the stock solution, the toxicity appears to increase to about 20%. This is possibly due to a reduction of the aggregation of the nanoparticles at these small concentrations. This makes it absorbtion by the cells easier, which could increase the toxicity.

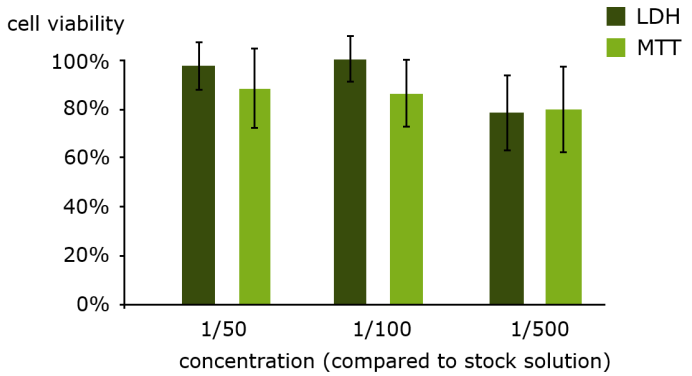

Figure 6.32: Calculated viability of cells in solutions of $Ca_2Si_5N_8$:Eu,Tm based on LDH and MTT experiments.

It should be noted that the above cytotoxicity tests were performed with nanoparticles without coating or functionalization. Since this coating or functionalization is required in practice to improve the biodistribution and circulation time in the body [16–18], the actual cytotoxicity of the particles used for *in vivo* imaging might differ from the values shown above, and further test remain necessary. However, it remains important to investigate the intrinsic toxicity of the uncoated particles as well.

6.3.4 Example of *in vivo* imaging

To prove the concept of *in vivo* medical imaging using persistent luminescent nanoparticles of $Ca_2Si_5N_8$:Eu,Tm, one of our samples was sent to the LCMCP research group (Chimie Paristech) in Paris, France. Thomas Maldiney and colleagues investigated the effect of functionalization with OH and PEG on the biodistribution of the particles when injected in mice. They used wet grinding and selective sedimentation to obtain nanoparticles with a diameter close to 200 nm.

Figure 6.33 shows the biodistribution of the $Ca_2Si_5N_8$:Eu,Tm nanoparticles 15 minutes after injection in the tail vain. The samples were excited for 5 minutes by 254 nm before injection, and the light emission was measured using a sensitive photon-counting system.

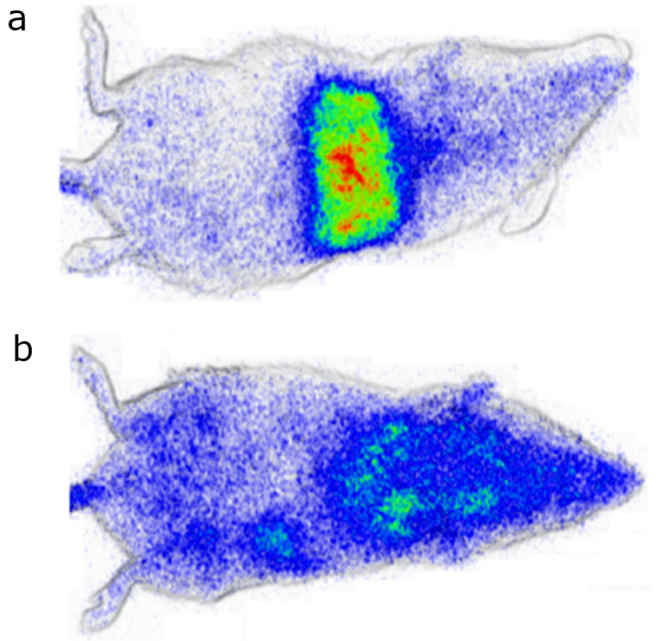

Figure 6.33: Biodistribution of (a) OH-terminated and (b) PEG-terminated $Ca_2Si_5N_8$:Eu,Tm nanoparticles in mice, 15 minutes after tail vain injection. The OH-terminated particles are mainly concentrated in the liver, while the PEG-terminated particles are distributed throughout the body.

In figure 6.33a, the distribution of OH-terminated particles is shown. Most of these particles are trapped almost instantly by the liver. The biodistribution of PEG-coated particles, shown in figure 6.33b, is much better. The emission from the nanoparticles can be detected anywhere in the body.

6.4 Summary

In our quest for new, bright and long-lasting persistent luminescent material, we have investigated the Eu^{2+}-doped $M_2Si_5N_8$ family, where M = Ca, Sr or Ba. After codoping

with various rare earth elements, we found that the longest afterglow could be achieved in $Ca_2Si_5N_8$:Eu,Tm, with an afterglow duration of up to 2,500 s. With the dark-adapted naked eye, this afterglow remains visible for multiple hours in the dark.

The preparation of $Ca_2Si_5N_8$:Eu,Tm was optimized by choosing the appropriate starting materials, adding small amounts of flux materials and increasing the preparation duration. The influence of the various rare earth codopants was investigated by TL measurements, and a good agreement with the Dorenbos model could be discerned. We also found that the $Ca_2Si_5N_8$:Eu,Tm powder is very stable. After two years storage in water, the afterglow intensity has only decreased by 2%. The persistent luminescence can be induced both by UV light and by visible light, with wavelengths up to 550 nm.

Finally, the size of the $Ca_2Si_5N_8$:Eu,Tm grains was reduced to around 100 nm by wet grinding. Cytotoxicity tests showed a high viability of cells exposed to these particles, and upon coating with PEG a good biodistribution could be achieved in mice, by our colleagues in Paris. This proves the possibility of using persistent luminescent nanoparticles as an alternative for radioactive tracers in *in vivo* medical imaging, one of the most promising applications of persistent phosphors.

References

[1] Nys, I. Master's thesis, Universiteit Gent, (2013).

[2] Höppe, H. A., Lutz, H., Morys, P., Schnick, W., and Seilmeier, A. *Journal of Physics and Chemistry of Solids* **61**, 2001–2006 (2000).

[3] Schlieper, T., Milius, W., and Schnick, W. *Zeitschrift fur Anorganische und Allgemeine Chemie* **621**, 1380–1384 (1995).

[4] Schlieper, T., Milius, W., and Schnick, W. *Zeitschrift fur Anorganische und Allgemeine Chemie* **621**, 1037–1041 (1995).

[5] Li, Y. Q., van Steen, J. E. J., van Krevel, J. W. H., Botty, G., Delsing, A. C. A., DiSalvo, F. J., de With, G., and Hintzen, H. T. *Journal of Alloys and Compounds* **417**, 273–279 (2006).

[6] Shannon, R. *Acta Crystallographica Section A* **32**, 751–767 (1976).

[7] Smet, P. F., Avci, N., and Poelman, D. *Journal of the Electrochemical Society* **156**, H243–H248 (2009).

[8] Clabau, F., Garcia, A., Bonville, P., Gonbeau, D., Le Mercier, T., Deniard, P., and Jobic, S. *Journal of Solid State Chemistry* **181**, 1456–1461 (2008).

[9] Smet, P. F., Parmentier, A. B., and Poelman, D. *Journal of the Electrochemical Society* **158**, R37–R54 (2011).

[10] Bos, A. J. J., van Duijvenvoorde, R. M., van der Kolk, E., Drozdowski, W., and Dorenbos, P. *Journal of Luminescence* **131**, 1465–1471 (2011).

[11] Miyamoto, Y., Kato, H., Honna, Y., Yamamoto, H., and Ohmi, K. *Journal of the Electrochemical Society* **156**, J235–J241 (2009).

[12] Lei, B., Machida, K.-i., Horikawa, T., Hanzawa, H., Kijima, N., Shimomura, Y., and Yamamoto, H. *Journal of The Electrochemical Society* **157**, J196–J201 (2010).

[13] Chung, K. S., Choe, H. S., Lee, J. I., Kim, J. L., and Chang, S. Y. *Radiation Protection Dosimetry* **115**, 343–349 (2005).

[14] Dorenbos, P. *Journal of Luminescence* **104**, 239–260 (2003).

[15] Huang, Y.-Y., Chen, A. C.-H., and Hamblin, M. *SPIE Newsroom* , DOI 10.117/2.1200906.1669 (2009).

[16] le Masne de Chermont, Q., Chanéac, C., Seguin, J., Pellé, F., Maîtrejean, S., Jolivet, J.-P., Gourier, D., Bessodes, M., and Scherman, D. *Proceedings of the National Academy of Sciences* **104**, 9266–9271 (2007).

[17] Maldiney, T., Richard, C., Seguin, J., Wattier, N., Bessodes, M., and Scherman, D. *ACS Nano* **5**, 854–862 (2011).

[18] Maldiney, T., Sraiki, G., Viana, B., Gourier, D., Richard, C., Scherman, D., Bessodes, M., Van den Eeckhout, K., Poelman, D., and Smet, P. F. *Optical Materials Express* **2**, 261–268 (2012).

Conclusions and perspectives

To conclude this dissertation, we summarize the main results of our work, and we discuss some of the remaining challenges for future research.

Main results

We have used two approaches to study the phenomenon of persistent luminescence. On one hand, we have investigated the origin and behaviour of the charge carriers and the trap levels in the phosphor, using a variety of common and novel experimental techniques. On the other hand, we have developed, optimized and studied our own orange-emitting persistent phosphor $Ca_2Si_5N_8$:Eu,Tm.

Mechanism of persistent luminescence

While the intensity and shape of the afterglow decay are commonly studied in persistent phosphors, the study of the emission during the excitation is much less frequently investigated. However, such a study can provide us with information on the whereabouts and the kinetics of the charge carriers during the trapping.

By simulating the expected behaviour during the excitation using a simple one- or two-trap energy level scheme, we can accurately model the emission intensity during the excitation of $Sr_2MgSi_2O_7$:Eu,Dy and $CaAl_2O_4$:Eu,Nd. It also shows us how shallow traps reach their final filled fraction much faster than deeper traps.

Using fast XANES measurements on the Eu L_{III} edge in $SrAl_2O_4$:Eu,Dy, we were able to monitor the valence state of the luminescent centers during the excitation and trapping process. We showed that, under x-ray excitation, the concentration of divalent Eu ions decreases in favor of that of the trivalent ions. Also, the change in the Eu^{3+} versus Eu^{2+} ratio could be related to the trap filling rate derived from radioluminescence measurements. This proves the assumption that the trapped charge carriers in $SrAl_2O_4$:Eu,Dy are electrons originating from the luminescent centers.

To study the trap system in persistent phosphors, we developed a procedure that combines series of thermoluminescence (TL) measurements with the initial rise analysis method. After exciting a persistent phosphor for various durations and at various temperatures, a change in the height and location of the glow peaks can indicate the presence of a continuous distribution of trap depths, rather than one or more discrete energy levels. Applying this procedure on an e-beam annealed $CaAl_2O_4$:Eu,Nd sample showed that the trap system consists of a continuous distribution with a Gaussian shape, centered around a depth of 0.9 eV, but extending from 0.7 to over 1.2 eV (figure 1).

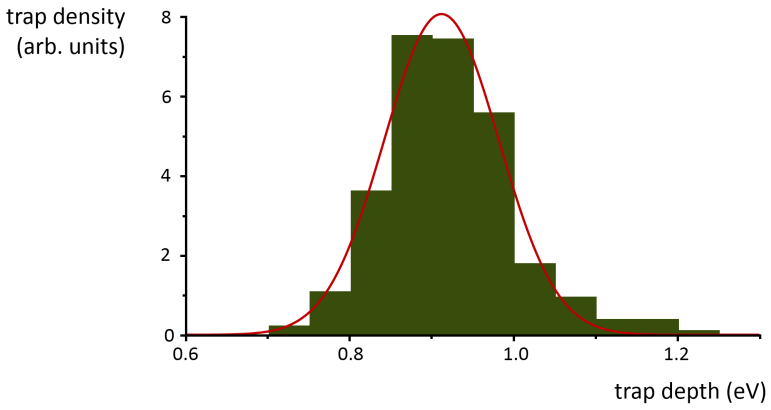

Figure 1: The trap system in $CaAl_2O_4$:Eu,Nd consists of a continuous distribution of trap depths with a Gaussian shape, centered around 0.9 eV (section 5.5.4).

Development of a persistent phosphor

In order to alleviate the need for orange- and red-emitting persistent phosphors, we investigated the Eu-doped nitrido-silicate family, $M_2Si_5N_8$:Eu. These materials are commonly used as conversion phosphor in white LEDs, but their persistent luminescent properties had not been described before.

Upon codoping with various rare earth ions, the influence on the trap levels (as studied with TL experiments) was found to be in accordance with the Dorenbos model. The addition of Tm to $Ca_2Si_5N_8$:Eu causes a spectacular increase in persistent luminescent intensity (figure 2). $Ca_2Si_5N_8$:Eu,Tm powder shows a bright orange afterglow lasting about 2500 seconds (before dropping below the 0.32 mcd/m^2 threshold).

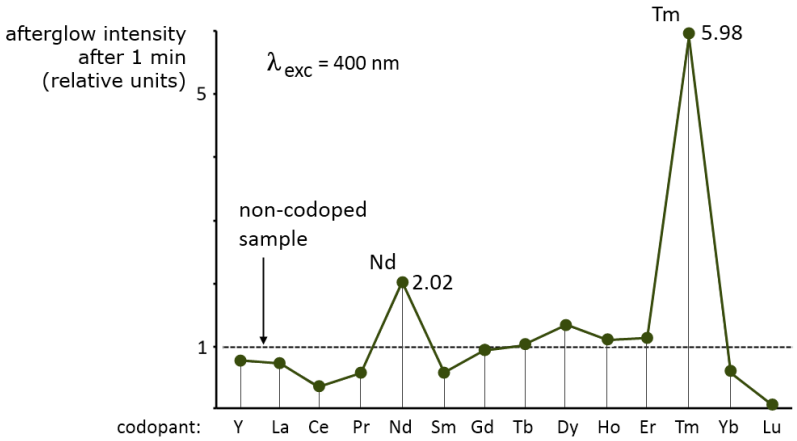

Figure 2: The addition of Tm to $Ca_2Si_5N_8$:Eu induces a spectacular increase in the afterglow intensity, compared to the non-codoped compound (section 6.2.1).

We optimized the preparation procedure, starting mixture, and dopant concentra-

tion in order to achieve the longest possible afterglow. TL-excitation mapping showed that the traps in the material can be filled using visible light, which is advantageous for indoor applications. Also, the phosphor has a very high stability, retaining its afterglow properties even after 2 years of storage in water.

As a final step, $Ca_2Si_5N_8$:Eu,Tm powder was downsized to nanoparticles, for use as tracer particles in *in vivo* medical imaging. Cytotoxicity measurements showed only low acute toxicity. As a proof of principle, these particles were injected into mice by the LCMCP research group (Chimie Paristech), enabling the *in vivo* tracking of the particles' biodistribution in the body. In the near future, such persistent luminescent nanoparticles might replace the commonly employed radioactive tracer particles for *in vivo* medical imaging techniques.

Perspectives for future research

The mechanism behind persistent luminescence is governed by a complex interplay between the host lattice, luminescent ions, trap levels, codopants and charge carriers. To complicate things even more, small changes in composition, material purity and crystallinity and dopant concentration can have a strong effect on the afterglow properties. It is very difficult to describe this with a simple model which is valid for every persistent phosphor, since the situation is different for every single compound. For example, while the emission during excitation in $Sr_2MgSi_2O_7$:Eu,Dy can be accurately modeled assuming only one trap level (section 4.2.1), the radioluminescent behaviour of $SrAl_2O_4$:Eu,Dy suggests at least the presence of two trap levels (section 4.2.3), and TL measurements in $CaAl_2O_4$:Eu,Nd have revealed the presence of a continuum of trap depths (section 5.5.3).

While the influence of codoping on the afterglow intensity cannot be overestimated (e.g. Dy in $SrAl_2O_4$:Eu or Tm in $Ca_2Si_5N_8$:Eu), it should not be forgotten that the majority of persistent phosphors also shows an afterglow without the addition of a codopant. It is clear that internal defects are somehow responsible for the traps in these materials. However, these defects are clearly of a different nature and origin for various host compounds.

For these reasons, every persistent phosphor needs its own individual study to fully understand the trap system and the trapping kinetics. Ideally, such a study consists of a large range of diverse experimental techniques. More conventional experimental data, such as the excitation and emission spectra, and measurement of the afterglow decay, could be combined with more uncommon techniques such as X-ray absorption (to monitor the valence state of the ions in question) or EPR (to monitor the presence of specific defects or, e.g., divalent europium). A thorough thermoluminescence study of each material can reveal the underlying trap system. Not all of these experimental techniques are ideally suited for all persistent phosphors, but such a broad view will help in unraveling the mechanism behind persistent luminescence.

A lot of research is going on in the field of persistent luminescent materials, and numerous material-dopant combinations have been and are being developed. It might simply be impossible to predict the afterglow properties of a certain combination of host lattice and activator before preparation, although energy level schemes such as

Dorenbos' model might allow to infer which codopants will have a positive or negative influence on the afterglow intensity and duration.

Up to recently, the best Eu^{2+}-based persistent phosphors such as $SrAl_2O_4$:Eu,Dy and its sister compound $CaAl_2O_4$:Eu,Nd were without competition in terms of absolute luminance or afterglow time. But while they are still unrivalled for blue and green emission, the use of other dopants - especially Cr^{3+} or Mn^{2+}- allows to extend the wavelength range that can be covered with persistent luminescence. The potential applications, especially in the red and near-infrared range, will be a driving force into further research and developments of new persistent phosphors.

List of Figures

4. Trapping and detrapping kinetics

5. Estimating trap depths

List of Tables

List of Acronyms

CCD	charge-coupled device
CRT	cathode ray tube
DFT	discrete Fourier transform
DUBBLE	Dutch Belgian beam line
EDX	energy-dispersive x-ray spectroscopy
EPR	electron paramagnetic resonance
ESRF	European Synchrotron Radiation Facility
FWHM	full width at half maximum
GOT	general one trap
IR	infrared
LCMCP	Laboratoire Chimie de la Matière Condensée de Paris
LED	light emitting diode
LDH	lactate dehydrogenase
MTT	3-(4,5-dimethylthiazol-2-yl)-2,5-diphenyltetrazolium bromide
PEG	polyethylene glycol
PLAL	pulsed laser ablation
QE	quantum efficiency
RE	rare earth
RL	radioluminescence
rpm	revolutions per minute
SEM	scanning electron microscopy
STE	self-trapped exciton
TL	thermoluminescence
UV	ultraviolet
XANES	x-ray absorption near-edge spectroscopy
XRD	x-ray diffraction

Examination committee

Chairman

Prof. dr. Jan Ryckebusch
Department of Solid State Sciences, Ghent University

Promoters

Prof. dr. Dirk Poelman (*)
Department of Solid State Sciences, Ghent University
Prof. dr. Philippe Smet
Department of Solid State Sciences, Ghent University

Other members of the examination committee

Prof. dr. Aurélie Bessière (*)
LCMCP, Chimie ParisTech (France)
Prof. dr. Adrie Bos (*)
Department of Radiation Science and Technology, TU Delft (The Netherlands)
Prof. dr. Klaartje De Buysser (*)
Department of Inorganic and Physical Chemistry, Ghent University
Prof. dr. Henk Vrielinck
Department of Solid State Sciences, Ghent University

(*) Reading committee

Publications

Papers in international, peer reviewed journals

- **Persistent luminescence in non-Eu^{2+}-doped compounds: A review**
  K. Van den Eeckhout, D. Poelman and P.F. Smet
  Materials **6** (2013) 2789-2818

- **Revealing trap depth distributions in persistent phosphors**
  K. Van den Eeckhout, A.J.J. Bos, D. Poelman and P.F. Smet
  Physical Review B **87** (2013) 045126

- **Persistent luminescence in $MSi_2O_2N_2$:Eu phosphors**
  J. Botterman, K. Van den Eeckhout, A.J.J. Bos, P. Dorenbos and P.F. Smet
  Optical Materials Express **2** (2012) 341-349

- **Extending the afterglow in $CaAl_2O_4$:Eu,Nd persistent phosphors by electron beam annealing**
  P.F. Smet, N. Avci, K. Van den Eeckhout and D. Poelman
  Optical Materials Express **2** (2012) 1306-1313

- **Mechanoluminescence in $BaSi_2O_2N_2$:Eu**
  J. Botterman, K. Van den Eeckhout, I. De Baere, D. Poelman and P.F. Smet
  Acta Materialia **60** (2012) 5494-5500

- **Temperature and wavelength dependent trap filling in $M_2Si_5N_8$:Eu (M = Ca, Sr, Ba) persistent phosphors**
  P.F. Smet, K. Van den Eeckhout, A.J.J. Bos, E. van der Kolk and P. Dorenbos
  Journal of Luminescence **132** (2012) 682-689

- **In vivo optical imaging with rare earth doped $Ca_2Si_5N_8$ persistent luminescence nanoparticles**
  T. Maldiney, G. Sraiki, B. Viana, D. Gourier, C. Richard, D. Scherman, M. Bessodes, K. Van den Eeckhout, D. Poelman and P.F. Smet
  Optical Materials Express **2** (2012) 261-268

- **Luminescent afterglow behaviour in the $M_2Si_5N_8$:Eu family (M = Ca, Sr, Ba)**
  K. Van den Eeckhout, P.F. Smet and D. Poelman
  Materials **4** (2011) 980-990

- **Luminescence and x-ray absorption measurements of persistent $SrAl_2O_4$:Eu,Dy powders: Evidence for valence state changes**
  K. Korthout, K. Van den Eeckhout, J. Botterman, S. Nikitenko, D. Poelman and P.F. Smet
  Physical Review B **84** (2011) 085140

- **Solvothermal synthesis, crystal structure, and properties of lanthanide-organic frameworks based on thiophene-2,5-dicarboxylic acid**
  Y. Sun, B. Jiang, T. Cui, G. Xiong, P.F. Smet, F. Ding, E. Gao, T. Lv, K. Van den Eeckhout, D. Poelman and F. Verpoort
  Dalton Transactions **40** (2011) 11581-11590

- **Persistent luminescence in Eu^{2+}-doped compounds: A review**
  K. Van den Eeckhout, P.F. Smet and D. Poelman
  Materials **3** (2010) 2536-2566

- **Persistent luminescence in rare-earth codoped $Ca_2Si_5N_8$:Eu^{2+}**
  K. Van den Eeckhout, P.F. Smet and D. Poelman
  Journal of Luminescence **129** (2009) 1140-1143

Contributions at international conferences

- **Probing trap depths in persistent phosphors**
  K. Van den Eeckhout, A.J.J. Bos, D. Poelman and P.F. Smet
  Luminescent Detectors and Transformers of Ionizing Radiation (LUMDETR), 8th international conference (2012)

- **Persistent luminescence and mechanoluminescence in $BaSi_2O_2N_2$:Eu**
  J. Botterman, K. Van den Eeckhout, A.J.J. Bos, P. Dorenbos, D. Poelman and P.F. Smet
  Luminescent Detectors and Transformers of Ionizing Radiation (LUMDETR), 8th international conference (2012)

- **Persistent luminescence: traps in materials and research**
  D. Poelman, K. Van den Eeckhout, K. Korthout, K. Meert, J. Botterman and P.F. Smet
  Optical, Optoelectronic and Photonic Materials and Applications (ICOOPMA), 5th international conference (2012)

- **Probing trap depths in persistent luminescent $CaAl_2O_4$:Eu,Nd**
  K. Van den Eeckhout, A.J.J. Bos, P. Dorenbos, D. Poelman and P.F. Smet
  Photoluminescence in Rare Earths (PRE), 4th international workshop (2012)

- **In vivo imaging with Eu,Tm:$Ca_2Si_5N_8$ persistent luminescence nanoparticles**
  T. Maldiney, G. Sraiki, B. Viana, D. Gourier, C. Richard, K. Van den Eeckhout, P.F. Smet and D. Poelman
  Photoluminescence in Rare Earths (PRE), 4th international workshop (2012)

- **Charging behaviour in persistent phosphors**
  K. Van den Eeckhout, P.F. Smet and D. Poelman
  Phosphoros (2011)

- **Persistent luminescence in rare-earth doped nitrido-silicates**
  K. Van den Eeckhout, P.F. Smet and D. Poelman
  Phosphoros (2011)

- **An x-ray absorption study of $SrAl_2O_4$:Eu,Dy powders**
  K. Korthout, K. Van den Eeckhout, P.F. Smet and D. Poelman
  Phosphoros (2011)

- **Persistent luminescence and mechanoluminescence in $MSi_2O_2N_2:Eu^{2+}$ (M = Ca, Sr, Ba)**
  J. Botterman, K. Van den Eeckhout, D. Poelman and P.F. Smet
  Phosphoros (2011)

- **Preparation and persistent luminescence in rare earth doped $Ca_2Si_5N_8$ nanoparticles**
  G. Sraiki, B. Viana, D. Gourier, T. Maldiney, C. Richard, K. Van den Eeckhout, P.F. Smet and D. Poelman
  Phosphoros (2011)

- **Charging mechanisms in persistent phosphors**
  P.F. Smet, K. Van den Eeckhout, K. Korthout, J. Botterman, E. van der Kolk, A.J.J. Bos, P. Dorenbos, D. Poelman
  Luminescence and Optical Spectroscopy of Condensed Matter (ICL), 16th international conference (2011)

- **Physics and applications of afterglow phosphors**
  P.F. Smet, K. Van den Eeckhout and D. Poelman
  Phosphor Global Summit (2011)

- **New classes of phosphors for emerging lighting applications**
  D. Poelman, A. Parmentier, K. Korthout, K. Van den Eeckhout, N. Avci, I. Cimieri, J. Botterman and P.F. Smet
  Electroluminescence (EL) (2010)

- **Persistent luminescence in the $M_2Si_5N_8:Eu^{2+},RE^{3+}$ family (M = Ca, Sr, Ba)**
  K. Van den Eeckhout, P.F. Smet and D. Poelman
  Excited States of Transition Elements (ESTE) (2010)

- **Revealing charge transfer by x-ray absorption and radioluminescence in $SrAl_2O_4$:Eu,Dy**
  K. Van den Eeckhout, K. Korthout, J. Botterman, S. Nikitenko, D. Poelman and P.F. Smet
  Excited States of Transition Elements (ESTE) (2010)

- **Seeing the light: new standards for quantifying specifications of low level light sources**
  D. Poelman, K. Van den Eeckhout and P.F. Smet
  Optical, Optoelectronic and Photonic Materials and Applications (ICOOPMA), 4th international conference (2010)

- **Persistent luminescence in rare earth doped oxynitrides**
  J. Botterman, K. Van den Eeckhout, P.F. Smet, A.J.J. Bos, E. van der Kolk, P. Dorenbos and D. Poelman
  Optical, Optoelectronic and Photonic Materials and Applications (ICOOPMA), 4th international conference (2010)

- **Resonance modes in rare earth doped microcrystals**
  K. Korthout, K. Van den Eeckhout, P.F. Smet and D. Poelman
  E-MRS, Spring meeting (2010)

- **Influence of rare-earth codoping on the afterglow behaviour in $Ca_2Si_5N_8$:Eu^{2+}**
  K. Van den Eeckhout, P.F. Smet and D. Poelman
  E-MRS, Spring meeting (2010)

- **Persistent luminescence in rare-earth co-doped $Ca_2Si_5N_8$:Eu^{2+}**
  K. Van den Eeckhout, P.F. Smet and D. Poelman
  International Conference on f-Elements (ICfE) (2009)

Contributions at national conferences

- **Probing trap depths in persistent phosphors**
  K. Van den Eeckhout, P.F. Smet and D. Poelman
  Belgian Physical Society (BPS), Annual general scientific meeting (2012)

- **Persistent luminescence in rare-earth doped nitrido-silicates**
  K. Van den Eeckhout, P.F. Smet and D. Poelman
  Belgian Physical Society (BPS), Annual general scientific meeting (2011)

- **The use of SEM-CL|EDX in phosphor research: merging luminescence and chemical information**
  P.F. Smet, K. Van den Eeckhout, K. Korthout, A. Parmentier and D. Poelman
  Belgian Society for Microscopy (BSM), 10th annual meeting (2009)

- **Persistent luminescence in rare-earth co-doped $Ca_2Si_5N_8$:Eu^{2+}**
  K. Van den Eeckhout, P.F. Smet and D. Poelman
  Belgian Physical Society (BPS), Annual general scientific meeting (2009)